Consideration of dynamic traffic conditions in the estimation of industrial vehicules energy consumption while integrating driving assistance strategies

Johana Cattin

N° d'ordre NNT : 2019LYSET003

THÈSE de DOCTORAT DE L'UNIVERSITÉ DE LYON
opérée au sein de
l'ENTPE (Ecole Nationale des Travaux Publics de l'Etat)

École Doctorale ED162
Mécanique - Energétique - Génie Civil - Acoustique

Spécialité / Discipline de doctorat : Génie Civil

Soutenue publiquement le 18/04/2019, par :
Johana CATTIN

Prise en compte des conditions de trafic dynamique dans l'évaluation des consommations énergétiques des véhicules industriels en intégrant les stratégies d'aide à la conduite

---

Devant le jury composé de :

Salima HASSAS, Professeur, UCBL / LIRIS,	Présidente
Azedine BOULMAKOUL, Professeur, Université Hassan II de Casablanca,	Rapporteur
Jérôme HÄRRI, Professeur, Eurecom,	Rapporteur
Nour-Eddin EL FAOUZI, Directeur de Recherche, IFSTTAR,	Directeur de thèse
Ludovic LECLERCQ, Directeur de Recherche, IFSTTAR,	Co-directeur de thèse
Florian PEREYRON, Ingénieur de Recherche, Renault Trucks,	Encadrant Industriel
Philippe DUTAL, Manager, Renault Trucks,	Invité

Thèse préparée au sein du laboratoire
LICIT - Laboratoire d'Ingénierie Circulation Transport

IFSTTAR
COSYS/LICIT
25, avenue François Mitterrand, Case 24
Cité des Mobilités
F-69675 Bron Cedex
France
www.ifsttar.fr

ENTPE
3, rue Maurice Audin
69518 Vaulx-en-Velin Cedex
France
www.entpe.fr

Et au sein de l'entreprise
Renault Trucks - Volvo Group
TER G50 1 57
99, route de Lyon
69806 Saint-Priest Cedex
France
www.volvogroup.com

Cette thèse a été financée par l'ANRT - Association Nationale Recherche Technologie Dans le cadre d'une convention CIFRE (Convention Industrielle de Formation par la REcherche)
ANRT
41, boulevard des Capucines
75002 Paris
France
www.anrt.asso.fr

NNT number : 2019LYSET003

PhD THESIS of the UNIVERSITY OF LYON
carried out inside
the ENTPE (Ecole Nationale des Travaux Publics de l'Etat)

Doctoral School ED162
Mécanique - Energétique - Génie Civil - Acoustique

Speciality / Doctoral discipline : Civil Engineering

Publicly defended on the 18/04/2019, by :
Johana CATTIN

Consideration of dynamic traffic conditions in the estimation of industrial vehicles energy consumption while integrating driving assistance strategies

---

In front of the jury composed of:

Salima HASSAS, Professor, UCBL / LIRIS,	President
Azedine BOULMAKOUL, Professor, Université Hassan II de Casablanca,	Reviewer
Jérôme HÄRRI, Professor, Eurecom,	Reviewer
Nour-Eddin EL FAOUZI, Research Director, IFSTTAR,	PhD supervisor
Ludovic LECLERCQ, Research Director, IFSTTAR,	PhD co-supervisor
Florian PEREYRON, Research Engineer, Renault Trucks,	PhD industrial supervisor
Philippe DUTAL, Manager, Renault Trucks,	Guest

PhD prepared with the lab
LICIT - Laboratoire d'Ingénierie Circulation Transport

IFSTTAR
COSYS/LICIT
25, avenue François Mitterrand, Case 24
Cité des Mobilités
F-69675 Bron Cedex
France
www.ifsttar.fr

ENTPE
3, rue Maurice Audin
69518 Vaulx-en-Velin Cedex
France
www.entpe.fr

And in collaboration with
Renault Trucks - Volvo Group
TER G50 1 57
99, route de Lyon
69806 Saint-Priest Cedex
France
www.volvogroup.com

This thesis was financed by ANRT - Association Nationale Recherche Technologie (ANRT)
As part of a CIFRE (Convention Industrielle de Formation par la REcherche) agreement.
ANRT
41, boulevard des Capucines
75002 Paris
France
www.anrt.asso.fr

Remerciements

Cette thèse s'est déroulée en collaboration avec le Laboratoire d'Ingénierie Circulation Transport (LICIT) et Renault Trucks (groupe Volvo). Je souhaiterai remercier toutes les personnes rencontrées durant ces trois années, qui ont contribué de près ou de loin à l'accomplissement de ce travail.

Je voudrais remercier dans un premier temps, le professeur Azedine Boulmakoul et le professeur Jérôme Härri qui ont rapporté ce mémoire de thèse. Je les remercie également, ainsi que la professeur Salima Hassas, d'avoir accepté d'évaluer mon travail lors de la soutenance de cette thèse.

Je remercie tout particulièrement mes directeurs de thèse : Ludovic Leclercq et Nour-Eddin El Faouzi ainsi que mon encadrant industriel : Florian Pereyron, pour leur accompagnement et leurs conseils qui ont permis la réalisation de ce travail. Merci de m'avoir soutenue tout au long de ces trois années et de m'avoir fait confiance.

Une thèse en convention CIFRE permet d'être à la fois en contact avec le monde de la recherche et le monde industriel. Durant cette magnifique expérience, j'ai pu rencontrer et travailler avec de nombreuses personnes que je tiens à remercier :

- Un grand merci tout d'abord à Philippe et Cédric, pour m'avoir permis d'effectuer mon stage de fin d'études d'ingénieur au sein de l'équipe System Simulation de Volvo. Ce stage a été ma première véritable expérience professionnelle mais également les prémices de cette thèse. Merci à vous pour votre accueil et votre sympathie.

- Merci à tous mes collègues de Renault Trucks qui ont rendu cette expérience très agréable: Thierry, Hellal, Réginald, Gérard, Florian D., Anthony, Thomas, Marc, Yves, Hocéane, Kéomany, Thomas, Wilfried et Célestin. Merci à Élie de m'avoir permis de travailler pour le projet Urban Lab 2.

- Je remercie également les membres du LICIT: Angelo, Bernard, Jean-Luc, Andrès, Arthur, Colette, Aurélien, Cécile, Jean, Delphine, Nicolas et Christine pour leur accueil, leur aide et les moments partagés.

- Anne-Christine, qui a relu avec attention mon mémoire et qui a fortement contribué à l'amélioration de mon niveau d'anglais. Merci aussi pour ta gentillesse et tes délicieux gâteaux du lundi matin.

- Sonia, qui permet chaque année aux doctorants de survivre à la difficile étape de la réinscription, merci pour ta gentillesse.

- Les doctorants du LICIT, passés et présents: Aurélien Jr, Sergio, Guilhem, Clélia, Nicole, Maxime, Pierre-Antoine, Raphaël, Loïc, Elise et Cécile.

- L'armée de doctorants/stagiaires/alternants rencontrée à Renault Trucks. En particulier, Élodie, ma comparse de voyage, Francesco, et Xavier, je vous souhaite bon courage pour vos thèses. Docteur Donatien, toutes mes félicitations ! Yoan, je te souhaite le meilleur pour la fin de ton apprentissage, et j'espère que l'on se croisera enfin sur une médiévale. Un pensée également pour Théo, mon super stagiaire.

- Je remercie finalement toutes les personnes rencontrées : professeurs, chercheurs, doctorants, industriels, lors des conférences pour les échanges autour de la problématique de la mobilité.

Je complète cette liste par quelques remerciements plus personnels. Tout d'abord une pensée pour l'ensemble des membres de la LIR avec qui je partage de superbes moments à chaque médiévale. Merci à vous pour ces bouffées d'air frais.

Je tiens à aussi à remercier mes amis, géographiquement éloignés, mais dont l'amitié sans faille me porte chaque jour. Camille, Alex, Angel, Laetitia, Auriane, Marine, Gil, Justine et Dorine, Sylvain, Gwen, et Astrid, merci.

Pour terminer, je remercie mes parents pour leur soutien sans faille depuis le début de mes études. Un énorme merci également à ma moitié, Jordi, qui a partagé cette expérience avec moi, et qui a su être présent lorsque j'avais besoin de soutien, mais également dans les meilleurs moments. Merci.

Consideration of dynamic traffic conditions in the estimation of industrial vehicles energy consumption while integrating driving assistance strategies

Summary

The industrial world, and in particular the automotive industry, is seeking to best represent the real world in order to design tools and products that are best adapted to current challenges and markets, by reducing development times and prototyping costs. To this end, modelling and simulation are increasingly used.

With this in mind, the Volvo Group has developed powerful tools to simulate the dynamics of industrial vehicles. These tools allow the optimization of vehicle components or control strategies. Many research activities focus on innovative technologies to reduce the consumption of industrial vehicles and increase the safety of their use in different environments. In particular, the development of driver assistance systems (ADAS) and intelligent transport systems (ITS) is booming.

In order to be able to develop these systems, a simulation environment must be set up to take into account the various factors that can influence the driving of a vehicle. As the vehicle kinematics simulation tools have already been developed, the work focuses on simulating the vehicle environment and the interactions between the vehicle and its direct environment, i.e. the vehicle in front of it.

The vehicle environment can be represented by two categories of parameters: (i) static parameters and (ii) dynamic parameters. Static parameters describe information related to the environment that does not change over time: the number of lanes, the slope, the speed limit, for example, while dynamic parameters are likely to change during the vehicle journey: the state of the traffic lights encountered, the speed and distance of the vehicle in front of it, the state of the network (congested or not), for example.

The interactions between the vehicle under study (Follower) and the vehicle in front of it (Leader) are modelled using mathematical models, called car-following models. Many models exist in the literature, most of which use as parameters the desired speed and acceleration of the Follower, the spacing and the speed difference between the two vehicles, the reaction time of the Follower for example.

The work done in this thesis is divided into two parts. The first part focuses on the study of car-following models and the calibration of their parameters on truck data. For this study, four car-following models frequently used for microscopic road traffic simulation were selected: the Gipps model, the Improved Intelligent Driver Model (IIDM), the Newell model and the Wiedemann model. The impact of the choice of the calibration method and the indicators on which errors are calculated is highlighted. Car-following models are assessed on their ability to produce vehicle trajectories similar to real trajectories but also sufficiently accurate to provide a relevant fuel consumption estimate.

The second part of the thesis presents a study of the usual environment encountered by an industrial vehicle during its use. In particular, statistical indicators of usual uses are estimated such as intersection density, number of lanes,... These indicators are evaluated according to different uses, urban or regional for example.

The first part of the thesis proposed a multi-objective calibration method based on three indicators (position, speed and acceleration) adapted for each of the four car-following models studied. The comparison of the calibration results of these models led to the conclusion that the most accurate model to represent the trajectory of a heavy vehicle and the most robust under the conditions of the tests performed is the Gipps model. The IIDM also allows to have correct results but with errors higher than the errors measured with the Gipps model. The other two models do not give satisfactory results and will not be retained for further study.

The impact of the calibration on the estimation of fuel consumption was then evaluated. The energy consumption corresponding to the routes used for calibration is estimated using a simulation tool used within the Volvo group. The comparison between measured and simulated consumption showed that errors could be quite high, so when the final objective is to estimate the energy consumption, a calibration of the car-following models based solely on trajectory related indicators (position, speed, acceleration) is not sufficient. To solve this problem, the estimation of energy consumption has been included in the calibration process of car-following models. This method made it possible to significantly improve the results without deteriorating the representativeness of the trajectories.

The second part of the thesis focuses on the implementation of methods to automatically generate simplified road networks for simulation while respecting the statistics of the usual cycles.

First, a statistical study was carried out over a set of standard cycles to determine the statistical data needed to define them, such as the number and type of intersections encountered, the slope, the number of lanes, legal speeds, etc. Five types of roads (urban, interurban, regional, ring road, highway) and two uses (local delivery, regional delivery) were also defined.

Then, a set of routines were developed to generate, from the statistical information defined above, a simplified network, usable in simulation with the SUMO software, statistically representative of a real use. The statistical relevance of the generated networks was verified.

Finally, the proposed simulation chain is illustrated by the evaluation of a driving assistance system that increases user safety, the ACC (Adaptive Cruise Control), on a long-haul cycle.

Keywords

Energy consumption, Heavy Duty Vehicles, Car-following models, Calibration, Statistics of use, Intelligent Transportation Systems (ITS), Advanced Driver Assistance System (ADAS)

Prise en compte des conditions de trafic dynamique dans l'évaluation des consommations énergétiques des véhicules industriels en intégrant les stratégies d'aide à la conduite

Résumé

Le monde industriel, et en particulier l'industrie automobile, cherche à représenter au mieux le réel pour concevoir des outils et produits les plus adaptés aux enjeux et marchés actuels, en diminuant les délais de mise au point et les coûts de prototypage. Dans ce but, il est de plus en plus fait appel à la modélisation et à la simulation.

Dans cette optique, le groupe Volvo a développé de puissants outils pour la simulation de la dynamique des véhicules industriels. Ces outils permettent notamment l'optimisation de composants véhicules ou de stratégies de contrôle. De nombreuses activités de recherche portent sur des technologies innovantes permettant de réduire la consommation des véhicules industriels et d'accroître la sécurité de leurs usages dans différents environnements. En particulier, le développement des systèmes d'aide à la conduite automobile (ADAS – *Advanced Driver Assistance Systems*) et des systèmes de transports intelligents (ITS – *Intelligent Transportation Systems*) est en plein essor.

Afin de pouvoir développer ces systèmes, un environnement de simulation permettant de prendre en compte les différents facteurs pouvant influencer la conduite d'un véhicule doit être mis en place. Les outils de simulation de la cinématique véhicule étant déjà développés, le travail se concentre sur la simulation de l'environnement du véhicule et des interactions entre le véhicule et son environnement direct, i.e. le véhicule qui le précède.

L'environnement du véhicule peut être représenté par deux catégories de paramètres : (i) les paramètres statiques et (ii) les paramètres dynamiques. Les paramètres statiques décrivent les informations liées à l'environnement qui ne changent pas au cours du temps : le nombre de voies, la pente, la limitation de vitesse par exemple, tandis que les paramètres dynamiques sont susceptibles d'évoluer au cours du trajet du véhicule : l'état des feux tricolores rencontrés, la vitesse et l'inter-distance du véhicule qui le précède, l'état du réseau (congestionné ou non), par exemple.

Les interactions entre le véhicule étudié (*Follower*) et le véhicule qui le précède (*Leader*) sont modélisées à l'aide de modèles mathématiques, nommés lois de poursuites (*car-following models*). De nombreux modèles existent dans la littérature, la plupart d'entre eux utilisent comme paramètres la vitesse désirée et l'accélération du *Follower*, l'inter-distance et la différence de vitesse entre les deux véhicules, le temps de réaction du *Follower* par exemple.

Le travail réalisé dans cette thèse se divise en deux parties. La première partie se concentre sur l'étude des lois de poursuites et le calage de leurs paramètres sur des données poids lourds. Pour cette étude, quatre lois de poursuite fréquemment utilisées pour la simulation microscopique du trafic routier ont été sélectionnées : le modèle de Gipps, l'*Improved Intelligent Driver Model* (IIDM), le modèle de Newell et le modèle de Wiedemann. L'impact du choix de la méthode de calibration ainsi que des indicateurs sur lesquels les erreurs sont calculées est mis en avant. Les lois de poursuites sont évaluées sur leur capacité à produire des trajectoires véhicules similaires aux trajectoires réelles mais également suffisamment précises pour une estimation de la consommation de carburant pertinente.

La seconde partie de la thèse présente une étude de l'environnement usuel rencontré par un véhicule industriel lors de son usage. En particulier, des indicateurs statistiques des usages usuels sont estimés tels que la densité d'intersections, le nombre de voies, ... Ces indicateurs sont évalués selon différents usages, urbain ou régional par exemple.

La première partie de la thèse a permis de proposer une méthode de calage multi-objectif basé sur trois indicateurs (la position, la vitesse et l'accélération) adaptée pour chacune des quatre lois de poursuite étudiées. La comparaison des résultats de calage de ces modèles a permis de conclure que le modèle le plus précis pour représenter la trajectoire d'un poids lourd et le plus robuste dans les conditions des tests effectués est le modèle de Gipps. L'IIDM permet également d'avoir des résultats corrects mais avec des erreurs supérieures aux erreurs mesurées avec le modèle de Gipps. Les deux autres modèles ne donnant pas de résultats satisfaisants, ils ne seront pas conservés pour la suite de l'étude.

L'impact du calage sur l'estimation des consommations de carburant a ensuite été évalué. Les consommations énergétiques correspondant aux trajets utilisés pour le calage sont estimées à l'aide d'un outil de simula-

tion utilisé au sein du groupe Volvo. La comparaison entre les consommations mesurées et simulées a montré que les erreurs pouvaient être assez élevées, ainsi lorsque l'objectif final est l'évaluation des consommations énergétiques, un calage des lois de poursuite uniquement basé sur des indicateurs liés à la trajectoire (position, vitesse, accélération) n'est pas suffisant. Pour résoudre ce problème, l'estimation des consommations énergétiques a été incluse dans le processus de calage des lois de poursuite. Cette méthode a permis d'améliorer de façon significative les résultats sans détériorer la représentativité des trajectoires.

La seconde partie de la thèse se concentre sur la mise en place de méthodes permettant de générer automatiquement des réseaux routiers simplifiés pour la simulation en respectant les statistiques des cycles usuels.

Dans un premier temps, une étude statistique a été réalisée sur un ensemble de cycles usuels afin de déterminer les données statistiques permettant de les définir, telles que le nombre et le type d'intersections rencontrées, la pente, le nombre de voies, les vitesses légales, etc... Cinq types de route (urbain, interurbain, régional, périphérique, autoroute) et deux usages (livraison locale, livraison régionale) ont également été définis.

Par la suite un ensemble de routines ont été développées permettant de générer, à partir des informations statistiques définies précédemment, un réseau simplifié, utilisable en simulation avec le logiciel SUMO, statistiquement représentatif d'un usage réel. La pertinence statistique des réseaux générés a été vérifiée.

Finalement, la chaîne de simulation proposée est illustrée par l'évaluation d'un système d'aide à la conduite augmentant la sécurité des usagers, l'ACC (*Adaptive Cruise Control*), sur un trajet long routier.

Mots clés

Consommation énergétique, Poids lourds, Lois de poursuite, Calibration, Statistiques d'usage, Système de Transport Intelligent (STI), Système d'Aide à la Conduite automobile

Contents

List of Figures

List of Tables

Glossary

car-following model A model describing how a vehicle follows the vehicle in front of it on a road. xvi, xix, I, III, IV, X, 2, 3, 5, 8, 11, 12, 17, 20, 21, 27, 34, 45, 48, 49, 51–53, 55–58, 60, 62, 63, 65, 66, 70–78, 80, 81, 83, 84, 87, 94, 113–115

EstimFC The simulation tool used within Volvo Group to estimate the fuel consumption of a vehicle along a defined path. xvi, 2, 70–72, 74

Follower The vehicle studied.. xv, xvi, xix, 11, 14, 18, 34, 37, 38, 40–45, 49, 63–65, 83, 113

Leader The vehicle preceding the vehicle studied on the road.. xv, xix, 11, 14, 18, 34, 37, 38, 40–42, 44, 45, 83, 84, 113

solver The method applied or integration or derivation of vehicle trajectory (position, speed and acceleration). 20, 21, 51, 56–58, 60, 66, 83, 114

Acronyms

ACC Adaptive Cruise Control. 108, 109, 111, 115

ADAS Advanced Driver Assistance System. 2, 5, 87, 90, 104, 108, 109, 111, 113, 115

CA Cellular Automata. 10

CADC Common Artemis Driving Cycles. 104

DC driving cycle. 104–109, 111, 114, 115

EV Electric Vehicle. 90

FC fuel consumption. xvi, xvii, xix, X–XVI, 2, 3, 5, 27, 51, 70–75, 77, 78, 80–84, 87, 90, 104–108, 111, 113–115

FD Fundamental Diagram. 8, 9, 14

GA Genetic Algorithm. 21, 62

GoF Goodness-of-Fit. xix, 20, 22, 48–51, 56, 62, 66, 83, 114

GPS Global Positioning System. 92

GSP Global Simulation Platform. 2

HDV Heavy Duty Vehicle. 5, 8, 11, 48, 66, 70, 87, 90, 99, 113–115

IDM Intelligent Driver Model. 13, 21, 62

IIDM Improved Intelligent Driver Model. xii, xix, II, 12, 13, 48–50, 52–55, 58, 60–63, 65, 66, 69–75, 78, 80, 81, 83, 84, 114

ITS Intelligent Transportation System. 2, 5, 9, 87, 90, 104, 108, 109, 111, 113, 115

LDV Light Duty Vehicle. 104

MAE Mean Absolute Error. 62

MANE Mean Absolute Normalized Error. 62

MO Multi-Objective. X, 20, 25, 48, 49, 51, 52, 63, 64, 71, 83

MoP Measure of Performance. xvi, XII, XIV, XVI, 20, 22, 24, 48, 51, 62, 70, 71, 73–75, 77, 78, 80–84, 114

MOPSO Multi-Objective Particle Swarm Optimization. 24, 25, 60, 83

NEDC New European Driving Cycle. 104

NGSIM Next Generation SIMulation. 11, 34, 42, 43, 48

OVM Optimal Velocity Model. 21

PCA Principal Component Analysis. xv, 54, 55

PSO Particle Swarm Optimization. 21, 25, 96

RK4 Runge-Kutta of order 4. 57, 58, 60

RMSE Root Mean Squared Error. 20, 37, 48, 51, 62

RMSPE Root Mean Squared Percentage Error. 20, 48, 51

SE Squared Error. 20, 48, 51, 62

SUMO Simulation of Urban MObility. xvi, xvii, xix, 90, 94–96, 99, 105–108, 111, 113–115

VECTO Vehicle Energy Consumption calculation TOol. 90

WLTC World Harmonized Light Vehicles Test Procedures. 104

Notations

a_n acceleration of the the follower vehicle.. 12

L_{n-1} length of the leader vehicle.. 15

U Theil's inequality coefficient.. xvi, 20, 48, 70, 71, 74

v_n speed of the the follower vehicle.. 14

x_n position of the the follower vehicle.. 15

v_{n-1} speed of the the leader vehicle.. 14

x_{n-1} position of the the leader vehicle.. 15

Chapter 1

Introduction, motivations and research questions

Contents

1.1 Context and motivations

The reduction of FC and pollutant emissions is one of the major challenges of vehicle manufacturers. In a world in which the protection of the environment is an important issue, industrial vehicles must consume less energy. In this context, many manufacturers have been developing strategies to consume less energy, produce less CO_2 and taking up new challenges in mobility (connected vehicles, autonomous vehicles, electromobility).

The research on new technologies for mobility is currently widely investigated by researchers and engineers. Industrial researches want to represent the real world to design the most adapted tools and products to propose new solutions to save energy and to answer the current market, while reducing prototyping delays and costs. In this context, modelling and simulation are more and more used, and very powerful tools are developed.

Volvo Group has developed and uses efficient simulation tools, Global Simulation Platform (GSP) and EstimFC, for the simulation of the kinematic of vehicles and fuel consumption estimation. These models allow for example the evaluation or optimization of vehicle components or control strategies and fuel consumption estimation. The knowledge of the environment and the current increase of communicating systems bring the possibility to develop new solutions allowing to optimize driving according to events around the vehicle.

In order to develop, evaluate and optimize driving strategies, Intelligent Transportation System (ITS) and Advanced Driver Assistance System (ADAS), it is necessary to model every parameter that can impact the driving of a vehicle in real situations. Two categories of parameters can be defined: the static parameters describing the environment encountered by the vehicle (slope, type of road, speed limit,...), and the dynamic parameters mainly linked to road traffic conditions (spacing to the leading vehicle and its speed, traffic lights,...). A lot of work has already be done with the Volvo tool on static parameters through the definition of a database of usual cycles representing different environments that can be encountered. The goal of this thesis is to work on the dynamic parameters integration into the Volvo simulation tool.

The integration of the environment dynamic parameters of a studied vehicle can be realized through the use of traffic simulation models. Traffic flow theory has already a long history but the coupling of traffic simulation models and emissions estimation tools for evaluation of new driving strategies is a new challenge to work on in the context of the development of intelligent mobility.

In traffic flow theory, several models and tools allowing the dynamic simulation of traffic exist. Those models are commonly classified in three categories: macroscopic scale (flow of vehicles), microscopic scale (individual vehicles are defined) and mesoscopic scale (aggregation of individual vehicles, between macroscopic and microscopic scale) (Barcelò, 2010; van Wageningen-Kessels et al., 2015).

These different models were originally used to evaluate road construction or new control strategies and predict traffic evolution (jam prediction, travel time estimation). Their validity was mainly validated in this context. Then, it was proved that they correctly model congestion propagation taking into account the road network capacity. However they are not design to accurately reproduce vehicle kinematics. Recent studies (Vieira da Rocha et al., 2015) have shown that these trajectories could be not enough relevant for these applications and it is important to keep in mind that the trajectories created by a traffic simulator could not be representative for the estimation of energy consumption.

These models are also used for the estimation of the environmental parameters associated to the road traffic such as energy consumption, CO_2 emissions or noise. Microscopic models are generally used in these cases because they directly provide the trajectories driven by the vehicles. Then, these trajectories can be set as the inputs of consumption tools to obtain a detailed estimation of the consumptions.

1.2 Research questions

This thesis aims at improving the simulation tool used in Volvo Group which estimates FC of industrial vehicles. Two main questions will be studied in order to answer to this problem.

The first one aims at integrating a realistic representation of the dynamic parameters that the vehicle can encounter in order to take into account the road traffic conditions in the estimation of FC. The realistic notion will be evaluated by the capacity of the model to generate trajectories which are relevant for both driving and consumption points of view. Then it will be important to develop a model which can take into account road traffic but which is also sufficiently accurate for FC estimation. This means designing a car-following model suitable for trucks, assess its performance for calculating emission by comparison with existing Volvo tools based on kinematic profile.

The second objective completes the previous one. It will still focus on the representativeness of traffic condition modelling while integrating network structure of the road by the research of indicators linked to the routes. This study will propose to develop statistical methods allowing to create simplified cycles from topography, geography and traffic information on usual one, that will be used to estimate energy consumption in simulation.

The integration of models and methods developed will be done in Volvo simulation tool and can be divided into 4 steps:

1. The definition of methods and scales of simulation adapted to take into account road traffic conditions and the reactions of the industrial vehicle to that traffic,

2. The definition of a methodology allowing the creation of cycles from information on topology, network and infrastructure for the simulation,

3. The coupling of the two preceding approaches to have a complete simulation tool,

4. The verification of the improved tool on a test case.

The first and second steps correspond to the first and second question that we want to answer. The two following steps are the application of the study.

1.3 General methodology and PhD organisation

The manuscript is divided into two main parts answering the two central questions proposed in the previous section.

To answer the first question it is first necessary to make the Volvo vehicle model capable of reacting to stimuli from other vehicles. As written previously, road traffic can be modelled in several ways called scales of simulation. The first part is divided into four chapters. The first one presents the materials and the methodology used in this part (Chapter 2). Particularly, the scales of simulation and models retained to model trucks reaction to other vehicles (car-following model) are presented. Then, the calibration method used to adapt usual car-following models to trucks behaviour is described.

The second chapter presents the setup of a database of real cycles needed for the calibration of the car-following models (Chapter 3). A method is proposed to reconstruct the entire needed trajectories from measurement containing only the speed of the studied vehicle and spacing to its leader.

The third chapter (Chapter 4) is about the calibration of these car-following models on real cycles presented in Chapter 3.

The last chapter of the first part (Chapter 5) highlights the influence of simulated trajectories on FC estimation. A solution is proposed to reduce gaps between measured and simulated values.

The first part of this thesis proposed methods to obtain a well calibrated car-following model to reproduce trucks behaviour and its energy consumption. Moreover, car-following models were calibrated and compared, and one of them is selected to be used with Volvo simulation tools.

The second part of the thesis is divided into two chapters. The first one (Chapter 6) deals with the statistical representation of usual cycles and the automatic generation of simplified cycles for simulation. This chapter presents the methodology used to easily create simulation cycles with traffic and so it completes the previous work.

The last chapter of the second part (Chapter 7) presents some results on a test case chosen to validate the developed complete simulation model.

The plan of this manuscript is described in Figure 1.1.

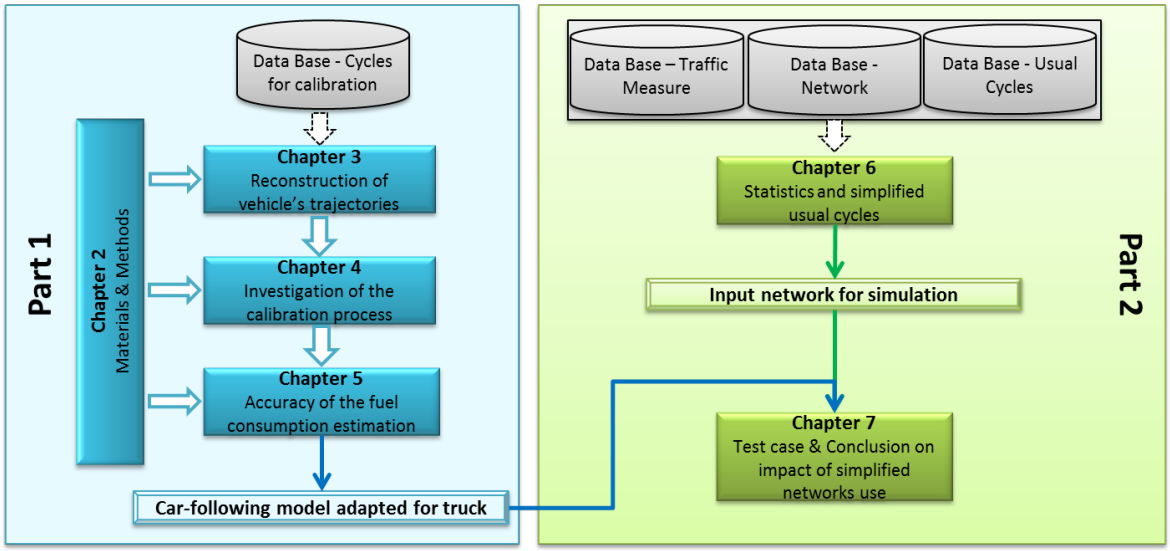

Figure 1.1 – Structure of the PhD manuscript

1.4 References

Jaume Barcelò. *Fundamentals of traffic simulations*. Jaume Barcelò, 2010. ISBN 978-1-4419-6141-9. p. 2

Femke van Wageningen-Kessels, Hans van Lint, Kees Vuik, and Serge Hoogendoorn. Genealogy of traffic flow models. *EURO Journal on Transportation and Logistics*, 4(4):445–473, December 2015. ISSN 2192-4376, 2192-4384. doi: 10.1007/s13676-014-0045-5. p. 2

Thamara Vieira da Rocha, Ludovic Leclercq, Marcello Montanino, Céline Parzani, Vincenzo Punzo, Biagio Ciuffo, and Daniel Villegas. Does traffic-related calibration of car-following models provide accurate estimations of vehicle emissions? *Transportation Research Part D: Transport and Environment*, 34:267–280, January 2015. ISSN 13619209. doi: 10.1016/j.trd.2014.11.006. p. 2

Part I

Adaptation of car-following models to heavy duty vehicles

The aim of this thesis is to evaluate the FC of industrial vehicles in a road traffic environment and to assess the benefits of new driving strategies like ITS and ADAS. The first step of this project is to make the studied and simulated vehicle able to react to surrounding road traffic and infrastructure.

According to Aghabayk et al. (2012, 2016); Nodine et al. (2017); Sarvi (2011) the following behaviour of a vehicle varies a lot according to its class (passenger car or Heavy Duty Vehicle (HDV)). However, so far, little has been done to adapt usual car-following models to HDV behaviour.

The first part of this thesis focuses on the development of calibration methods to adapt usual car-following models parameters to the behaviour of HDV. This work is divided into four parts:

i. The definition of the methods and data needed for the calibration, Chapter 2 - *Materials and Methods*,
ii. The definition of a database of trajectories to calibrate, Chapter 3 - *Reconstruction of vehicles' trajectories for car-following calibration*,
iii. The comparison of several calibration methods and different car-following models, Chapter 4 - *Calibration of car-following models from trucks trajectories*,
iv. The impact of the calibration method on the FC estimation, Chapter 5 - *Fuel consumption estimation from simulated trajectories*.

A synthesis of this study has been plublished in an article of the IET Journal, and presented at the ITS World Congress 2018 in Copenhagen (Cattin et al., 2019).

References

Kayvan Aghabayk, Majid Sarvi, and William Young. Understanding the Dynamics of Heavy Vehicle Interactions in Car-Following. *Journal of Transportation Engineering*, 138(12):1468–1475, December 2012. ISSN 0733-947X, 1943-5436. doi: 10.1061/(ASCE)TE.1943-5436.0000463. p. 5

Kayvan Aghabayk, Majid Sarvi, and William Young. Including heavy vehicles in a car-following model: modelling, calibrating and validating. *Journal of Advanced Transportation*, 50(7):1432–1446, November 2016. ISSN 01976729. doi: 10.1002/atr.1409. [3]. p. 5

Johana Cattin, Ludovic Leclercq, Florian Pereyron, and Nour-Eddin El Faouzi. Calibration of Gipps' car-following model for trucks and the impacts on fuel consumption estimation. *IET Intelligent Transport Systems*, 13(2):367–375, February 2019. ISSN 1751-956X, 1751-9578. doi: 10.1049/iet-its.2018.5303. p. 5

Emily Nodine, Andy Lam, Mikio Yanagisawa, and Wassim Najm. Naturalistic Study of Truck Following Behavior. *Transportation Research Record: Journal of the Transportation Research Board*, 2615:35–42, January 2017. ISSN 0361-1981. doi: 10.3141/2615-05. [2]. p. 5

Majid Sarvi. Heavy commercial vehicles-following behavior and interactions with different vehicle classes: Following behavior analysis in heavy vehicles. *Journal of Advanced Transportation*, pages n/a–n/a, October 2011. ISSN 01976729. doi: 10.1002/atr.182. URL http://doi.wiley.com/10.1002/atr.182. p. 5

Chapter 2

Materials and Methods

Contents

As presented previously, the first part of the thesis focuses on the definition of adjusted micro-simulation tools to HDV. This chapter focuses on the description of the data and the methods which are used in this part. First, a brief review of traffic simulation methods is presented, then the four well-known car-following models that will be investigated later are presented (Chapters 4 and 5). The definition of a simulation model adapted to HDV will be based on real data recorded in Lyon (France), that are presented in section 2.4. The way recorded data are processed to be used for calibration will be detailed in Chapter 3.

In order to define properly the simulation models, usual car-following models must be calibrated on measurements. Different calibration methods are presented in this chapter and will be investigated more in details in Chapter 4.

2.1 Road traffic simulation - General definitions

Mathematical description of the traffic flows dynamics began in the 1930s with the pioneering studies on the fundamental relations between traffic flow, mean speed and vehicle density conducted by Greenshield (Gerlough and Huber, 1975; May, 1990). By the 1950s, scientists had started to describe the physical propagation of traffic flows by means of macroscopic (flow dynamics) and microscopic models - car-following models (Gerlough and Huber, 1975).

There are different ways to model the dynamics of traffic flows in order to simulate their temporal propagation through traffic networks (Figure 2.1). Traffic flows can be represented macroscopically from an aggregated point of view based on a fluid dynamic analogy. They can also be modelled microscopically, from a fully disaggregated point of view, by modelling each vehicle individually. An intermediate scale, named mesoscopic simulation, takes place between the macroscopic and the microscopic scales, where the traffic is modelled as packets of vehicles (Barcelò, 2010). The macroscopic and microscopic scales will be described in the following sections.

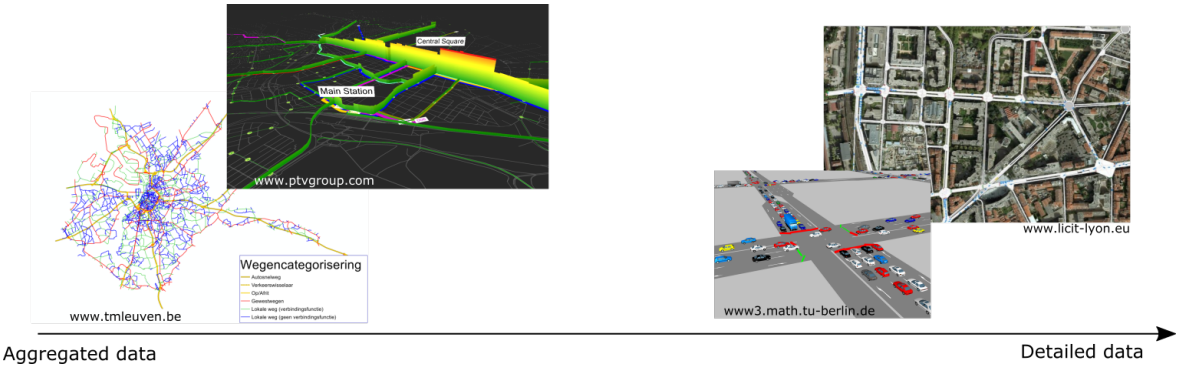

Figure 2.1 – Scales of traffic simulation

2.1.1 Macroscopic scale

The macroscopic modelling is mainly used for the static modelling of a big network. Macroscopic models have applications when detailed information about behaviour of a single vehicle is not required but only an evaluation of traffic flows in a network (Maciejewski, 2010). In this view, traffic appears to be a compressive fluid whose state (speed, flow and density) propagates like waves. These models are often used for regional transportation planning.

Macroscopic measures of effectiveness are mean speed, traffic flow and traffic density. These models are similar to models of fluid dynamics, macroscopic modelling is usually based on the continuum traffic flow theory whose objective is to describe the time-space evolution of the variables characterizing the macroscopic flows: volume $q(x,t)$, speed $u(x,t)$ and density $k(x,t)$ (Barcelò, 2010).

The Fundamental Diagram (FD) is a macroscopic description of traffic states: (i) free flow, and (ii) congested situations. This kind of diagrams is based on field data.

Many FD exist, about 25 according to Gerlough and Huber (1975). The main diagrams are the parabolic fundamental diagram of Greenshield (Greenshields, 1935) where the speed u is a linear decreasing function of

the density k (see Figure 2.2) and the triangular FD LWR-model (Lighthill, Whitham, Richards, (Lighthill and Whitham, 1955; Richards, 1956)) (see Figure 2.3). Experimental studies (Cassidy and Mauch, 2001; Chiabaut et al., 2009; Coifman and Wang, 2005; Windover and Cassidy, 2001) show that the FD is triangular on freeways, and linear in congestion situations for urban areas (Leclercq, 2005).

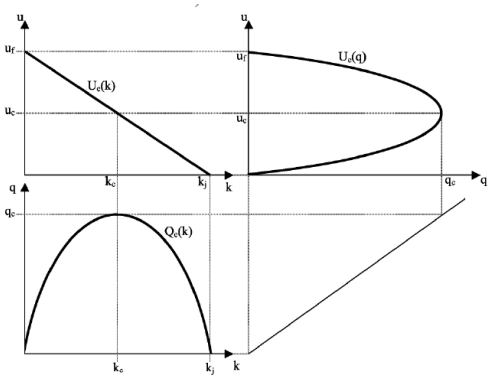

Figure 2.2 – Greenshield Fundamental Diagram

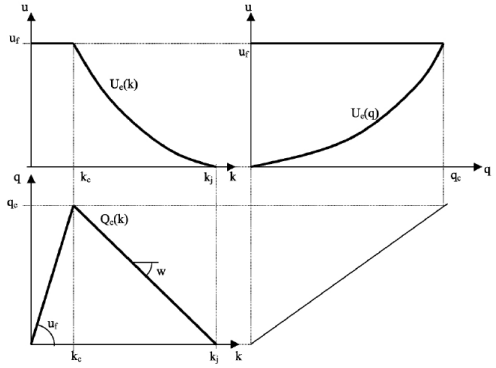

Figure 2.3 – Triangular Fundamental Diagram

2.1.2 Microscopic scale

From the microscopic point of view, the simulation is done thanks to moving particles that interact with each other in order to maintain safe position in the traffic stream (Ni, 2011).

The microscopic traffic models are used for a wide range of applications in network design, analysis of transportation problems, traffic management strategies and the evaluation of ITS.

Microscopic traffic models are especially recommended to the study of heterogeneous traffic stream consisting of different and individual types of driver-vehicle units or agents (Kesting et al., 2008).

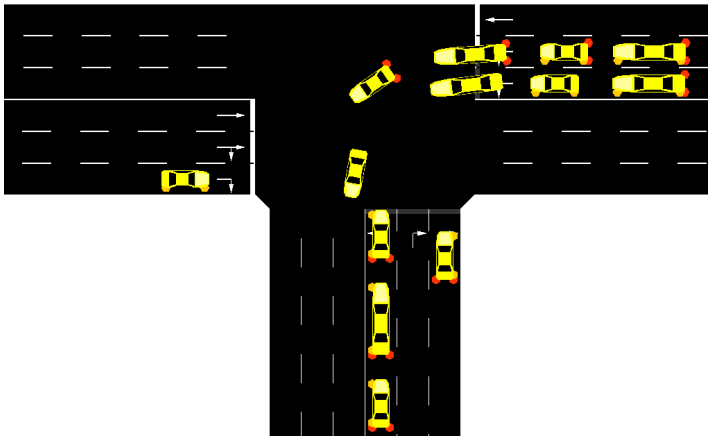

Figure 2.4 – Example of microscopic network

This scale of simulation is based on the description of the motion of each individual vehicle composing the traffic stream (Barcelò, 2010).

Microscopic models describe information about the behaviour of each single vehicle. For this reason, they can be applied to narrow-range transportation systems, however, with a much higher level of details (Maciejewski, 2010). The dynamical aspects of these traffic flow models are formed by the underlying interactions between the drivers of the vehicles. This is largely determined by the behaviour of each driver, as well as the physical characteristics of the vehicles (Maerivoet and De Moor, 2005).

Microscopic models can continuously or discretely predict the state of individual vehicles (Boxill and Yu, 2000). Classically, microscopic models have two main goals:

- Describing the behaviour of a vehicle when following a vehicle: **car-following models**,

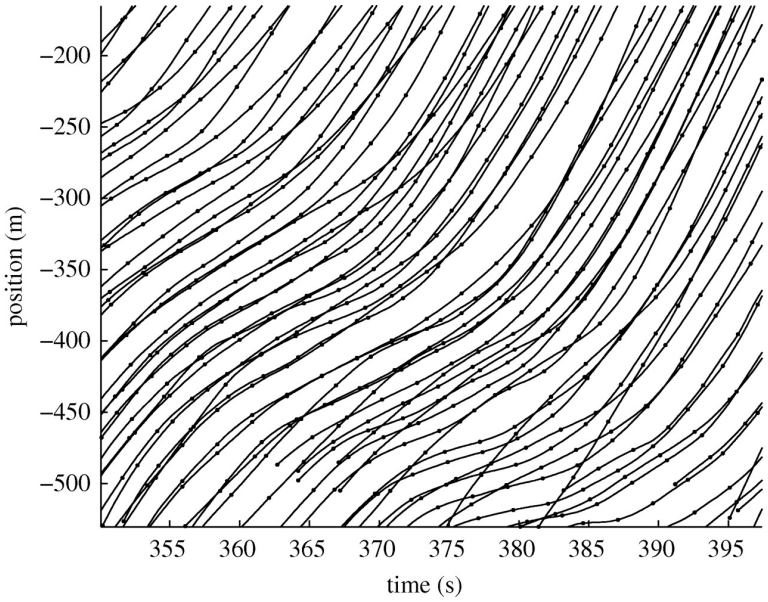

Figure 2.5 – Microscopic state diagram (Hoogendoorn and Hoogendoorn, 2010)

- Describing the behaviour of a vehicle when changing lane: **lane-changing and gap acceptance models**.

Within traffic flow community, microscopic models treat driver-vehicle unit as massless particles with personalities. The behaviour of these particles is governed by car-following models in the longitudinal direction and discrete choice (lane-changing and gap acceptance) models in the lateral direction (Ni, 2011).

The trajectory of each vehicle can be tracked in the longitudinal direction $x_i(t)$ with the lateral direction being discretized per lanes $LN_i(t)$. Hence, $(x_i(t), LN_i(t))$ is the state variable that describes the state and dynamics of traffic flow at the microscopic level. The corresponding state diagram (Figure 2.5) consists of vehicle trajectories in a two-dimensional domain (x,t) (Hoogendoorn and Hoogendoorn, 2010).

There are several classification of microscopic models, one of which is described in (Kesting et al., 2008):

- **Time-continuous models**:
  They are formulated as ordinary or delay-differential equations and consequently, space and time are treated as continuous variables.
  Car-following models are the most prominent examples of this approach. In general, these models are deterministic but stochastic variables can be added in a natural way.
- **Cellular Automata (CA)**:
  These models use integer variable to describe the dynamic state of the system. Time is discretized and the road is divided into cells which can be either occupied by a vehicle or empty.
  Compared to time-continuous models, they lack accuracy due to their simplicity, however, this is a benefit for simulation of large road network.
  The first CA model was proposed by Nagel and Schreckenberg (1992).
- **Iterated coupled maps**:
  These models are between CA and time-continuous models: the update time is considered as an explicit model parameter rather than an auxiliary parameter needed for numerical integration. Consequently, the time is discretized while the spatial coordinate remains continuous.
  The most popular examples are the Gipps' model and the Newell's model, which are typically associated with car-following models as well.

Another classification of microscopic models of traffic could be done based on the following logic of the model (Aghabayk et al., 2015; Brackstone and McDonald, 1999; Kessels, 2019; Treiber and Kesting, 2013a,b; Van Wageningen-Kessels, 2013). This classification provides 7 categories that are described in Table 2.1:

	Principle	**Authors**	**Software**
Stimulus-response model	The response of a driver is proportional to the stimulus he perceives (relative speed)	Chandler et al. (1958)	DYNASIM SITRA
Safe distance model	The driver of a following vehicle chooses his speed based on a safe following distance	Pipes (1953) Gipps (1981) Krauß (1998)	AIMSUN CARSIM SUMO MOVSIM
Psychophysical model	It considers psychophysical aspects of driving behaviour, implying the use of perceptual thresholds	Wiedemann and Reiter (1992); Wiedemann (1974) Leutzbach and Wiedemann (1986) Fritzsche (1994)	PTV VISSIM SUMO
Cell based model	The road is divided into cells which have two possible states: empty or not	Nagel and Schreckenberg (1992)	MOVSIM
Optimal velocity model	The following driver response is proportional to the difference between his optimum speed and his actual speed	Bando et al. (1995)	MOVSIM
Intelligent driver model	The acceleration is a continuous function which takes into account distance to the leader, actual speed and relative speed	Treiber et al. (2000)	SUMO MOVSIM
Trajectory based model	A driver will maintain a minimum space and time gap between him and his leader	Newell (2002)	Symuvia

Table 2.1 – Car-following models

2.2 Heavy vehicles modelling in literature

The study of car-following models has already a long history but very few studies focus specifically on HDV behaviour (Aghabayk et al., 2015; Nodine et al., 2017), although trucks reactions to traffic are different from those of cars as shown in (Aghabayk et al., 2012, 2016; Sarvi and Ejtemai, 2011). For the trucks trajectory, we can observe that spacing would be larger, acceleration capabilities are smaller and speed profiles are more complex due to more complex engine chains. Inertia also modifies the driving behaviour of HDV due to the important weights of vehicles. The main studies taking into account truck-following behaviour focus on the differences in following reactions (Aghabayk et al., 2012, 2016; Nodine et al., 2017; Sarvi, 2011) depending of the Follower and Leader type: passenger car or HDV. Other existing studies which consider truck-following behaviour describe the influence of heterogeneous traffic flow on traffic instabilities (Chen et al., 2016; Liu et al., 2016; Yang et al., 2014).

To model the heterogeneity of real road traffic, several modified car-following models were previously developed. Previous studies about truck-following rule were based either on specific mode formulation (Aghabayk et al., 2016; Liu et al., 2016), on quite complex existing car-following models (Aghabayk et al., 2016) or on new developed models based on the local linear tree approach, LOLIMOT (Aghabayk, 2013; Aghabayk et al., 2013). All of these studies used data from the Next Generation SIMulation (NGSIM) project. The trajectories used were collected on the Hollywood freeway (U.S.101) and on the Berkeley Highway (I-80) in California. They were, respectively, 640 and 503m long. In this thesis we want to assess if an existing and usual car-following model, with dedicated parameter settings can accurately reproduce trucks behaviour under different applications: urban, mid-urban, regional and ring road. The data used for this study come from measures done in Lyon (France) and will be detailed in section 2.4 (p.17) and in Chapter 3 (p.33).

The following section (section 2.3) will describe the four car-following models that will be studied in this

thesis. These models have been chosen because they represent different levels of complexity, and different following logic. The characteristics of these models are presented in Table 2.2.

Microscopic model	**Category**	**Number of parameters to calibrate**	**Output of the model**	**Software**
Gipps' model (Gipps, 1981)	Iterated-Coupled map Safe distance model	6	Speed	SUMO DLR
IIDM (Treiber and Kesting, 2013a)	Time-continuous model Intelligent Driver model	5	Acceleration	MOVSIM
Newell's model (Newell, 2002)	Iterated-Coupled map Trajectory based model	2	Position	Symuvia
Wiedemann's model (Wiedemann, 1974) (Wiedemann and Reiter, 1992)	Time-continuous model Psychophysical model	9 (after simplification)	Acceleration	PTV VISSIM

Table 2.2 – Characteristics of the four car-following models studied

2.3 Description of studied car-following models

2.3.1 Gipps' model

Model

Gipps' model is part of the safe distance models category: the driver of the following vehicle chooses his speed based on a safe following distance to avoid possible collisions with the leader vehicle (Kometani and Sasaki, 1959). This type of models does not try to reproduce a following behaviour but to transcribe the trajectory of a vehicle according to a minimum safe distance.

Gipps' model was first introduced in Gipps (1981). The empirical model developed by Gipps consists of two components: acceleration and deceleration. The first represents the intention of a driver to achieve a certain desired speed, while the second reproduces the limitations imposed by the preceding vehicle when trying to drive at the desired speed. The output of Gipps' model is the speed. The expression of the velocity of this model is given by eq.((2.1)), and comes from Wilson (2001).

$$\begin{aligned} \dot{x}_n(t+T) &= min\left\{ \begin{array}{l} \dot{x}_n^a(t+T) \\ \dot{x}_n^d(t+T)) \end{array} \right\} \\ &= min\left\{ \begin{array}{l} \dot{x}_n(t)+2.5a_nT\left(1-\frac{\dot{x}_n(t)}{V_n}\right)\sqrt{0.025+\frac{\dot{x}_n(t)}{V_n}}; \\ b_n\left(\frac{\tau_n}{2}+\theta\right)+\sqrt{b_n^2\left(\frac{\tau_n}{2}+\theta\right)^2-b_n\left[2(x_{n-1}(t)-x_n(t)-S_{n-1})-\dot{x}_n(t)T-\frac{\dot{x}_{n-1}(t)^2}{\hat{b}_{n-1}}\right]} \end{array} \right\} \end{aligned} \tag{2.1}$$

On eq.((2.1)), a_n is the maximum acceleration rate of the Follower, $S_{n-1} = L_{n-1} + SafetyMargin$ represents the length of the Leader vehicle including a minimum safe distance, T is the response time of the Follower, V_n is the maximum desired speed, b_n is the maximum braking rate of the Follower and $\hat{b}_{n-1}$ is the assumed braking rate of the Leader. These 6 parameters have to be calibrated.

Gipps' model includes also a safety margin time θ (Ciuffo et al., 2012; Gipps, 1981; Wilson, 2001). This parameter represents the ability of a driver to always stop safely if he begins to brake at $\tau_n + \theta$ after a change in the leader's behaviour. As demonstrated by Gipps (1981), a good value for θ to ensure safety is $\frac{\tau_n}{2}$.

Stability

Besides, the Gipps' car-following model has to fulfill two constraints to keep feasible values of speeds during simulation. The first one is a feasible constraint on the initial state (Punzo et al., 2012) that ensures that in case of emergency stop, the follower will stop safely at the beginning of the simulation. It is represented by

eq.((2.2)).

$$b_n\left(\frac{\tau_n}{2}+\theta\right)^2+b_n\left(2(x_{n-1}(0)-x_n(0)-S_{n-1})-\tau_n v_n(0)+\frac{v_{n-1(0)^2}}{\hat{h}_{n-1}}\right)\geq 0 \tag{2.2}$$

The second constraint (eq.((2.3))) applied to Gipps' model is a stability constraint demonstrated in (Wilson, 2001). This constraint ensures that the speed has a unique value at equilibrium and it takes place in the case where $\hat{b}_{n-1} < b_n$.

$$V_n^{des} \leq \frac{\tau_n+\theta}{\frac{1}{\hat{b}_{n-1}}-\frac{1}{b_n}} \tag{2.3}$$

2.3.2 IIDM

Model

The IIDM (Treiber and Kesting, 2013a) is as its name suggests an improved model of the Intelligent Driver Model (IDM) proposed in (Treiber et al., 2000). The direct output of this model is the acceleration of the current step depending of the current speed, relative speed and spacing between the two vehicles. The IIDM is defined as follows (eq.((2.4))):

$$\ddot{x}_n(t)=\begin{cases} a_n.(1-z(s,v,\Delta v)^2) & \text{if } \dot{x}_n(t)\leq v_0 \text{ and } z(s,v,\Delta v)\geq 1 \\ a_{free}(t).\left(1-z(s,v,\Delta v)^{\frac{2a_n}{a_{free}(t)}}\right) & \text{if } \dot{x}_n(t)\leq v_0 \text{ and } z(s,v,\Delta v)<1 \\ a_{free}(t)+a_n.(1-z(s,v,\Delta v)^2) & \text{if } \dot{x}_n(t)>v_0 \text{ and } z(s,v,\Delta v)\geq 1 \\ a_{free} & \text{if } \dot{x}_n(t)>v_0 \text{ and } z(s,v,\Delta v)<1 \end{cases} \tag{2.4}$$

With:

- $z(s,v,\Delta v)=\dfrac{s^*(v,\Delta v)}{s(t)}=\dfrac{s_0+v_n(t).T+v_n(t).\left(\frac{v_{n-1}(t)-v_n(t)}{2\sqrt{ab}}\right)}{x_{n-1}(t)-x_n(t)}$

- $a_{free}(t)=\begin{cases} a_n\left(1-\left(\frac{v_n(t)}{v_0}\right)^{\delta}\right) & \texttt{if } v_n(t)\leq v_0 \\ -b\left(1-\left(\frac{v_0}{v_n(t)}\right)^{\frac{a_n\delta}{b}}\right) & \texttt{if } v_n(t)>v_0 \end{cases}$

In the IIDM, five parameters have to be calibrated. a_n is the maximum speed of the Follower, v_0 is its desired speed, $s0$ is the minimum bumper-to-bumper gap between the two vehicles, T represents the bumper-to-bumper time gap and b_n is the comfortable braking rate of the follower.

Stability

Just like the Gipps' car-following model, the IIDM is subject to stability constraint (Treiber and Kesting, 2013a). Its stability constraint is the same as that of the IDM for congested situations and it is defined in eq.(2.5).

$$a_n \geq \frac{s_0}{T^2} \tag{2.5}$$

2.3.3 Newell's model

The Newell's car-following model (Newell, 2002) differs from preceding car-following models presented above. The Newell's model is far simpler and uses fewer parameters (eq.(2.6)).

The main idea of this model is that a vehicle will maintain a minimum space and time gap between itself and its leader: when the leader changes its velocity, the follower changes also its speed. In this theory, a driver selects its preferred minimum space for each velocity of its leader (assumed to be less than its desired velocity) after reaching its desired spacing, in this way his trajectory looks like that of its leader, with a translation in

time and space. The output of Newell's car-following model is the position at the next time step.

$$\begin{cases} x_n(t) &= min\left(x_n^F(t); x_n^C(t)\right) & \\ x_n^F(t) &= x_n(t-\Delta t) + v_f.\Delta t & \text{vehicle } n \text{ under free flow conditions} \\ x_n^C(t) &= x_{n-1}(t-\Delta t) - \rho & \text{vehicle } n \text{ under congested conditions} \end{cases} \tag{2.6}$$

According to Leclercq (2009) and Daganzo (2005), Newell's model (eq.(2.6)) corresponds to the exact solution of the LWR model (triangular FD).

To solve the Lagrangian expression of the LWR model, Leclercq (2007); Leclercq et al. (2007) proposed to use the Godunov scheme. When the FD is triangular, the Godunov scheme can be expressed as eq.(2.7):

$$x_n(t) = min\begin{pmatrix} x_n(t-\Delta t) + u\Delta t \\ (1-\alpha)x_n(t-\Delta t) + \alpha x_{n-\Delta n}(t-\Delta t) - |w|\Delta t \end{pmatrix} \tag{2.7}$$

With $\alpha = \dfrac{|w|\Delta t}{\rho \Delta n}$, u the desired speed in free flow situations, w the wave speed and ρ the minimum safety spacing desired by the Follower between itself and its Leader in congestion situations. The variables of this model are the position of the follower $x_n(t)$, the position of the leader $x_{n-\Delta n}$ and the number of leading vehicles considered, Δn.

This expression is exact in Lagrangian coordinates when the Courant-Friedrihs-Lewy condition is satisfied (Leclercq, 2009), that implies $\alpha = 1$. Under this condition, eq.(2.7) can be simplified (eq.(2.8)):

$$x_n(t) = min\begin{pmatrix} x_n(t-\Delta t) + u\Delta t \\ x_{n-\Delta n}(t-\Delta t) - \rho \Delta n \end{pmatrix} \tag{2.8}$$

The previous expression (eq.(2.8)) is strictly equivalent to the definition of the Newell's model in eq.(2.6).

2.3.4 Wiedemann's model

The Wiedemann's model was first introduced in Wiedemann (1974). It is said to be a psychophysical model because it considers psychophysical aspects of driving behaviour and several perceptual thresholds (Figure 2.6) such that, only when they are reached, the driver of a following vehicle reacts to the vehicle in front of him. Perceptual thresholds depend on the front to rear distance and the speed difference between the Follower and the Leader. This model is based on two main assumptions (Van Wageningen-Kessels, 2013):

(i) At large spacing, the driver of a following vehicle is not influenced by the size of the speed difference, and,
(ii) At small spacing, there are combinations of relative speeds and distance headways for which there is, as in (i), no response from the driver of a following vehicle because the relative motion is too small.

The Wiedemann's microscopic traffic model supposes the existence of four driving situations (Wiedemann and Reiter, 1992; Wiedemann, 1974): uninfluenced driving, closing process, following process and emergency braking. The output of this model is the acceleration.

An example of a trajectory (bold blue line) is presented, with the perceptual thresholds (in black), in Figure 2.6. The vehicle is driving with a speed equal to v_n, and it follows a vehicle with the speed $v_{n-1} < v_n$ at the constant relative speed Δv, upon reaching the threshold SDV, the driver reacts by reducing his speed. Once the threshold SDX is reached, the diver is in the following situation and he tries to decelerate in order to reach a point at which $\Delta v = 0$. Because a driver cannot to do it accurately (he cannot to perceive small differences or control his speed accurately), he will reach the opposite threshold $OPDV$, and then accelerate and again try to achieve the desired spacing, and so on.

Thresholds definition and simplification of the model

In this manuscript, the original thresholds presented in Wiedemann and Reiter (1992) are indicated with the index $W74$ whereas the simplified thresholds will be named without any index.

The thresholds used in Wiedemann's model are presented on Figure 2.6. The horizontal axis represents the speed difference between the Leader and the Follower, defined as $\Delta V = v_n - v_{n-1}$, $\Delta V > 0$ corresponds to a

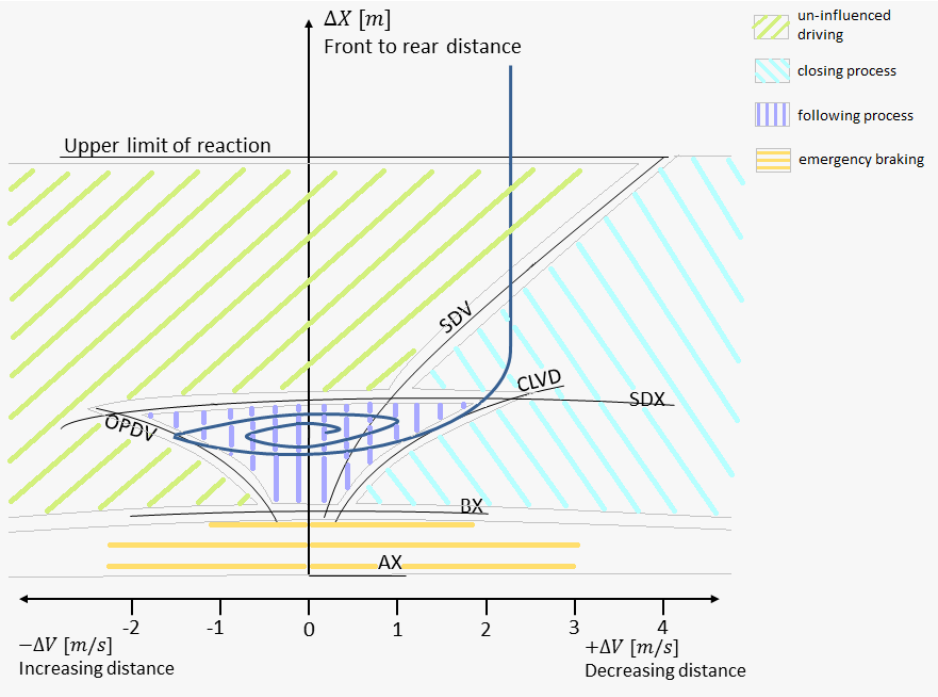

Figure 2.6 – Thresholds of the Wiedemann car-following model (Wiedemann and Reiter, 1992)

closing process. The vertical axis is the front bumper to rear bumper distance defined as $\Delta X = x_{n-1} - L_{n-1} - x_n$, with L_{n-1}, the length of the leader vehicle.

The thresholds presented on Figure 2.6 are detailed below (Wiedemann and Reiter, 1992; Wiedemann, 1974).

AX_{W74} is the desired distance for standing vehicles (front bumper to front bumper distance). It consists of the length of the Leader and the desired front-to-rear distance depending on the safety need of the Follower.

$$AX_{W74} = lL + AXadd + RND1 * AXmult \tag{2.9}$$

$RND1$ is a normally distributed parameter; between 0 and 1 with 0.5 as mean and a standard deviation of 0.15, representing the differences between drivers.

Because we work with trajectories of only one driver, we will consider $RND1$ (and all other random parameters) equal to 1. This leads to a simplified expression of AX_{W74} (eq.(2.10)), named AX in the rest of the thesis.

$$AX = lL + AXadd \tag{2.10}$$

ABX_{W74} is the desired minimum following distance at low speed differences. It is defined by:

$$ABX_{W74} = AX_{W74} + BX_{W74} = AX_{W74} + (BXadd + BXmult.RND1).\sqrt{min(v_n, v_{n-1})} \tag{2.11}$$

Considering the simplification explained above, we have:

$$ABX = AX + BX.\sqrt{min(v_n, v_{n-1})} \tag{2.12}$$

With $BX = BXadd + BXmult$.

SDV_{W74} is the perception threshold of speed difference at long distances. When this limit is reached the driver is conscious that he is closing on another vehicle. This threshold is defined by:

$$SDV_{W74} = \left(\frac{\Delta X - AX_{W74}}{CX_{W74}}\right)^2 = \left(\frac{\Delta X - AX_{W74}}{CXconst.(CXadd + CXmult.(RND1 + RND2))}\right)^2 \tag{2.13}$$

$RND2$ is defined in the same manner as $RND1$. The simplification of the previous equation leads to:

$$SDV = \left(\frac{\Delta X - AX}{CX}\right)^2 \tag{2.14}$$

With $CX = CXconst.(CXadd + CXmult)$.
According to Wiedemann and Reiter (1992), CX should represent the range between 25 and 75.

SDX_{W74} is the threshold representing a growing distance during the following process. It is defined by the following equation:

$$SDX_{W74} = AX_{W74} + EX_{W74}.BX_{W74} = AX_{W74} + (EXadd + EXmult.(NRND - RND2)).BX_{W74} \tag{2.15}$$

$NRND$ has the same range of variation than $RND1$ and $RND2$, and it is driver independent. Moreover, to simplify, it is considered to be equal to 1. The simplified equation of SDX is represented by eq.(2.16).

$$SDX = AX + EX.BX \tag{2.16}$$

With $EX = EXadd$.

$CLDV_{W74}$ is used to recognize small speed differences, at short and decreasing distances.

$$CLDV_{W74} = SDV_{W74}.EX_{W74}^2 \tag{2.17}$$

The simplification of the equations leads to $CLDV = SDV.EX^2$.

$OPDV_{W74}$ is used to recognize small speed difference, at short and increasing distances.

$$OPDV_{W74} = CLDV_{W74}.(-OPDVadd - OPDVmult.NRND) \tag{2.18}$$

Using the fact that $NRND = 1$, we obtain the following simplified equation:

$$OPDV = -CLDV.OPDVadd \tag{2.19}$$

According to measurements presented in Wiedemann and Reiter (1992), $OPDV$ used to be about 1 to 3 times higher than $CLDV$.

Another threshold is defined and proposes a value of $150m$ for the upper limit of reaction, i.e. the spacing beyond which the Follower does not take into account the vehicle in front of it.

The thresholds described above define 4 driving situations which are explained in the next paragraphs.

Driving situations

The **uninfluenced situation** is described by the fact that the driver is driving at his desired speed or tries to reach this desired speed. The oscillations around his desired speed are modeled using acceleration $BNULL$ with positive and negative speed. Until the desired speed is reached, the driver will accelerate using maximum acceleration value. For heavy vehicle, the maximum acceleration is defined as follow in Wiedemann and Reiter (1992):

$$\begin{aligned} BMAX = min(&2.5, \\ &(-BMAXadd + BMAXmult * KWperTo).exp((-BMAXVadd + BMAXVmult.KWperTo).V)) \end{aligned} \tag{2.20}$$

Because we focus on the following process in this study, this expression is simplified by considering $BMAX$ equal to the minimum between $2.5m/s$ and the maximum value of acceleration encountered during the cycle.

The **closing process** is defined by a deceleration, the driver tries to reduce his own speed to the speed of the leader, always keeping a spacing longer than ABX. This deceleration is defined by eq. (2.21).

$$B_n = 0.5 * \frac{\Delta V^2}{ABX - \Delta X} + B_{n-1} \tag{2.21}$$

$BMIN$ is defined as $BMIN = -BMINadd - BMINmult * RND3 + BMINVmult * V$, the simplification leads to $BMIN = -BMINadd + BMINVmult * V$.

The deceleration applied during closing process is the maximum value between deceleration desired, B_n and deceleration capacity of the vehicle $BMIN$.

During the **following process** the driver follows the leader at quite the same speed and tries to keep acceleration low. This is represented by the lowest value of acceleration $BNULL$ which is used with positive or negative sign. The sign of $BNULL$ is kept until ΔV reaches $CLDV$ or $OPDV$, or until ΔX reaches SDX or ABX. $BNULL$ has a mean value of $0.2m/s$ and its expression is:

$$BNULL = BNULLmult.(RND4 + NRND) \tag{2.22}$$

As in the previous paragraphs, the random parameters are not considered and so $BNULL$ is considered as a constant.

The **emergency braking** occurs when the spacing ΔX is lower than the threshold ABX.
If the spacing becomes lower than AX, a collision occurs between the Leader and the Follower. The expression of the deceleration in emergency mode is presented in equation (2.23).

$$B_n = 0.5.\frac{\Delta X^2}{AX - \Delta X} + B_{n-1} + BMIN.\frac{ABX - \Delta X}{BX} \tag{2.23}$$

2.4 Setup of a trajectories database from measurements

The definition of the data used for the car-following models calibration takes an important place in calibration studies. Trajectories needed for calibration can come from different sources: probe vehicles, video-based trajectory data or driving simulation (Thiemann et al., 2008; Toledo et al., 2007; Vieira da Rocha et al., 2015). This section presents the reconstruction methods employed to compute the entire trajectories from measured speed. The data on which the car-following models are calibrated is presented more in details in Chapter 3, section 3.1.1 (p.34).

Several studies have already been done on the influence of the method used to reconstruct the trajectories. Ossen and Hoogendoorn (2008b) verify the impacts of errors on vehicles movement on car-following models calibration. It has been shown that measurements errors lead to considerable bias in calibration results. Moreover, the way trajectories are derived from measurement data can have an influence on platoon consistency (Punzo et al., 2005) or internal consistency (Toledo et al., 2007). The platoon consistency criterion verifies whether trajectories of following vehicles are consistent with regard to space travelled. The internal consistency implies that the differentiation process must preserve the basic equations of motion, that means that the estimated speeds and accelerations after integration must return the measured travelled space. An overview of existing methods and studies for trajectories reconstruction is proposed in Punzo et al. (2011). These studies mainly focus on which smoothing method to use or in which order to apply smoothing and derivation of the data, but do not really consider derivation schemes.

The methods tested here differ since the order smoothing and derivation methods are applied: we want to know if it is necessary to smooth speed and acceleration or if smoothing one of them is enough. Moreover, they differ in the derivation scheme applied (explicit, implicit, or trapezoidal). The methods used are presented in the following paragraphs.

First, the position of the Follower is computed from measured speed and smoothed measured speed (moving average, $1.5s$). The integration schemes used are Euler Explicit (eq.(2.24)), Euler Implicit (eq.(2.25)) and Midpoint method (or Trapezoidal rule) (eq.(2.26)). From this first step, six position vectors are available for each cycle (Figure 2.7).

$$x(t + \Delta t) = x(t) + \dot{x}(t).\Delta t \tag{2.24}$$

$$x(t + \Delta t) = x(t) + \dot{x}(t + \Delta t).\Delta t \tag{2.25}$$

$$x(t + \Delta t) = x(t) + \frac{\dot{x}(t) + \dot{x}(t + \Delta t)}{2}.\Delta t \tag{2.26}$$

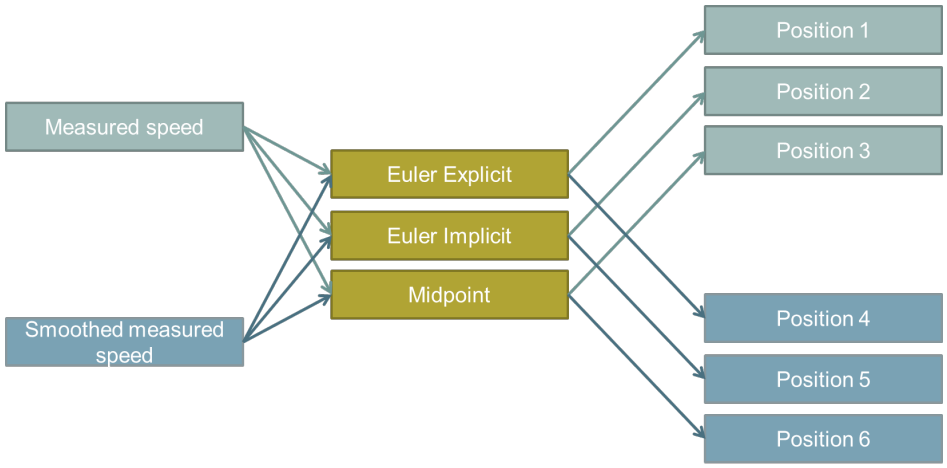

Figure 2.7 – Construction of the six sets of position

Then, the position of the Leader is easily computed by adding the spacing and the length of the Leader vehicle. Since positions of the two vehicles are known, one can reconstruct from those vectors their speed and their acceleration.

Three methods have been defined to derive data:

- Method (1): Direct derivation of the data, with the time step of the measure ($0.1s$)
- Method (2): Smoothing of the resulting vector of method (1) with a moving average ($1.5s$ for the speed and $1s$ for the acceleration)
- Method (3): Direct derivation of the data, with time step equal to $1s$ and interpolation with cubic spline to complete the resulting vector.

To compute the Follower's positions and accelerations, we could have directly used the speed measured by the odometer instead of calculating it again from position. But, as we do not have a direct measure of the Leader speed, we could not apply the same method for both vehicles (to obtain a complete couple of trajectories created with the same method). That is why we compute speed from positions even for the Follower. Figure 2.8 illustrates the different methods of trajectories reconstruction. This leads to 54 possible trajectories for each of the 35 cycles, listed on Table 2.3.

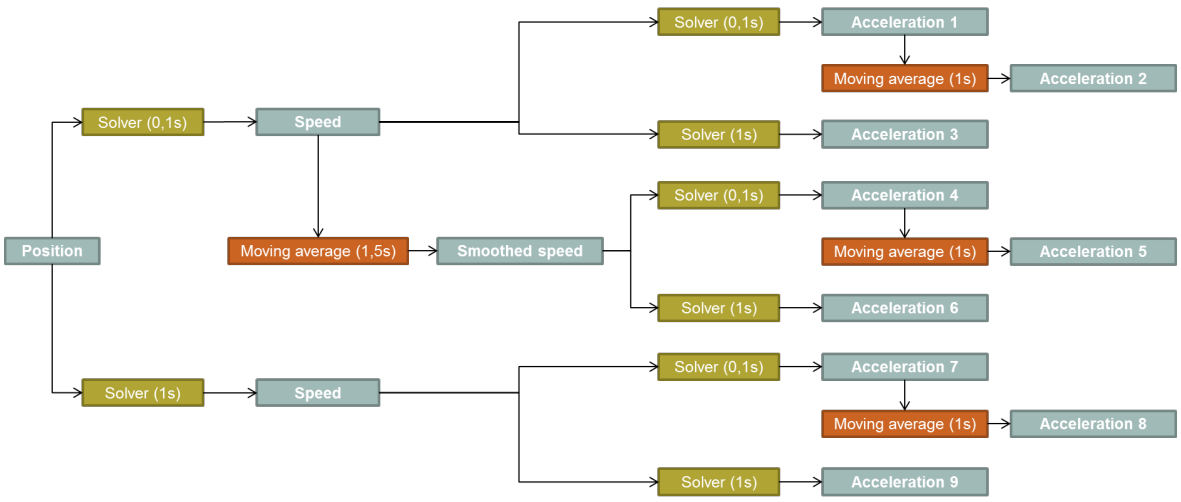

Figure 2.8 – Construction of the speeds and acceleration

Table 2.3 – Reconstruction methods

			Acceleration derived	
Measured speed	Position Euler Explicit	Speed derived 0.1s	0.1s	1
			0.1s, smoothed	2
			1s	3
		Speed derived 0.1s, smoothed	0.1s	4
			0.1s, smoothed	5
			1s	6
		Speed derived 1s	0.1s	7
			0.1s, smoothed	8
			1s	9
	Position Euler Implicit	Speed derived 0.1s	0.1s	10
			0.1s, smoothed	11
			1s	12
		Speed derived 0.1s, smoothed	0.1s	13
			0.1s, smoothed	14
			1s	15
		Speed derived 1s	0.1s	16
			0.1s, smoothed	17
			1s	18
	Position Midpoint	Speed derived 0.1s	0.1s	19
			0.1s, smoothed	20
			1s	21
		Speed derived 0.1s, smoothed	0.1s	22
			0.1s, smoothed	23
			1s	24
		Speed derived 1s	0.1s	25
			0.1s, smoothed	26
			1s	27
Measured speed smoothed	Position Euler Explicit	Speed derived 0.1s	0.1s	28
			0.1s, smoothed	29
			1s	30
		Speed derived 0.1s, smoothed	0.1s	31
			0.1s, smoothed	32
			1s	33
		Speed derived 1s	0.1s	34
			0.1s, smoothed	35
			1s	36
	Position Euler Implicit	Speed derived 0.1s	0.1s	37
			0.1s, smoothed	38
			1s	39
		Speed derived 0.1s, smoothed	0.1s	40
			0.1s, smoothed	41
			1s	42
		Speed derived 1s	0.1s	43
			0.1s, smoothed	44
			1s	45
	Position Midpoint	Speed derived 0.1s	0.1s	46
			0.1s, smoothed	47
			1s	48
		Speed derived 0.1s, smoothed	0.1s	49
			0.1s, smoothed	50
			1s	51
		Speed derived 1s	0.1s	52
			0.1s, smoothed	53
			1s	54

2.5 Calibration methods for car-following models

2.5.1 Problem statement

The calibration of car-following models aims at finding the set of parameters which would minimize the errors between the simulated trajectory of the truck and the measured one. To calibrate the models, several parameters must be defined:

(i) The GoF function, the function which computes the error between measurements and simulation,

(ii) The MoP, the indicator(s) on which the error will be computed,

(iii) The simulation time step, and,

(iv) The solver, the integration/derivation scheme, to link position, speed and acceleration.

2.5.2 Definition of the GoF functions and MoPs

This study will focus on four well-known GoF functions. The influence of the GoF function on calibration results has already be widely studied (see for example Ciuffo and Punzo (2010)). However, here we propose another approach to find a well adapted GoF function for our case study. This approach will focus on the shapes of the GoF functions, it is presented in Chapter 4, section 4.2 (p.48). The studied GoF functions are presented in the following paragraphs. The first one is the Root Mean Squared Error (RMSE) defined by (2.27). This function is widely used to calibrate car-following models: Ciuffo et al. (2012); Duret et al. (2008); Punzo and Simonelli (2005); Punzo et al. (2012); Vieira da Rocha et al. (2015) and Song et al. (2015).

$$RMSE = \sqrt{\frac{1}{N}\sum_i \left(Y_i^{obs} - Y_i^{sim}\right)^2} \tag{2.27}$$

With Y_i^{obs} the observed data, and Y_i^{sim} the simulated data.

The second GoF function is the Root Mean Squared Percentage Error (RMSPE) defined by eq.(2.28) used in Punzo and Simonelli (2005) and Kesting and Treiber (2008b).

$$RMSPE = \sqrt{\frac{1}{N}\sum_i \left(\frac{Y_i^{obs} - Y_i^{sim}}{Y_i^{obs}}\right)^2} \tag{2.28}$$

The third GoF function is more simple than the two previous ones, and it is named Squared Error (SE), presented in eq.(2.29) (Treiber and Kesting, 2013c).

$$SE = \frac{1}{N}\sum_i \left(Y_i^{obs} - Y_i^{sim}\right)^2 \tag{2.29}$$

The last GoF function studied, Theil's inequality coefficient, is more complex than the three others, and it is defined by eq.(2.30). This function is used in Ciuffo et al. (2012); Duret et al. (2008); Kim and Mahmassani (2011); Punzo and Simonelli (2005); Punzo et al. (2012); Vieira da Rocha et al. (2015) and Song et al. (2015).

$$U = \frac{\sqrt{\frac{1}{N}\sum_i \left(Y_i^{obs} - Y_i^{sim}\right)^2}}{\sqrt{\frac{1}{N}\sum_i (Y_i^{obs})^2} + \sqrt{\frac{1}{N}\sum_i (Y_i^{sim})^2}} \tag{2.30}$$

The different studies comparing the calibration of car-following models mainly focus on spacing or speed errors (Kesting and Treiber, 2008a; Kim and Mahmassani, 2011; Ossen and Hoogendoorn, 2008b; Punzo and Simonelli, 2005; Punzo et al., 2012; Ranjitkar et al., 2004). It has been previously shown (Punzo and Montanino, 2016) that it is better to use as MoP the spacing (or the position) instead of the speed when we want to minimize error on both spacing (or position) and speed. However, these studies were done by using a single MoP (Kesting and Treiber, 2008b; Punzo and Montanino, 2016; Punzo and Simonelli, 2005) or combined MoP (Kim and Mahmassani, 2011; Ossen and Hoogendoorn, 2008a), but not using a Multi-Objective (MO) calibration. This solution is investigated in this thesis and four MoP are compared in Chapter 4: the position, the spacing, the speed and the acceleration.

2.5.3 Variation of the simulation time step in calibration process

Some investigations are realized to conclude on the influence of the simulation time step on calibration results. To the author best knowledge, this issue has not been studied a lot so far. Treiber and Kesting (2013c) highlighted that too small a time step ($0.1s$ for example) does not improve calibration results of the IDM and the Optimal Velocity Model (OVM) (Bando et al., 1994).

In this thesis we will study the impact of the use of small or high time steps on errors after calibration between the measured and simulated trajectories, but also the impact on optimal parameters values. The studied simulation time steps are listed below:

- $0.01s$,
- $0.1s$, the measurement time step,
- $0.5s$,
- $1s$.

2.5.4 Variation of the solver in the calibration process

In (Ciuffo et al., 2012) different methods to compute acceleration from speed produced by Gipps car-following model are tested: the Euler explicit scheme (eq.(2.24)) and the approach adopted in the AIMSUN software (System, 2014) where the integration step Δt is a submultiple of the delay τ (up to a minimum of $0.1s$) and the Gipps' model is applied at each simulation step.

Treiber and Kesting (2013b) pointed out that the performances of complex update schemes are generally inferior to simpler lower-order update methods. For example, on single-lane simulations, the Runge Kutta scheme of order 4 is less efficient by a factor of about two compared to a mixed Euler explicit - Midpoint scheme. The integration/derivation scheme is not often studied in calibration of microscopic models studies, this is why this work investigates the influence of the use of different integration/derivation schemes listed below. These schemes will be named solvers in the rest of this thesis.

- The Euler Explicit scheme (eq.(2.24)),
- The Euler Implicit scheme (eq.(2.25)),
- The Midpoint scheme (eq.(2.26)),
- The method proposed by Treiber and Kesting (2013b): the Euler Explicit scheme to link the speed and the acceleration, and the Midpoint scheme to link the speed and the position. It is called Mixed solver in the rest of the thesis,
- Runge-Kutta of order 4.

2.5.5 Particle Swarm Optimization

The method chosen to calibrate car-following models is the Particle Swarm Optimization (PSO). It is a global optimization method like Genetic Algorithms (GA). This method was first introduced by Kennedy and Eberhart (1995). It was first used to describe birds or fish movements.

Description of the algorithm

This algorithm is based on a swarm of particles which represent the values of the variables (stored in vectors) we want to calibrate. At each iteration, the error between the simulation and the measure is computed, and the value of the particles (called 'position') is updated depending on:

(i) the best position in the history of the particle itself (its value which has provided the smallest error), and,

(ii) the best position in the history of the entire swarm (the value which has provided the smallest error in the entire swarm)

The calibration ends when the maximum number of iterations or the accepted error is reached.

Seven parameters have to be defined for the calibration:

- the number of particles N,
- the upper and lower bounds into which the particles will move,
- the maximum number of iteration max_iter (and/or the minimum error to reach),
- the minimum error to reach min_error (and/or the maximum number of iterations),
- c_1 and c_2 which are used to update the particles positions,
- the GoF function,
- the MoP.

Initialization

At the beginning of the simulation, a set of N particles is defined randomly between the upper and lower bounds defined: each particle is given a position x^i, and a speed v^i. The position corresponds to the value of the particle. The speed at the initialization phase is defined randomly and will be used to update the position of the particles.

If there are conditions on the particles values (stability, feasibility), the initialization is done until every particle fulfils the conditions(s).

Then, simulations are run for each particles and the errors between the simulation and the reference are computed thanks to the GoF function. The errors for each particle are saved, and the best position of each particle (the initial state at Initialization phase), called p^i with $i \in [1,N]$; and the global best position in the entire swarm, g are computed. Then, the position of the particles is updated according to eq.(2.31) and eq.(2.32).

$$x^i(k+1) = x^i(k) + v^i(k+1) \tag{2.31}$$

$$v^i(k+1) = K * (v^i(k) + r_1 c_1 (p^i - x^i) + r_2 c_2 (g - x^i)), i \in [1,N] \text{ and } k \in [1, max\_iter - 1] \tag{2.32}$$

With, $K = \dfrac{2}{|2 - \varphi - \sqrt{\varphi^2 - 4\varphi}|}$ and $\varphi = c_1 + c_2$.

r_1 and r_2 are random numbers between 0 and 1, they are used to add a little randomness in the movement of the particles and to ensure that they do not get stuck in a local minimum. For convergence, φ must be greater than 4 (Eberhart and Shi, 2000), we chose $c_1 = c_2 = 2.05$.

Iterations

Then the following process is run for each particles:

1. (if necessary) we check if the conditions are satisfied, if not the error for the particle is set to Infinity and they will not be used for simulation, if conditions are satisfied, the following steps are done,
2. Simulations are run for the (kept) particles,
3. The errors between simulated and reference values are computed,
4. The global (g) and personal (p^i with $i \in [1,N]$) best positions are computed and saved,
5. The particle positions are updated thanks to equations (2.31) and (2.32),
6. Return to step 1. while the maximum number of iterations or the minimum accepted error is not reached.

The algorithm is presented on Figure (2.9).

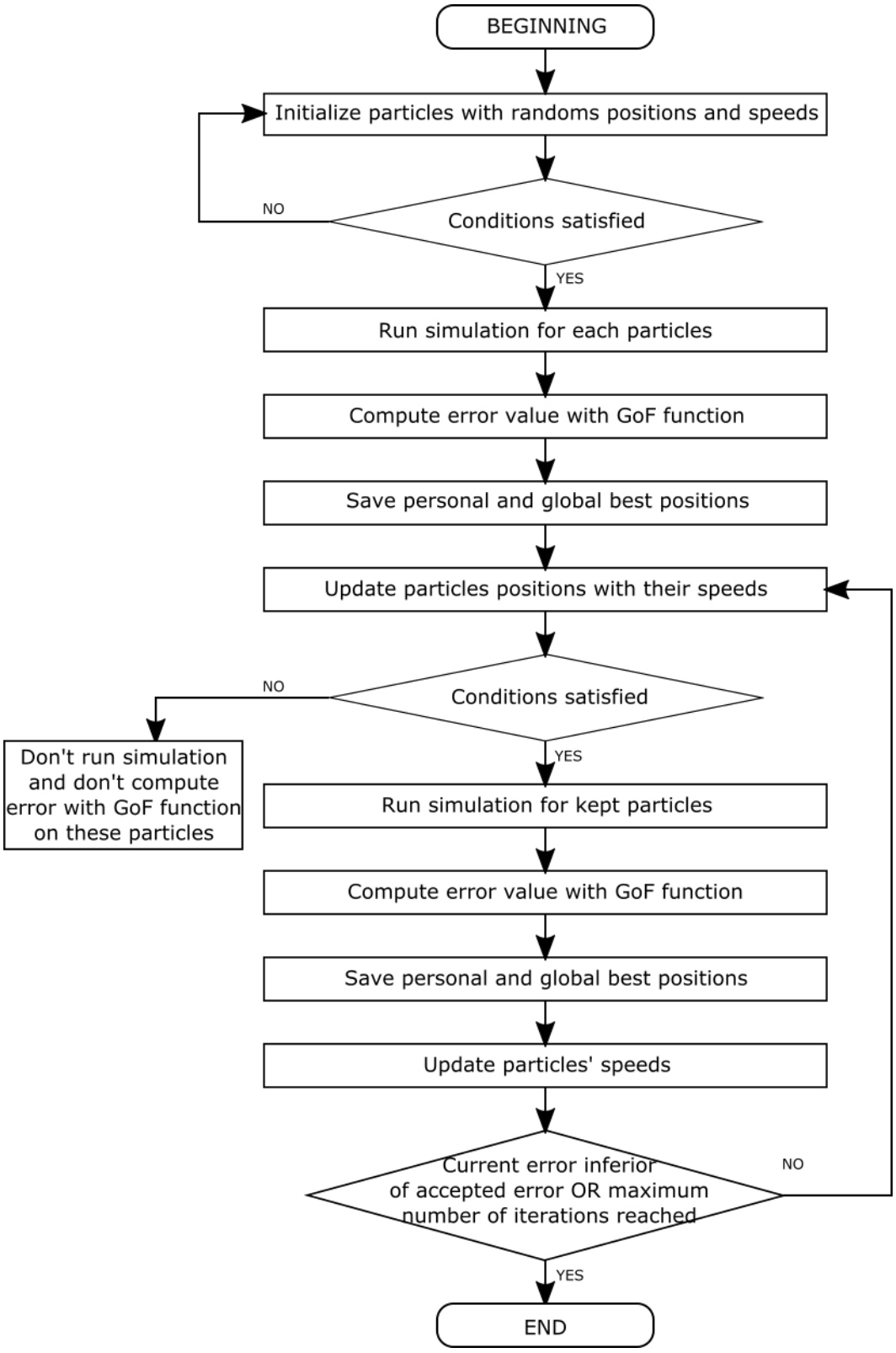

Figure 2.9 – PSO algorithm

Multi-Objective Particle Swarm Optimization

The Multi-Objective Particle Swarm Optimization (MOPSO) is used to minimize the error on several MoP at the same time. In this algorithm, an archive is created containing the particles which dominates (in Pareto sense) the swarm of particles. Figure 2.10 shows an example of a Pareto front where the blue points are the positions of the swarm (for all the iterations) and the red points correspond to the dominating particles called Pareto front.

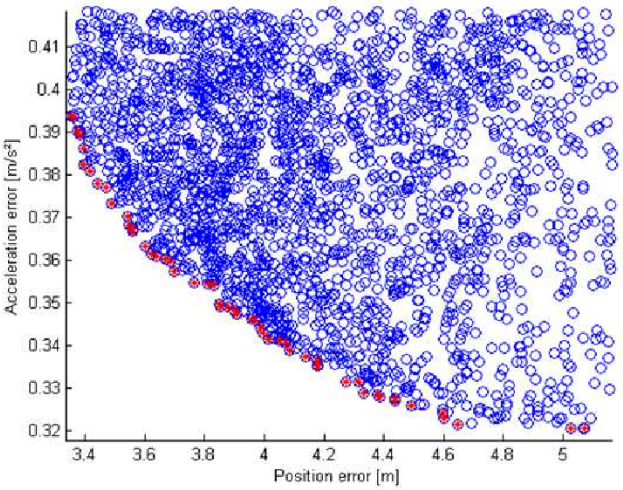

Figure 2.10 – Example of a Pareto front

Dominance definition in Pareto sense

The MOPSO is based on the dominance definition of Pareto (Coello Coello and Lechuga, 2002), see Definitions 2.1 and 2.2.

Definition 2.1

$\overrightarrow{x}^* \in \Omega$ is **Pareto Optimal** if $\forall \overrightarrow{x} \in \Omega$ and $I = \{1,..,k\}$, either

$$\forall i \in I,\ f_i(\overrightarrow{x}) = f_i(\overrightarrow{x}^*)$$

or,

$$\exists i \in I,\ f_i(\overrightarrow{x}) > f_i(\overrightarrow{x}^*)$$

Definition 2.2

$\overrightarrow{u} = (u_1,...,u_k)$ is said to **dominate in the sense of Pareto** $\overrightarrow{v} = (v_1,...,v_k)$ ($\overrightarrow{u} \preceq \overrightarrow{v}$) if and only if

$$\forall i \in \{1,..,k\},\ u_i \leq v_i \text{ and } \exists i \in \{1,..,k\},\ u_i < v_i$$

Algorithm

The MOPSO algorithm is defined in Figure 2.11. This algorithm is really close to the PSO algorithm. The main change is on the choice of the value of the global best particle g. For the MO calibration, there is not only one global best particle for the all swarm because there are several objectives to minimize: g in PSO becomes g^i with $i \in [1,N]$ in MOPSO. The choices of the g^i is based on the RANDOM global guides' selection proposed in Alvarez-Benitez et al. (2005):

- if the particle is in the archive containing the dominating particles, its g^i is defined randomly as one of the particle of the dominating archive,
- else, if the particle is not in the archive, its g^i is chosen randomly in the set of the particles dominating it.

The last choice is different from what is proposed in Alvarez-Benitez et al. (2005) in the sense that they only consider as a possible g^i the particles in the archive which dominates the particle for which g^i is computed.

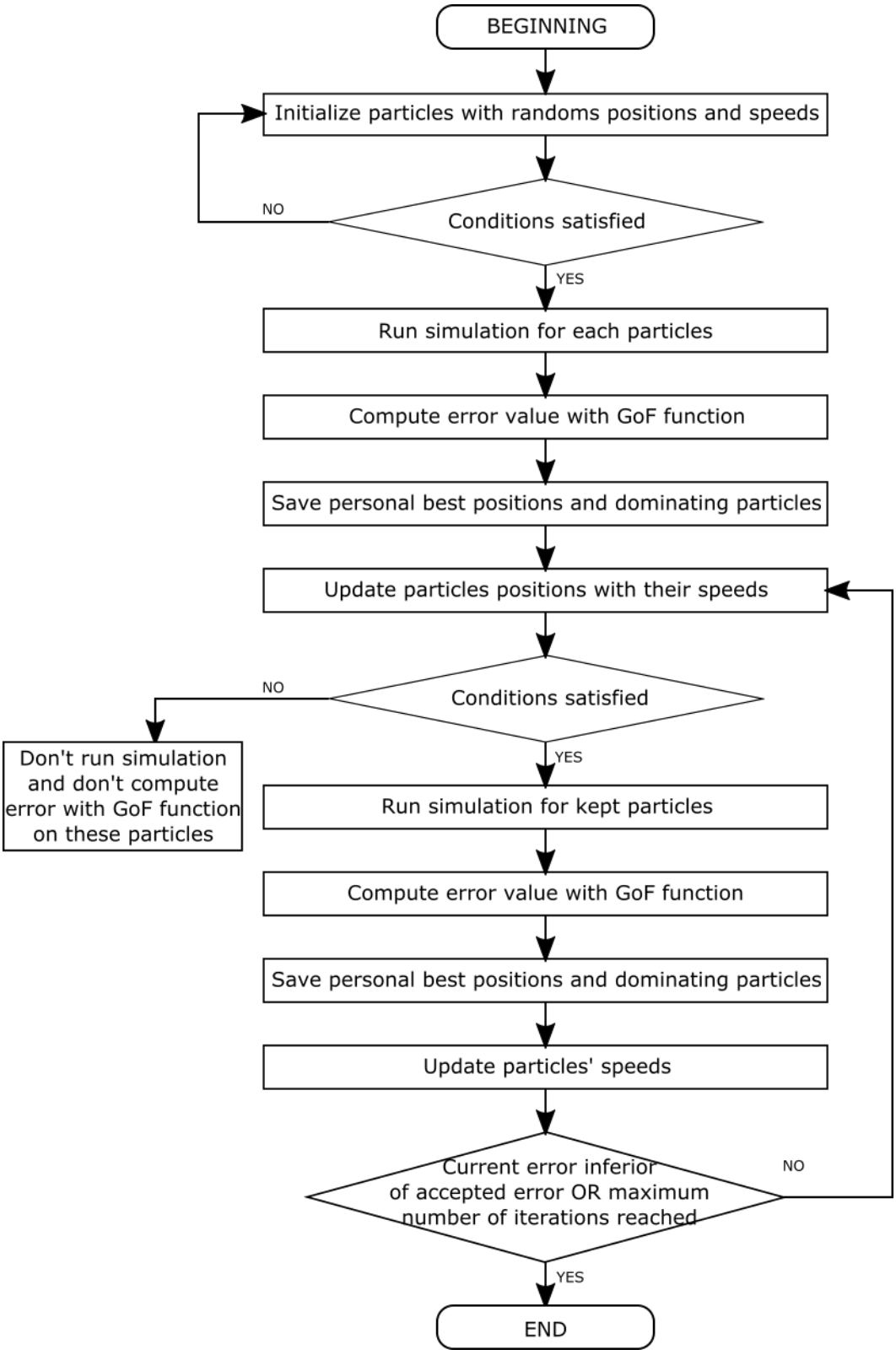

Figure 2.11 – MOPSO algorithm

2.6 Study presentation

This chapter introduced the data and methodology that is applied to calibrate car-following models on truck's trajectories, and to verify the accuracy of these models when computing the vehicle FC. Next chapter (Chapter 3) details the construction of a database of trajectories for the calibration, then Chapter 4 details the definition of an adapted calibration method for each car-following model studied. Finally, Chapter 5 presents the results of the car-following model calibration and their accuracy when using simulated trajectory to estimate the vehicle FC.

2.7 References

Kayvan Aghabayk. *Modelling heavy vehicle car-following in congested traffic conditions*. PhD thesis, Institute of Transport Studies, SDepartment of Civil Engineering, Monash University, 2013. p. 11

Kayvan Aghabayk, Majid Sarvi, and William Young. Understanding the Dynamics of Heavy Vehicle Interactions in Car-Following. *Journal of Transportation Engineering*, 138(12):1468–1475, December 2012. ISSN 0733-947X, 1943-5436. doi: 10.1061/(ASCE)TE.1943-5436.0000463. p. 11

Kayvan Aghabayk, Majid Sarvi, Nafiseh Forouzideh, and William Young. New Car-Following Model Considering Impacts of Multiple Lead Vehicle Types. *Transportation Research Record: Journal of the Transportation Research Board*, 2390:131–137, December 2013. ISSN 0361-1981. doi: 10.3141/2390-14. p. 11

Kayvan Aghabayk, Majid Sarvi, and William Young. A State-of-the-Art Review of Car-Following Models with Particular Considerations of Heavy Vehicles. *Transport Reviews*, 35(1):82–105, January 2015. ISSN 0144-1647, 1464-5327. doi: 10.1080/01441647.2014.997323. p. 11

Kayvan Aghabayk, Majid Sarvi, and William Young. Including heavy vehicles in a car-following model: modelling, calibrating and validating. *Journal of Advanced Transportation*, 50(7):1432–1446, November 2016. ISSN 01976729. doi: 10.1002/atr.1409. [3]. p. 11

Julio E. Alvarez-Benitez, Richard M. Everson, and Jonathan E. Fieldsend. A MOPSO Algorithm Based Exclusively on Pareto Dominance Concepts. In David Hutchison, Takeo Kanade, Josef Kittler, Jon M. Kleinberg, Friedemann Mattern, John C. Mitchell, Moni Naor, Oscar Nierstrasz, C. Pandu Rangan, Bernhard Steffen, Madhu Sudan, Demetri Terzopoulos, Dough Tygar, Moshe Y. Vardi, Gerhard Weikum, Carlos A. Coello Coello, Arturo Hernández Aguirre, and Eckart Zitzler, editors, *Evolutionary Multi-Criterion Optimization*, volume 3410, pages 459–473. Springer Berlin Heidelberg, Berlin, Heidelberg, 2005. ISBN 978-3-540-24983-2 978-3-540-31880-4. doi: 10.1007/978-3-540-31880-4_32. URL http://link.springer.com/10.1007/978-3-540-31880-4_32. p. 25

M. Bando, K. Hasebe, A. Nakayama, A. Shibata, and Y. Sugiyama. Structure stability of congestion in traffic dynamics. *Japan Journal of Industrial and Applied Mathematics*, 11(2):203–223, June 1994. ISSN 0916-7005, 1868-937X. doi: 10.1007/BF03167222. URL http://link.springer.com/10.1007/BF03167222. p. 21

M. Bando, K. Hasebe, A. Nakayama, A. Shibata, and Y. Sugiyama. Dynamical model of traffic congestion and numerical simulation. *Physical Review E*, 51(2):1035–1041, 1995. doi: 10.1103/PhysRevE.51.1035. p. 11

Jaume Barcelò. *Fundamentals of traffic simulations*. Jaume Barcelò, 2010. ISBN 978-1-4419-6141-9. p. 8, 9

Sharon Adams Boxill and Lei Yu. An evaluaytion of traffic simulation models for supporting ITS development. Technical Report SWUTC/00/167602-1, Center for Transportation Training and Research, Texas Southern University, 2000. p. 9

Mark Brackstone and Mike McDonald. Car-following: a historical review. *Transportation Research Part F: Traffic Psychology and Behaviour*, 2(4):181–196, December 1999. ISSN 13698478. doi: 10.1016/S1369-8478(00)00005-X. p. 11

M. J. Cassidy and Michael Mauch. An observed traffic pattern in long freeway queues. *Transportation Research Part A: Policy and Practice*, 35(2):143–156, 2001. ISSN 0965-8564. p. 9

Robert E. Chandler, Robert Herman, and Elliott W. Montroll. Traffic dynamics: Studies in car-following. *Operations Research*, 6(2):165–184, 1958. p. 11

Danjue Chen, Soyoung Ahn, Soohyuk Bang, and David Noyce. Car-Following and Lane-Changing Behavior Involving Heavy Vehicles. *Transportation Research Record: Journal of the Transportation Research Board*, 2561:89–97, January 2016. ISSN 0361-1981. doi: 10.3141/2561-11. [9]. p. 11

N. Chiabaut, C. Buisson, and L. Leclercq. Fundamental Diagram Estimation Through Passing Rate Measurements in Congestion. *IEEE Transactions on Intelligent Transportation Systems*, 10(2):355–359, June 2009. ISSN 1524-9050, 1558-0016. doi: 10.1109/TITS.2009.2018963. p. 9

Biagio Ciuffo, Vincenzo Punzo, and Marcello Montanino. Thirty Years of Gipps' Car-Following Model. *Transportation Research Record: Journal of the Transportation Research Board*, 2315:89–99, December 2012. ISSN 0361-1981. doi: 10.3141/2315-10. p. 12, 20, 21

Biagio Filippo Ciuffo and Vincenzo Punzo. Verification of Traffic Micro-simulation Model Calibration Procedures: Analysis of Goodness-of-Fit Measures. 2010. p. 20

C.A. Coello Coello and M.S. Lechuga. MOPSO: a proposal for multiple objective particle swarm optimization. volume 2, pages 1051–1056. IEEE, 2002. ISBN 978-0-7803-7282-5. doi: 10.1109/CEC.2002.1004388. p. 24

Benjamin A. Coifman and Yun Wang. Average Velocity of Waves Propagating through Congested Freeway Traffic. 2005. ISBN 978-0-08-044680-6. p. 9

Carlos F. Daganzo. A variational formulation of kinematic waves: Solution methods. *Transportation Research Part B: Methodological*, 39(10):934–950, December 2005. ISSN 01912615. doi: 10.1016/j.trb.2004.05.003. p. 14

Aurélien Duret, Christine Buisson, and Nicolas Chiabaut. Estimating individual speed-spacing relationship and assessing ability of Newell's car-following model to reproduce trajectories. In *Transportation Research Record: Journal of the Transportation Research Board*, volume 2088, pages 188–197, Washington, D.C., 2008. doi: 10.3141/2088-20. p. 20

R.C. Eberhart and Y. Shi. Comparing inertia weights and constriction factors in particle swarm optimization. In *Proceedings of the 2000 Congress on Evolutionary Computation. CEC00 (Cat. No.00TH8512)*, volume 1, pages 84–88, La Jolla, CA, USA, 2000. IEEE. ISBN 978-0-7803-6375-5. doi: 10.1109/CEC.2000.870279. p. 22

Hans-Thomas Fritzsche. A Model for Traffic Simulation. *Traffic Engineering & Control*, 35(5):317–321, May 1994. ISSN 0041-0683. p. 11

Daniel L. Gerlough and Matthew J. Huber. *Traffic Flow Theory - A monograph*. Transportation Research Board Special Report 165. H.P. Orland, Washington, D.C., 1975. p. 8

P.G. Gipps. A behavioural car-following model for computer simulation. *Transportation Research Part B: Methodological*, 15(2):105–111, April 1981. ISSN 01912615. doi: 10.1016/0191-2615(81)90037-0. p. 11, 12

B. d Greenshields. A study of traffic capacity. *Proceedings of the 14th Annual Meeting of the Highway Research Board*, 1935:448–477, 1935. ISSN 0096-1027. p. 8

Serge Hoogendoorn and Raymond Hoogendoorn. Calibration of microscopic traffic-flow models using multiple data sources. *Philosophical Transactions of the Royal Society of London A: Mathematical, Physical and Engineering Sciences*, 368(1928):4497–4517, October 2010. ISSN 1364-503X, 1471-2962. doi: 10.1098/rsta.2010.0189. p. xv, 10

J. Kennedy and R. Eberhart. Particle swarm optimization. volume 4, pages 1942–1948. IEEE, 1995. ISBN 978-0-7803-2768-9. doi: 10.1109/ICNN.1995.488968. p. 21

Femke Kessels. *Traffic Flow Modelling: Introduction to Traffic Flow Theory Through a Genealogy of Models*. EURO Advanced Tutorials on Operational Research. Springer International Publishing, Cham, 2019. ISBN 978-3-319-78694-0 978-3-319-78695-7. doi: 10.1007/978-3-319-78695-7. p. 11

Arne Kesting and Martin Treiber. Calculating travel times from reconstructed spatiotemporal traffic data. In *Proceedings of the 4th International Symposium*, Stuttgart, 2008a. ISBN 978-3-921882-24-5. p. 20

Arne Kesting and Martin Treiber. Calibrating car-following models by using trajectory data: Methodological Study. volume 2088, pages 148–156, Washington, D.C., December 2008b. doi: 10.3141/2088-16. p. 20

Arne Kesting, Martin Treiber, and Dirk Helbing. Agents for traffic simulation. In *Multi-Agents Systems: Simulation and Applications*, pages 325–356, 2008. p. 9, 10

Jiwon Kim and Hani Mahmassani. Correlated Parameters in Driving Behavior Models: Car-Following Example and Implications for Traffic Microsimulation. *Transportation Research Record: Journal of the Transportation Research Board*, 2249:62–77, December 2011. ISSN 0361-1981. doi: 10.3141/2249-09. p. 20

E. Kometani and T. Sasaki. Dynamic Behaviour of Traffic with a Non-Linear Spacing-Speed Relationship. 1959. p. 12

Stefan Krauß. *Microscopic modeling of traffic flow: Investigation of collision free vehicle dynamics*. PhD thesis, 1998. p. 11

Ludovic Leclercq. Calibration of Flow-Density Relationships on Urban Streets. *Transportation Research Record: Journal of the Transportation Research Board*, 1934:226–234, January 2005. ISSN 0361-1981. doi: 10.3141/1934-24. p. 9

Ludovic Leclercq. Hybrid approaches to the solutions of the "Lighthill–Whitham–Richards" model. *Transportation Research Part B: Methodological*, 41(7):701–709, August 2007. ISSN 01912615. doi: 10.1016/j.trb.2006.11.004. p. 14

Ludovic Leclercq. *Le modèle LWR: théorie, confrontation expérimentale et applications au milieu urbain*. HDR, Université Claude Bernard Lyon 1, Lyon, 2009. p. 14

Ludovic Leclercq, Jorge Andres Laval, and Estelle Chevallier. The Lagrangian Coordinates and What it Means for First Order Traffic Flow Models. 2007. ISBN 978-0-08-045375-0. p. 14

W. Leutzbach and R. Wiedemann. Development and Applications of Traffic Simulation Models at the Karlsruhe Institut fur Verkehrwesen. *Traffic Engineering & Control*, 27(5), May 1986. ISSN 0041-0683. p. 11

M. J. Lighthill and G. B. Whitham. On Kinematic Waves. II. A Theory of Traffic Flow on Long Crowded Roads. *Proceedings of the Royal Society A: Mathematical, Physical and Engineering Sciences*, 229(1178):317–345, May 1955. ISSN 1364-5021, 1471-2946. doi: 10.1098/rspa.1955.0089. p. 9

Lan Liu, Liling Zhu, and Da Yang. Modeling and simulation of the car-truck heterogeneous traffic flow based on a nonlinear car-following model. *Applied Mathematics and Computation*, 273:706–717, January 2016. ISSN 00963003. doi: 10.1016/j.amc.2015.10.032. [8]. p. 11

Michal Maciejewski. A comparison of microscopic traffic flow simulation systems for an urban area. *Transport problems: an International Scientific Journal*, 5(4):27–38, 2010. p. 8, 9

Sven Maerivoet and Bart De Moor. Traffic flow theory. *arXiv:physics/0507126*, July 2005. p. 9

Adolf D May. *Traffic flow fundamentals*. Prentice Hall, Englewood Cliffs, N.J., 1990. ISBN 978-0-13-926072-8. OCLC: 20354224. p. 8

Kai Nagel and Michael Schreckenberg. A cellular automaton model for freeway traffic. *Journal de Physique I*, 2(12):2221–2229, December 1992. ISSN 1155-4304, 1286-4862. doi: 10.1051/jp1:1992277. p. 10, 11

G.F. Newell. A simplified car-following theory: a lower order model. *Transportation Research Part B: Methodological*, 36(3):195–205, March 2002. ISSN 01912615. doi: 10.1016/S0191-2615(00)00044-8. p. 11, 12, 13

Daiheng Ni. Multiscale modeling of traffic flow. *Mathematica Aeterna*, 1(01):27–54, 2011. p. 9, 10

Emily Nodine, Andy Lam, Mikio Yanagisawa, and Wassim Najm. Naturalistic Study of Truck Following Behavior. *Transportation Research Record: Journal of the Transportation Research Board*, 2615:35–42, January 2017. ISSN 0361-1981. doi: 10.3141/2615-05. [2]. p. 11

Saskia Ossen and Serge Hoogendoorn. Calibrating car-following models using microscopic trajectory data: A Critical Analysis of Both Microscopic Trajectory Data Collection Methods, and Calibration Studies Based on These Data. Technical report, Delft Univ. Technol., The Netherlands, 2008a. p. 20

Saskia Ossen and Serge P. Hoogendoorn. Validity of Trajectory-Based Calibration Approach of Car-Following Models in Presence of Measurement Errors. *Transportation Research Record: Journal of the Transportation Research Board*, 2088(1):117–125, January 2008b. ISSN 0361-1981, 2169-4052. doi: 10.3141/2088-13. p. 17, 20

Louis A. Pipes. An operational analysis of traffic dynamics. *Journal of Applied Physics*, 24(3):274–281, April 1953. doi: 10.1063/1.1721265. p. 11

Vincenzo Punzo and Marcello Montanino. Speed or spacing? Cumulative variables, and convolution of model errors and time in traffic flow models validation and calibration. *Transportation Research Part B: Methodological*, 91:21–33, September 2016. ISSN 01912615. doi: 10.1016/j.trb.2016.04.012. p. 20

Vincenzo Punzo and Fulvio Simonelli. Analysis and Comparison of Microscopic Traffic Flow Models with Real Traffic Microscopic Data. In *Transportation Research Record: Journal of the Transportation Research Board*, volume 1934, pages 53–63, Washington D.C., 2005. doi: 10.3141/1934-06. p. 20

Vincenzo Punzo, Domenico Formisano, and Vincenzo Torrieri. Nonstationary Kalman Filter for Estimation of Accurate and Consistent Car-Following Data. *Transportation Research Record: Journal of the Transportation Research Board*, 1934:1–12, January 2005. ISSN 0361-1981. doi: 10.3141/1934-01. p. 17

Vincenzo Punzo, Maria Teresa Borzacchiello, and Biagio Ciuffo. On the assessment of vehicle trajectory data accuracy and application to the Next Generation SIMulation (NGSIM) program data. *Transportation Research Part C: Emerging Technologies*, 19(6):1243–1262, December 2011. ISSN 0968-090X. doi: 10.1016/j.trc.2010.12.007. p. 17

Vincenzo Punzo, Biagio Ciuffo, and Marcello Montanino. May we trust results of car-following models calibration based on trajectory data? In *Proceedings of the 91st Transportation Research Board Annual Meeting*. Transportation Research Board of the National Academies, 2012. p. 12, 20

Prakash Ranjitkar, Takashi Nakatsuji, and Motoki Asano. Performance Evaluation of Microscopic Traffic Flow Models with Test Track Data. *Transportation Research Record: Journal of the Transportation Research Board*, 1876(1):90–100, January 2004. ISSN 0361-1981, 2169-4052. doi: 10.3141/1876-10. p. 20

Paul I. Richards. Shock Waves on the Highway. *Operations Research*, 4(1):42–51, February 1956. ISSN 0030-364X, 1526-5463. doi: 10.1287/opre.4.1.42. p. 9

M. Sarvi and O. Ejtemai. Exploring heavy vehicles car-following behaviour. volume 34, September 2011. [4]. p. 11

Majid Sarvi. Heavy commercial vehicles-following behavior and interactions with different vehicle classes: Following behavior analysis in heavy vehicles. *Journal of Advanced Transportation*, pages n/a–n/a, October 2011. ISSN 01976729. doi: 10.1002/atr.182. [6]. p. 11

Guohua Song, Lei Yu, and Zhongbo Geng. Optimization of Wiedemann and Fritzsche car-following models for emission estimation. *Transportation Research Part D: Transport and Environment*, 34:318–329, January 2015. ISSN 13619209. doi: 10.1016/j.trd.2014.11.023. p. 20

TSS Transport Simulation System. Aimsun 8 User's Manual, May 2014. p. 21

Christian Thiemann, Martin Treiber, and Arne Kesting. Estimating Acceleration and Lane-Changing Dynamics from Next Generation Simulation Trajectory Data. In *Transportation Research Record: Journal of the Transportation Research Board*, volume 2088, pages 90–101, Washington D.C., 2008. doi: 10.3141/2088-10. p. 17

Tomer Toledo, Haris N. Koutsopoulos, and Kazi I. Ahmed. Estimation of Vehicle Trajectories with Locally Weighted Regression. In *Transportation Research Record: Journal of the Transportation Research Board*, volume 1999, pages 161–169, Washington D.C., 2007. doi: 10.3141/1999-17. p. 17

Martin Treiber and Arne Kesting. Car-Following Models based on Driving Strategies. In *Traffic Flow Dynamics*. Springer Berlin Heidelberg, Berlin, Heidelberg, 2013a. ISBN 978-3-642-32459-8 978-3-642-32460-4. doi: 10.1007/978-3-642-32460-4. p. 11, 12, 13

Martin Treiber and Arne Kesting. Elementary Car-Following models. In *Traffic Flow Dynamics*. Springer Berlin Heidelberg, Berlin, Heidelberg, 2013b. ISBN 978-3-642-32459-8 978-3-642-32460-4. doi: 10.1007/978-3-642-32460-4. p. 11, 21

Martin Treiber and Arne Kesting. Microscopic Calibration and Validation of Car-Following Models – A Systematic Approach. *Procedia - Social and Behavioral Sciences*, 80:922–939, June 2013c. ISSN 18770428. doi: 10.1016/j.sbspro.2013.05.050. p. 20, 21

Martin Treiber, Ansgar Hennecke, and Dirk Helbing. Congested traffic states in empirical observations and microscopic simulations. *Physical Review E*, 62(2):1805–1824, August 2000. ISSN 1063-651X, 1095-3787. doi: 10.1103/PhysRevE.62.1805. p. 11, 13

F.L.M. Van Wageningen-Kessels. *Multi-class continuum traffic flow models: Analysis and simulation methods*. PhD thesis, TRAIL, 2013. p. 11, 14

Thamara Vieira da Rocha, Ludovic Leclercq, Marcello Montanino, Céline Parzani, Vincenzo Punzo, Biagio Ciuffo, and Daniel Villegas. Does traffic-related calibration of car-following models provide accurate estimations of vehicle emissions? *Transportation Research Part D: Transport and Environment*, 34:267–280, January 2015. ISSN 13619209. doi: 10.1016/j.trd.2014.11.006. p. 17, 20

R. Wiedemann and U. Reiter. Microscopic traffic simulation: the simulation system MISSION, background and actual state. Proj. ICARUS Final report, Brussels, 1992. p. xv, 11, 12, 14, 15, 16

Rainer Wiedemann. Simulation des Strassenverkehrsflusses. Technical report, Instituts für Verkehrswesen des Universität Karlsruhe, 1974. p. 11, 12, 14, 15

R. E. Wilson. An analysis of Gipps's car-following model of highway traffic. *IMA Journal of Applied Mathematics*, 66(5):509–537, October 2001. ISSN 0272-4960, 1464-3634. doi: 10.1093/imamat/66.5.509. p. 12, 13

John R. Windover and Michael J. Cassidy. Some observed details of freeway traffic evolution. *Transportation Research Part A: Policy and Practice*, 35(10):881–894, 2001. p. 9

Da Yang, Peter (Jing) Jin, Yun Pu, and Bin Ran. Stability analysis of the mixed traffic flow of cars and trucks using heterogeneous optimal velocity car-following model. *Physica A: Statistical Mechanics and its Applications*, 395:371–383, February 2014. ISSN 03784371. doi: 10.1016/j.physa.2013.10.017. [7]. p. 11

Chapter 3

Reconstruction of vehicles trajectories for car-following calibration

Contents

The definition of the data used for the calibration of car-following models takes an important place in calibration studies. Trajectories needed for calibration can be defined in different ways: probe vehicles, loop detector data or video records (Thiemann et al., 2008; Toledo et al., 2007; Vieira da Rocha et al., 2015).

As far as the study of trucks reaction to traffic is concerned, existing studies have used the NGSIM (US_-Dept_Transportation, 2006) data base (Aghabayk et al., 2016) or data acquisition on vehicles (Nodine et al., 2017). In this thesis, the data used for car-following models calibration was recorded with a truck, equipped with two sensors, a radar and a camera, on a trip of 80.5kms.

This chapter presents the comparison of several reconstruction methods of vehicles trajectory: position, speed and acceleration. These methods differ on the integration (or derivation) schemes used and the filtering (or not) of the data.

The objective of this study is to propose a method to reconstruct couples of trajectories (Leader and Follower) from the measured data available: the speed of the truck and the spacing to the leader vehicle.

This chapter begins with the presentation of the processed sensors data used and the selection of the interesting route sections (section 3.1.1). Then, the methods that will be compared are detailed. The trajectories will be compared in sections 3.1.2.1, 3.1.2.2, 3.1.2.3 and 3.1.2.4.

3.1 Trajectories reconstruction

The vehicle travelled about 80.5km in 2h45 in and around the city of Lyon (France). The route travelled by the vehicle is presented in Figure 3.2, the starting and ending points are represented by the yellow circle.

3.1.1 Data processing

The recorded data contains three pieces of information that will be used for the trajectory reconstruction. The first one is the speed of the truck (in m/s) registered thanks to the vehicle odometer.

The two other signals are the outputs of two of the sensors that equipped the vehicle. These sensors are a radar and a camera which measure the spacing between the truck and the Leader vehicle. They will be respectively called Follower and Leader in the following pages of this thesis.

Sensor data

The measured spacings could not be used directly for trajectory reconstruction. First of all, the two signals are merged. The process applied to merge the signals is illustrated on Figure 3.1. The blue line represents the radar signal and the green line represents the camera signal. If the sensors values are equal to 250, no object is detected. The reconstructed spacing is illustrated with the pink line, it has been filtered with a moving average to remove measurement noise.

First, we examine the sensors signals to find the first point where the two sensors detect the same target. Then, the time when it was first detected by one of the sensors is found and used as the beginning of the final spacing. In this example, the camera detects the target before the radar. In the same manner we search for the last point where the target is detected. Moreover, in the case where the two sensors lose their target during less than 2.5s, but the signal(s) could be extrapolated to the next point where the target is seen without losing its consistency, the combined signal is extrapolated.

Then, a new signal is computed as the weighted average of the radar and camera signals. A bigger weight is given to the radar which is more stable than the camera, for more than 90% of the cycles. This signal is used as the final spacing between the Follower and its Leader. This process is equivalent to the scalar formulation of the Kalman filter. Interaction situations are situations where the spacing value is different from 250.

Division into sub-cycles

To create operational cycles for the calibration of car-following models, the entire cycle was divided into sub-cycles separated by stops (speed less than $0.1m/s$) of at least 6s. This division leads to 61 sub-cycles with distances between 2m and 40km. In these sub-cycles, some contain one interaction situation, some contain several interaction situations and others do not contain any interaction. These sub-cycles are divided again in order to create 111 sub-cycles, each one containing at most one interaction situation.

Following behaviours are defined by a short distance ($< 20m$) between the Leader and the Follower. Moreover, a variation in the speed is necessary to the calibration process to catch the following behaviour. In urban areas, a change in speed profile usually occurs at the scale of a link which corresponds to a distance of $150-200m$ in general. Therefore, in urban areas, cycles smaller than 150m are not kept, and in other locations, cycles without any change in the speed profile are also deleted.

Finally, 35 sub-cycles are selected for the calibration study, with distances varying from 166m to 2.6km. The location of the selected sub-cycles is presented in Figure 3.2 (green and pink roads).

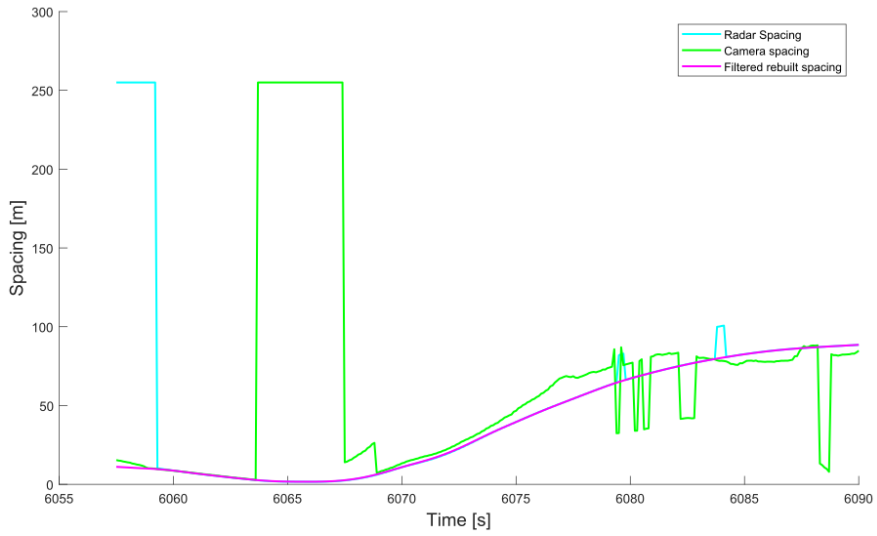

Figure 3.1 – Post processing of sensors spacing signals

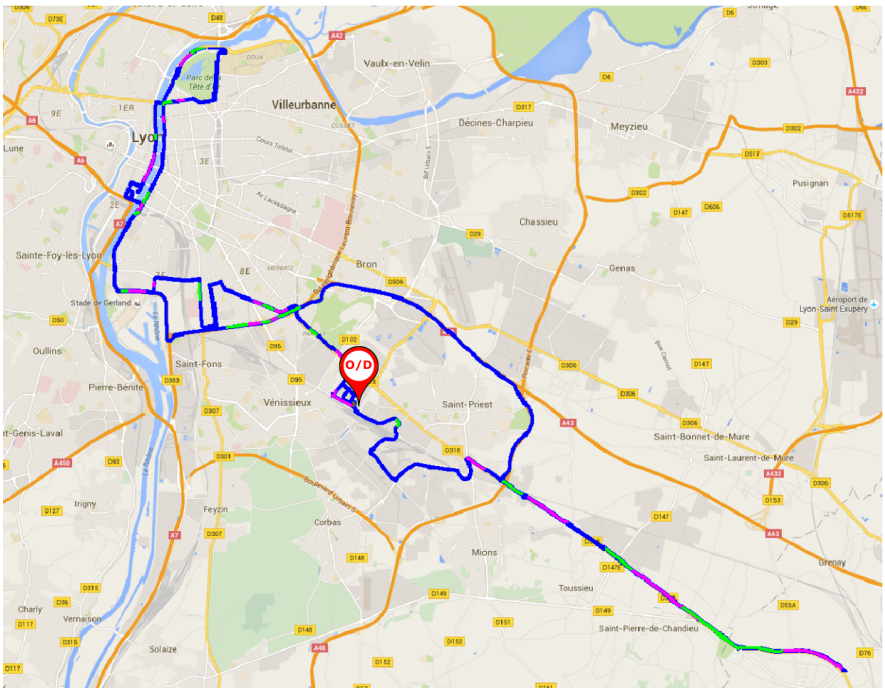

Figure 3.2 – Selected cycles location, on the route driven by the studied vehicle

3.1.2 Comparison of the methods

The different methods that will be compared are detailed in Chapter 2, section 2.4, they are reminded in Table 3.1. The 54 possible trajectories are compared to define one method for which the trajectories of the vehicles fulfill the following requirements: (i) the lowest error possible between measured speed and computed speed, and (ii) physical consistency of acceleration values, i.e. values between $+/-3m/s^2$. In order to select one method, positions, speeds, accelerations and jerk values are compared.

Table 3.1 – Reconstruction methods

			Acceleration derived	
Measured speed	Position Euler Explicit	Speed derived 0.1s	0.1s	1
			0.1s, smoothed	2
			1s	3
		Speed derived 0.1s, smoothed	0.1s	4
			0.1s, smoothed	5
			1s	6
		Speed derived 1s	0.1s	7
			0.1s, smoothed	8
			1s	9
	Position Euler Implicit	Speed derived 0.1s	0.1s	10
			0.1s, smoothed	11
			1s	12
		Speed derived 0.1s, smoothed	0.1s	13
			0.1s, smoothed	14
			1s	15
		Speed derived 1s	0.1s	16
			0.1s, smoothed	17
			1s	18
	Position Midpoint	Speed derived 0.1s	0.1s	19
			0.1s, smoothed	20
			1s	21
		Speed derived 0.1s, smoothed	0.1s	22
			0.1s, smoothed	23
			1s	24
		Speed derived 1s	0.1s	25
			0.1s, smoothed	26
			1s	27
Measured speed smoothed	Position Euler Explicit	Speed derived 0.1s	0.1s	28
			0.1s, smoothed	29
			1s	30
		Speed derived 0.1s, smoothed	0.1s	31
			0.1s, smoothed	32
			1s	33
		Speed derived 1s	0.1s	34
			0.1s, smoothed	35
			1s	36
	Position Euler Implicit	Speed derived 0.1s	0.1s	37
			0.1s, smoothed	38
			1s	39
		Speed derived 0.1s, smoothed	0.1s	40
			0.1s, smoothed	41
			1s	42
		Speed derived 1s	0.1s	43
			0.1s, smoothed	44
			1s	45
	Position Midpoint	Speed derived 0.1s	0.1s	46
			0.1s, smoothed	47
			1s	48
		Speed derived 0.1s, smoothed	0.1s	49
			0.1s, smoothed	50
			1s	51
		Speed derived 1s	0.1s	52
			0.1s, smoothed	53
			1s	54

3.1.2.1 Comparison of Positions

For all of the 35 cycles, we can observe that the 6 possible position vectors are very similar. The maximum gap (the maximum RMSE error) between two methods is about $0.6m$. No method outperforms another based on this criterion.

3.1.2.2 Comparison of Speeds

The comparison of the speed vectors is done by computing the RMSE defined in eq.(2.27) between the measured speed or the filtered measured speed and the computed one for the Follower.

For the Leader, we do not have a measured speed as reference, then one of the computed speeds will be defined as a reference for the study. We have chosen to use the simplest method as reference, i.e. the direct derivation of the reconstructed positions (from measured and filtered measured speeds of the Follower) with explicit scheme, a time step equal to the measurement time step ($0.1s$), and no filtering for the speed.

This comparison points out very low differences between the methods for the Follower and the Leader, however we can say that some methods are always underperforming the others. These methods are those using Euler explicit (eq. (2.24)) and implicit (eq. (2.25)) derivation schemes to compute the position from measured and filtered measured speed, and then the derivation with a time step equal to $1s$ to obtain the reconstructed speed. This result is illustrated in Figure 3.3 and 3.4, where the green horizontal lines represent, from bottom to top, the 50^{th}, 75^{th} and 95^{th} quantiles. In these figures, we can see that for the 35 sub-cycles, methods represented by medium blue circles and dark red stars are always above the 75^{th} quantile and sometimes above the 95^{th} quantile. That means that these methods always provide error between the measurements and the reconstructed speed that are in the upper quarter of the set. However, the error never exceeds $1m/s$ for the speed of the Follower and $1.5m/s$ for the speed of the leader.

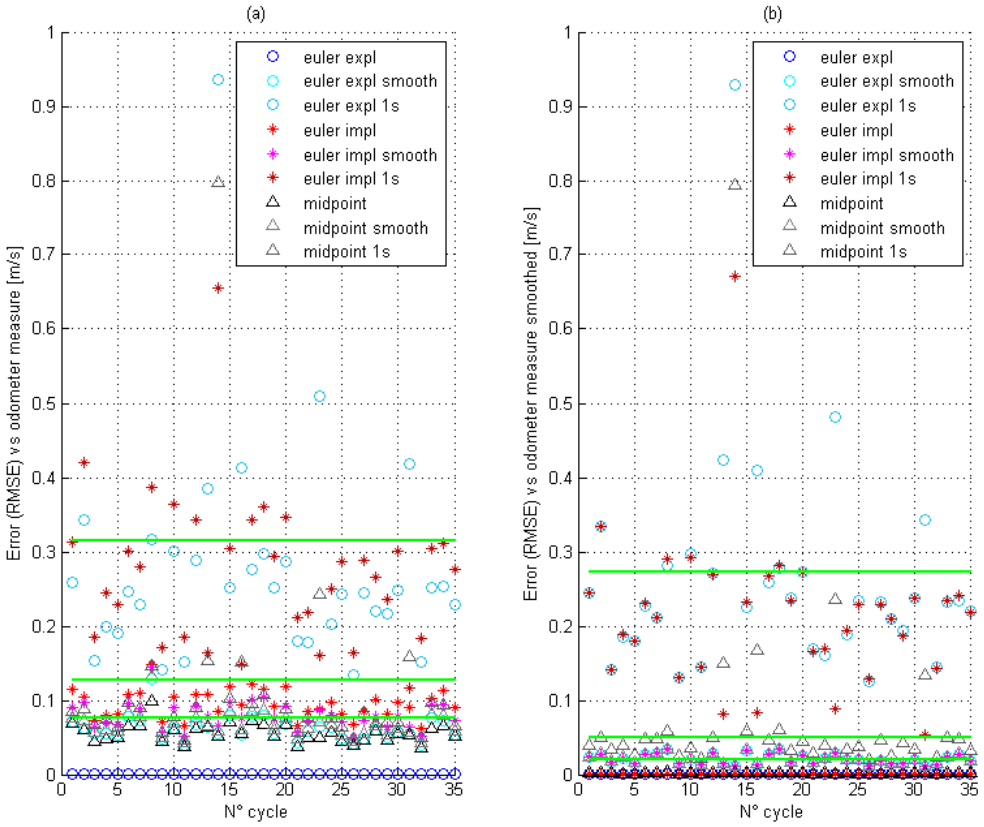

Figure 3.3 – (a) Comparison of the errors between measured speed and computed speed for the trajectory of the Follower; (b) Comparison of the errors between smoothed measured speed and computed speed for the trajectory of the Follower

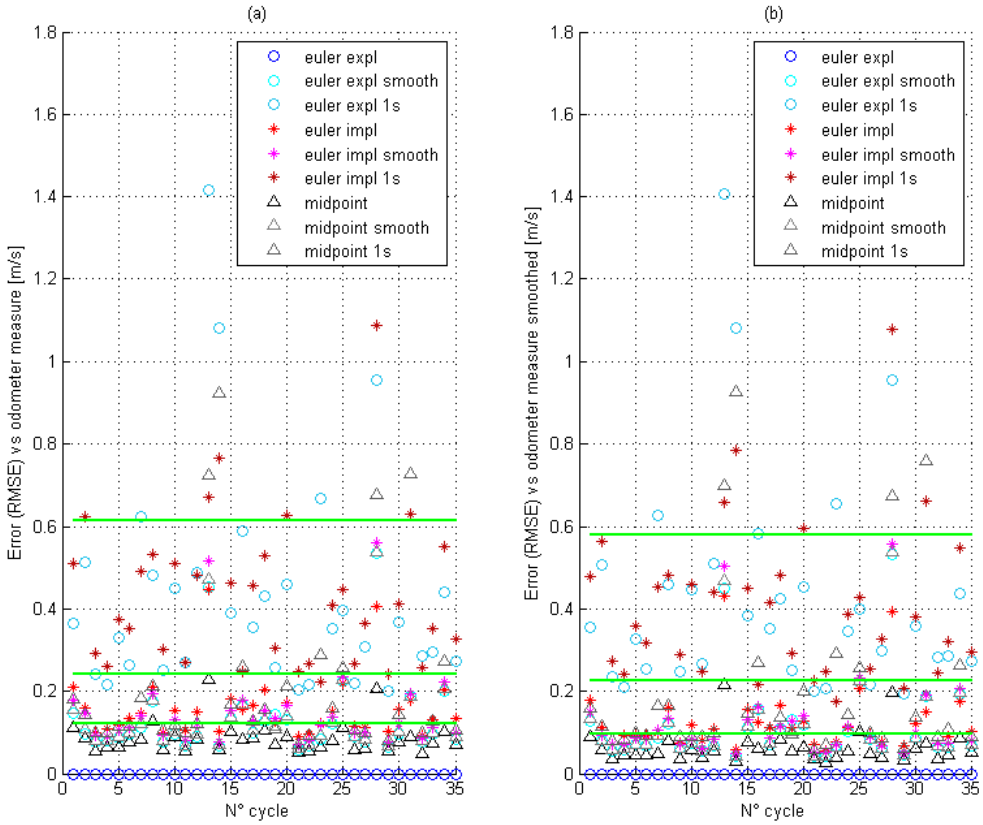

Figure 3.4 – (a) Comparison of the errors between measured speed and computed speed for the trajectory of the Leader; (b) Comparison of the errors between smoothed measured speed and computed speed for the trajectory of the Leader

3.1.2.3 Comparison of Accelerations

Extreme values of acceleration - Quantiles 10% ***and*** 90%

The acceleration vectors will be compared differently, because no reference measurement is available for this data. For the acceleration, we first compare the the 10^{th} and 90^{th} quantiles, respectively D1 and D9, of the 54 methods, for each cycle. The results are presented in Figure 3.5 and Figure 3.6. Figure 3.5 represents accelerations computed from measured speed by odometer. Figure 3.6 represents acceleration from smoothed measured speed.

In Figure 3.5 and Figure 3.6, blue points are the acceleration computed with Euler explicit derivation method, red points correspond to the acceleration computed with Euler implicit and black points come from the midpoint method (eq. (2.26)). The markers correspond to different derivations: circles correspond to direct derivation, stars represent the direct derivation smoothed and triangles are the derivation with time step equal to $1s$.

First, some methods can be easily removed from the set of feasible ones because their values of $D1$ and $D9$ are far from the others. These methods (red and blue circles) correspond to direct derivation, without smoothing, with Euler explicit and implicit derivation schemes. This difference is less visible for the Follower acceleration which comes from the smoothed measured speed. Moreover, some methods provide unrealistic values for maximum and/or minimum acceleration. Considering that we try to find a universal method, they can also be removed from the set of feasible methods for the reconstruction of the trajectories. This first selection leads to a reduced set of 20 possible methods. Kept methods are the methods number: 4, 5, 13, 21, 22, 23, 24, 25, 26, 31, 32, 39, 41, 42, 48, 49, 50, 51, 52 and 53. They are summarized in Table 3.2.

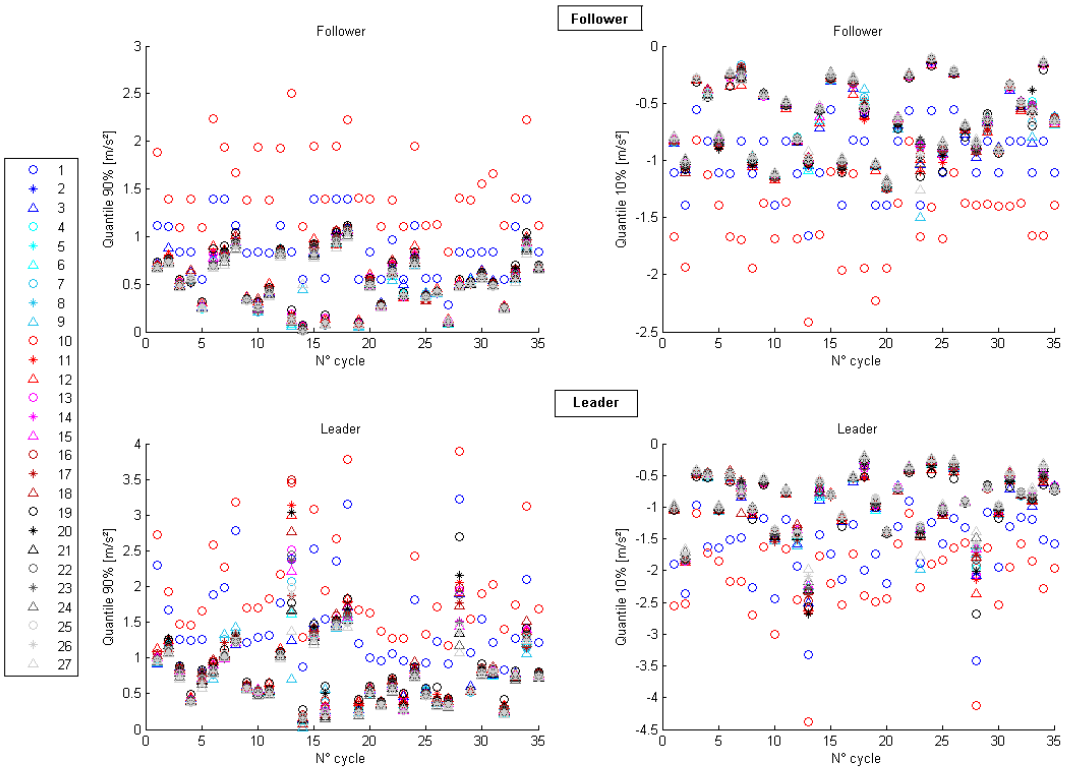

Figure 3.5 – Comparison of the 10^{th} and 90^{th} of the accelerations quantiles for methods from measured speed

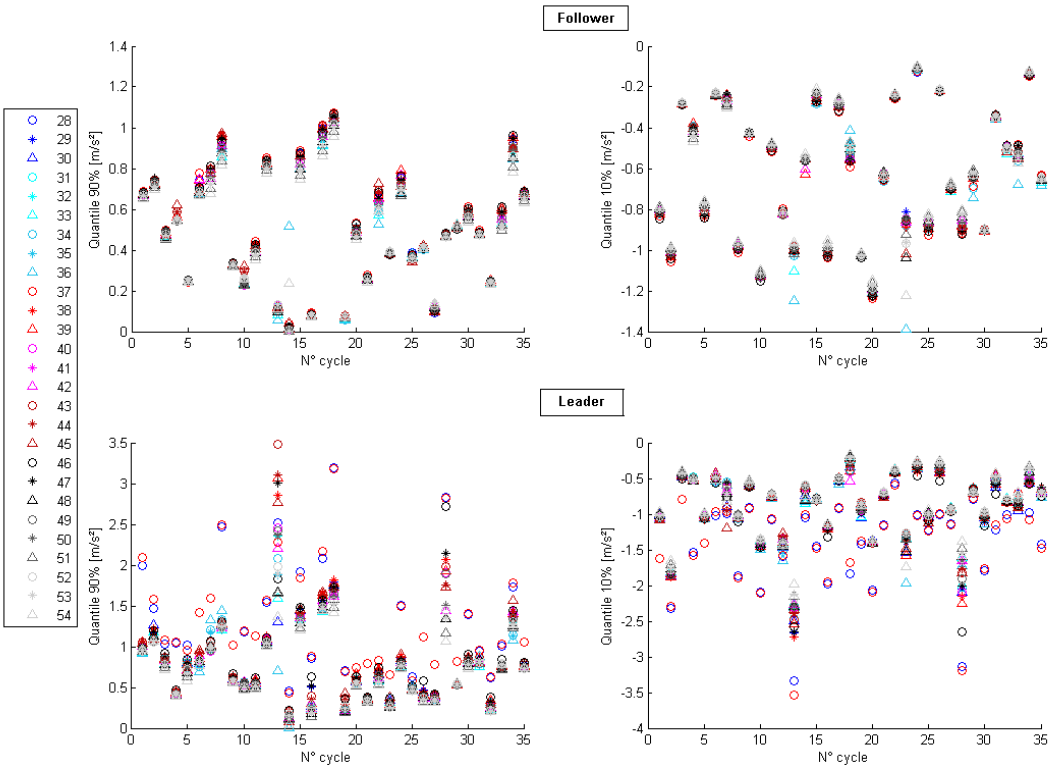

Figure 3.6 – Comparison of the 10^{th} and 90^{th} of the accelerations quantiles for methods from smoothed measured speed

Table 3.2 – Methods providing consistent values of acceleration

Measured speed	Position Euler Explicit	Speed derived 0.1s, smoothed	Acceleration derived 0.1s	4
			Acceleration derived 0.1s, smoothed	5
	Position Euler Implicit	Speed derived 0.1s, smoothed	Acceleration derived 0.1s	13
	Position Midpoint	Speed derived 0.1s	Acceleration derived 1s	21
		Speed derived 0.1s, smoothed	Acceleration derived 0.1s	22
			Acceleration derived 0.1s, smoothed	23
			Acceleration derived 1s	24
		Speed derived 1s	Acceleration derived 0.1s	25
			Acceleration derived 0.1s, smoothed	26
Measured speed smoothed	Position Euler Explicit	Speed derived 0.1s, smoothed	Acceleration derived 0.1s	31
			Acceleration derived 0.1s, smoothed	32
	Position Euler Implicit	Speed derived 0.1s	Acceleration derived 1s	39
		Speed derived 0.1s, smoothed	Acceleration derived 0.1s, smoothed	41
			Acceleration derived 1s	42
	Position Midpoint	Speed derived 0.1s	Acceleration derived 1s	48
		Speed derived 0.1s, smoothed	Acceleration derived 0.1s	49
			Acceleration derived 0.1s, smoothed	50
			Acceleration derived 1s	51
		Speed derived 1s	Acceleration derived 0.1s	52
			Acceleration derived 0.1s, smoothed	53

Distributions of accelerations

The remaining methods are compared using the distribution of acceleration along each cycle. For almost each cycle, the distributions are similar (Figure 3.7 for Follower's acceleration and Figure 3.8 for Leader's acceleration on cycle n°8). Nevertheless, we can observe some differences on some cycles, two or three groups of accelerations can be observed. To point out similarities between the methods, they are clustered using the K-means method over 4 indicators:

- (1) the minimum value of acceleration reached,
- (2) the maximum value of acceleration reached,
- (3) the percentage of time spent at low acceleration, ($|a| <= 0.1 m/s^2$)
- (4) the value of acceleration at which the driver drives most fo the time.

The clustering technique was done with a maximum of three clusters. For indicators (1) and (2) listed above, we can observe that in most cases, three clusters are identified. For indicator (3), there are also generally three clusters but with one which contains one or two methods only. The last indicator gives in most cases only one cluster, which will not be considered for further analysis. The first three indicators studied allow to identify which methods are similar to others according to minimum and maximum values of acceleration reached and according to time spent at low acceleration ($|a| < 0.1 m/s^2$). The three groups that can be highlighted are the following:

- Cluster 1: 4, 5, 13, 22, 23, 39 (Table 3.3)
- Cluster 2: 24, 48, 51, 52, 53 (Table 3.4)
- Cluster 3: 21, 25, 26, 31, 32, 41, 42, 49, 50 (Table 3.5)

The reconstruction methods classification with clusters has allowed to point out similarities between methods. The 20 methods selected in paragraph 3.1.2.3 are 20 possible methods to reconstruct data. Punzo et al. (2011) propose different ways to analyze trajectory data accuracy. One of them uses jerk values as an indicator. This study is presented in the next paragraph.

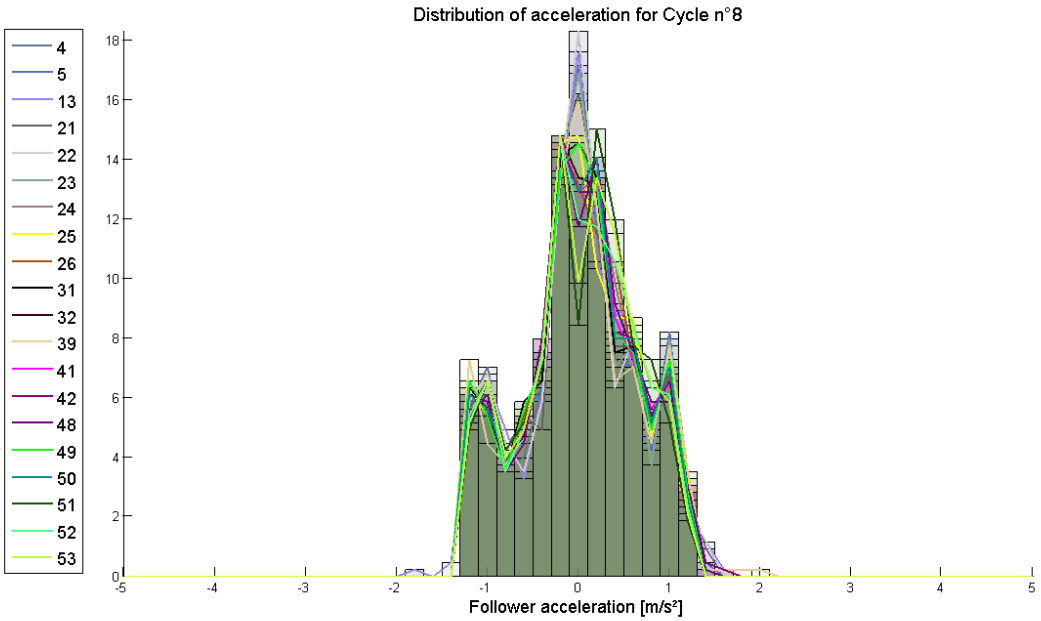

Figure 3.7 – Distribution of Follower's acceleration along Cycle n°8

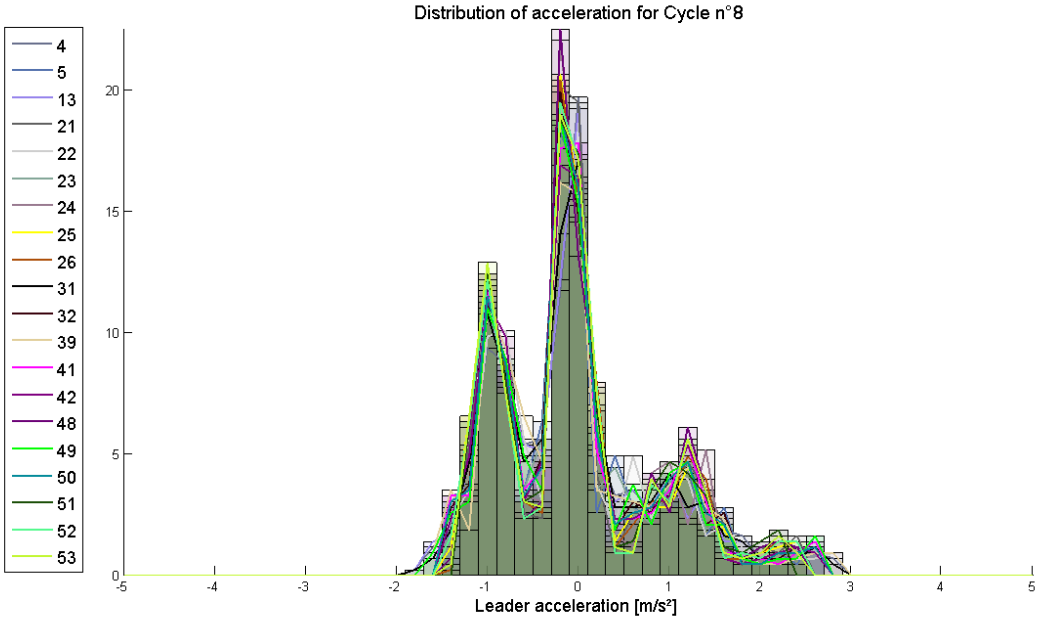

Figure 3.8 – Distribution of Leader's acceleration along Cycle n°8

Table 3.3 – Methods providing similar values of acceleration - Cluster 1

Measured speed	Position Euler Explicit	Speed derived 0.1s, smoothed	Acceleration derived 0.1s	4
			Acceleration derived 0.1s, smoothed	5
	Position Euler Implicit	Speed derived 0.1s, smoothed	Acceleration derived 0.1s	13
	Position Midpoint	Speed derived 0.1s, smoothed	Acceleration derived 0.1s	22
			Acceleration derived 0.1s, smoothed	23
Measured speed smoothed	Position Euler Implicit	Speed derived 0.1s	Acceleration derived 1s	39

Table 3.4 – Methods providing similar values of acceleration - Cluster 2

Measured speed	Position Midpoint	Speed derived 0.1s, smoothed	Acceleration derived 1s	24
Measured speed smoothed	Position midpoint	Speed derived 0.1s	Acceleration derived 1s	48
		Speed derived 0.1s, smoothed	Acceleration derived 1s	51
		Speed derived 1s	Acceleration derived 0.1s	52
			Acceleration derived 0.1s, smoothed	53

Table 3.5 – Methods providing similar values of acceleration - Cluster 3

Measured speed	Position Midpoint	Speed derived 0.1s	Acceleration derived 1s	21
		Speed derived 1s	Acceleration derived 0.1s	25
			Acceleration derived 0.1s, smoothed	26
Measured speed smoothed	Position Euler Explicit	Speed derived 0.1s, smoothed	Acceleration derived 0.1s	31
			Acceleration derived 0.1s, smoothed	32
	Position Euler Implicit	Speed derived 0.1s, smoothed	Acceleration derived 0.1s, smoothed	41
			Acceleration derived 1s	42
	Position Midpoint	Speed derived 0.1s, smoothed	Acceleration derived 0.1s	49
			Acceleration derived 0.1s, smoothed	50

3.1.2.4 Comparison of jerk values

An analysis of the jerk values is presented in Punzo et al. (2011). The jerk values (in m/s^3) represent the variation of the acceleration, its derivative. They are computed with explicit derivation scheme from the 20 possible accelerations selected in the previous paragraphs and for each of the 35 cycles.

In Martinez and Canudas-de Wit (2007), they mentioned that jerk values can reach $10m/s^3$ while comfortable values of jerk do not exceed $2m/s^3$. These thresholds are kept for the Follower, but for the Leader, the thresholds are respectively set to $12m/s^3$ and $3m/s^3$.

The indicators which are studied are the ones presented in Punzo et al. (2011), and also the percentage of time with comfortable jerk values:

- the percentage of time with jerk values higher than the defined maximum thresholds ($10m/s^3$ and $12m/s^3$),
- the percentage of time with jerk values lower than the defined comfortable thresholds ($2m/s^3$ and $3m/s^3$),
- the maximum value of the jerk reaches,
- the minimum value of the jerk reaches,
- the percentage of one-second window which contains more than one sign change of the jerk.

These five indicators are computed for each of the 20 reconstruction methods remaining, and for each of the 35 cycles.

Table 3.6 and Table 3.7 present the results of the jerk values analysis for the cycle n°8, respectively for the Follower and the Leader. The results are very similar for every cycle.

First, we can observe that those statistics are quite better than the ones observed on NGSIM data and presented in Punzo et al. (2011). In this study, the maximum absolute value of jerk reached is higher than $75m/s^3$ whereas the maximum absolute value reached here is equal to $22m/s^3$. Moreover, the percentage of jerk values greater than the maximum admissible threshold is very low. It does not exceed 1.7% for the Follower and 4% for the Leader, against percentages greater than 10% for NGSIM data with a higher threshold, and this only for two or three over the 20 reconstruction methods studied, the others never exceed the thresholds. There is the same observation for the percentage of $1s$ window with more than one sign change of the jerk. Only some methods imply a number of sign change greater than 50% and 60%, the other methods are generally around 30% and around 40% respectively for the Follower's trajectories and for Leader's trajectories.

The statistics on the entire set of trajectories show that methods n°4, 13 and 22 provide for the majority of the cycles the worst values. Accelerations n°25, 31 and 49 provide statistics which are not really good compared to the others. We can observe that those two trios of accelerations contain methods which are respectively in the same clusters.

Table 3.6 – Results of the jerk values analysis for the cycle n°8 for the Follower

Cycle n°8	%jerk > $\lvert 10m/s^3 \rvert$	%jerk < $\lvert 2m/s^3 \rvert$	Maximum jerk	Minimum jerk	% 1s window with sign change >1
4	0.47	93.0	41.3	-14.0	96.6
5	0.0	100.0	1.95	-1.5	46.5
13	1.64	84.0	22.2	-21.0	99.3
21	0.0	100.0	0.57	-1.8	23.5
22	0.0	98.4	3.03	-2.5	58.0
23	0.0	100.0	1.09	-1.5	38.4
24	0.0	100.0	0.5	-1.3	26.6
25	0.0	99.8	0.71	-6.2	27.8
26	0.0	100.0	0.58	-1.2	29.0
31	0.0	99.8	0.26	-2.2	38.1
32	0.0	100.0	0.62	-0.8	27.6
39	0.0	100.0	0.76	-1.9	34.5
41	0.0	100.0	0.62	-1.7	27.3
42	0.0	100.0	0.6	-1.2	25.7
48	0.0	100.0	0.49	-1.4	26.9
49	0.0	99.8	0.9	-2.2	31.2
50	0.0	100.0	0.61	-1.5	27.1
51	0.0	100.0	0.44	-1.1	16.8
52	0.0	99.8	0.56	-5.7	26.4
53	0.0	100.0	0.5	-1.1	24.5

To select the method, which will be used in the next part of this study, we will take into account recommendation given in the literature with respect to pre-processing of data for calibration (Punzo et al., 2011). In this article, measurements (from NGSIM) provide the position of the vehicles, contrary to our case in which the vehicle speed is the input. The authors propose to compute speed from position by direct derivation, then, to filter the speed, then, to derive the speed to obtain acceleration and, again, filter the acceleration vector. They mentioned that "this process would guarantee smooth speeds and accelerations while preserving the internal and platoon consistency of trajectories". In our case we have chosen to study the influence of three integration/derivation methods. In the 14 possible methods, only 5 methods respect this scheme: methods n°5, 23, 32, 41 and 50.

Methods n°5 and 23 come from measured speed whereas methods n°32, 41 and 50 come from smoothed measured speed. The Explicit scheme is used for methods n°5 and 32, the implicit scheme for method n°41 and the midpoint method for methods n°23 and 50. The method selected will be the midpoint method (or Trapezoidal rule) because it can be considered as a mean of the two others (Euler explicit and Euler implicit), moreover, in order to limit as far as possible the measurement noise, the selected method will come from the smoothed measured speed. So, the method selected is the method number 50.

3.1.3 Conclusion

In this study, we have studied different methods to reconstruct trajectory data from odometer measurements. We can finally observe that many of these methods provide results in acceleration that are not accurate. At the end of the study only 14 methods over the 54 tested provide realistic values for position, speed and acceleration; and only 5 are possible to reconstruct the entire trajectory in a realistic manner, taking into account traffic consistency. The strategy that seems the most suitable for trajectory reconstruction from speed measurements is the following: first, smooth the measure with a moving average (1.5s), then, compute position with trapezoidal rule (midpoint method), then, derive the position to obtain speed, smooth speed with a moving average, then derive to obtain acceleration and smooth acceleration with a moving average.

Moreover, we can note that the reconstruction method is independent of the type of the cycle (urban, mid-urban, regional or ring road).

Table 3.7 – Results of the jerk values analysis for the cycle n°8 for the Leader

Cycle n°8	%jerk > $\lvert 10m/s^3 \rvert$	%jerk < $\lvert 2m/s^3 \rvert$	Maximum jerk	Minimum jerk	% 1s window with sign change >1
4	0.47	82.6	13.6	-15.0	94.5
5	0.0	100.0	2.2	-1.9	59.2
13	1.88	79.1	21.8	-22.0	97.4
21	0.0	99.1	4.92	-1.2	36.9
22	0.0	98.8	6.77	-4.6	63.5
23	0.0	99.5	4.23	-1.6	37.2
24	0.0	100.0	2.48	-0.9	32.4
25	0.23	99.8	12.7	-1.3	36.5
26	0.0	100.0	2.72	-1.0	30.0
31	0.0	87.6	6.5	-6.4	93.0
32	0.0	100.0	2.15	-1.8	51.8
39	0.0	100.0	2.61	-2.2	46.5
41	0.0	99.8	3.3	-1.8	51.8
42	0.0	100.0	1.68	-1.4	44.4
48	0.0	98.8	5.12	-1.3	39.1
49	0.0	98.8	6.77	-4.4	62.8
50	0.0	99.5	3.81	-1.4	42.2
51	0.0	100.0	2.68	-0.9	35.7
52	0.23	99.8	13.2	-1.2	37.2
53	0.0	100.0	2.82	-1.0	35.5

3.2 Cycles Categorisation

The previous section proposed and compared several methods to reconstruct the complete trajectories (position, speed and acceleration) of the Follower and its Leader. The method was used to compute the different couples of trajectories for the 35 cycles mentioned in section 3.1.1. These cycles are presented more in detail in the following sections. The cycles are classified into four sub-categories (urban, mid-urban, regional and ring road) and their characteristics (length, average and legal speed) are presented.

3.2.1 Criteria descriptions

This set of 35 cycles is divided into 4 sub-groups according to mean speed, maximum speed and location:

(i) **Urban** category, characterized by a maximum speed smaller than $50km/h$, a mean speed less than $40km/h$ and an urban location. It contains 17 cycles.

(ii) **Regional** category is defined by a maximum speed greater than $55km/h$ and a regional location. This set contains 8 cycles.

(iii) **Mid-urban** category is between the urban and the regional category. The maximum speed is higher than $50km/h$, the mean speed is higher than $30km/h$ and the cycles are in the urban part of the recording data. This category contains 5 cycles.

(iv) **Ring road** category contains the 5 cycles which are located on the ring road.

3.2.2 Representative cycles

The cycles that will be used for the calibration process are different in length and speed. These characteristics are detailed in Table 3.8.

For each category of cycles, a cycle is defined as the representative cycle of the category and it will be used in the calibration study of the next Chapter (Chapter 4). For the urban category, the representative cycle is the cycle number 4, for mid-urban, it is the cycle number 11, for regional areas it is the cycle number 26 and for ring road cycles, it is the number 21.

Table 3.8 – Description of the 35 cycles kept

Urban									
N°	2	3	4	5	6	7	8	9	10
Length [m]	269.24	409.52	361.61	267.93	511.37	166.04	248.01	865.95	167.37
Average speed [km/h]	23.42	12.39	28.38	21.59	33.15	21.87	20.98	37.78	31.35
Legal speed [km/h]	70-50	50	50	50	50-30	50	50	50	50
N°	13	14	15	16	17	18	33	34	Average
Length [m]	194.72	307.54	212.30	350.06	245.70	210.49	627.05	306.55	336.38
Average speed [km/h]	33.84	26.29	20.78	38.16	24.59	23.33	29.97	28.59	26.85
Legal speed[km/h]	50	50	50	50	50	50	50	50	30-50-70

Mid-urban						
N°	1	11	12	19	35	Average
Length [m]	786.24	686.38	539.80	432.78	469.01	582.84
Average Speed [km/h]	43.37	36.56	42.17	32.97	39.98	39.01
Legal Speed [km/h]	50	70-50	50	50	50	50-70

Regional									
N°	25	26	27	28	29	30	31	32	Average
Length [m]	490.93	2634.34	1777.08	1771.01	1717.75	962.00	1380.27	663.57	1424.62
Average speed [km/h]	47.01	58.04	62.83	65.87	60.45	47.59	56.76	43.82	55.30
Legal speed [km/h]	90	90	90	90	90-70	90-70	70	70	70-90

Ring road						
N°	20	21	22	23	24	Average
Length [m]	614.70	364.67	280.75	250.66	622.79	426.71
Average speed [km/h]	18.38	22.86	46.42	29.34	29.22	29.24
Legal speed [km/h]	90	90	90	90	90	90

Urban cycles are in average 336m long, with an average speed of 26.85km/h and a legal speed equal to 50km/h in most cases. Mid-urban cycles a little longer and faster than urban ones, with an average length of 582m and an average speed of 39km/h. Ring road cycles are located close to on-ramps/off-ramps that could explain the small average speed observed: 29km/h. These cycles are 426m long in average. The average length of regional cycles is about 1.4km with a maximum cycle length of 2.6km. These cycles are also faster than the ones of the other categories, their average observed speed is equal to 55km/h.

3.3 Conclusion of the chapter

This chapter proposed several methods to reconstruct the trajectory of the Follower and its Leader. Moreover, these methods were compared and one of them has been defined as the most suitable for our study. This method first consists in filtering the measured speed of the truck with a moving average to remove noise due to the measure. Then, its position is computed thanks to the trapezoidal scheme, and the position of its leader is computed by adding the measured spacing and the length of the vehicle to the position of the truck. Then, the speeds are computed by derivating the positions with trapezoidal scheme, and they are filtered. The acceleration profiles are computed in the same manner.

Once the reconstruction method has been defined, the complete couples of trajectories are computed and the cycles are classified into four categories: urban, mid-urban, regional and ring road cycles, having similar characteristics.

The cycles computed in this chapter will be used in Chapter 4 to calibrate, assess and compare the car-following models ability to reproduce the truck behaviour. In Chapter 5, these cycles will be used to evaluate the car-following models on fuel consumption estimation.

3.4 References

Kayvan Aghabayk, Majid Sarvi, and William Young. Including heavy vehicles in a car-following model: modelling, calibrating and validating. *Journal of Advanced Transportation*, 50(7):1432–1446, November 2016. ISSN 01976729. doi: 10.1002/atr.1409. [3]. p. 34

John-Jairo Martinez and Carlos Canudas-de Wit. A Safe Longitudinal Control for Adaptive Cruise Control and Stop-and-Go Scenarios. *IEEE Transactions on Control Systems Technology*, 15(2):246–258, March 2007. ISSN 1063-6536. doi: 10.1109/TCST.2006.886432. p. 42

Emily Nodine, Andy Lam, Mikio Yanagisawa, and Wassim Najm. Naturalistic Study of Truck Following Behavior. *Transportation Research Record: Journal of the Transportation Research Board*, 2615:35–42, January 2017. ISSN 0361-1981. doi: 10.3141/2615-05. [2]. p. 34

Vincenzo Punzo, Maria Teresa Borzacchiello, and Biagio Ciuffo. On the assessment of vehicle trajectory data accuracy and application to the Next Generation SIMulation (NGSIM) program data. *Transportation Research Part C: Emerging Technologies*, 19(6):1243–1262, December 2011. ISSN 0968-090X. doi: 10.1016/j.trc.2010.12.007. p. 40, 42, 43

Christian Thiemann, Martin Treiber, and Arne Kesting. Estimating Acceleration and Lane-Changing Dynamics from Next Generation Simulation Trajectory Data. *Transportation Research Record: Journal of the Transportation Research Board*, 2088:90–101, December 2008. ISSN 0361-1981. doi: 10.3141/2088-10. p. 34

Tomer Toledo, Haris Koutsopoulos, and Kazi Ahmed. Estimation of Vehicle Trajectories with Locally Weighted Regression. *Transportation Research Record: Journal of the Transportation Research Board*, 1999:161–169, January 2007. ISSN 0361-1981. doi: 10.3141/1999-17. p. 34

US_Dept_Transportation. Federal Highway Administration, 2006. URL https://www.fhwa.dot.gov/publications/research/operations/06137/index.cfm/. p. 34

Thamara Vieira da Rocha, Ludovic Leclercq, Marcello Montanino, Céline Parzani, Vincenzo Punzo, Biagio Ciuffo, and Daniel Villegas. Does traffic-related calibration of car-following models provide accurate estimations of vehicle emissions? *Transportation Research Part D: Transport and Environment*, 34:267–280, January 2015. ISSN 13619209. doi: 10.1016/j.trd.2014.11.006. p. 34

Chapter 4

Calibration of car-following models from HDV trajectories

Contents

The previous chapter presented and compared several methods to compute the complete trajectory of a vehicle from its speed. The selected method consists in integrating the filtered measured speed to obtain the vehicle position, then adding the spacing and the length of the Leader to obtain its position. The positions are then derived with a trapezoidal scheme and filtered. The same process is applied to the speed to compute the acceleration. Using this method, a set of 35 cycles, varying from 166m to 2.6km has been created. Chapter 4 focuses on the calibration of four well-known car-following models: the Gipps model (Gipps, 1981), the IIDM (Treiber and Kesting, 2013a), the Newell's model (Newell, 2002) and the Wiedemann's model (Wiedemann, 1974). The cycles used to calibrate the models were computed in the previous chapter (Chapter 3). Chapter 4 not only focuses on the models calibration but also on the definition of an appropriate method to calibrate each of them.

The study of car-following models already has a long history, but very few studies focus specifically on HDV behaviour (Aghabayk et al., 2015; Nodine et al., 2017) although HDV reactions to traffic are different from those of passenger cars as shown in Aghabayk et al. (2016), Sarvi and Ejtemai (2011) and Aghabayk et al. (2012). For the trucks trajectory we can observe that spacing would be larger, acceleration capabilities are smaller, speed profiles are more complex due to more complex engine chains. Inertia also modifies the driving behaviour of HDV due to the important weight of vehicles. The main studies taking into account truck-following behaviour focus on the differences in following reactions (Aghabayk et al., 2012, 2016; Nodine et al., 2017; Sarvi and Ejtemai, 2011) depending on the follower and the leader type (passenger car or HDV). Some other studies describe the influence of heterogeneous vehicle flow on traffic instabilities (Chen et al., 2016; Liu et al., 2016; Yang et al., 2014).

To capture the heterogeneity of actual road traffic, several modified car-following models were previously developed. Previous studies about truck-following rule were either based on specific mode formulation (Aghabayk et al., 2016; Liu et al., 2016), on quite complex existing car-following rules (Aghabayk et al., 2016) or on new developed models based on the local linear mode tree approach, LOLIMOT, (Aghabayk, 2013; Aghabayk et al., 2013). All these studies used data from the NGSIM project. The trajectories used were collected on the Hollywood freeway (U.S.101) and on the Berkeley Highway (I-80) in California. They are respectively 640m and 503m long. Here, we want to assess if usual car-following models, with dedicated parameters settings can accurately reproduce truck behaviour under different applications: urban, mid-urban, regional and ring road.

This chapter is divided into five sections. The first three sections are about the definition of the calibration method and a particular attention is given to the GoF and to the MoP on which computing the error between measured and simulated data. The first section focuses on the choice of the GoF function, four functions are compared. The second section investigates the influence of the simulation time step on calibration results and on the value of car-following parameters. Then, the third section examines the influence of the derivation/integration scheme (named solver in this thesis) on calibration results. Finally, the ability to reproduce truck behaviour under different applications of the four car-following models studied is compared, and the robustness of the calibration is verified.

4.1 Data description

The first part of this study is based on a subset of cycles created in previous chapter. For each cycle category, urban, mid-urban, regional and ring road, a representative cycle is selected for the study. These cycles are detailed in Chapter 3, section 3.2.2 p.44.

4.2 Influence of the GoF function and choice of the MoPs

The different studies comparing the calibration of car-following models mainly focus on error on position or speed. It has been previously shown (Punzo and Montanino, 2016) that it is better to use as MoP the spacing (or the position) instead of the speed when we want to minimize error on both position (or spacing) and speed. However, these studies were done by using a single MoP (Kesting and Treiber, 2008; Punzo and Montanino, 2016; Punzo and Simonelli, 2005) or combined MoP (Kim and Mahmassani, 2011; Ossen and Hoogendoorn, 2008), but not using a MO calibration. This solution is investigated here.

The GoF functions studied in this thesis are often used for the calibration of car-following models. These functions are the RMSE, the RMSPE, the SE and the Theil's inequality coefficient (U). These functions are described in Chapter 2, section 2.5.2 p.20.

4.2.1 Method

Prior to looking for optimal parameters values, we first investigate the response of the GoF function to a large range of parameter values. For each car-following model, a range of variation of the parameters to calibrate is defined (Table 4.1). Gipps' model, IIDM and Wiedemann's model have a parameter representing the desired speed of the Follower. The range of variation of this parameter depends on the type of cycle: urban, mid-urban, regional and ring road. It is defined according to the category of cycle in Table 4.2.

Actually, if the GoF function is flat, the optimal domain is large and so the calibration process will not lead to a narrow definition of optimal parameters. Moreover, due to the truck kinematics that is more complex than the passenger car one and because of the important vehicle weight that results in high inertia, we want to focus on multiple objectives (position, spacing, speed and acceleration) when calibrating the models. The calibration problem is then formulated as a MO optimization problem. It is also interesting to evaluate the intersection of optimal domains obtained independently for position, spacing, speed and acceleration. If this intersection is close to the union, it means that all independent processes converge to the same consistent region for optimal parameters. If this intersection is void it means that a single but MO calibration process is mandatory to determine a relevant set of optimal parameter values.

To compute a surface grid of the GoF functions, trajectories are simulated for each possible combination of parameters and the error between the simulated trajectory and the measured one is computed with each of the four GoF functions. To study the shape of the GoF functions, we compare the size of optimal domains.

Optimal domains are defined for each of the criteria that we want to optimize the error on. These variables are, as mentioned in previous paragraphs:

- the position of the Follower,
- the spacing between the Follower and the Leader,
- the speed of the Follower and,
- the acceleration of the Follower.

The optimal domains are defined as follow: we search for the point which provides the minimum error for the variable, then, five optimal domains are defined. The first one contains the points for which the error is between the minimum error and the minimum error plus 10%. The second domain contains points between the minimum error and the minimum error plus 20%, and so on until the minimum error plus 50%.

Table 4.1 – Variation of car-following models parameters for meshing of the GoF functions

Car-following model	Parameter	Minimum	Step	Maximum
Gipps	τ_n $[s]$	0.2	0.3	3.8
	V_n^{des} $[m/s]$			
	a_n $[m/s^2]$	0.5	0.4	2.9
	$SafetyMargin$ $[m]$	0.1	0.5	4.6
	$\hat{b}_{n-1}$ $[m/s^2]$	-6.1	0.5	-0.1
	b_n $[m/s^2]$	-4.1	0.5	-0.1
IIDM	a_n $[m/s^2]$	0.1	0.2	3.9
	V_n^{des} $[m/s]$			
	$s0$ $[m]$	0.1	0.5	4.6
	T $[s]$	0.1	0.2	2.9
	b_n $[m/s^2]$	-2.1	0.2	-0.1
Newell	w $[m/s]$	5	1	70
	ρ $[m]$	0.2	0.5	50.2
Wiedemann	$AXadd$ $[m]$	1.3	0.5	5.3
	$BXadd$ $[m]$	5	5	5
	$CXconst$	25	5	75
	$EXadd$	1	1	5
	$OPDVadd$	1	1	3
	$BNULLmult$ $[m/s^2]$	0.05	0.05	0.2
	$BMINadd$	5	3	20
	$BMINVmult$	0.05	0.05	0.5
	V_n^{des} $[m/s]$			

Table 4.2 – Variation of parameter V_n^{des} for meshing of GoF functions in km/h

Category	Minimum	Step	Maximum
Urban	40	2	50
Mid-Urban	48	3	68
Regional	70	3	85
Ring road	75	3	85

Moreover, the Gipps' model and the IIDM are subject to constraints (see 2, section 2.3 p.12 for details). For these models, as for the optimal domain, an optimal and stable domain is defined containing the points of the optimal domains which fulfil the constraints.

The number of points in each optimal domain, expressed as a percentage of the total number of tested points, is compared. First, the evolution with the accepted error of the size of the optimal domains is studied. If the size of the domain increases a lot with the percentage of accepted error, it means that the optimal domain is quite flat, so a large range of parameters are acceptable.

4.2.2 Size of optimal domains

The evolution of the size of the optimal domains is similar whatever the car-following model studied and the type of cycle. An illustration of this evolution is presented in figures 4.1 to 4.4, for Gipps' car-following model, on an urban cycle. Its first axis represents the optimal domains for the four variables (position, speed, acceleration and spacing) and two intersection domains. The first intersection domain represents the common points of optimal domains in position, speed, and acceleration. The second is for common points for optimal domains in spacing, speed and acceleration. The second axis corresponds to the percentage of accepted error, from 10% to 50%. And the last axis (vertical) represents the percentage of points in the optimal domain.

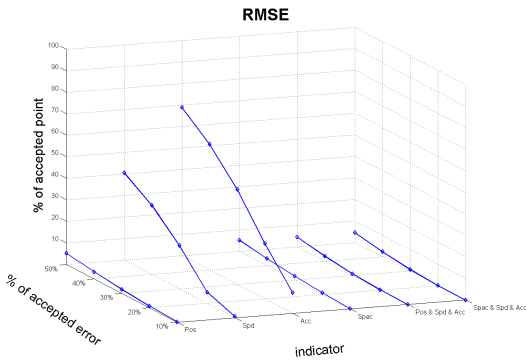

Figure 4.1 – Evolution of the size of optimal domains for RMSE function

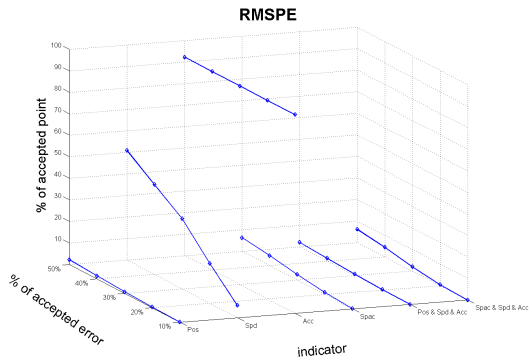

Figure 4.2 – Evolution of the size of optimal domains for RMSPE function

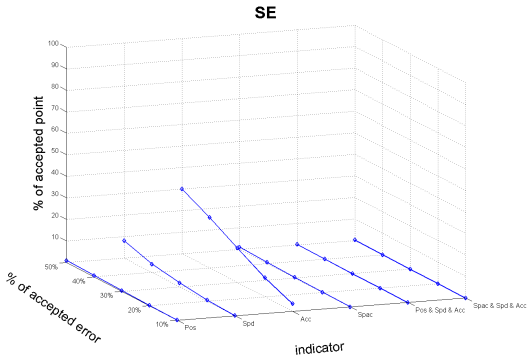

Figure 4.3 – Evolution of the size of optimal domains for SE function

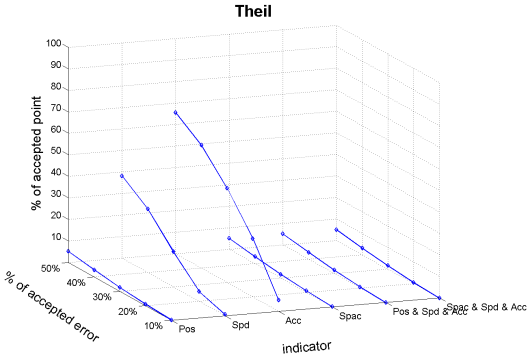

Figure 4.4 – Evolution of the size of optimal domains for Theil's inequality coefficient

For the optimal domains in position and spacing, the results are quite identical. The sizes of the optimal domains increase very little with the accepted percentage of error. Moreover, these two domains are really close to each other even if the optimal domain for spacing is a bit larger. This observation is valid for the four GoF functions.

The RMSPE function is not usable in our case. Its mathematical formulation prevents it from being used because we would like to take into account position (or spacing), speed and acceleration. When the values of the speed or acceleration are small or null, the value of the error computed with the RMSPE immediately increases a lot (Figure 4.2), which makes this function not relevant for this application.

The optimal domains for speed and acceleration are very sensitive to the percentage of accepted error. From 20% of accepted error, their sizes increase quickly. The three GoF functions (RMSE, SE and Theil's coefficent) behave in the same way. However, the optimal domains of the RMSE and Theil's inequality coefficient have almost the same size; whereas for the SE, domains are smaller. It means that the SE GoF function is less flat than the RMSE and Theil's inequality coefficient.

4.2.3 Intersection of optimal domains

To conclude on which GoF functions to use, the sizes of the intersection domains are compared. For the SE function, the intersections are always inexistent (Figure 4.3). This inexistence of intersections means that the optimal domains obtained independently for position, spacing, speed and acceleration are distinct and running a MO calibration in that case would imply to arbitrate between objectives. In the case presented here, intersection domains exist for the RMSE (Figure 4.1) and Theil's inequality coefficient (Figure 4.4). However, this is not the case for all models and cycles. Only Theil's inequality coefficient ensures the existence of intersection of optimal domains in most of the cases studied. Moreover, when both RMSE and Theil's coefficient provide the existence of intersections, for equivalent percentage of accepted error, the size of intersection domains is a little greater with Theil's function than with the RMSE.

4.2.4 Conclusion

To conclude, the RMSPE is not a relevant function to use in our case even if it seems good for calibration of position and spacing. The SE function does not provide good results for the research of intersection of optimal domains. Considering RMSE and Theil's inequality coefficient, they are similar if we want to calibrate on position or speed or acceleration or spacing. However, only Theil's inequality performs better than the RMSE in providing the intersection of optimal domains. This function is chosen for the rest of the study.

It was previously demonstrated that it is preferable to use spacings as MoP (Kesting and Treiber, 2008; Punzo and Montanino, 2016; Punzo and Simonelli, 2005). This result is consistent with the one we found. As illustrated in Figures 4.1 to 4.4, the optimal domain for spacing is really less flat than speed or acceleration optimal domains, that ensure to find a minimum more easily than for the other MoP. However, the final objective of the calibration method developed in this paper is to have a car-following model well calibrated to compute the FC of industrial vehicles: the error on speeds and accelerations must be minimized too. Then, MO calibration is needed for the application considered in this study.

Two intersections of optimal domains were defined. The second intersection domain (spacing, speed and acceleration) is generally greater than the first one (position, speed and acceleration) because the optimal domain for spacing is a little bigger than the optimal domain for position. To ensure that the MO calibration algorithm will find the maximum of possible optimal points and the best, it will be run with the three variables which allow the biggest intersection domain: spacing, speed and acceleration.

4.3 Influence of the time step

In order to define a calibration method adapted to each car-following model, the influence of the simulation time step value on calibration results is investigated. This study is made on the four car-following models presented previously. The influence of the time step will be investigated on two points: the value of the cost function according to the value of the time step and the sensitivity of the parameters value to time step variation.

4.3.1 Method

The calibration of the car-following models is done on the four cycles used in the previous paragraph and with Theil's inequality coefficient as GoF function. Four time steps are compared: $0.01s$, $0.1s$ (the time step of the measurements), $0.5s$ and $1s$. The time step and solver influences are studied independently. The Mixed solver is arbitrarily chosen here.

4.3.2 Evolution of errors with respect to simulation time steps

The different time steps tested do not have the same influence on the value of the error depending of the car-following model. The MO calibration generate a set of possible solutions (*particles*) for the problem we want to solve. Error values mentioned in the following sections refer to the particle *Compromise* (defined in Chapter 2, section 2.5.5, p.24). The *Compromise* particle is the one for which the error is the closest, according to the Euclidian distance, to the optimal point $(0,0,0)$. The evolution of the error for growing time steps values are summarized in Table 4.3.

Table 4.3 – Evolution of errors with respect to simulation time steps

		Error on			
		Position	Spacing	Speed	Acceleration
Gipps	Urban	→	↗↘	→	→↗
	Mid-Urban	→	→↗	→	→
	Ring Road	→	→↗	→	↗↘↗
	Regional	→	↗↘↗	→	↗↘↗
IIDM	Urban	→	→↘	→	→↗
	Mid-Urban	→	↗↘↗	→	↗↘↗
	Ring Road	→	↘	→	↗
	Regional	→	↗↘↗	→	→↗
Newell	Urban	→	→↗	→	→
	Mid-Urban	→	↗↘↗	→	→
	Ring Road	→	↗↘	→	↗
	Regional	→	↗↘↗	→	↗
Wiedemann	Urban	↗↘↗	↗↘↗	↗↘↗	↗↘↗
	Mid-Urban	→↘	↗↘↗	→↘	↗
	Ring Road	↗↘↗	↗↘↗	↗↘↗	→
	Regional	→	↗↘↗	→↗	↗

a) Gipps' car-following model

The error on position is generally stable whatever the values of the time step (around 1%).

However there is not a global tendency that can be highlighted, regarding the evolution of the errors values. These errors depend both on the type of cycle and the particle selected. But a bigger time step provides greater error on spacing (Figure 4.5), where in this case the value of the error increases from 5% to 12%.

b) Improved Intelligent Driver Model

For the four cycles and the four particles, the values of the error in position and speed do not change with time step, the gap does not exceed 1.5% (Figure 4.6). Globally, whatever the particle, the error on acceleration is lower with the smaller time step ($0.01s$), 36% instead of 45% as illustrated in Figure 4.6, which is consistent with the model initial formulation (analytic and continuous). The evolution of the error on spacing is less stable than the others.

c) Newell's car-following model

For the values of the error in position and in speed, the time step has no influence. The variations of the values of the errors in position and speed do not exceed 2%.

For the acceleration, the evolution of the values of the error depends on the type of cycle. On the ring road cycle, the error increases a lot ($+7\%$) with time step (Figure 4.7), for the regional road, the error is quite stable whatever the time step ($+/-1\%$), whereas for mid-urban and urban cycles, its error decreases a little (-2%).

So, an intermediate time step, seems to be better to be used with Newell's model.

d) Wiedemann's car-following model

There is not a global tendency that can be highlighted for Wiedemann's car-following model.

For the urban cycle (Figure 4.8), values of error in position for a time step equal to $0.01s$ and $0.5s$ are close to each other (around 3%), whereas for a time step of $1s$, the error is really higher (22%). For a time step of $0.1s$, the value of the error is a bit higher than for $0.01s$ and $0.5s$ time steps. On a mid-urban cycle, errors on position, speed and acceleration are lower for intermediate time steps. The gap between error values is at least of 10%.

On regional and ring road cycles, errors on position, speed and acceleration vary little with time steps.

For the error in spacing, values vary a lot with the particle and the cycle. Time step equal to 1s is globally not as good as the others, particularly on urban and mid-urban cycles. Errors in spacing are lower for a time step of 0.5s whatever the category of the cycle for the particle *Compromise*. Moreover, time step 0.1s provides a higher error on spacing for *Compromise* particle. It is illustrated in Figure 4.8.

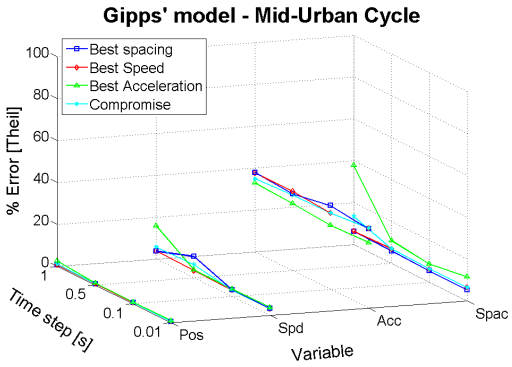

Figure 4.5 – Evolution of the error vs simulation time step for Gipps' model on a mid-urban cycle

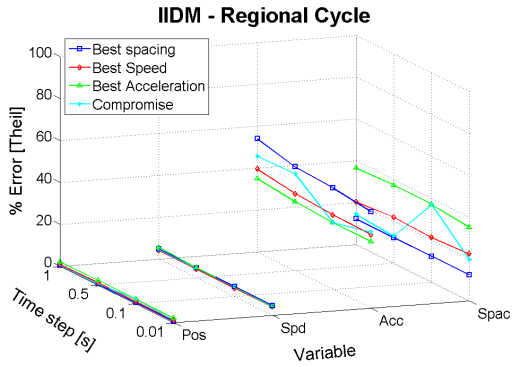

Figure 4.6 – Evolution of the error vs simulation time step for IIDM on a regional cycle

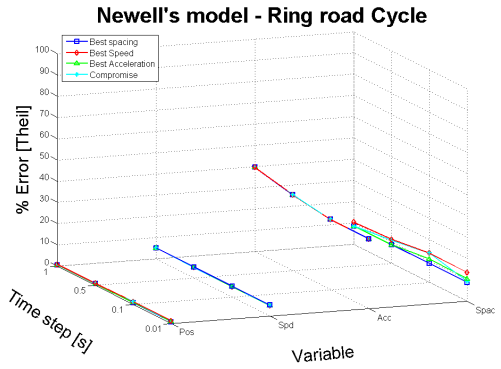

Figure 4.7 – Evolution of the error vs simulation time step for Newell's model on a ring road cycle

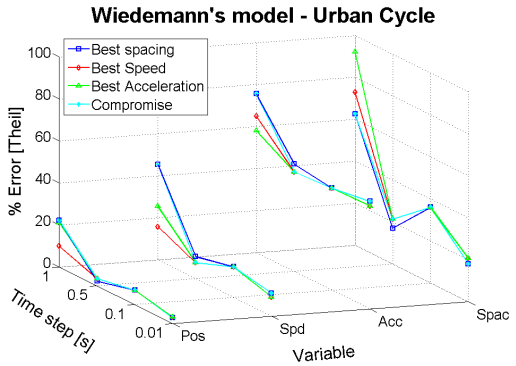

Figure 4.8 – Evolution of the error vs simulation time step for Wiedemann's model on an urban cycle

4.3.3 Parameters values evolution with time step

Observation of the time step influence on the values of optimal parameters

The simulation time step has also a strong influence on the values of the optimal parameters of the Pareto front. Qualitative observations are detailed in the following paragraphs.

For the Gipps's car-following model and the IIDM, deceleration parameters (b_n and $\hat{b}_{n-1}$) are really sensitive to time step variation whereas distance parameters ($SafetyMargin$ and $s0$) do not depend on time step (Figure 4.9 and Figure 4.10). Moreover, the optimal values found with time steps equal to 1s and 0.5s are generally close to each other.

For Newell's model, parameter w does not depend on the time step (Figure 4.11 and Figure 4.12). However, the distributions of the parameter ρ of the Newell's model are similar for the time steps equal to 0.01s and 0.1s. The time steps 0.5s and 1s, provide another distribution of this parameter.

The dependence to the value of the time steps for Wiedemann's car-following parameters depends on the cycle. For regional cycles, $CXconst$, V_n^{des}, $EXadd$, $BXadd$ and $OPDVadd$ are not sensitive to the time step whereas for the other categories of cycles, their values completely depend on it (Figure 4.13 and Figure 4.14). For the other parameters, if there is dependence, one can observe similar distributions for the lowest time steps, and another one for the highest time steps like for the Newell's model.

Finally, we can observe that some parameters are really sensitive to the value of the time step. In particular for Gipps' car-following model and the IIDM, the deceleration parameters are really dependent contrary to

parameters related to distance $SafetyMargin$ and $s0$.

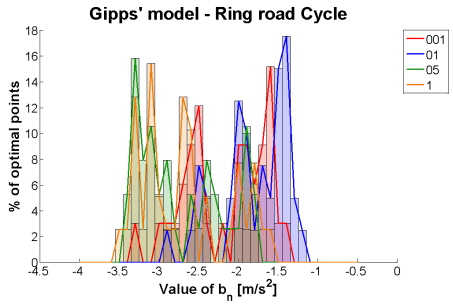

Figure 4.9 – Influence of time step on b_n value for Gipps' model on ring road cycle

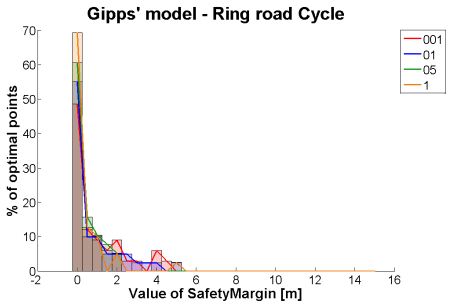

Figure 4.10 – Influence of time step on $SafetyMargin$ value for Gipps' model on ring road cycle

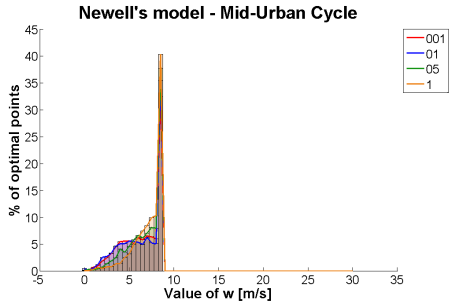

Figure 4.11 – Influence of time step on w value for Newell's model on mid-urban cycle

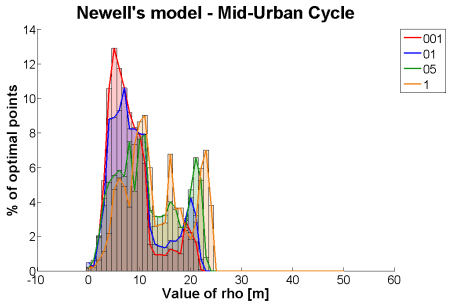

Figure 4.12 – Influence of time step on rho value for Newell's model on mid-urban cycle

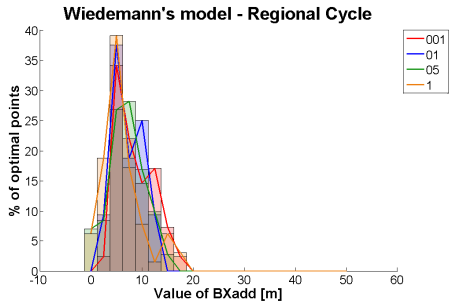

Figure 4.13 – Influence of time step on $BXadd$ value for Wiedemann's model on regional cycle

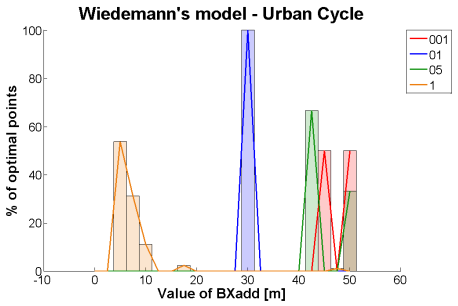

Figure 4.14 – Influence of time step on $BXadd$ value for Wiedemann's model on urban cycle

Synthesis of the time step influence using a PCA

In order to highlight more precisely the relation between car-following parameters values and the simulation time step, a PCA is applied to the calibration results of the Gipps' model and the IIDM. Some interesting results are highlighted in the following paragraphs.

Figures 4.15 and 4.16 present the distribution and classification of the results of Gipps' model calibration on a regional cycle. Four classes have been achieved using both PCA and hierarchical clustering technique. We can observe that Class 1 is placed on the negative side (b_n, V_n^{des}) of the first axis, it is opposed to Class 4, on τ side. Moreover, the majority of points from $t_{step} = 0.01s$ and $t_{step} = 0.1s$ are in Class 1, whereas the majority of points from $t_{step} = 0.5s$ and $t_{step} = 1s$ are in Class 4. The smaller time steps are opposed to the higher time steps.

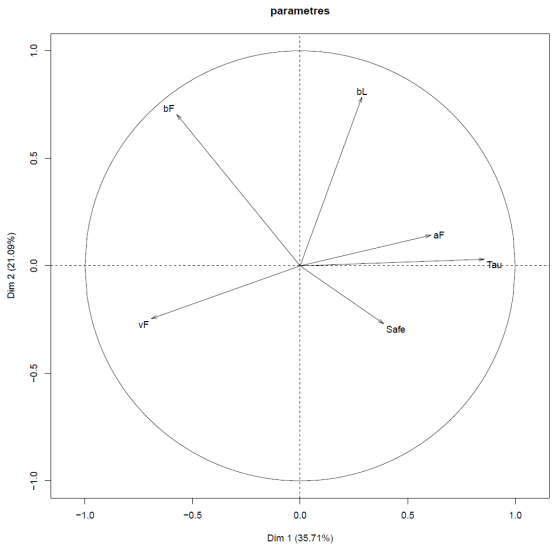

Figure 4.15 – Correlation circle, Axis 1 and 2 of the PCA of the Gipps' model on regional cycle

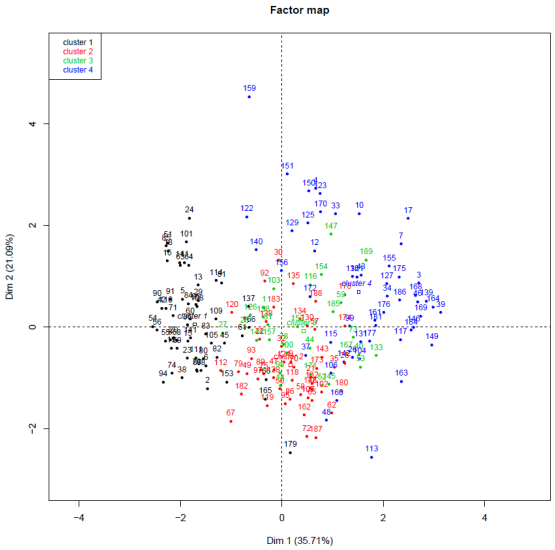

Figure 4.16 – Classification (4 classes) of calibration results of Gipps' model on regional cycle

Figures 4.17 and 4.18 present the distribution and classification of the results of IIDM calibration on a regional cycle. The higher time step (Class 5) implies high b_n and τ, and small a_n and V_n^{des}. Class 1 and 3 (containing in majority points from small time steps groups) imply high values of a_n and V_n^{des}, and small values of $s0$ and b_n. As for the Gipps' model, the smaller time steps are opposed to the higher time steps for the IIDM.

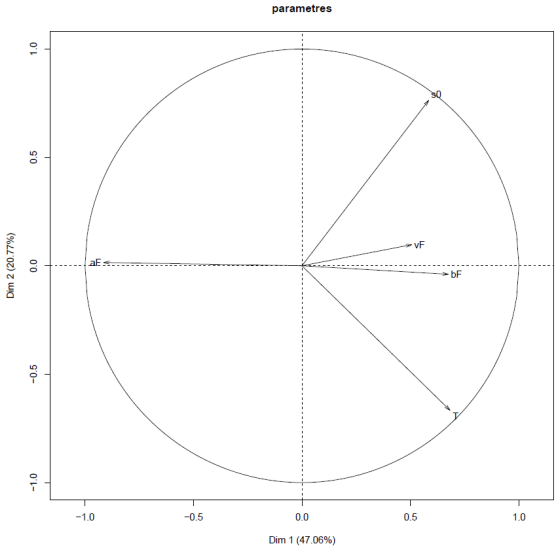

Figure 4.17 – Correlation circle, Axis 1 and 2 of the PCA of the Gipps' model on regional cycle

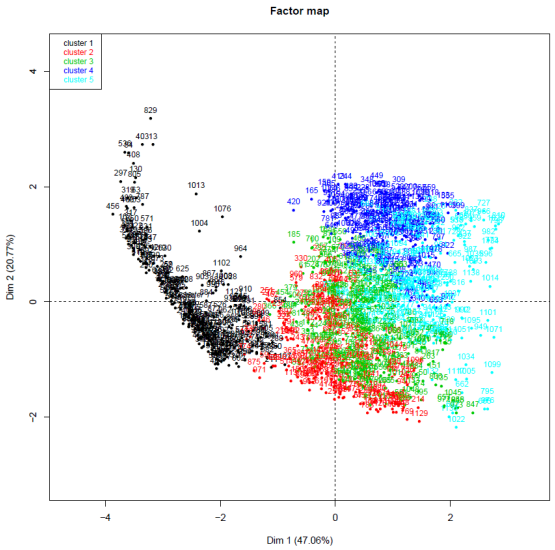

Figure 4.18 – Classification (4 classes) of calibration results of Gipps' model on regional cycle

4.3.4 Conclusion

According to the error values, some time steps seem more relevant than others. For Gipps' car-following model, the time step which provides generally the lowest error should be consistent with the measurement time step, i.e. $0.1s$. However, for the IIDM, it is the smaller time step ($0.01s$) which provides the smallest errors. Newell's and Wiedemann's car-following model calibration are better with an intermediate time step equal to $0.5s$.

Those results are not consistent with the one presented in Treiber and Kesting (2013c) where the conclusion

is that a smaller time step ($0.1s$) is not better than a greater one ($1s$). This could be due to the use of a different set of data or to a more complex kinematic for trucks rather than cars. The values of the error on position, speed, acceleration and spacing are presented in Table 4.4 for the selected time steps on the four cycles used for the study.

Table 4.4 – Errors on the trajectories for the selected time steps

	Category of cycle	Error on position [%]	Error on speed [%]	Error on acceleration [%]	Error on spacing [%]
Gipps [0.1s]	Urban	0.67	4.36	33.31	5.49
	Mid-urban	0.71	3.67	30.62	7.75
	Regional	0.67	2.72	30.69	15.24
	Ringroad	1.73	3.86	25.94	8.73
IIDM [0.01s]	Urban	3.97	5.75	37.10	24.57
	Mid-urban	1.53	8.51	62.08	15.93
	Regional	0.91	4.07	36.24	19.66
	Ringroad	2.11	7.32	45.49	20.82
Newell [0.5s]	Urban	1.68	5.90	37.92	12.21
	Mid-urban	2.80	6.28	45.59	24.12
	Regional	1.13	3.34	35.34	23.28
	Ringroad	0.96	5.02	35.79	10.95
Wiedemann [0.5s]	Urban	3.44	7.73	47.38	21.57
	Mid-urban	1.78	6.03	44.80	22.40
	Regional	3.14	19.43	75.58	61.67
	Ringroad	1.30	8.93	39.35	16.49

4.4 Influence of the solver

This section investigates the influence of the solver on calibration results. The solver influence will be investigated based on two different considerations: the value of the GoF function according to the solver and the sensitivity of the parameters value to the solver used. As in the previous sections, error values mentioned refer to the particle *Compromise*, it will be precised when it will not be the case.

4.4.1 Method

The calibration of the car-following models is done on the four cycles used in previous sections of this chapter and with Theil's inequality coefficient as GoF function. The simulation time step used was defined in the previous section: $0.1s$ for the Gipps' model, $0.01s$ for the IIDM and $0.5s$ for the Newell's and the Wiedemann's model. Five solvers are compared: the Euler Explicit scheme, the Euler Implicit scheme, the Trapezoidal scheme, the Mixed solver and Runge-Kutta of order 4. These solvers are detailed in Chapter 2, section 2.5.4 p.21.

Due to the mathematical formulation of the car-following models, all solvers cannot be tested for each model. Table 4.5 presents the mapping of the car-following and the solver. Empty cells refer to impossible combinations.

Table 4.5 – Usage of solvers with car-following models

	Euler Explicit	Euler Implicit	Trapezoidal	Mixed	RK4
Gipps	√	√	√	√	√
IIDM	√			√	√
Newell	√	√	√	√	
Wiedemann	√			√	√

4.4.2 Different error values for different solvers

a) Gipps' car-following model

The most complex solver, Runge-Kutta of order 4 (RK4), provides the largest errors on spacing, around 55% compared to less than 20% for the other solvers. The errors on position and speed also increase with this solver up to 10% whereas the other solvers provide errors around 1% and 5% respectively for the position and the speed, and this for all the cycles types.

The four other solvers perform similarly (Figure 4.19). The error on position is around 1% and around 5%, respectively for the position and the speed. For the acceleration, the errors oscillate between 25% and 30%, and between 8% and 15% for the spacing.

b) Improved Intelligent Driver Model

In most of the cases, RK4 provides largest errors than the other solvers for the four indicators: position, speed, acceleration and spacing. For the acceleration the error value resulting from the use of the RK4 solver is from 5% to 20% higher than the error resulting from the use of the Mixed or the Euler Explicit solvers. For the spacing on the regional and mid-urban cycles, the error value is almost multiplied by 4 when using the RK4 solver instead of the Euler Explicit solver (Figure 4.20).

The two other solvers perform similarly for the position and the speed. However for the acceleration the smallest error is provided by the Mixed solver on mid-urban and regional cycles, for the two other cycles, the errors are similar. On ring road and urban cycles, the Mixed solver provides the lowest errors for the spacing, whereas for regional and mid-urban cycles the smallest errors are found when using the Euler Explicit solver.

c) Newell's car-following model

Errors increase with Euler Implicit solver, in particular for urban and mid-urban cycles (Figure 4.21) on acceleration and spacing. The three other solvers perform similarly. The Newell's model is the one which is the less sensitive to the solver.

For all cycles, errors are around 1% and between 5% and 10%, respectively for the position and the speed. On urban and mid-urban cycles, the errors on acceleration are lower than on regional and ring road cycles, respectively around 28% and around 40%.

d) Wiedemann's car-following model

For Wiedemann's model, the influence of the solver depends on the category of the cycle and on the particle.

On urban cycle, the Mixed solver performs better than the other solvers. On error on spacing, there is a big increase of the value of the error for RK4 (Figure 4.22).

On regional cycle, the Mixed solver globally performs well except for *Compromise* particle on the error on spacing where there is a big increase of the error.

On ring road cycle, for the error on spacing, particles *Best Spacing* and *Best Speed* provide highest error with RK4, whereas particles *Best Acceleration* and *Compromise* provide lowest error with RK4.

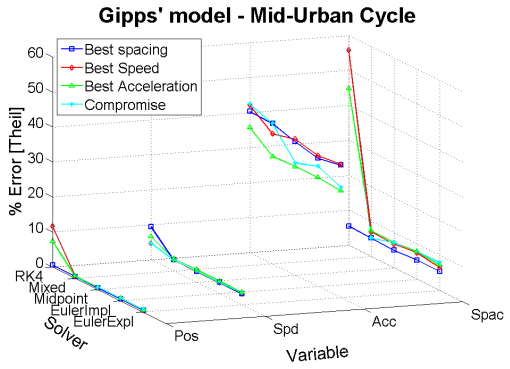

Figure 4.19 – Evolution of the error vs solver for Gipps' model on a mid-urban cycle

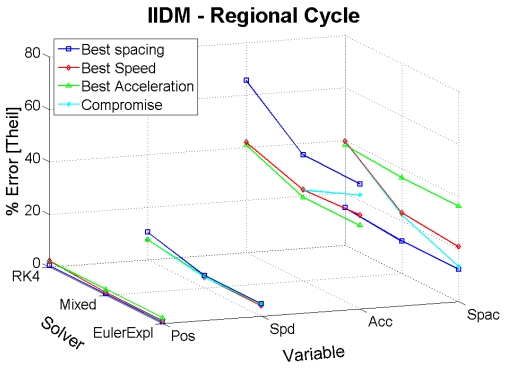

Figure 4.20 – Evolution of the error vs solver for IIDM on a regional cycle

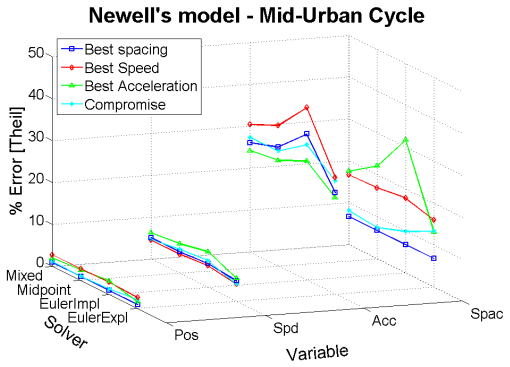

Figure 4.21 – Evolution of the error vs solver for Newell's model on a mid-urban cycle

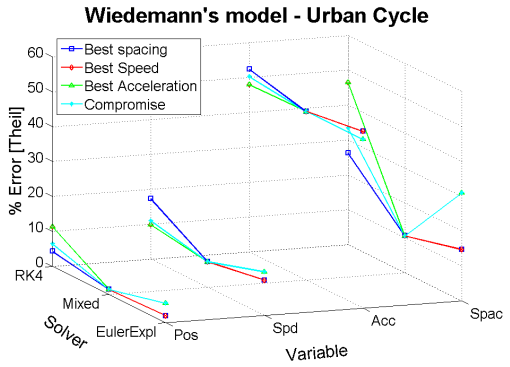

Figure 4.22 – Evolution of the error vs solver for Wiedemann's model on an urban cycle

4.4.3 Relation between parameter values and solver

a) Gipps' car-following model

We can observe that RK4 solver often provides really different distributions of values (Figure 4.24) for the parameters of Gipps' car-following model. Sometimes it is close to the Euler Explicit or the Euler Implicit scheme. Moreover, we can say that the deceleration parameters b_n and $\hat{b}_{n-1}$, and the acceleration a_n are really sensitive to the solver used (Figure 4.23). Using RK4 solver leads to higher acceleration values and higher deceleration absolute values. The other parameters values are not so much influenced by the choice of the solver.

b) Improved Intelligent Driver Model

For the IIDM, parameters for ring road cycles do not depend much on the solver used (Figure 4.25). The distribution of the optimal parameters values are similar whatever the solver used.

As for Gipps' car-following model, the deceleration parameter b_n and a_n are more sensitive to the solver than other parameters. Moreover $s0$ and T also depend on the solver used: values of parameters in the Pareto front are generally close if the solver used is Euler Explicit or the Mixed solver, but different if we choose RK4 (Figure 4.26).

With the RK4 solver, the deceleration capacity is smaller, the acceleration is higher, the minimum bumper-to-bumper gap is higher for mid-urban and regional cycles and the bumper-to-bumper time gap is smaller for urban and regional cycles.

c) Newell's car-following model

The values of the Pareto points resulting of the calibration of Newell's car-following model do not depend on the solver used (Figure 4.27 and Figure 4.28). The distribution of the optimal parameters are almost identical whatever the solver used, the calibrations lead to small values of ρ and w.

d) Wiedemann's car-following model

For the Wiedemann's model, we can observe that the values of the parameters for regional cycle do not depend a lot on the solver used, except $BMINadd$, $BMINVmult$ and $BNULLmult$, contrary to the values for urban, mid-urban and ring road cycles (Figure 4.29 and Figure 4.30).

For these cycles, $BMINadd$ and $BMINVmult$ do not depend on the solver used contrary to regional cycle. Moreover, $AXadd$, $BXadd$, $CXconst$, $EXadd$, $OPDVadd$, $BNULLmult$ and V_n^{des} strongly depend on the solver used. The three solvers provide three different distributions of parameters values, a difference between RK4 and the other solvers is not observable like for the Gipps' model or the IIDM.

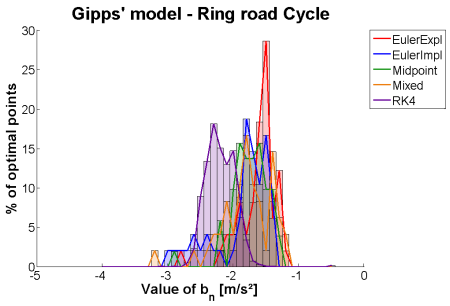

Figure 4.23 – Influence of solver on b_n value for Gipps' model on ring road cycle

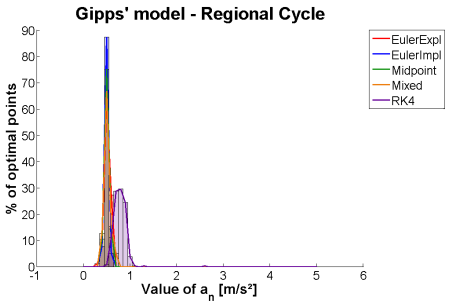

Figure 4.24 – Influence of solver on a_n value for Gipps' model on regional cycle

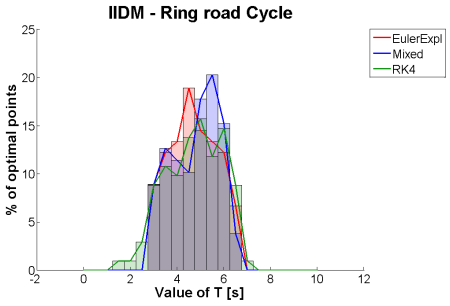

Figure 4.25 – Influence of solver on T value for IIDM on ring road cycle

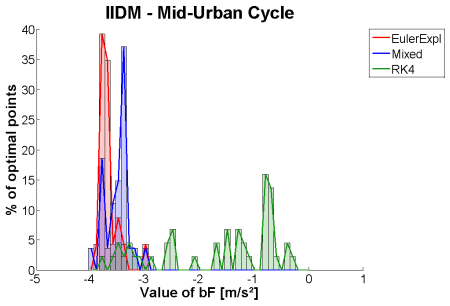

Figure 4.26 – Influence of solver on T value for IIDM on mid-urban cycle

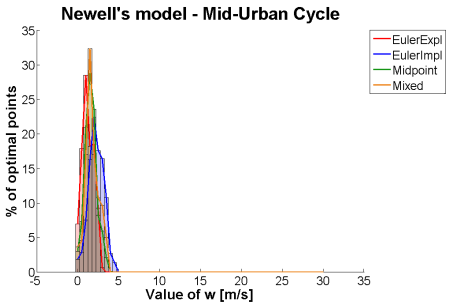

Figure 4.27 – Influence of solver on w value for Newell's model on mid-urban cycle

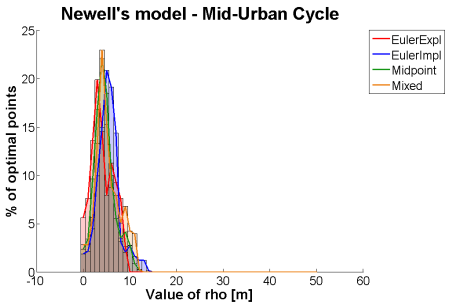

Figure 4.28 – Influence of solver on ρ value for Newell's model on mid-urban cycle

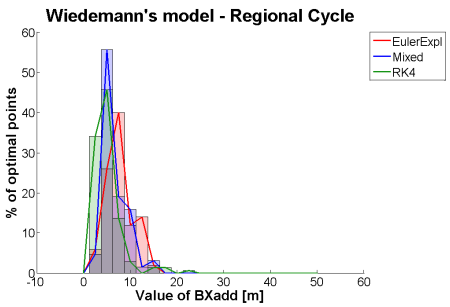

Figure 4.29 – Influence of solver on $BXadd$ value for Wiedemann's model on regional cycle

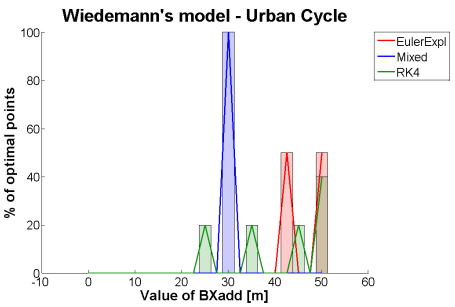

Figure 4.30 – Influence of solver on $BXadd$ value for Wiedemann's model on urban cycle

4.4.4 Conclusion

RK4 leads to a different distribution of parameters that explains the fact that it provides trajectories with higher errors than the other solvers studied.

The same conclusion as the one proposed in the literature (Treiber and Kesting, 2013b) can be done. RK4 does not perform better than simpler solvers. The four other solvers are generally close to each other but in most cases it is the Mixed solver which performs the best by providing the smallest errors on the major part of the indicators. This solver will be used for the calibration of the four car-following models.

4.5 Calibration of the four car-following models

The previous sections allow defining an optimal calibration method for each car-following model tested here. These methods were defined on some cycles extracted from the original set of 35 cycles. The following sections present the calibration results of the car-following models on the entire set of cycles.

The four car-following models studied are calibrated with their own optimal method (summarized in Table F.1) using MOPSO method (see Chapter 2, section 2.5.5 p.24) on spacing, speed and acceleration.

Table 4.6 – Optimal method to calibrate car-following models

	Goodness-of-Fit function	Measure of Performance	Simulation time step	Solver
Gipps	Theil's inequality coefficient	Spacing/Speed/Acceleration	0.1s	Mixed
IIDM	Theil's inequality coefficient	Spacing/Speed/Acceleration	0.01s	Mixed
Newell	Theil's inequality coefficient	Spacing/Speed/Acceleration	0.5s	Mixed
Wiedemann	Theil's inequality coefficient	Spacing/Speed/Acceleration	0.5s	Mixed

4.5.1 Results of the calibration

Comparison of the error values

The calibration of the four car-following models with their optimal method leads to similar results in terms of error in position for all the set of trajectories, except for Wiedemann's model (Figure 4.31). The error in position for the Gipps and the Newell models are respectively 0.89% and 0.86% in average (Figure 4.31). The IIDM provides errors which are slightly higher, 1.96% in average. The position estimation error for the Wiedemann model is really higher, 9.97% in average. The same observations can be done for the error on spacing (Figure 4.32). The Gipps and the Newell models perform the best with average error equal to 7.44% and 7.41% respectively. The error computed with the IIDM is two times greater 14.96%, and the Wiedemann's model is the one which gives the largest error 36.22%.

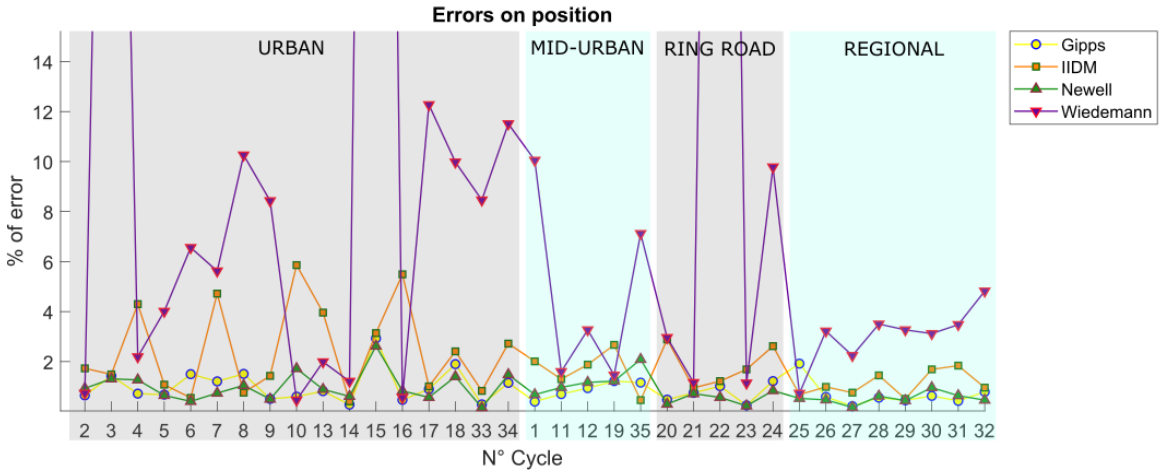

Figure 4.31 – Comparison of position estimation errors

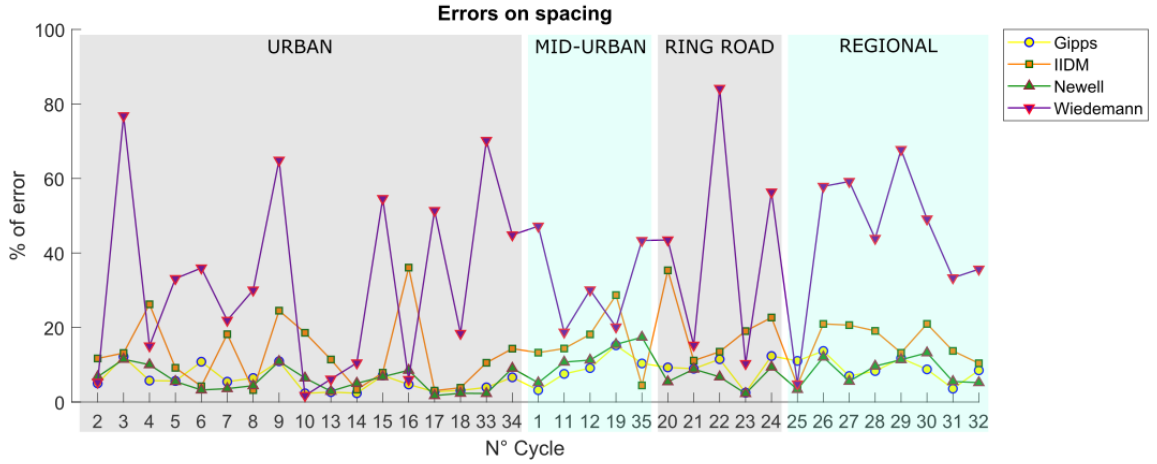

Figure 4.32 – Comparison of spacing estimation errors

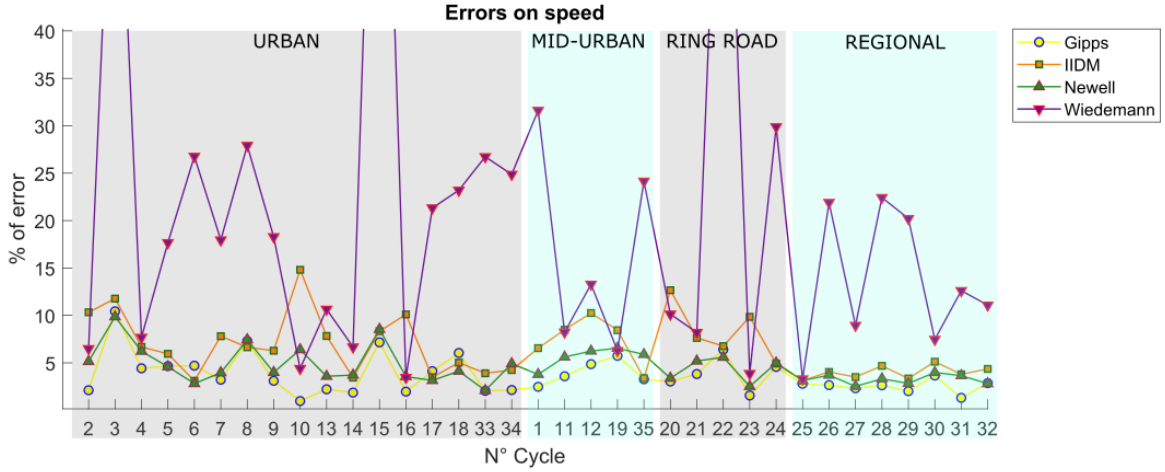

Figure 4.33 – Comparison of speed estimation errors

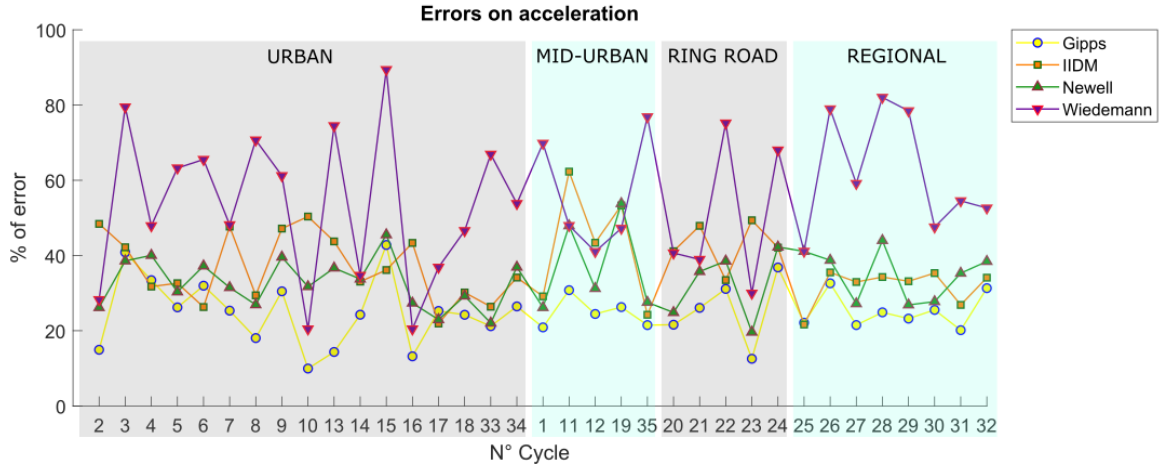

Figure 4.34 – Comparison of acceleration estimation errors

As for the position and the spacing, the Gipps and Newell models are the ones which provide the smallest errors on speed and acceleration. The IIDM also give acceptable errors even if they are a little higher. However, the Wiedemann's model is the one which performs the worst for all the indicators. For the speed the errors with

the Gipps and the Newell models are 3.66% and 4.56% respectively. For the IIDM the error is 6.59% and for the Wiedemann model it is equal to 20.78%. The errors on acceleration are higher than on the other variables, the errors are equal to 25.03%, 33.81%, 37.28% and 55.37% respectively for the Gipps' model, the Newell's model, the IIDM and the Wiedemann's model in average.

In Aghabayk (2013) the author proposed a new model (LOLIMOT) to represent truck-following behaviour and compared it to Gipps' model calibrated with a GA using the SE as GoF function. The MoP used in this study is the speed of the truck. The results presented by Aghabayk are expressed as the RMSE of the speed (in km/h). The results for a truck following a car are $3.27 km/h$ and $6.84 km/h$ respectively for LOLIMOT and Gipps' model. For comparison, the RMSE has been computed on the simulated speed, the results are presented in Table 4.7. In Liu et al. (2016), the authors calibrated the IDM for the four following combinations: car-truck, car-car, truck-car and truck-truck. The IDM has been calibrated with a GA using Theil's inequality coefficient as GoF function. The MoP is the acceleration. The results presented in Liu et al. (2016) are expressed using the Mean Absolute Error (MAE) and the Mean Absolute Normalized Error (MANE) functions, respectively defined in equation (4.1) and (4.2). For the truck-car combination, the results are $5.75 m$ / 3.0% (MAE / MANE), $4.32 km/h$ and $1.24 m/s^2$ respectively for the position, the speed and the acceleration. For comparison, the error on the trajectories simulated thanks to the Gipps' model, the Newell's model, the IIDM and the Wiedemann's model are computed with the MAE and MANE functions. The results are detailed in Table 4.7.

$$MAE = \frac{1}{N}\sum_{i=1}^{N}|Y_i^{obs} - Y_i^{sim}| \tag{4.1}$$

$$MANE = \frac{1}{N}\sum_{i=1}^{N}\frac{|Y_i^{obs} - Y_i^{sim}|}{Y_i^{obs}} \tag{4.2}$$

Table 4.7 – Comparison of calibration results with existing studies

Car-following model	Cycle	RMSE (speed $[km/h]$)	MAE (position $[m]$)	MANE (position $[\%]$)	MAE (speed $[km/h]$)	MAE (acceleration $[m/s^2]$)
Gipps	Urban	2.14	2.91	3.30	1.71	0.18
	Mid-Urban	3.24	5.36	1.91	2.62	0.19
	Ring Road	2.23	3.17	2.68	1.78	0.16
	Regional	2.84	8.22	1.65	2.20	0.15
	Average	2.47	4.51	2.64	1.96	0.17
IIDM	Urban	4.10	7.11	6.77	3.26	0.34
	Mid-Urban	6.03	9.89	4.99	4.94	0.40
	Ring Road	5.19	9.16	4.84	4.18	0.35
	Regional	4.57	16.30	3.43	3.67	0.23
	Average	4.64	9.90	5.48	3.72	0.32
Newell	Urban	2.74	2.79	3.85	2.22	0.25
	Mid-Urban	4.64	8.26	3.71	3.85	0.29
	Ring Road	2.58	2.44	1.48	2.08	0.22
	Regional	3.69	7.29	2.16	2.94	0.21
	Average	3.21	4.55	3.11	2.60	0.24
Wiedemann	Urban	11.65	26.62	16.09	8.74	0.51
	Mid-Urban	13.00	24.59	5.64	9.41	0.53
	Ring Road	11.89	38.52	21.69	9.24	0.38
	Regional	16.45	42.08	6.04	12.79	0.56
	Average	12.98	31.56	13.10	9.83	0.51
Aghabayk (2013) - LOLIMOT		3.27	-	-	-	-
Aghabayk (2013) - Gipps		6.84	-	-	-	-
Liu et al. (2016) - IDM		-	3.60	3.80	1.82	0.17

In Table 4.7, we can see that the Wiedemann's model always provides errors greater than the other models. In contrast, the Gipps' model provides smaller errors than the other models, including the one described in the literature. The Newell's model is better than models proposed in the literature for the position, however, its errors on speed or acceleration are a little higher. The IIDM generates errors which are higher than the errors of the models proposed in Aghabayk (2013) and Liu et al. (2016) but the values are not so high and could be considered as acceptable.

Comparison of the parameters values

The previous section presents the results of the car-following models calibration from the error side. It is highlighted that for the position and the spacing, the Newell and Gipps models perform the best (with the lowest error values). For the simulation of the speed and the acceleration, the Gipps' model is the one which provides the smallest errors.

This section focuses on the optimal parameter values. Because of MO calibration, the distribution of optimal parameters can be very wide (Figure 4.35). The following figures present some distributions of the car-following models optimal parameters. In these figures, the blue line represents urban cycles, the red line represents the mid-urban cycles, the green line represents regional cycles and the yellow line represents ring road cycles. The *Compromise* particle value is shown with the star marker, the same color code as for the distributions is used. The optimal parameter values will be studied for each car-following model.

The distribution of optimal parameters values is very wide for the Gipps' model (Figure 4.35) except for the reaction time τ as illustrated in Figure 4.36. However, we can observe that the values of the *Compromise* particles are generally close to each other. The values of the Follower are around $-1.6m/s^2$ for urban cycles and between -2 and $-2.2m/s^2$ for the other categories. The smaller b_n value on urban compared to other cycles could be explained be the smaller speed on urban cycles. The $SafetyMargin$ value is around $7m$ for the mid-urban cycles, whereas it is around $2m$ for the other cycles. For the acceleration a_n and the reaction time τ, the values are respectively between 1 and $1.6m^2$, and between 0.5 and $1.5s$ for all the cycles, corresponding to physical values.

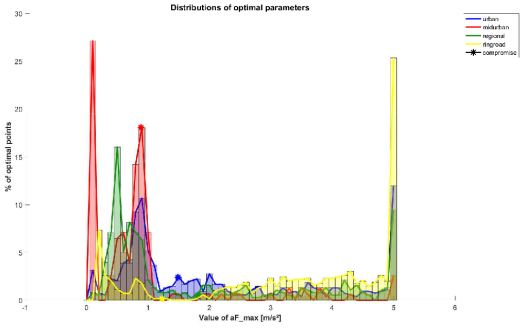

Figure 4.35 – Comparison of Follower deceleration (b_n) estimation errors

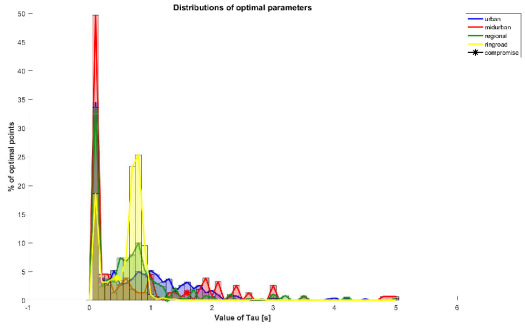

Figure 4.36 – Comparison of reaction time (τ) estimation errors

The calibration of the IIDM provides distribution of optimal parameters which are not wide (Figure 4.37) except for the time gap T (Figure 4.38). As for Gipps' model, the parameter values of *Compromise* are in the same range of value whatever the cycle. Acceleration a_n and deceleration b_n values are a little high, respectively between 3 and $4m/s^2$ and between -4 and $-3m/s^2$. The time gap values are in the range $[3;4.5]s$. The values of the minimum gap between the two vehicles $s0$ is around $3m$ for ring road cycles, and lower for the other categories, between 0.1 and $1.5m$.

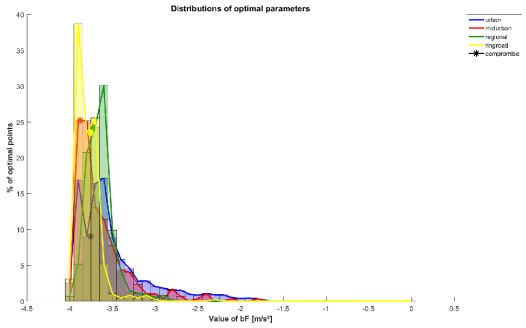

Figure 4.37 – Comparison of Follower deceleration (b_n) estimation errors

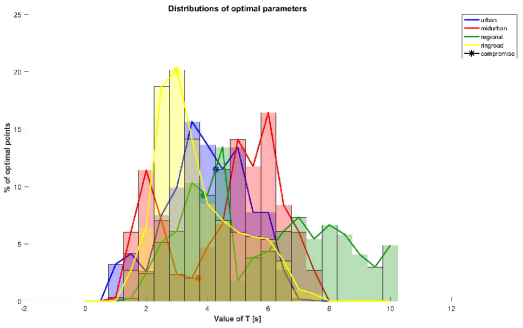

Figure 4.38 – Comparison of the time gap (T) estimation errors

The calibration of the two parameters of Newell model, ρ and w, leads to small values, not really physical, for both of them (Figures 4.39 and 4.40). These results can be due to the use of a MO calibration and the fact that the output of Newell's model is the position of the vehicle. As we search for optimal parameters looking also to errors on speed and acceleration, derivating twice the position could lead to a bias in the estimation of the trajectory and a model with only two parameters could not be accurate enough for this application.

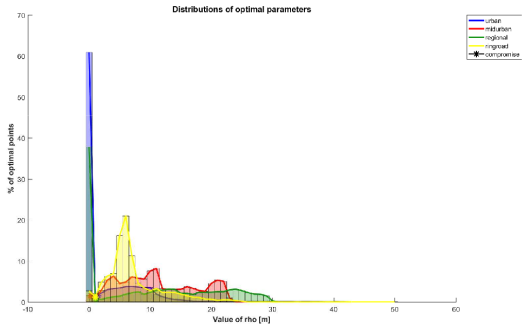

Figure 4.39 – Comparison of Follower deceleration (b_n) estimation errors

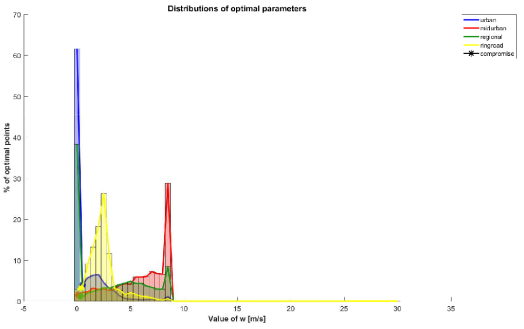

Figure 4.40 – Comparison of the time gap (T) estimation errors

Wiedemann's model has nine parameters to calibrate. Parameters related to deceleration *BMINadd* and *BMINVmult*, have similar values whatever the type of cycle (Figure 4.41), the other optimal parameters cover a wide range of values.

BMINadd and *BMINVmult* values are respectively around $1m/s^2$ and $0.15s^{-1}$. *BNULLmult* which represents the small acceleration oscillations when trying to keep a constant speed has very different values depending on the cycle (Figure 4.42). Its optimal value varies from 0.22 to $0.65m/s^2$.

The parameter related to the minimum distance for standing vehicles, *AXadd*, has similar values for regional and ring road cycles, around $2.2m$, whereas the value for urban cycle is smaller: $1m$ and the one for mid-urban cycle is greater: $4.2m$. The parameter *BXadd* which is linked to the minimum distance for following at low speed difference, has similar values for ring road, urban and mid-urban cycles: between 35 and $40m$ whereas the value for regional cycles is really smaller, around $21m$.

CXconst, *EXadd* and *OPDVadd* optimal values vary a lot, respectively from 33 to 50, from 3.6 to 9.5 and from 2.2 to 6.2.

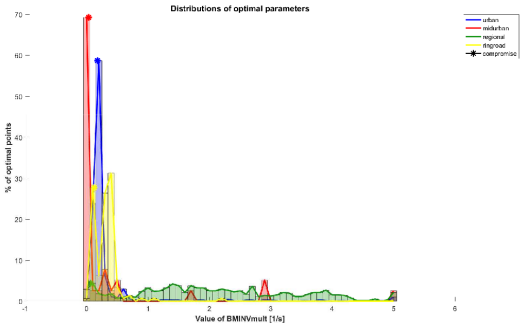

Figure 4.41 – Comparison of Follower deceleration (b_n) estimation errors

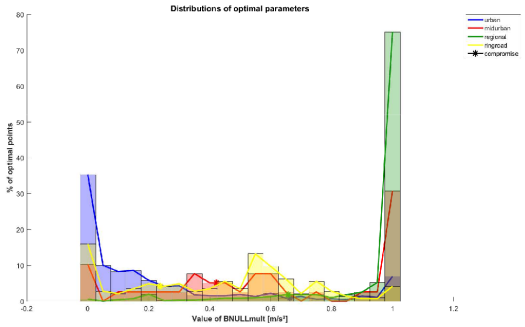

Figure 4.42 – Comparison of the time gap (T) estimation errors

4.5.2 Robustness to mean parameters

The previous section presented the results of the calibration of the four car-following model studied. We have seen that the Gipps' and the Newell's models are the more precise, followed by the IIDM. However, the Wiedemann's model is not so good at modelling the truck's behaviour.

The validation of the calibration could not be done in a usual way (calibrating the models on a part of the cycles, and validating the calibration on another part) because there are not enough cycles available do to this properly. Then to conclude on the robustness of the calibrated models, we study the response of the models to averaged parameters. A set of averaged parameters is defined, for each category, as the average of the values of the particles *Compromise*. For all the cycles, simulations are run with the optimal parameters and with averaged parameters of their category. The influence of the use of averaged parameters on the value of the error instead of the optimal one is studied.

The method is relevant here, because, in practice, we may not have optimal parameters for each trajectory. If we want to have a tool including both traffic and fuel consumption models, it would be necessary to have a well calibrated model for different situations and not to calibrate the model for each particular case. It is interesting to study the sensibility of the car-following models to averaged parameters in order to define a generic model per type of road.

Table 4.8 – Comparison of errors on simulated trajectories with optimal and averaged parameters

		Optimal parameters				Averaged parameters			
		Position	Spacing	Speed	Accel.	Position	Spacing	Speed	Accel.
Gipps	Urban	1.03	5.75	4.03	24.87	2.14	11.98	5.99	33.44
	Mid-Urban	0.88	9.08	3.99	24.78	3.43	25.76	8.29	39.15
	Ring Road	0.74	8.91	3.88	25.63	0.78	10.40	4.43	33.87
	Regional	0.70	9.08	2.53	25.16	1.17	17.26	3.88	35.91
	Average	0.89	7.44	3.66	25.03	1.91	14.93	5.61	34.88
IIDM	Urban	2.46	12.91	7.04	36.75	3.22	16.64	8.26	40.53
	Mid-Urban	1.66	15.78	7.42	42.47	2.79	24.01	10.03	51.85
	Ring Road	1.88	20.34	8.36	42.79	1.63	17.25	9.36	57.32
	Regional	1.11	15.44	4.00	31.72	1.62	22.14	6.18	45.40
	Average	1.96	14.96	6.59	37.28	2.56	18.89	8.14	45.48
Newell	Urban	1.01	5.93	4.94	32.73	96.48	74.12	100.00	100.00
	Mid-Urban	1.23	12.00	5.61	37.33	95.25	84.02	100.00	100.00
	Ring Road	0.53	6.53	4.33	32.19	98.51	87.04	100.00	100.00
	Regional	0.53	8.23	3.24	34.91	98.72	88.32	100.00	100.00
	Average	0.86	7.41	4.56	33.81	97.11	80.63	100.00	100.00
Wiedemann	Urban	12.79	32.18	23.89	53.42	48.81	56.21	69.97	74.60
	Mid-Urban	4.70	31.90	16.71	56.57	18.72	73.63	29.83	60.45
	Ring Road	16.70	41.92	25.96	50.55	36.22	91.95	43.25	61.49
	Regional	3.05	43.96	13.50	61.79	13.56	88.06	24.66	65.96
	Average	9.97	36.22	20.78	55.37	34.65	79.99	43.38	66.48

The results of the simulation with averaged parameters are presented in Table 4.8. Newell and Wiedemann models are not robust at all to the use of averaged parameters.

We can see that for the Newell's model, the errors increase significantly. For the position and the spacing, they are respectively greater than 95% and 75%. For the speed and the acceleration, they reach the 100%. On the Wiedemann's model side, the results are also poor. The errors on position and spacing reach values up to 48% and 91% respectively. The errors on speed and acceleration are also high, with average values equal to 43% and 66% respectively.

Gipps' model and the IIDM are robust to the use of averaged parameters. The errors on the trajectories increase less for the IIDM, however, errors are still lower with the Gipps' car-following model. The main difference between these two models is on the acceleration where the average error is about 35% for the Gipps' model whereas it is around 45% for the IIDM. On the other indicators, the errors are in average 1.9% and 2.6% for the position, 15% and 19% for the spacing and 5.6% and 8.1% for the speed, respectively for the Gipps' model and the IIDM.

4.6 Conclusion of the chapter

The study presented in this chapter proposed a robust method to calibrate each of the selected car-following models on trucks' trajectories by comparing several GoF functions (section 4.2), several simulation time steps (section 4.3) and several solvers (section 4.4).

According to the results of the calibration, the Gipps' car-following model appears to be more relevant to reproduce the behaviour of a HDV. It is the model with the lowest error values even when optimal parameters are switched to mean values. Moreover, the importance of calibrating car-following models not only based on spacing, speed or acceleration but based on the joint combination of all these variables has been demonstrated by studying the intersections of optimal parameters domains (section 4.2).

On the contrary to the Wiedemann's model and the Newell's model, the Gipps' model and the IIDM are more robust and less sensitive to the use of averaged parameters instead of optimal one per cycles. The models proposed by Newell and Wiedemann are clearly not enough robust to be used as shown in section 4.5.2. The rest of the work will focus on the two other models: the Gipps one and the IIDM. The mean parameters of these models for the four types of roads are presented in the tables below (Table 4.9 and Table 4.10).

Table 4.9 – Gipps' model mean optimal parameters per road category

	$\tau_n[s]$	$V_n^{des}[km/h]$	$a_n[m/s^2]$	$SafetyMargin[m]$	$\hat{b}_{n-1}[m/s^2]$	$b_n[m/s^2]$
Urban	0.95	44.2	1.48	1.79	−3.39	−1.60
Mid-urban	1.60	51.7	0.89	7.12	−3.43	−2.00
Regional	1.27	78.7	1.81	2.75	−3.36	−2.20
Ring road	0.45	83.2	1.23	0.70	−4.58	−2.18

Table 4.10 – IIDM mean optimal parameters per road category

	$a_n[m/s^2]$	$V_n^{des}[km/h]$	$s0[m]$	$T[s]$	$b_n[m/s^2]$
Urban	3.47	46.8	0.42	4.29	−3.75
Mid-urban	3.97	61.1	0.10	3.71	−3.88
Regional	2.96	77.3	3.21	3.87	−3.73
Ring road	3.01	77.9	1.41	2.98	−3.75

This chapter also highlights some dependencies of the car-following model parameters to the simulation time step (section 4.3.3) and to the solver (4.4.3).

Furthermore, to complete this work, the energy consumption of the vehicle has to be estimated on all cycles simulated with the Gipps' model and the IIDM. The evaluation of the fuel consumption was not included in this first study of calibration methods due to high computation times for a complete model including traffic and fuel consumption. The study of the accuracy of fuel consumption estimation could be done in two ways. The first one consists in using directly the tool which computes energy consumption with the output trajectories of the car-following models. Since the domains of variation of the optimal parameters and the sensitivity of

the models are now known, it is also possible to include the fuel consumption calculation tool directly into the calibration process. The computation time would not be too high because the optimal calibration method has already be defined here.

This will allow concluding on the best model to represent truck's behaviour in order to compute its energy consumption, because, as shown in (Vieira da Rocha et al., 2015), it is not because a model is the best to represent vehicle trajectory, that it will be the best for the calculation of its energy consumption.

The accuracy of the fuel consumption estimation is investigated in the following chapter (Chapter 5).

4.7 References

Kayvan Aghabayk. *Modelling heavy vehicle car-following in congested traffic conditions*. PhD thesis, Institute of Transport Studies, SDepartment of Civil Engineering, Monash University, 2013. p. 48, 62, 63

Kayvan Aghabayk, Majid Sarvi, and William Young. Understanding the Dynamics of Heavy Vehicle Interactions in Car-Following. *Journal of Transportation Engineering*, 138(12):1468–1475, December 2012. ISSN 0733-947X, 1943-5436. doi: 10.1061/(ASCE)TE.1943-5436.0000463. p. 48

Kayvan Aghabayk, Majid Sarvi, Nafiseh Forouzideh, and William Young. New Car-Following Model Considering Impacts of Multiple Lead Vehicle Types. *Transportation Research Record: Journal of the Transportation Research Board*, 2390:131–137, December 2013. ISSN 0361-1981. doi: 10.3141/2390-14. p. 48

Kayvan Aghabayk, Majid Sarvi, and William Young. A State-of-the-Art Review of Car-Following Models with Particular Considerations of Heavy Vehicles. *Transport Reviews*, 35:82–105, January 2015. doi: 10.1080/01441647.2014.997323. [1]. p. 48

Kayvan Aghabayk, Majid Sarvi, and William Young. Including heavy vehicles in a car-following model: modelling, calibrating and validating. *Journal of Advanced Transportation*, 50(7):1432–1446, November 2016. ISSN 01976729. doi: 10.1002/atr.1409. [3]. p. 48

Danjue Chen, Soyoung Ahn, Soohyuk Bang, and David Noyce. Car-Following and Lane-Changing Behavior Involving Heavy Vehicles. *Transportation Research Record: Journal of the Transportation Research Board*, 2561:89–97, January 2016. ISSN 0361-1981. doi: 10.3141/2561-11. [9]. p. 48

P.G. Gipps. A behavioural car-following model for computer simulation. *Transportation Research Part B: Methodological*, 15(2):105–111, April 1981. ISSN 01912615. doi: 10.1016/0191-2615(81)90037-0. p. 48

Arne Kesting and Martin Treiber. Calibrating Car-Following Models by Using Trajectory Data: Methodological Study. *Transportation Research Record: Journal of the Transportation Research Board*, 2088:148–156, December 2008. ISSN 0361-1981. doi: 10.3141/2088-16. p. 48, 51

Jiwon Kim and Hani Mahmassani. Correlated Parameters in Driving Behavior Models: Car-Following Example and Implications for Traffic Microsimulation. *Transportation Research Record: Journal of the Transportation Research Board*, 2249:62–77, December 2011. ISSN 0361-1981. doi: 10.3141/2249-09. p. 48

Lan Liu, Liling Zhu, and Da Yang. Modeling and simulation of the car-truck heterogeneous traffic flow based on a nonlinear car-following model. *Applied Mathematics and Computation*, 273:706–717, January 2016. ISSN 00963003. doi: 10.1016/j.amc.2015.10.032. [8]. p. 48, 62, 63

G.F. Newell. A simplified car-following theory: a lower order model. In *Transportation Research Part B: Methodological*, volume 36, pages 195–205, 2002. doi: 10.1016/S0191-2615(00)00044-8. p. 48

Emily Nodine, Andy Lam, Mikio Yanagisawa, and Wassim Najm. Naturalistic Study of Truck Following Behavior. *Transportation Research Record: Journal of the Transportation Research Board*, 2615:35–42, January 2017. ISSN 0361-1981. doi: 10.3141/2615-05. [2]. p. 48

Saskia Ossen and Serge Hoogendoorn. Calibrating car-following models using microscopic trajectory data. *A Report Submitted on A Critical Analysis of Both Microscopic Trajectory Data Collection Methods, and Calibration Studies Based on These Data, Delft Univ. Technol., Delft, The Netherlands*, 2008. p. 48

Vincenzo Punzo and Marcello Montanino. Speed or spacing? Cumulative variables, and convolution of model errors and time in traffic flow models validation and calibration. *Transportation Research Part B: Methodological*, 91:21–33, September 2016. ISSN 01912615. doi: 10.1016/j.trb.2016.04.012. p. 48, 51

Vincenzo Punzo and Fulvio Simonelli. Analysis and Comparison of Microscopic Traffic Flow Models with Real Traffic Microscopic Data. *Transportation Research Record: Journal of the Transportation Research Board*, 1934:53–63, January 2005. ISSN 0361-1981. doi: 10.3141/1934-06. p. 48, 51

Majid Sarvi and Omid Ejtemai. Exploring heavy vehicles car-following behaviour. In *Proceedings of the 34th Australasian Transport Research Forum (ATRF)*, pages 1–11, Adelaide, South Australia, Australia, September 2011. p. 48

Martin Treiber and Arne Kesting. Car-Following Models based on Driving Strategies. In *Traffic Flow Dynamics: Data, Models and Simulation*, pages 187–198. Springer, 2013a. ISBN 978-3-642-32459-8. p. 48

Martin Treiber and Arne Kesting. Elementary Car-Following models. In *Traffic Flow Dynamics*. Springer Berlin Heidelberg, Berlin, Heidelberg, 2013b. ISBN 978-3-642-32459-8 978-3-642-32460-4. doi: 10.1007/978-3-642-32460-4. p. 60

Martin Treiber and Arne Kesting. Microscopic Calibration and Validation of Car-Following Models – A Systematic Approach. *Procedia - Social and Behavioral Sciences*, 80:922–939, June 2013c. ISSN 18770428. doi: 10.1016/j.sbspro.2013.05.050. p. 55

Thamara Vieira da Rocha, Ludovic Leclercq, Marcello Montanino, Céline Parzani, Vincenzo Punzo, Biagio Ciuffo, and Daniel Villegas. Does traffic-related calibration of car-following models provide accurate estimations of vehicle emissions? *Transportation Research Part D: Transport and Environment*, 34:267–280, January 2015. ISSN 13619209. doi: 10.1016/j.trd.2014.11.006. p. 67

Rainer Wiedemann. Simulation des Strassenverkehrsflusses. Technical report, Instituts für Verkehrswesen des Universität Karlsruhe, 1974. p. 48

Da Yang, Peter (Jing) Jin, Yun Pu, and Bin Ran. Stability analysis of the mixed traffic flow of cars and trucks using heterogeneous optimal velocity car-following model. *Physica A: Statistical Mechanics and its Applications*, 395:371–383, February 2014. ISSN 03784371. doi: 10.1016/j.physa.2013.10.017. [7]. p. 48

Chapter 5

Fuel consumption estimation from simulated trajectories

Contents

In the previous chapter (Chapter 4), calibration methods have been defined for each studied car-following model. These models have been compared and it has been highlighted that the Newell's model and Wiedemann's model are not accurate enough to reproduce truck behaviour under different applications: urban, mid-urban, regional and ring road. However, the Gipps' model and the IIDM provide quite accurate results.

The current chapter (Chapter 5) investigates the connection between car-following models and FC estimation. This is important because it is a common practice to calibrate the model for traffic applications and then determinate the FC (or CO_2 emissions) as an output. As mentioned earlier, we restrict our analysis to the Gipps' model and the IIDM as the other two do not provide accurate trajectories.

The FC is calculated using EstimFC, a simulation tool used within the Volvo Group to estimate the FC of HDV.

First, we want to know if a calibration based on traffic MoP provided accurate results when calculating the FC (section 5.1). Second, we determine the improvements related to a direct integration of FC in the calibration process through multi-objective optimization (section 5.2).

5.1 Influence of the calibration on the calculation of fuel consumption

5.1.1 Validation of EstimFC configuration

EstimFC tool is used within Volvo Group to estimate the FC of an industrial vehicle on a given path. This tool takes as input the configuration of the vehicle and the definition of the road cycle (the speed profile and the slope) (Figure 5.1). In order to verify the representativeness of the EstimFC simulation model, the measured trajectories are used to estimate the FC. The results of these simulations are compared to the instantaneous measured FC (the fuel injected) and the cumulated FC. The error on cumulated and instantaneous FC is computed with the Theil's inequality coefficient (U) defined by expression in eq.(2.30) (Chapter 2). This function describes the similarities between two vectors of data. $U = 0$ indicates a perfect fit whereas $U = 1$ indicates worst fit. For convenience, the value of the Theil's inequality coefficient is expressed in % varying from 0% (perfect fit) to 100% (worst fit).

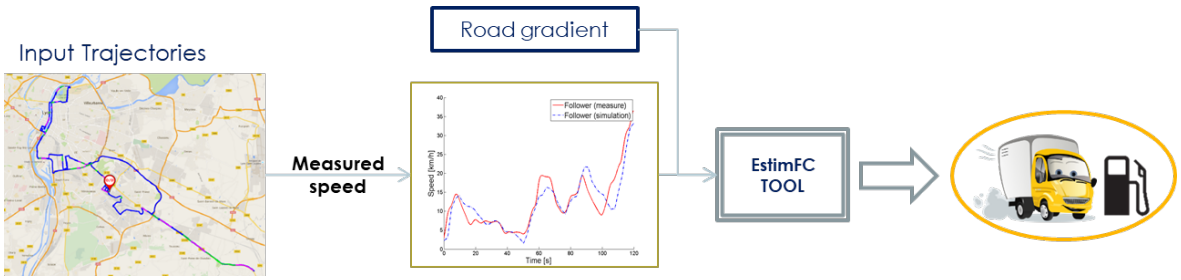

Figure 5.1 – Estimation of FC on measurements with EstimFC

The detailed results are presented in Appendix B, in Table B.1. The average gap in liters (L) is equal to $0.8L$ and corresponds to an error of 1.2% in average. The median is at $0.2L$ (0.7%), and the standard deviation is $3.9L$ (10.7%).

From Table B.1 (p.V), we can see that the errors on the cumulated FC (6.1% in average with a standard deviation of 4.7%) are really lower than the errors on the instantaneous FC (31.9% in average with a standard deviation of 9.6%). The errors on the instantaneous FC are higher than on the cumulated FC because this signal oscillates a lot, therefore it is more difficult to represent it. However, regarding the coefficients of variation values, $\sigma/\bar{U}$, the variations inside the errors values evoluate in the opposite direction. For the instantaneous FC, the coefficients of variation are between 0.20 and 0.34 that means that the errors generally differ between 20% and 34% from the average depending of the cycle type, while for the cumulated FC the errors differ between 31% and 97% from the average. This indicates that the estimation of the cumulated FC is less stable the instantaneous one.

We can also highlight that the urban cycles provides higher errors than the three other categories as illustrated in Table 5.1. This should be explained by the fact that urban cycles are smaller than the cycles in the other categories and will have more variations of traffic conditions. The behaviour of a vehicle in an urban environment is also less stable so more difficult to model than in a regional environment for example, because of the highest number of interactions due to the road traffic or due to the infrastructure.

Table 5.1 – Comparison of errors depending of the category of cycles

		Urban	Mid-urban	Regional	Ring road
FC cumulated	Average [%]	7.93	4.72	4.32	4.28
	Standard deviation [%]	5.30	2.33	4.19	1.31
	$\sigma/\bar{U}$	0.67	0.49	0.97	0.31
FC instantaneous	Average [%]	37.80	26.93	24.80	28.33
	Standard deviation [%]	7.40	7.38	6.99	9.49
	$\sigma/\bar{U}$	0.20	0.27	0.28	0.34

The following figure illustrates the results of the simulations. Figure 5.2 presents the errors (value of the Theil's inequality coefficient U) respectively between the measured and the simulated cumulated FC (red line woth squares) and between the measured and the simulated instantaneous FC (red line with stars). The cycles are presented with the same category order as in the tables: urban cycles (from 2 to 34), mid-urban cycles (from 1 to 35), ring road cycles (from 20 to 24) and regional cycles (from 25 to 32).

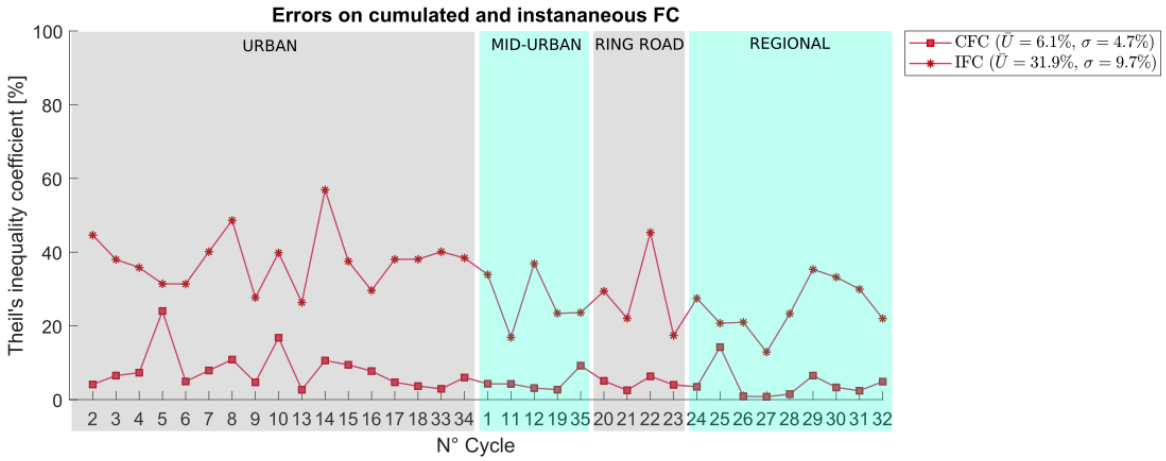

Figure 5.2 – Comparison of cumulated and instantaneous FC estimation errors U

5.1.2 FC estimation from the simulated trajectories

The simulated trajectories of the vehicle computed with the Gipps' car-following model and the IIDM are used to estimate the FC of the vehicle with EstimFC tool. The results are presented in the sections below.

Because the calibration was done thanks to a MO algorithm based on the dominance of some particles on the others (in the Pareto sense, see Chapter 2, section 2.5.5 for details), it implies that the output of the calibration is not only a vector of optimal parameters but a set of optimal vectors for the different MoP chosen. The error values and results presented here refer to a specific particle of the Pareto swarm. This particle is named *Compromise* and is defined to be a compromise between all the MoP; it is the closest particle to the origin (point with null coordinates). If the results refer to another particle of the particle swarm, this is mentioned in the corresponding section.

This section describes the results of the FC estimations along the 35 cycles studied for the Gipps' car-following model and the IIDM.

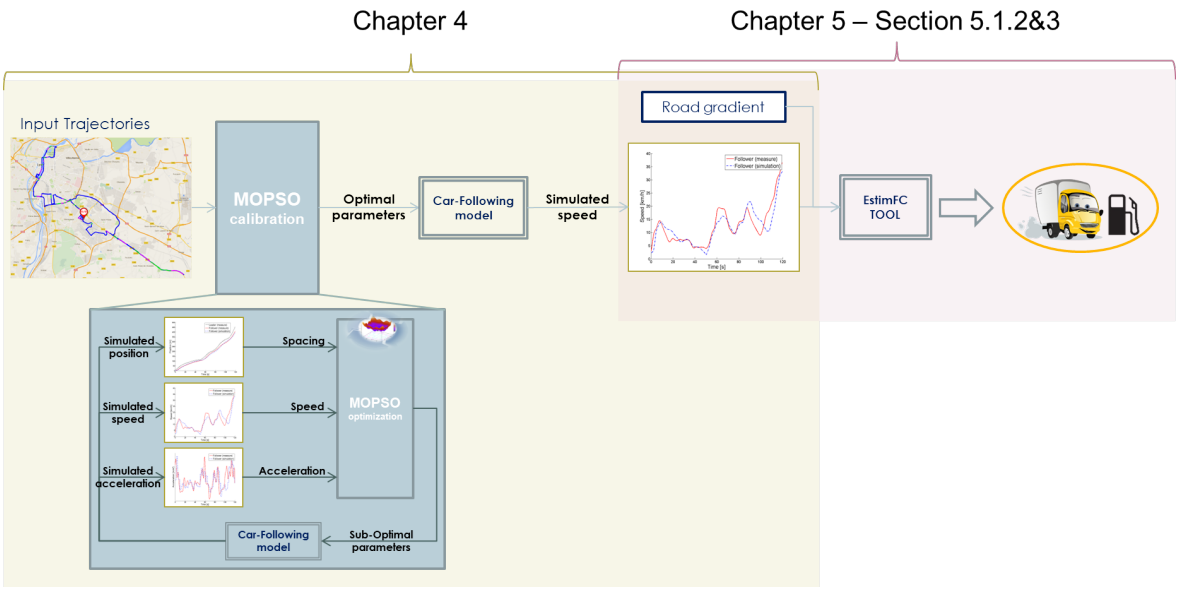

Figure 5.3 – Estimation of FC on simulated trajectories with EstimFC

Gipps' car-following model

The results of the simulation with EstimFC are presented in Table C.1 (p.VII).

The error on the cumulated FC is on average equal to 10.1% with a standard deviation of 9.6%. For the instantaneous FC the results are higher, with an average error of 38.0% and a standard deviation of 8.6%.

The error values are very different for the urban category with values varying from 2.7% to 53.1% for the cumulated FC, with a standard deviation close to 12%. However, the errors on regional cycles are more stable, 6.3% in average for the cumulated FC, with a standard deviation equal to 7.0%.

IIDM

The results of the simulation with EstimFC are presented in Table C.2 (p.VIII) for the IIDM. The same observations as for the Gipps' model apply for the IIDM, but errors are lower with the Gipps' car-following model than with the IIDM.

The errors on the cumulated and instantaneous FC are high, respectively 22.2% in average (with a standard deviation of 17.9%) and 46.9% in average (with a standard deviation of 12.6%).

The error values are smaller for regional cycles than for cycles of the other categories, with an average error respectively equal to 15.7% and 34.9% for the cumulated FC and the instantaneous FC.

5.1.3 Differences between the Gipps' model and the IIDM

The previous sections have shown that the cycles computed thanks to the calibrated Gipps' model and the calibrated IIDM are not good to estimate the FC of the truck although the models were good to reproduce its trajectories, see Chapter 4. The comparison of the errors is illustrated in Figure 5.4 and Figure 5.5. We can observe that the Gipps' car-following model is significantly better than the IIDM to generate trajectories for the estimations of the cumulated FC. For the estimation of the instantaneous FC both the Gipps' car-following model and the IIDM provide results that are not accurate, but the Gipps' car-following model is again a little better than the IIDM.

In average, the errors are about 1.2% (standard deviation of 10.7%), 6.1% (standard deviation of 4.6%) and 31.9% (standard deviation of 9.6%) for the simulation of the FC on measured trajectories, 11.2% (standard deviation of 32.3%), 10.1% (standard deviation of 9.6%) and 38.0% (standard deviation of 8.6%) for the trajectories generated with the Gipps' car-following model, and 66.5% (standard deviation of 96.4%), 22.2% (standard deviation of 17.9%) and 46.9% (standard deviation of 12.6%) for the trajectories generated with the IIDM, respectively for the FC in $L/100km$, the cumulated FC and the instantaneous FC. This result is consistent with the conclusion of Chapter 4, the Gipps model also provides trajectories for which the differences with the

measurements were lower than the one from the IIDM.

The following figures illustrate the results described in the preceding paragraphs. Figure 5.4 and Figure 5.5 respectively show the errors on the estimation of the cumulated FC and on the estimation of the instantaneous FC. The black diamonds are the errors previously computed on measured trajectories (see previous section 5.1.1), the yellow circles are the errors for Gipps' car-following model while the orange circles are the errors resulting of the trajectories simulated thanks to the IIDM.

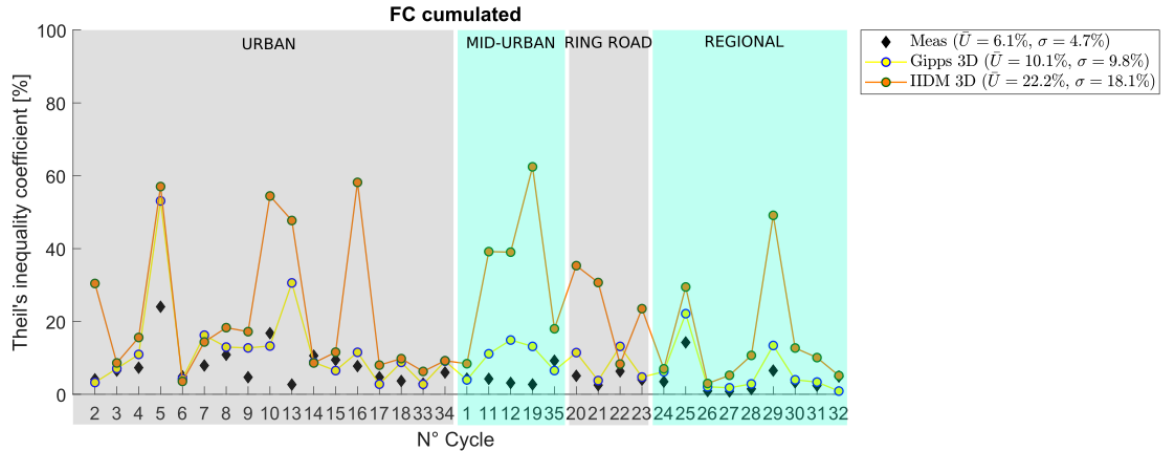

Figure 5.4 – Comparison of cumulated FC estimation errors

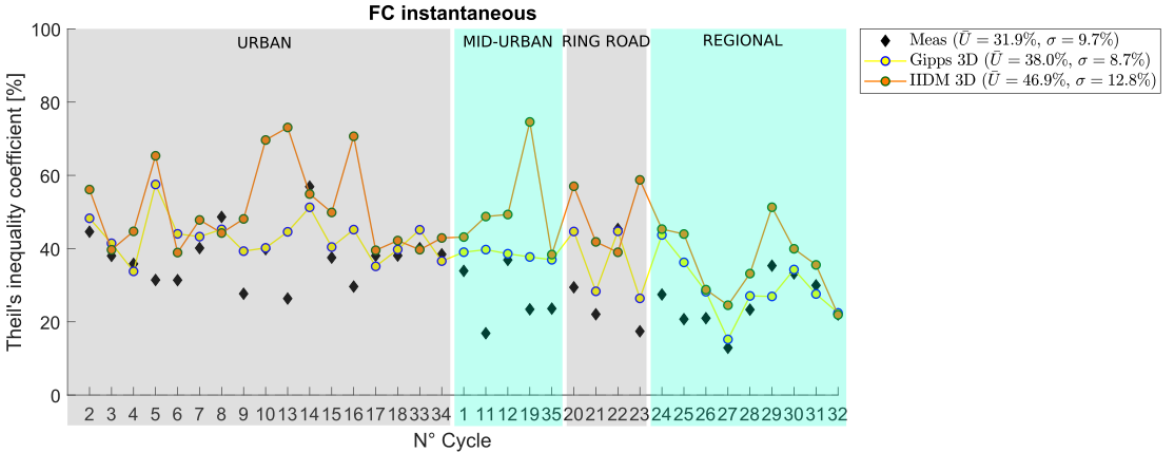

Figure 5.5 – Comparison of instantaneous FC estimation errors

As shown in (Song et al., 2012; Vieira da Rocha et al., 2015) for passenger cars, we can say that a car-following model can be well calibrated from a traffic point of view but not satisfactory to estimate the related FC. However, car-following models or traffic models are generally calibrated regarding traffic indicators, and they are used to estimate energy consumption or pollutant emissions (Song et al., 2013). As we can see in this study, this method can lead to bias in FC values, particularly for heavy vehicles.

Figure 5.6 illustrates the calibration result of a regional cycle. The Theil's inequality coefficient is highlighted for spacing, speed and acceleration and errors on cumulated FC have been computed for all points of the Pareto archive. The FC errors are illustrated thanks to the color scale. We can observe that the compromise point leads to a high FC error, while the three best points for trajectory (illustrated with diamond points) provide lower FC errors. However, choosing the best acceleration point implies high errors on spacing and speed modelling, and vice versa.

To solve this issue, we propose to incorporate the FC estimation into the calibration process as a fourth MoP of the car-following models' calibration which leads to multi-objective calibration mechanism.

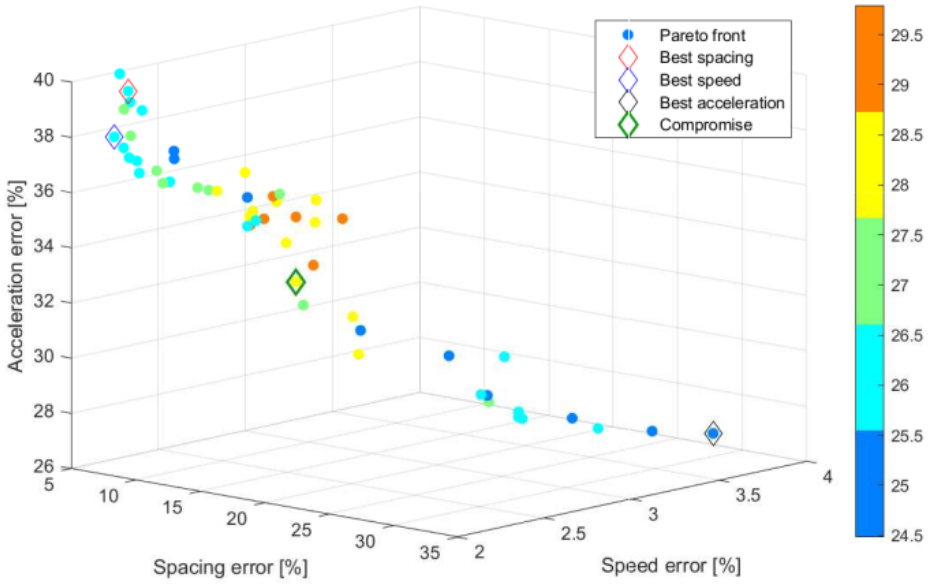

Figure 5.6 – Pareto front errors for a regional cycle

5.2 Including the FC estimation into the car-following models calibration

The Gipps' car-following model and the IIDM are calibrated again but with four MoP namely: the spacing, the speed, the acceleration and the FC (estimated using EstimFC). The car-following models have been calibrated for two FC indicators: the cumulated FC and the instantaneous FC. The results are compared for these two indicators.

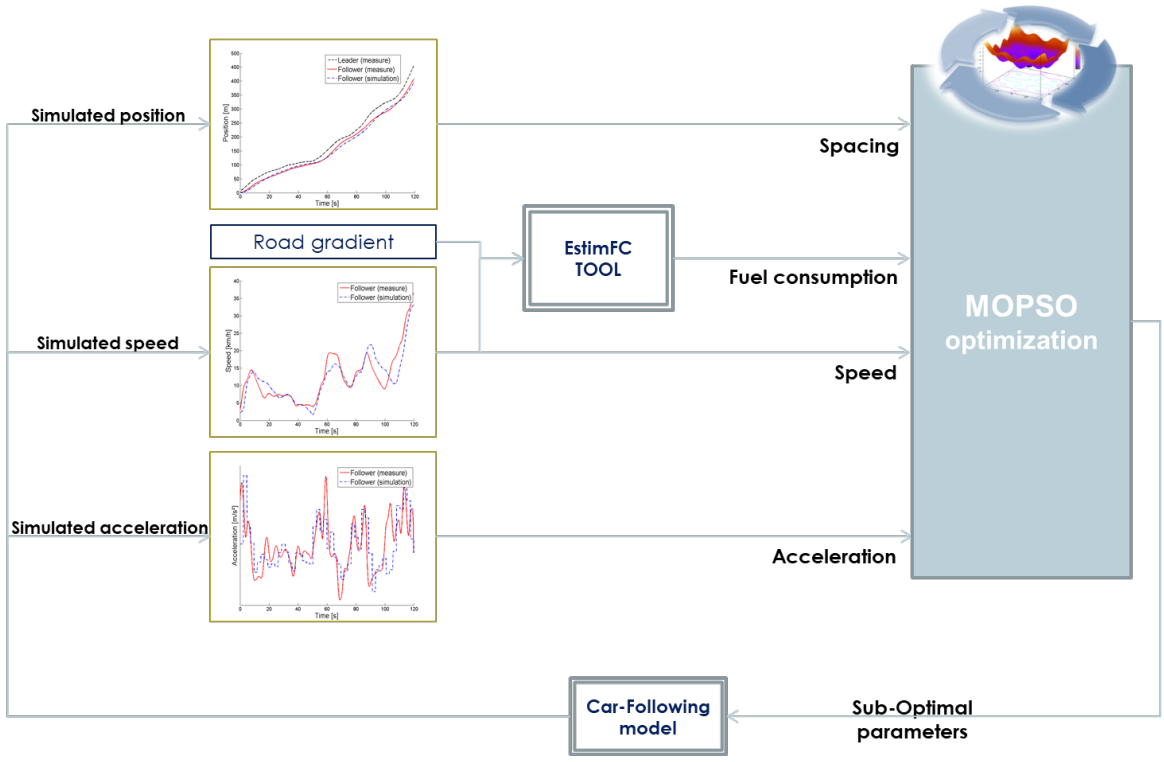

Figure 5.7 – Comparison of FC, cumulated in blue and instantaneous in black, estimation errors *U*

We observe that the errors on position, spacing, speed or acceleration are really close to the errors resulting of the calibration without taking into account the FC estimation. However, the errors on the FC estimation are significantly reduced. This means that the optimal domain from a traffic point of view is large and flat and including another indicator in the calibration process easily improves FC estimation results.

The results of this new and global calibration method are presented more in depth in the following sections, first for the Gipps' car-following model (section 5.2.1), and then for the IIDM (section 5.2.2).

5.2.1 Gipps' car-following model

5.2.1.1 Cumulated FC as the fourth MoP

The errors on FC estimation are presented in Table D.1 (p.IX).

Considering the results of the calibration one by one, we can say that the estimation of the FC is improved drastically on some cycles (7 ,8, 9, 10 for example) and not really changed on others (2, 30, 31 for example). However, considering the entire set of cycles the results are improved significantly. The average error is reduced for all FC estimations and not deteriorated for trajectory indicators.

We can observe that the errors on the cumulated FC estimations have been significantly reduced by adding this indicator to the calibration process of the car-following models. In average, this error has decreased from 10.1% (with a standard deviation of 9.6%) to 7.0% (with a standard deviation of 6.3%), the error has been reduced by 40%. Moreover, the errors on the position, the spacing, the speed, and the acceleration are quite similar: 0.9% and 0.9% for the position, 7.4% and 7.8% for the spacing, 3.7% and 3.8% for the speed, and 25.0% and 25.5% for the acceleration, respectively for calibration without and with a FC indicator. The most impacted indicator is the spacing.

5.2.1.2 Instantaneous FC as the fourth MoP

The errors on FC estimation are presented in Table D.2 (p.XI).

As for the calibration using the cumulated FC as objective, we can observe that adding the FC estimation to the calibration process with the instantaneous FC as objective allows to improve the energy consumption estimation without deteriorating too much the representativeness on the other MoP (spacing, speed and acceleration).

The error on the instantaneous FC estimation is quite the same from 38.0% in average to 37.4% (the standard deviation goes from 8.6% to 7.7%).

The resulting average errors for the calibration, respectively without and with the FC estimation, are equal to 0.9% and 1.1% for the position, 7.4% and 9.2% for the spacing, 3.7% and 3.9% for the speed, 25.0% and 27.2% for the acceleration, and 10.1% and 7.0% for the cumulated FC. The most impacted MoP are the spacing and the acceleration.

Results for the instantaneous FC are globally better for regional cycles, around 25%, than for the three other categories: urban, mid-urban and ring road cycles, where the errors remains around 34%.

5.2.1.3 Conclusion

The FC estimation has been added to the calibration process as a fourth MoP. It has allowed to reduce the error on the FC estimation without deteriorating too much the error on the trajectory of the vehicle.

The following figures compare the error on the simulated trajectories for the three calibrations: without including the FC estimation ('3D', yellow line with circles), with the cumulated FC as MoP ('4D cumul', blue line with squares) and with the instantaneous FC as MoP ('4D instant', purple line with triangles). Figure 5.8 illustrates the error on the position, Figure 5.9 illustrates the error on the spacing, Figure 5.10 illustrates the error on the speed of the vehicle and Figure 5.11 illustrates the error on the acceleration.

We can observe that the results are similar for the three calibrations. However, the results for the calibration with the cumulated FC as MoP are closer to the results of the calibration without FC estimation than the calibration with the instantaneous FC as MoP. This is particularly noticeable on the errors of the spacing, which is the most impacted indicator.

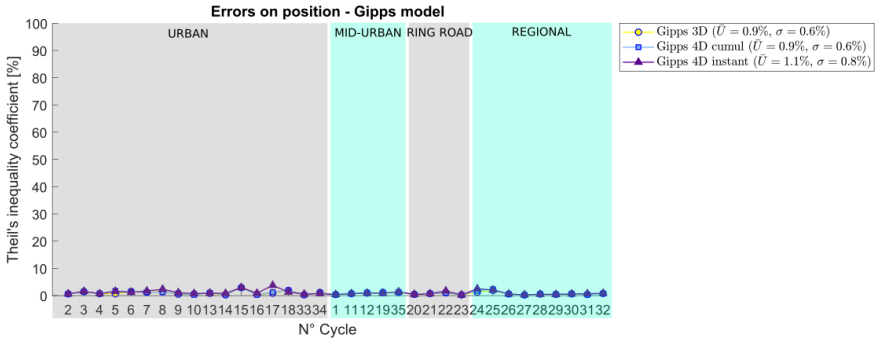

Figure 5.8 – Comparison of position estimation errors for Gipps' car-following model

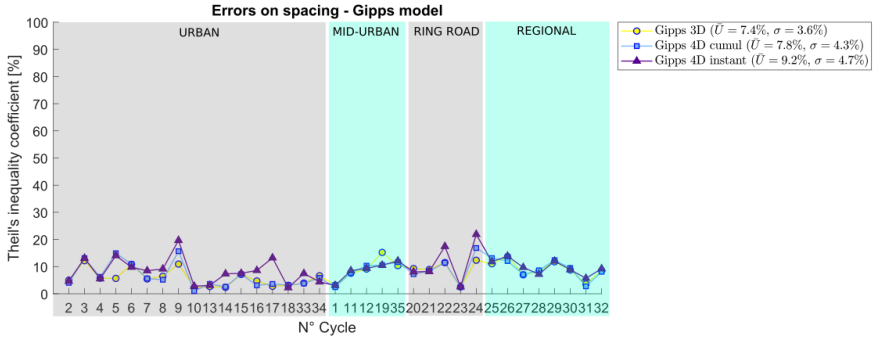

Figure 5.9 – Comparison of spacing estimation errors for Gipps' car-following model

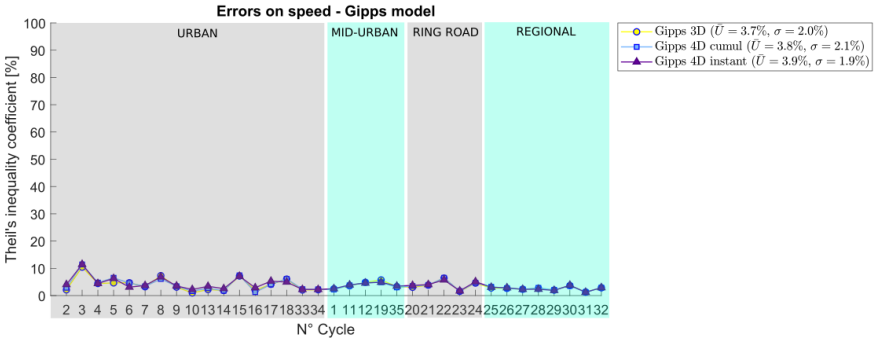

Figure 5.10 – Comparison of speed estimation errors for Gipps' car-following model

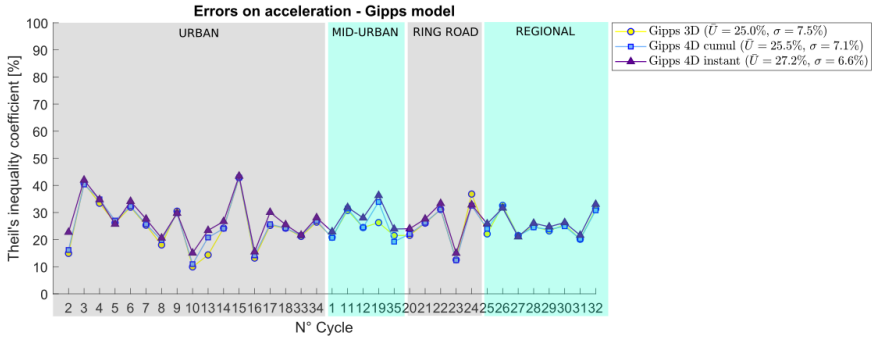

Figure 5.11 – Comparison of acceleration estimation errors for Gipps' car-following model

The comparison of all the calibration for the Gipps' car-following model is presented in the figures below (Figure 5.12 and Figure 5.13). On these figures, the black diamonds represent the errors resulting of the simulation of the measure, the yellow circles represent the errors resulting of the trajectories generated after the calibration without a FC indicator, the blue squares are the errors for the trajectories generated thanks to the Gipps' model calibrated with the cumulated FC as a fourth MoP, and the violet triangles represent the error for the trajectories generated thanks to the Gipps' car-following model calibrated using the instantaneous FC as the fourth MoP.

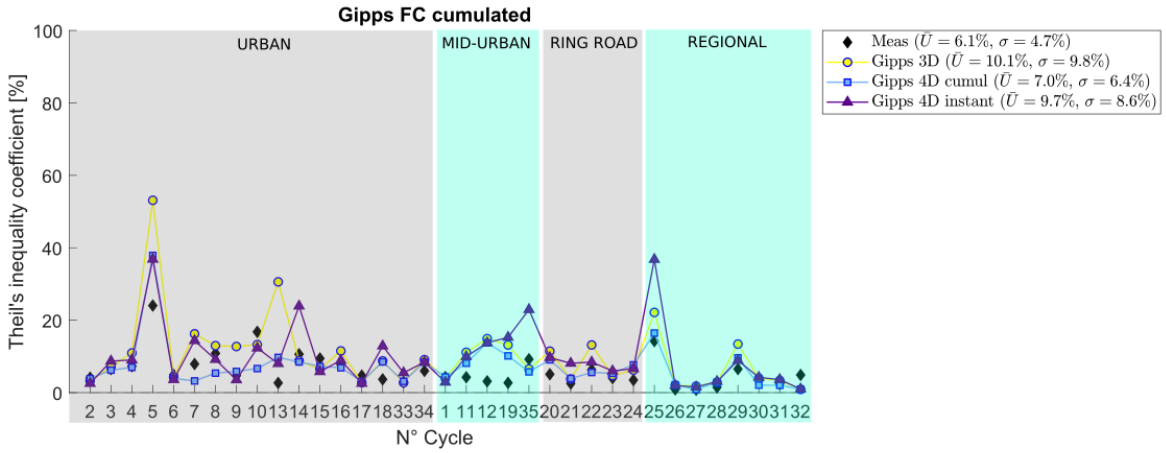

Figure 5.12 – Comparison of cumulated FC estimation errors, resulting of calibration without and with a FC indicator

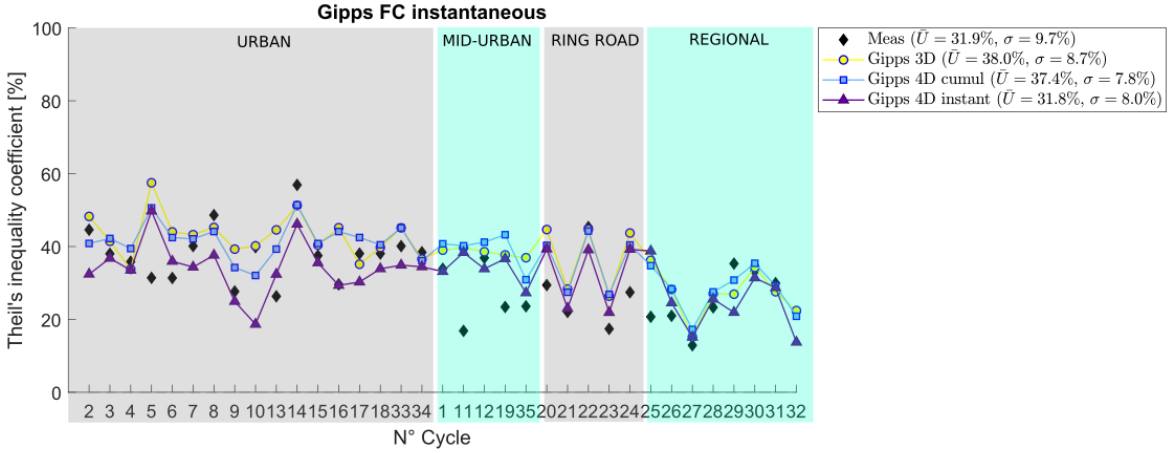

Figure 5.13 – Comparison of instantaneous FC estimation errors, resulting of calibration without and with a FC indicator

We can observe, on Figures 5.12 and 5.13 that the errors on the FC MoP (cumulated and instantaneous) are reduced. Furthermore, the results are more stable, the standard deviation is smaller, for the trajectories generated after the calibration with cumulated FC as MoP (than with instantaneous FC).

We can notice that best results are achieved for regional cycles, which are longer, and with less variability in the speed.

It is also interesting to highlight that being better on instantaneous FC does not lead to better cumulative FC. It may seem counterintuitive in a first step, but it could be explained by the fact that the instantaneous FC oscillates a lot and even if it is better represented after the calibration considering it as the fourth MoP, it is still not accurate enough to see an improvement on the cumulative FC.

5.2.2 IIDM

5.2.2.1 Cumulated FC as the fourth MoP

The errors on FC estimation are presented in Table D.3 (p.XIII).

The IIDM provided very bad results on the estimation of the FC when it was calibrated only using trajectories MoP (see Figure 5.4 and Figure 5.5). The new calibration of this model, adding a fourth MoP for the FC estimation, has allowed to improve the results a lot.

In average, the mean error drops from 22.2% to 10.3% for the cumulated FC and from 46.9% to 42.6% for the instantaneous FC. As highlighted previously for the Gipps' car-following model, adding the cumulated FC to the calibration process has allowed to reduce the average FC error and also to make the model more accurate with smaller standard deviation on the errors. The standard deviations of the errors respectively go from 17.9% to 6.7%, and from 12.6% to 9.1% for the cumulated and instantaneous FC.

However, the errors on the trajectories are worse than for the previous calibration without FC MoP. The most impacted indicators are the spacing between the follower and the leader, and the acceleration of the follower. The errors increase from 2.0% to 4.7% for the position, from 15.0% to 26.6% for the spacing, from 6.6% to 10.8% for the speed and from 37.3% to 53.2% for the acceleration.

The standard deviation calculated on the trajectories errors also increases, from 1.4% to 5.3% for the position, from 8.5% to 20.7% for the spacing, from 3.0% to 7.5% for the speed and from 9.5% to 22.4% for the acceleration.

The errors on trajectories behave in the opposite direction of errors on FC estimation. The average errors and the standard deviation increase. It means that the trajectories are not only less well represented but the accuracy of the model is reduced.

5.2.2.2 Instantaneous FC as the fourth MoP

The errors on FC estimation are presented in Table D.4 (p.XV).

The errors on the FC estimation have also been reduced by adding the instantaneous FC estimation as the fourth MoP of the calibration process. However, as for the previous section, the errors on the trajectory indicators increase.

In average the error on the instantaneous FC drops from 46.9%, with a standard deviation of 12.6%, to 39.4%, with a standard deviation of 8.1%. The cumulated FC error decreases from 22.2%, with a standard deviation of 17.9%, to 13.5%, with a standard deviation of 7.6%. As mentioned previously, both average errors on FC and standard deviation values are reduced.

For the trajectory indicators, the average errors increase from 2.0% to 3.8% for the position, from 15.0% to 23.3% for the spacing, from 6.6% to 9.4% for the speed and from 37.3% to 51.5% for the acceleration. The standard deviations also increase in this case, with values similar to those of the previous section.

5.2.2.3 Conclusion

The FC estimation has been added to the calibration process as a fourth MoP. It has allowed to reduce the error on the FC estimation but the errors on the trajectory of the vehicle have been increased.

The following figures compare the error on the simulated trajectories for the three calibrations: without including the FC estimation ('3D', orange line with circles), with the cumulated FC as MoP ('4D cumul', green line with squares) and with the instantaneous FC as MoP ('4D instant', blue duck line with triangles). Figure 5.14 illustrates the error on the position, Figure 5.15 illustrates the error on the spacing, Figure 5.16 illustrates the error on the speed of the vehicle and Figure 5.17 illustrates the error on the acceleration.

We can observe that the results are better for the calibration without a FC MoP. This is particularly noticeable on the errors of the spacing and the acceleration, which are the most impacted indicators. Moreover, we can observe that the results are a little better for regional cycles.

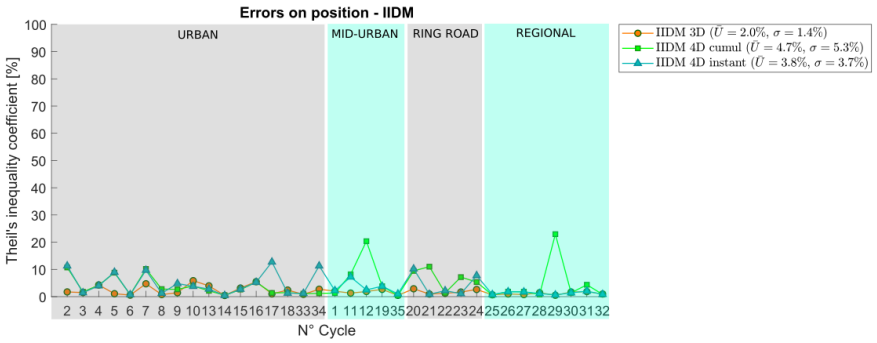

Figure 5.14 – Comparison of position estimation errors

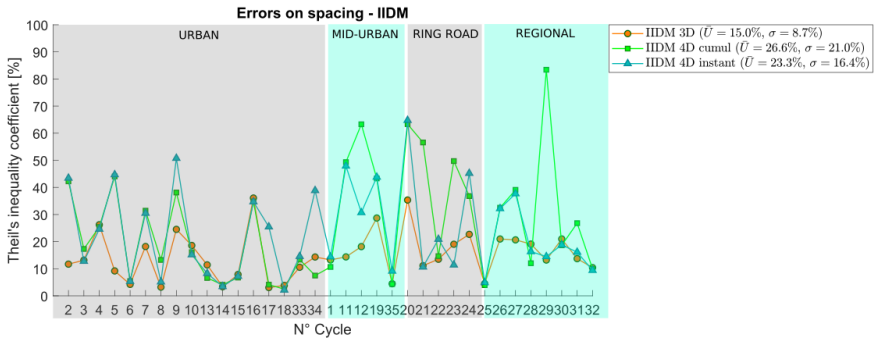

Figure 5.15 – Comparison of spacing estimation errors

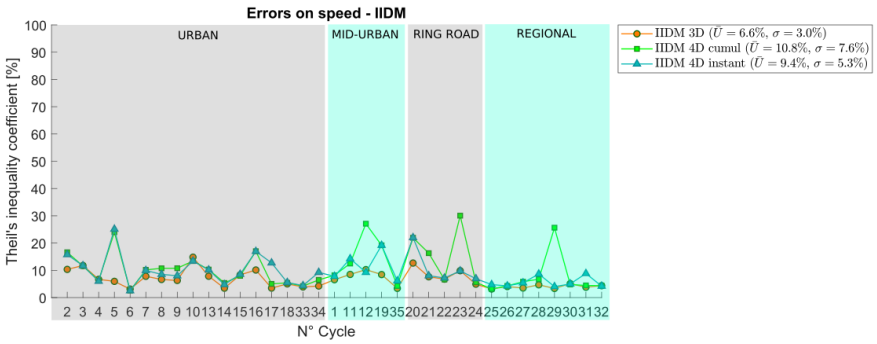

Figure 5.16 – Comparison of speed estimation errors

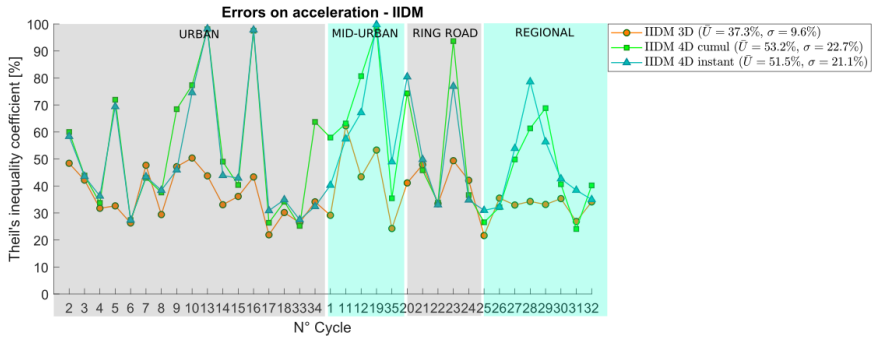

Figure 5.17 – Comparison of acceleration estimation errors

The comparison of all the calibrations for the IIDM is presented in Figure 5.18 and Figure 5.19. In these figures, the black diamonds represent the errors resulting of the simulation of the measure, the orange circles represent the errors resulting of the trajectories generated after the calibration without a FC MoP, the green squares are the errors for the trajectories generated thanks to the MoP calibrated with the cumulated FC as the fourth MoP, and the blue duck triangles represent the error for the trajectories generated thanks to the IIDM calibrated using the instantaneous FC as the fourth MoP. The cycles are presented with the same category order as in the tables: urban cycles (from 2 to 34), mid-urban cycles (from 1 to 35), ring road cycles (from 20 to 24) and regional cycles (from 25 to 32).

We can observe that the error on the FC estimation has been significantly reduced thanks to the calibration including FC estimation for the cumulated and instantaneous FC.

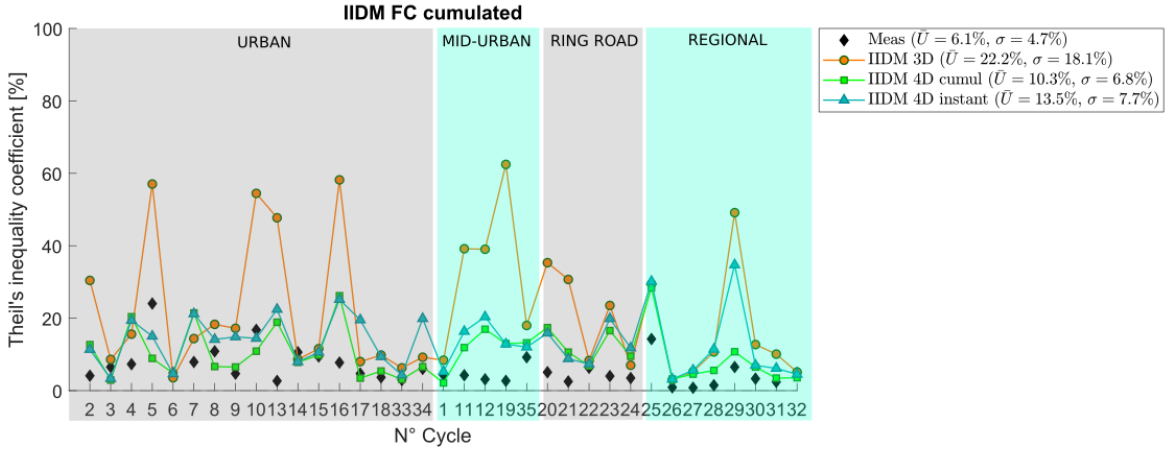

Figure 5.18 – Comparison of cumulated FC estimation errors, resulting of calibration without and with a FC MoP

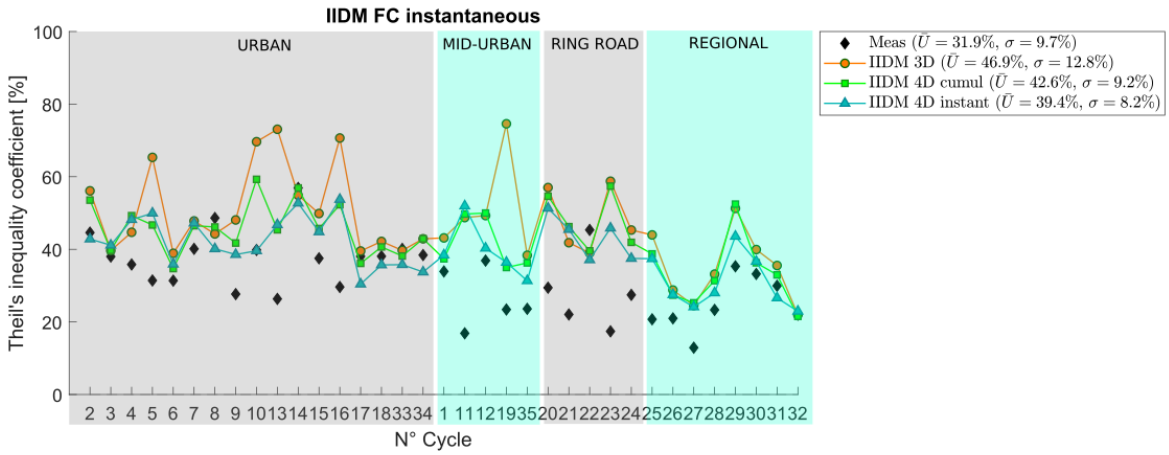

Figure 5.19 – Comparison of instantaneous FC estimation errors, resulting of calibration without and with a FC MoP

As illustrated in the Figures (5.18 and 5.19), there are less differences between FC estimations from calibration with cumulated or instantaneous FC as MoP, than for the Gipps' car-following model.

We can notice that for the IIDM the results are not better for regional cycles than for the cycles of the other categories.

5.3 Conclusion of the chapter

The two car-following models: the Gipps' car-following model and the IIDM, are compared on their ability to provide trajectories accurate enough to estimate properly the FC of the vehicle studied.

The first comparison is realized using the trajectories resulting on the models calibration on trajectory MoP (spacing, speed and acceleration). Even though these models provide good results in terms of trajectory

representativeness, the errors on the FC estimation are high. To solve this issue, it has been proposed to calibrate the models again including the FC estimation in the process. Two calibrations are done: one with the cumulated FC as the fourth MoP, and the other with the instantaneous FC as the fourth MoP.

The computation time is increased, but the results are really better. The error on the FC estimation has been reduced for the two models.

However, the two models do not react in the same way to these new parameters. For the Gipps' car-following model, the error on the trajectory indicators are only a little higher than previously (Figures 5.8, 5.9, 5.10 and 5.11), whereas for the IIDM these errors increase significantly (Figures 5.14, 5.15, 5.16 and 5.17). The Gipps' model is still better than the IIDM to represent the truck's trajectory.

The comparison of the Gipps' model FC results and the IIDM FC results are summarized in Table 5.2. The Figures 5.20 and 5.21 illustrate for each cycle the comparison between the Gipps' model and the IIDM ability to provide acurate trajectory to estimate properly the FC, respectively for the FC expressed in $L/100km$, the cumulated FC and the instantaneous FC.

Table 5.2 – Comparison of average errors provided by Gipps' model and IIDM on FC estimation

Cycle Category	Error on	Gipps		IIDM	
		FC cumul	FC instant	FC cumul	FC instant
Urban	Cumulated FC	7.97%	10.35%	10.38%	13.97%
	Instantaneous FC	41.64%	34.17%	45.63%	42.19%
Mid-Urban	Cumulated FC	8.42%	12.95%	11.43%	13.36%
	Instantaneous FC	39.26%	33.86%	41.67%	39.69%
Ring Road	Cumulated FC	6.31%	7.76%	12.18%	12.73%
	Instantaneous FC	35.87%	32.52%	47.95%	43.44%
Regional	Cumulated FC	4.63%	7.63%	8.25%	12.85%
	Instantaneous FC	28.02%	24.97%	33.25%	30.85%
All cycles	Cumulated FC	7.03%	9.73%	10.30%	13.45%
	Instantaneous FC	37.36%	31.79%	42.56%	39.42%

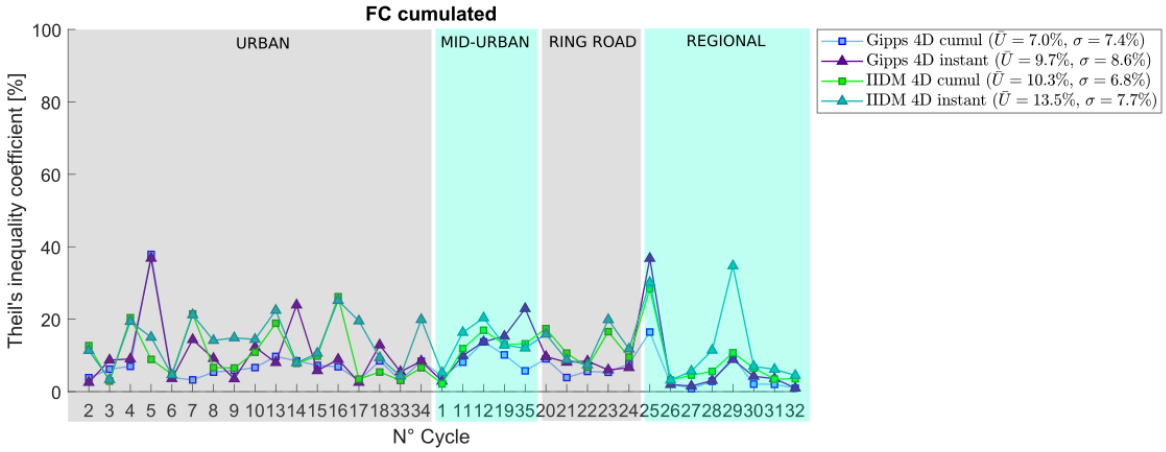

Figure 5.20 – Comparison of cumulated FC estimation errors, resulting of calibration with a MoP on the cumulated or instantaneous FC

For all categories, the calibration of the IIDM with the instantaneous FC as the fourth MoP is the least efficient.

For the cumulated and instantaneous FC, the Gipps' model results are always better than the IIDM results. Considering the standard deviation of the errors, the results from the calibration of the Gipps' model with the cumulated FC as a fourth MoP are more stable than with the instantaneous FC as the fourth MoP. We can observe this result in the figures. In Figure 5.20 we can see that the results from the Gipps' model calibrated with the cumulated FC are most of the time better than the others and really more stable.

According to these observations, a good compromise between the values of the errors on position and on FC and the stability of the method seems to be the use of the Gipps' car-following model, calibrated on four MoP: the spacing, the speed, the acceleration and the cumulated FC.

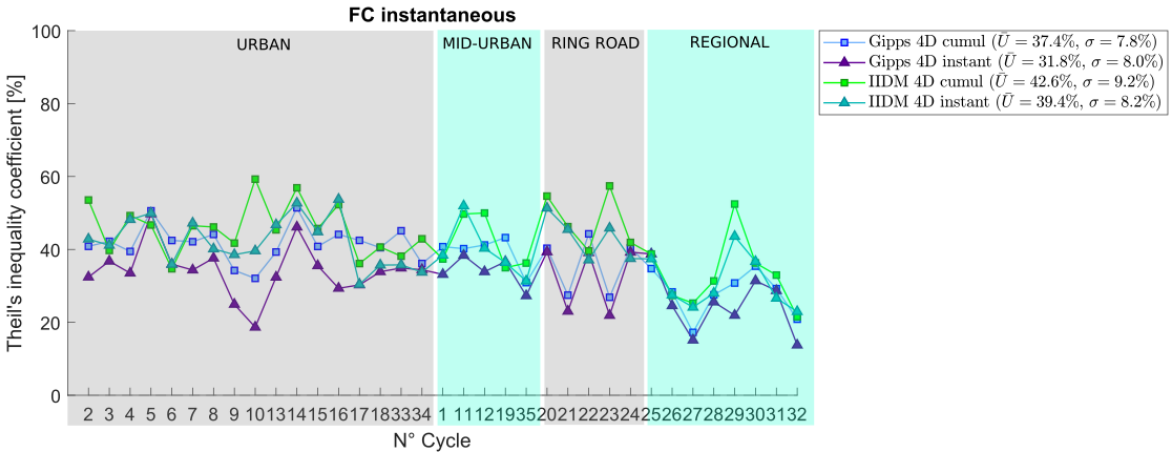

Figure 5.21 – Comparison of instantaneous FC estimation errors, resulting of calibration with a MoP on the cumulated or instantaneous FC

5.4 References

Guohua Song, Lei Yu, and Yanhong Zhang. Applicability of Traffic Microsimulation Models in Vehicle Emissions Estimates: Case Study of VISSIM. *Transportation Research Record: Journal of the Transportation Research Board*, 2270(1):132–141, January 2012. ISSN 0361-1981, 2169-4052. doi: 10.3141/2270-16. URL http://journals.sagepub.com/doi/10.3141/2270-16. p. 73

Guohua Song, Lei Yu, and Long Xu. Comparative analysis of car-following models for emissions estimation. volume 2341, pages 12–22, Washington, D.C., December 2013. doi: 10.3141/2341-02. p. 73

Thamara Vieira da Rocha, Ludovic Leclercq, Marcello Montanino, Céline Parzani, Vincenzo Punzo, Biagio Ciuffo, and Daniel Villegas. Does traffic-related calibration of car-following models provide accurate estimations of vehicle emissions? *Transportation Research Part D: Transport and Environment*, 34:267–280, January 2015. ISSN 13619209. doi: 10.1016/j.trd.2014.11.006. p. 73

Conclusion of Part I

The first part of this thesis focuses on the design of a car-following model dedicated to trucks. Its ability to reproduce the truck behaviour and the accuracy of the model when using it to estimate the vehicle FC is investigated.

The first chapter of this part (Chapter 2) presents the methods and data used to design a suitable model to reproduce truck trajectories and to compute its energy consumption.

In the second chapter (Chapter 3), several trajectory reconstruction methods have been compared. They were evaluated on their ability to produce speed profiles close to the measured ones, and physically realistic acceleration and jerk values. This study has highlighted that the best method, among the ones tested to generate truck trajectory from measured speed profiles, first consists in filtering the measured speed of the trucks with a moving average to remove noise due to the measure. Then, its position is computed thanks to the trapezoidal scheme, and the position of its leader is computed by adding the measured spacing and the length of the vehicle to the position of the truck. Then, the speeds are computed by derivating the positions with trapezoidal scheme, and they are filtered. The acceleration profiles are computed in the same manner as the speed.

After computing the trajectories, the calibration methods and car-following models (Gipps, IIDM, Newell and Wiedemann models) can be compared (Chapter 4).
The study proposes to define a robust calibration method for each car-following models and then to compare these models. The algorithm used for the calibration is the MOPSO and several configurations have been investigated here: the choice of the GoF function and the MoP, the simulation time step and the solver. It has been pointed out that Theil's inequality coefficient is the most adapted method for the case studied here. Moreover, in order to obtain an accurate representation of the vehicle trajectory (position, speed, and acceleration), a MO calibration is necessary. The spacing between the Follower and the Leader, the speed and the acceleration of the Follower are the MoP of this optimization problem.
The influences of the simulation time step and the solver have been investigated. It has been highlighted that the four car-following models need different time steps. However, the Mixed solver is adapted to all the models. The calibration methods are summarized in the table below.
The robustness of the models is also tested. For each car-following model, trajectories are simulated with averaged parameters per category, then optimal and averaged trajectories are compared. We have observed that the Gipps' model is the most robust, followed by the IIDM. However, the Newell's and Wiedemann's models are not robust at all, and therefore could not be used for the rest of the study.

Optimal method to calibrate car-following models

	Goodness-of-Fit function	Measure of Performance	Simulation time step	Solver
Gipps	Theil's inequality coefficient	Spacing/Speed/Acceleration	$0.1s$	Mixed
IIDM	Theil's inequality coefficient	Spacing/Speed/Acceleration	$0.01s$	Mixed
Newell	Theil's inequality coefficient	Spacing/Speed/Acceleration	$0.5s$	Mixed
Wiedemann	Theil's inequality coefficient	Spacing/Speed/Acceleration	$0.5s$	Mixed

The last chapter, Chapter 5, studied the accuracy of FC estimation from simulated trajectories. This work has highlighted that the previous calibration based only on trajectory MoP is not sufficient to estimate properly the FC due to the flatness of the optimal parameter domain. To solve this issue, the FC estimation has been added into the calibration loop. Two FC MoP were tested: the instantaneous and the cumulated FC. Results show that using the cumulated FC as the fourth MoP provide lowest errors than using the instantaneous FC. Moreover, as observed previously, Gipps' model is still more accurate than the IIDM.

In conclusion, a good compromise between the accuracy of the trajectory and the FC estimation is to use the Gipps' car-following model, calibrated on four MoP: the spacing, the speed, the acceleration and the cumulated FC. The averaged parameters values per category are presented in the following table.
We can observe that the reaction time values are small for urban and ring road cycles and the acceleration values are higher than for the other cycles. It implies that on urban roads or ring roads, the vehicle has a more dynamic behaviour than on other roads, with higher accelerations and quicker reactions. This could be explained in urban areas by the fact that there are more interactions with other vehicles and the infrastructure than on regional roads for example. For ring roads, the cycles correspond to on/off-ramp zones that lead to huge interactions between vehicles. This can explain such values for the acceleration and the reaction time.
The deceleration values are a little high, particularly for the Leader, but coherent because they do not represent a comfortable deceleration in Gipps' model, but a maximum deceleration. The desired speed values are consistent with the roads type and the truck capabilities.

Gipps' model mean optimal parameters per road category

	$\tau_n[s]$	$V_n^{des}[km/h]$	$a_n[m/s^2]$	$SafetyMargin[m]$	$\hat{b}_{n-1}[m/s^2]$	$b_n[m/s^2]$
Urban	0.79	44.3	1.61	2.41	-3.48	-1.58
Mid-urban	1.10	51.7	0.87	4.23	-3.56	-2.40
Regional	1.20	79.9	1.09	2.88	-3.81	-2.72
Ring road	0.33	81.1	1.27	2.01	-4.58	-2.05

Part II

Automatic generation of simulation cycles from statistics on usual routes for ITS evaluation

Chapter 1 highlighted the two questions studied in this thesis to improve the vehicle simulation model used in Volvo Group.

The first one, studied in Part I, deals with the definition of methods and scales of simulation adapted to take into account road traffic conditions and the reactions of a HDV to that traffic. This question was studied thanks to the definition of an adapted calibration method for usual car-following models, to generate truck trajectories which are relevant for both driving and FC points of view. This part has allowed to define sets of parameters for the Gipps car-following model for different applications: urban, mid-urban, regional and ring road.

The second part of the thesis investigates the second issue, related to the definition of a methodology allowing the creation of simulation cycles from information on topology, road network and infrastructure. This focuses on the research of statistical indicators linked to the usual routes driven by the HDV.
This study proposes to develop statistical methods allowing to create simplified road networks for a traffic simulation software. In this way, the coupling between the Volvo vehicle model and a traffic simulation software will allow the evaluation of ITS and ADAS.
The generated network would be statistically realistic but would not reproduce the real infrastructure that can be encountered by the vehicle. Using a simplified network will allow a quicker and simpler creation of the networks for simulation.

This part is divided in two chapters. The first one, Chapter 6 (p.89), introduces a statistical study of usual cycles and the creation method of simplified networks. First, it presents the usual cycles used in the study, then a description on how these cycles are sorted into five categories (corresponding to those of Part I): urban, mid-urban, regional, ring road and highway. On each of these categories, the defined statistics are computed. Finally, these statistics are used to automatically generate simplified road networks for simulation.
Chapter 7 (p.103) presents an application of the entire simulation chain (road traffic and vehicle modelling), on a long-haul cycle. This chapter compares the simulation results, in terms of average speed and fuel consumption, obtained with the method developed in this thesis, with the previously used tool and measurements. An evaluation of an ADAS is finally presented.

Chapter 6

Using usual driving cycle statistics for road traffic network generation via simulation tools

Contents

The coding of roads networks for traffic simulation purposes can be very time consuming. This chapter investigates the statistical information of a database of usual cycles. Several indicators are studied, the static ones like the number of lanes, the intersections, and the dynamic ones such as average speed under different traffic conditions. The aim of this chapter is to propose a methodology allowing the automatic generation of simplified networks for traffic simulation. These networks are based on usual cycles statistics. This information are used to generate networks having the same statistics as usual cycles but without reproducing the real geometry of infrastructure encountered by the vehicle.

To the author's best knowledge, automatic generation of network for simulation has not been widely investigated. The majority of works on that topic are about the definition of accurate driving cycles. Driving cycles, or driving schedules, are characterized by a plot of vehicle speed versus time, representing the typical driving behaviour or traffic conditions in a given city or region for different vehicles classes (Xiao et al., 2012). Driving cycles can also include information regarding road grade.

Barlow (2009) and Xiao et al. (2012) propose a review of the existing reference driving cycles and methodologies to develop them. Barlow (2009) references a total of 256 driving cycles that are grouped according to the purpose or the measurement program they belong to. As highlighted in Barlow (2009) driving cycles are often developed for a specific country or city: Gong et al. (2018); Liu et al. (2018); Qiu et al. (2018); Shen et al. (2018); Wang et al. (2008); Zhang et al. (2014); Zhao et al. (2018) for China, Arun et al. (2017); Mayakuntla and Verma (2018) for India, Amirjamshidi and Roorda (2015) for Toronto, Mahayadin et al. (2018) for Malaysia and Charadsuksawat et al. (2018) for Thailand for example. In Europe, the recent development of Vehicle Energy Consumption calculation TOol (VECTO) for trucks CO_2 certification (EuropeanCommission), has also lead to the definition of representative cycles for CO_2 calculation (Luz et al., 2014). For driving cycle creation, most existing studies use microtrips extracted from a set of driving measurements (Xiao et al., 2012). However, in this thesis we would like to propose a generic methodology that could be used whatever the country or the city, requiring only to compute the network statistics from GPS data.

The development of Electric Vehicles (EV) also implies the development of new driving cycles adapted for the evaluation and optimization of this type of vehicles. Much work has already been done to define accurate simulation driving cycles for EV (Brady and O'Mahony, 2016; Chrenko et al., 2012; Degrenne and Mollov, 2016; Gong et al., 2018; Schwarzer and Ghorbani, 2013), hybrid EV (Charadsuksawat et al., 2018; Shen et al., 2018) and plug-in hybrid EV tests (Guo et al., 2018).

However, in the development objective of ITS and ADAS, the representation of the vehicle environment is an important parameter that cannot be done only with driving cycles. The ITS and ADAS development requires the modelling of the other vehicles and the infrastructure that the vehicle under study needs to interact with.

In this chapter, we would like to propose a methodology for the automatic generation of representative networks based on statistical information instead of recorded speed profiles. These networks, coupled with the Volvo vehicle simulation model, will allow the estimation of the vehicle FC but also the test of ITS and ADAS. This chapter first presents the usual cycles and their statistics. Then, the traffic simulation software, SUMO, is presented with the process of the simplified networks generation. Finally, the statistics of generated networks are compared with the usual cycles.

6.1 Usual cycles

6.1.1 Usual cycles and HERE database presentation

This chapter is based on the statistical information collected on usual cycles. Usual cycles are defined as journeys done by HDV for their daily usages. The usual cycles used in this part were provided by the traffic engineering lab (LICIT) of IFSTTAR and Volvo Group.

Usual cycles database

This database contains 23 cycles located in and around the city of Lyon (France). These cycles are representative of two usages: (i) local delivery and (ii) regional delivery. They are composed of several types of roads: urban, mid-urban, regional, ring roads, and highways. Moreover, three single-type cycles (one urban, one ring road and one highway) complete the database. The highway cycle will be our reference cycle for the application presented in Chapter 7 (p.103).

The cycles are first classified into five categories: urban, mid-urban, regional, ring road and highway. These categories are based on the legal speed, the maximum and average observed speed according to the HERE database and the mean number of lanes. Then, single-type cycles are created. The five categories are

defined in Table 6.1. An example of the classification is presented in Figures 6.1 and 6.2, respectively for local and regional delivery cycles.

Table 6.1 – Characteristics of cycles categories

	Urban	Mid-Urban	Regional	Ring road	Highway
Legal Speed km/h	$0 \leq v \leq 50$	$50 \leq v \leq 70$	$50 \leq v \leq 90$	$70 \leq v \leq 110$	$90 \leq v$
Maximum observed speed km/h	$0 \leq v \leq 63$	$46 \leq v \leq 73$	$65 \leq v \leq 95$	$73 \leq v \leq 102$	$95 \leq v$
Average speed km/h	$0 \leq v \leq 53$	$43 \leq v \leq 67$	$64 \leq v \leq 92$	$68 \leq v \leq 94$	$94 \leq v$
Mean lanes number	-	-	< 1.9	≥ 1.9	≥ 2.3

Figure 6.1 – Classification of local delivery cycle

Figure 6.2 – Classification of regional delivery cycle

The cycles classification leads to the creation of 158 urban cycles with an average length of 5.2km, 138 mid-urban cycles which are 765m long in average, 41 regional cycles of 2.6km in average, 68 ring road cycles and 14 highway cycles, respectively 4.4km and 16.1km long in average. This results is detailed in Figure 6.3.

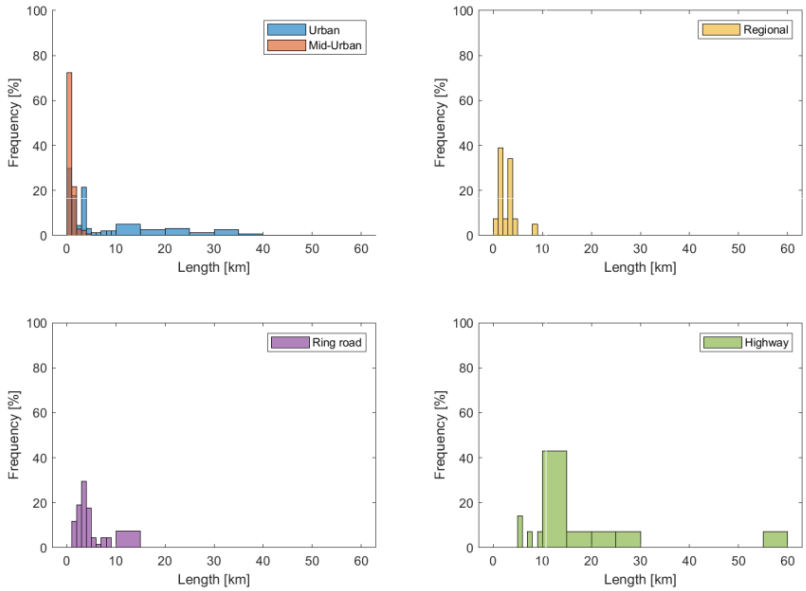

Figure 6.3 – Average length of the cycles categories

HERE Maps database

HERE Maps (HereMaps) is a database which contains many information regarding the road infrastructure and traffic conditions. From a Global Positioning System (GPS) trace, many information can be exported such as:

- the type of infrastructure (bridges for example),
- the number of lanes of the road,
- the altitude,
- the road signs,
- the legal speed, and,
- the average speed (historical information), stored for all edges, every days and every 15 minutes

This information is used here to define the required statistics of usual cycles for simplified network generation.

6.1.2 Statistical indicators investigated

The statistical indicators defined to represent usual cycles can be separated into two categories: (i) information related to the infrastructure (static) and (ii) information related to the road traffic conditions (dynamic).

Several indicators are defined to represent the usual cycles as best as possible. The indicators are presented in Table 6.2 and Table 6.3, respectively the static ones and the dynamic ones. The classical time slots corresponding to the three road traffic conditions in Lyon (on peak, off peak and free flow) are detailed in section 6.3.1. They are computed for each single-type cycle and averaged per road categories.

The succession of events (change in number of lanes, next intersection type, next speed limit...) is defined thanks to Markov Matrices. Markov Matrices have been often used in the literature for the generation of driving cycles (Liessner et al., 2016; Nyberg et al., 2014, 2016; Sun and Qiao, 2016). Moreover, the validity of Markov Property for driving cycles has been investigated and proven in Shuming Shi et al. (2013) and Shi et al. (2016), we assume that the Markov property is also verified for networks.

A Markov process is a mathematical stochastic model. It represents a memoryless system: the evolution of the system depends only on the present state (see Definition 6.1). The Markov Matrices or Probability Matrices are computed according to Definition 6.2.

Definition 6.1

Let $\mathbb{S}$ be a discrete set and X a $(\mathbb{S},\mathbb{S})$-valued stochastic process. X is said to fulfil the **Markov property** if, $\forall n \in \mathbb{N}$

$$P_r(X_{n+1} = x | X_1 = x_1, ..., X_n = x_n) = P_r(X_{n+1} = x | X_n = x_n)$$

Definition 6.2

A **Markov Process**, having n number of states, has a **Probability Matrix** $\mathbb{P}$ of size $n \times n$. $P_{i,j}$ is the probability to go from state i to state j, $\mathbb{P}$ defined as:

$$\mathbb{P} = \begin{bmatrix} P_{1,1} & . & . & P_{1,n} \\ . & & & . \\ . & & & . \\ P_{n,1} & . & . & P_{n,n} \end{bmatrix}$$

With $P_{i,j} = \dfrac{T_{i,j}}{\sum_{k=1}^{n} T_{i,k}}$, where $T_{i,j}$ is the number of times a transition from state i to j occurs.

Table 6.2 – Static indicators investigated

Type of information	Details
Length of cycles	- Minimum, maximum, mean, and standard deviation values of length
Intersection	- Number of intersections - Percentage of each type of intersections (Traffic light, Yield, Stop, Roundabout) - Type and position from the beginning of the first intersection - Density of intersections (number of intersections per kilometre) - Minimum, maximum, mean, and standard deviation values of spacing between two consecutive intersections - Markov Matrix to describe the succession of intersection types
Slope	- Number of valleys and peaks - Minimum, maximum, mean, and standard deviation values length of valleys and peaks - Markov Matrix describing the succession of slope differences every $20m$
Number of lanes	- Minimum, maximum, mean, and standard deviation values of the number of lanes - Number of lanes of the first edge (to begin the process) - Markov Matrix describing the succession of the number of lanes
Speed Limit	- Minimum, maximum, mean, and standard deviation values of the speed limit - Markov Matrix describing the succession of speed limits

Table 6.3 – Dynamic indicators investigated

Type of information	Details
Road Traffic on peak	- Minimum, maximum, mean, and standard deviation values of average speed - Markov Matrix describing how the average speed evolves
Road Traffic off peak	- Minimum, maximum, mean, and standard deviation values of average speed - Markov Matrix describing how the average speed evolves
Road Traffic free flow	- Minimum, maximum, mean, and standard deviation values of average speed - Markov Matrix describing how the average speed evolves

6.1.3 Usual cycles statistics

The indicators defined previously have been computed and averaged per road type. The results are presented in Table 6.4.

The usual cycles database contains cycles that represent local and regional deliveries. For these usages, the same statistics as for single-type cycles are computed. Moreover, the road type composition of these usages and the succession of road types described with Markov Matrices are computed. The statistics of local and regional usages are detailed in Appendix E.

The process to compute statistical information can be applied on any cycle type. It can be used to generate statistics for single-type cycles, for multi-type cycles corresponding to particular usage (local or regional delivery for example), but also to describe and simplify a particular cycle that would be used for simulation. This last case will be applied on a long-haul cycle in Chapter 7 to evaluate the impact of using a simplified network instead of a classical speed profile as input for simulation.

Results presented in Table 6.4 are consistent with the types of cycles. The number of intersections is high (19 in average) for urban cycles, the major part of intersections are traffic lights, and there are short (around $150m$) valleys and peaks. In contrast, for regional roads, the valleys and peaks are longer, around $315m$, and the major part of intersections are roundabouts. On highways, there are no intersections and the valleys and peaks are larger than $1km$ long. Highway cycles are in average $16km$ long.

Statistics presented in Appendix E highlight that local delivery cycles are composed of 75% of urban roads and 20% of ring roads and they are $42.1km$ long in average. Regional delivery cycles are made of 29% of urban roads, 26% of highway, 17% of Regional roads and ring roads, and 11% of mid-urban roads. They are in average $200.2km$ long.

Table 6.4 – Statistics of usual cycles

	Urban	**Mid-Urban**	**Regional**	**Ring Road**	**Highway**
Number of samples	158	138	41	68	14
Mean length $[m]$	5167	765	2642	4406	16082
Mean number of intersections	19.4	0.9	1.3	0.1	0.0
Percentage of intersection type					
Traffic lights	88.7	61.9	11.3	0.0	0.0
Yields	2.2	10.2	3.8	66.7	0.0
Stops	1.7	4.2	11.3	0.0	0.0
Roundabouts	7.4	23.7	73.6	33.3	0.0
Density of intersections	0.37	0.23	0.07	0.03	0.0
Mean spacing between intersections $[m]$	332.3	441.5	566.0	562.5	0.0
Mean number of peaks	18.6	2.1	4.5	5.3	8.5
Mean length of peaks $[m]$	145.1	221.1	307.1	401.9	1182.0
Mean number of valleys	18.2	2.0	4.5	5.1	9.0
Mean length of valleys $[m]$	148.3	196.2	333.1	473.1	1192.8
Mean number of lanes	1.5	1.5	1.2	2.6	2.6
Mean speed limit $[km/h]$	49.2	71.1	85.6	91.0	122.5
Mean speed under ON peak conditions $[km/h]$	29.9	49.1	65.7	73.2	110.9
Mean speed under OFF peak conditions $[km/h]$	33.3	55.2	68.6	80.7	111.0
Mean speed under FREE flow conditions $[km/h]$	36.1	59.6	71.8	84.9	114.5

6.2 SUMO, an open source traffic simulation software

The previous sections presented the statistics of usual cycles. These statistics are computed to generate realistic simplified networks for road traffic simulation. The simulations are implemented using the open source software SUMO (Krajzewicz et al., 2012). This simulator accounts for different types of network, urban or at larger scales. The microsimulation is based on the Krauß car-following model (Krajzewicz et al., 2012) which is a variant of the Gipps car-following model.

SUMO simulations are based on five main files. The road network is defined through two files, containing the positions of the nodes (geometrical points) and the information about edges (road segments defined by the nodes they connect, their number of lane and speed limit). These two files are referenced in a main file named *network.net.xml*. The configuration file, *network.sumocfg*, contains references to the network file and to the one containing the routes driven by vehicles. An example of a network modelled with SUMO is presented in Figure 6.4. SUMO has been chosen for this study because it is an open source simulation software. Moreover, the simulations files are based on XML language that allows to generate them simply and quickly thanks to Python scripts.

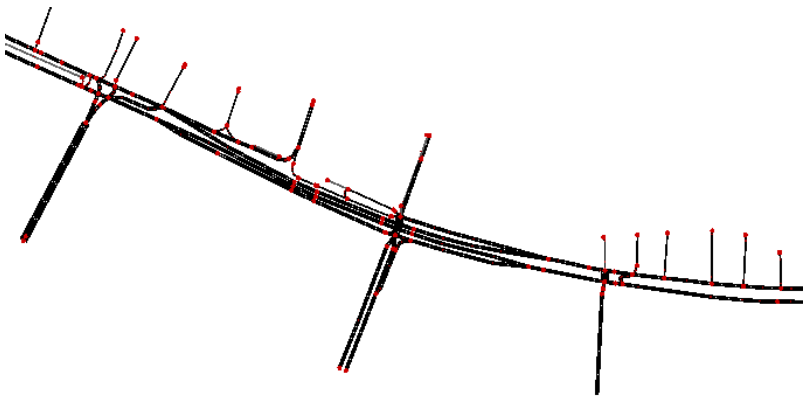

Figure 6.4 – Example of a SUMO network

6.3 The generation of simplified networks

6.3.1 Methodology

The creation of road network for simulation can be very time-consuming. To help the creation of road networks, SUMO for example, proposes to import data from map data provider like Open Street Map (OpenStreetMaps). However, this process needs to correct the imported network, particularly on intersections where junctions between roads can be difficult to represent.

SUMO offers the possibility to generate random networks (SUMOGit, 2019). These networks can have three geometries:

- *grid-like* networks (Figure 6.5 (a)),
- *spider-like* networks (Figure 6.5 (b)) or,
- random networks (Figure 6.5 (c)).

For representativeness reasons, these solutions are not usable here.

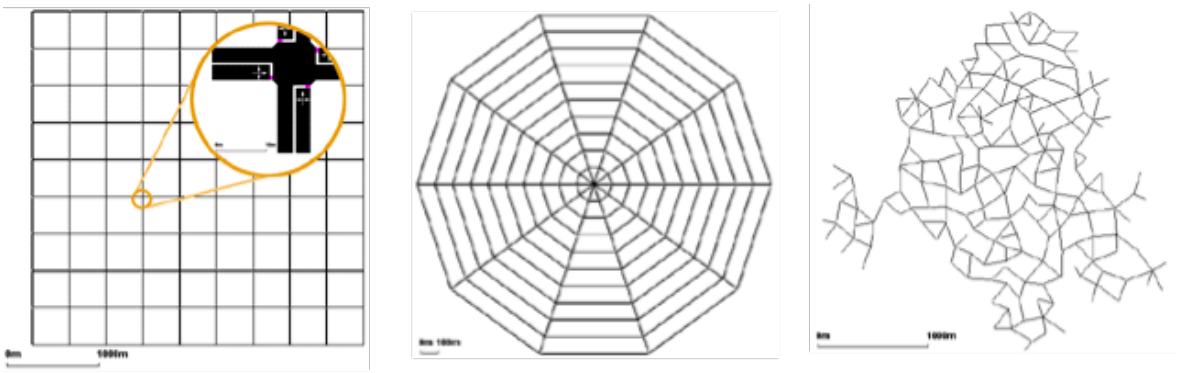

(a) grid-like network (b) spider-like network (c) random network

Figure 6.5 – SUMO type of network

The work presented here proposes a method to generate SUMO networks for simulation. The method proposed allows to choose between different types of cycles (single-type, delivery-type or particular roads), different route lengths and different road traffic conditions. The options of the process are detailed in Table 6.5.

Table 6.5 – Options for automatic SUMO network creation

Road Type			Length	Road Traffic conditions
Single-type	Delivery-type	Specific road		
Urban Mid-Urban Regional Ring Road Highway	Local Regional	To be defined by the user	To be defined by the user except for specific roads where it is adapted to the real road length	On peak Off peak Free flow

On-peak traffic conditions correspond to the traffic encountered between 8:30 and 9:45 in the morning and between 17:45 and 18:45 in the afternoon. The off-peak traffic conditions deal with road traffic between 6:00 and 7:15 in the morning and between 20:00 and 21:30 in the evening. The free flow condition is achieved for the highest average speed observed on the roads.

The generation of a simplified network follows the same process whatever the type of cycle chosen. Figure 6.6 presents the road traffic network creation process.

First, the main road is divided into edges of $20m$ long. Then, the number of intersections and their types are computed, based respectively on the intersection density (the average number of intersections per kilometre) and the Markov Matrix describing the sequence of intersection types. Afterwards, the number of lanes, the slope and the speed limit of each edge are defined according to the corresponding Markov Matrices computed. Next, the average vehicles speed on the edges are defined for the three road traffic conditions cited in Table 6.5. Finally, the consecutive edges having the same characteristics are merged to reduce the number on edges in the network. The generated information for the network is stored in four files. The two first ones contain the data related to the edges and their lanes. A third file contains the average speed information while the last

one references the intersections (stops, yields and traffic lights). These four files are then processed to generate SUMO network configuration files.

The time needed to generate such a network is very short, less than one minute in major cases. The process can reach about ten minutes in some cases due to the constraints that speed values must fulfil. For more realism, in the generation process, the speed limit must be observed in at least 90% of the network edges. Moreover, the average speed under on peak traffic conditions must be smaller than the average speed under off-peak traffic conditions which has to be smaller than the average speed under free flow traffic conditions.

Once the SUMO network has been created, it has to be calibrated. The calibration method has been developed within the Volvo Group. The calibration of the network consists in defining several routes on the network that cover a percentage (defined by the user) of the available roads. Several vehicle types are also defined based on observations of the traffic composition in different sites. Then, a calibration method based on the PSO algorithm is applied to determine the needed vehicles on the network and their departure times which ensures the observation of average speed on edges corresponding to the one defined when generating automatically the network. The calibration lasts less than a day, it is not so long due to the simplification of the network.

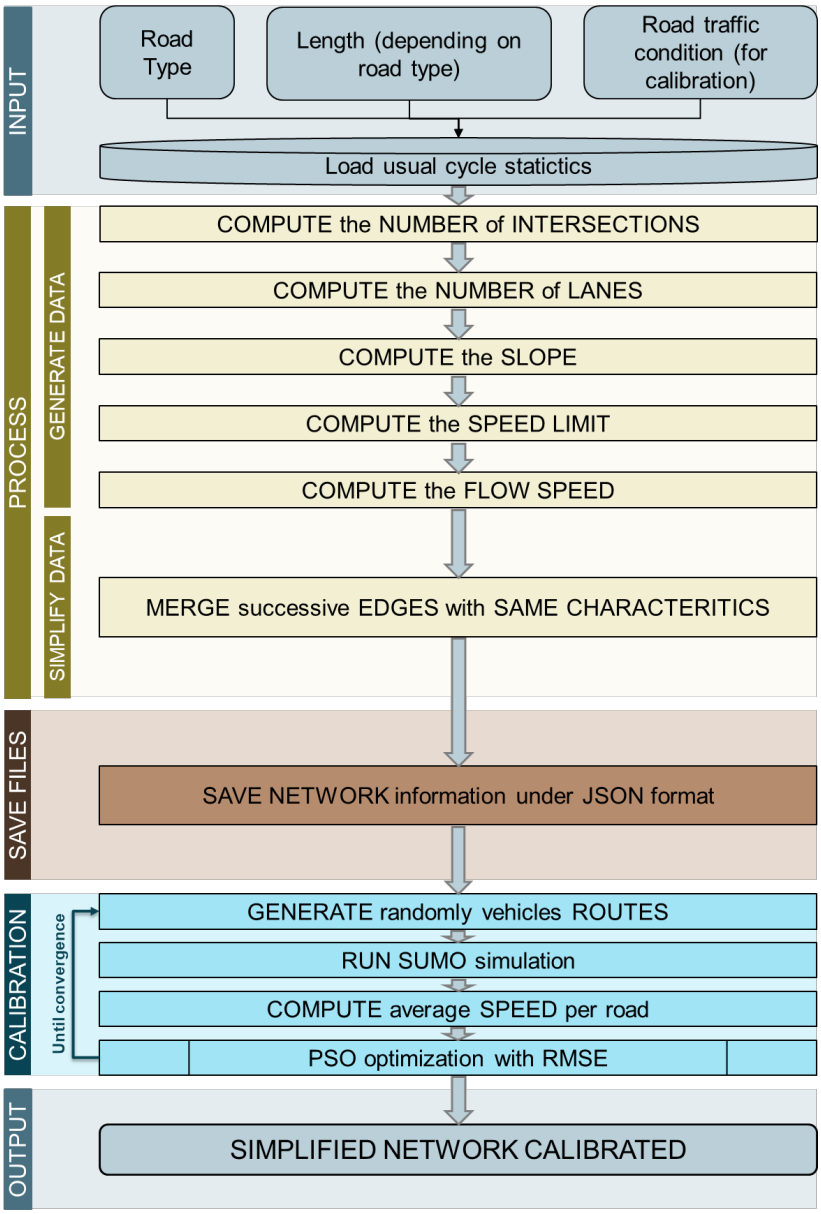

Figure 6.6 – Process of simplified SUMO network creation

6.3.2 Validation

This section presents the comparison between the statistics of usual cycles presented in section 6.1.3 (p.93) with respect to the statistics of networks created through the process detailed in the previous section. Two cycle types will be detailed here, but the results are relevant for all cycles options.

For both urban and regional cycles, 100 simplified cycles are generated, with a length close to the average length of usual cycles. The characteristics of the generated simplified networks are compared to the one of the usual cycles.

Urban cycles

Urban simplified networks are about 5000m long. The comparison between usual cycles and generated networks for intersections and average speed are illustrated in Figures 6.7 and 6.8 respectively. In these figures, the red circles refer to the mean values for generated network while the green stars refer to mean values for usual cycles.

The generated urban networks have an average intersection density equal to 0.43 $intersections/km$ while it is equal to 0.37 $intersections/km$ for usual cycles. The distribution of intersections is fulfilled, with a majority of traffic lights, some roundabouts, and very few yields or stops. However, the proportion of traffic lights in generated networks is a little smaller than in usual cycles (62% instead of 89%) while the roundabouts one is bigger (31% instead of 7%).

The average speed limits are close for usual cycles and generated networks, respectively 49.2km/h and 48.3km/h. On generated cycles, we can observe a smaller average flow speed than on usual cycles (Figure 6.8). Particularly, under on peak traffic conditions, the average speed in generated networks is equal to 26.2km/h while it is equal to 32.7km/h in usual cycles. However, the speed observed in usual cycles are in the range of observed values in generated cycles.

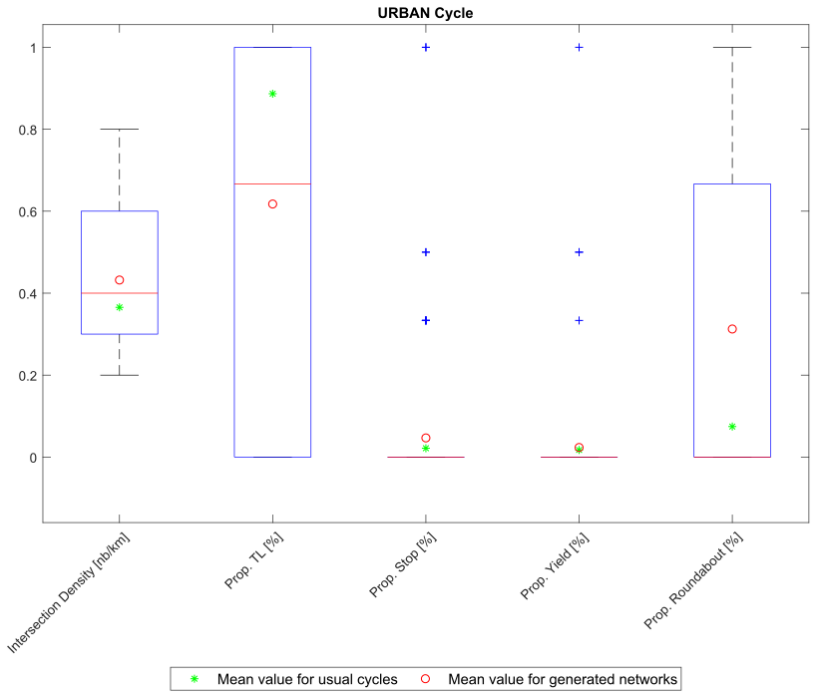

Figure 6.7 – Comparison of intersection density between urban usual cycles and urban generated networks

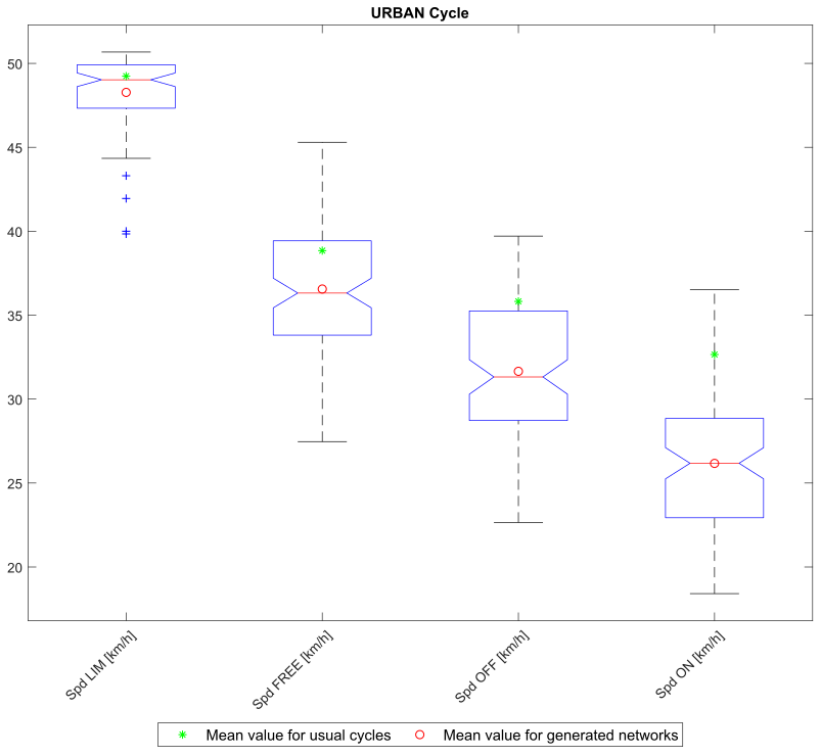

Figure 6.8 – Comparison of average speeds between urban usual cycles and urban generated networks

Regional cycles

Generated regional networks are about 2500m long. The comparison between usual cycles and generated networks for intersections and average speed are illustrated in Figures 6.9 and 6.10 respectively. In these figures, the red circles refer to the mean values for generated network while the green stars refer to mean values for usual cycles.

The generated regional networks have an average intersection density equal to 0.35 $intersections/km$ while it is equal to 0.1 $intersections/km$ for usual cycles. The generated networks contains a little more intersections than usual cycles, however, the distribution of intersections is fulfilled, with a majority of roundabouts, and some yields or stops. It appears here that the generated networks do not contain traffic lights whereas usual cycles do. This can be explained by three parameters: (i) the intersection density is low, (ii) the cycle is small and (iii) there is a high proportion of roundabouts. The intersection density value and the length of regional networks allow only one intersection. Moreover, the first intersection is chosen randomly according to the proportion of the first intersection types encountered into usual cycles. In the available data, the first intersection was never a traffic light that explain that the generated cycles do not contain any traffic light. The proportion of roundabouts, yields and stops in generated networks and usual cycles are close as it is illustrated in Figure 6.9.

The average speed limits, average free flow speed and average off peak speed are really close for usual cycles and generated networks, respectively 85.6km/h and 84.4km/h, 67.9km/h and 70.1km/h and, 64.5km/h and 62.2km/h. On generated cycles, we can observe smaller average flow speed under on peak traffic conditions than on usual cycles (Figure 6.10). The average speed in generated networks is equal to 53.2km/h while it is equal to 61.7km/h in usual cycles. However, the speed observed in usual cycles are in the range of values observed in generated cycles.

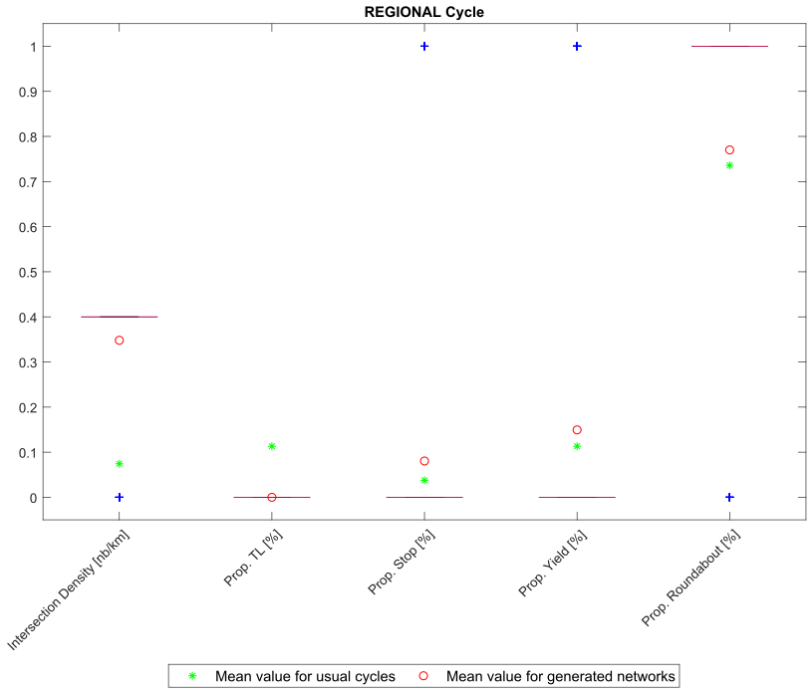

Figure 6.9 – Comparison of intersection density between regional usual cycles and regional generated networks

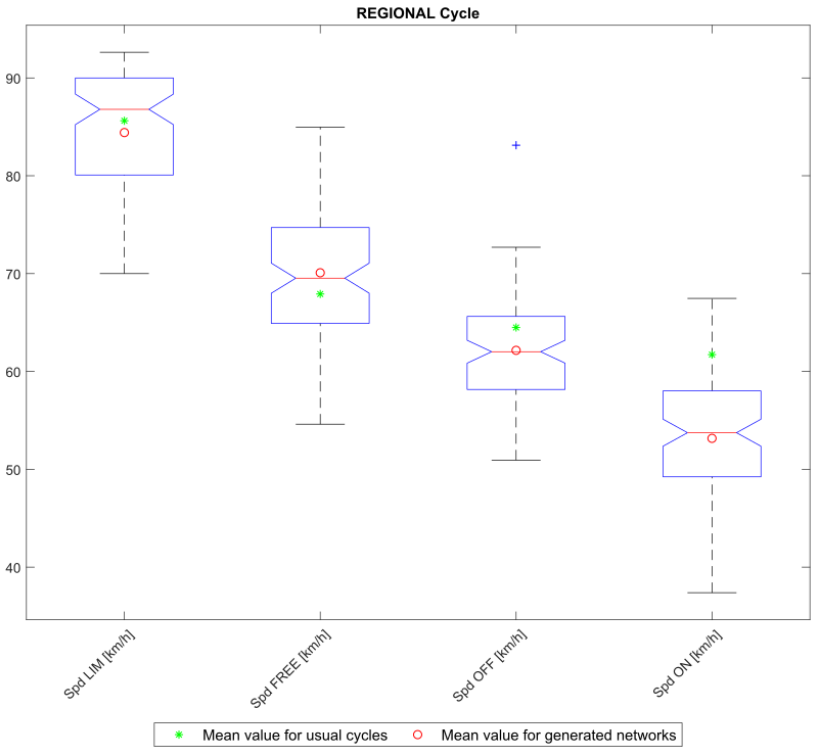

Figure 6.10 – Comparison of average speeds between regional usual cycles and regional generated networks

6.4 Conclusion of the chapter

In this chapter, a highlight on usual cycle of HDV was done. The static and dynamic statistics of these cycles are presented.

Then, a methodology to generate simplified SUMO networks for simulation based on these statistics is presented. It is pointed out that the proposed methods allow an easy creation of relevant simulation networks.

Figures 6.7 to 6.10 illustrate the representativeness of the generated networks with regards to the usual cycles. The accuracy of the generated networks can be increased by the improvement of the road classification (to prevent from errors into statistics) and also by merging several road data base (Open Street Map, Google Maps) instead of using only one.

6.5 References

Glareh Amirjamshidi and Matthew J. Roorda. Development of simulated driving cycles for light, medium, and heavy duty trucks: Case of the Toronto Waterfront Area. *Transportation Research Part D: Transport and Environment*, 34:255–266, January 2015. ISSN 13619209. doi: 10.1016/j.trd.2014.11.010. p. 90

N.H. Arun, Srinath Mahesh, Gitakrishnan Ramadurai, and S.M. Shiva Nagendra. Development of driving cycles for passenger cars and motorcycles in Chennai, India. *Sustainable Cities and Society*, 32:508–512, July 2017. ISSN 22106707. doi: 10.1016/j.scs.2017.05.001. p. 90

T. J Barlow. *A reference book of driving cycles for use in the measurement of road vehicle emissions*. IHS, Bracknell, 2009. OCLC: 751482569. p. 90

John Brady and Margaret O'Mahony. Development of a driving cycle to evaluate the energy economy of electric vehicles in urban areas. *Applied Energy*, 177:165–178, September 2016. ISSN 03062619. doi: 10.1016/j.apenergy.2016.05.094. p. 90

A. Charadsuksawat, Y. Laoonual, and N. Chollacoop. Comparative Study of Hybrid Electric Vehicle and Conventional Vehicle Under New European Driving Cycle and Bangkok Driving Cycle. In *2018 IEEE Transportation Electrification Conference and Expo, Asia-Pacific (ITEC Asia-Pacific)*, pages 1–6, Bangkok, June 2018. IEEE. ISBN 978-1-5386-5782-9. doi: 10.1109/ITEC-AP.2018.8432599. p. 90

Daniela Chrenko, Irene Garcia Diez, and Luis Le Moyne. Artificial driving cycles for the evaluation of energetic needs of electric vehicles. In *2012 IEEE Transportation Electrification Conference and Expo (ITEC)*, pages 1–5, Dearborn, MI, USA, June 2012. IEEE. ISBN 978-1-4673-1408-4 978-1-4673-1407-7 978-1-4673-1406-0. doi: 10.1109/ITEC.2012.6243426. p. 90

N. Degrenne and S. Mollov. Real-life vs. standard driving cycles and implications on EV power electronic reliability. In *IECON 2016 - 42nd Annual Conference of the IEEE Industrial Electronics Society*, pages 2177–2182, Florence, Italy, October 2016. IEEE. ISBN 978-1-5090-3474-1. doi: 10.1109/IECON.2016.7793633. p. 90

EuropeanCommission. VECTO - European Commission. URL https://ec.europa.eu/clima/policies/transport/vehicles/heavy_en. p. 90

Huiming Gong, Yuan Zou, Qingkai Yang, Jie Fan, Fengchun Sun, and Dietmar Goehlich. Generation of a driving cycle for battery electric vehicles: A case study of Beijing. *Energy*, 150:901–912, May 2018. ISSN 03605442. doi: 10.1016/j.energy.2018.02.092. p. 90

Jinquan Guo, Chao Sun, Hongwen He, and Jiankun Peng. Urban Global Driving Cycle Construction Method and Global Optimal Energy Management in Plug-in Hybrid Electric Vehicle. *Energy Procedia*, 152:593–598, October 2018. ISSN 18766102. doi: 10.1016/j.egypro.2018.09.216. p. 90

HereMaps. HERE. URL https://www.here.com. p. 92

Daniel Krajzewicz, Jacob Erdmann, Michael Behrisch, and Laura Bieker. Recent development and applications of SUMO–Simulation of Urban MObility. *International Journal On Advances in Systems and Measurments*, 5(3&4):128–138, December 2012. p. 94

R. Liessner, A.M. Dietermann, B. Bäker, and K. Lüpkes. Derivation of Real-World Driving Cycles Corresponding to Traffic Situation and Driving Style on the Basis of Markov Models and Cluster Analyses. In *6th Hybrid and Electric Vehicles Conference (HEVC 2016)*, pages 1 (7 .)–1 (7 .), London, UK, 2016. Institution of Engineering and Technology. ISBN 978-1-78561-294-7. doi: 10.1049/cp.2016.0961. p. 92

Bingjiao Liu, Qin Shi, Lin He, and Duoyang Qiu. A study on the construction of Hefei urban driving cycle for passenger vehicle. *IFAC-PapersOnLine*, 51(31):854–858, 2018. ISSN 24058963. doi: 10.1016/j.ifacol.2018.10.100. p. 90

Raphael Luz, Martin Rexeis, Stefan Hausberger, Dalibor Jajcevic, Wolfgang Lang, Leif-Erik Schulte, Jan Hammer, Lutz Lessmann, Mensch van Pim, Ruud Verbeek, and Steven Heinz. Development and validation of a methodology for monitoring and certification of greenhouse gas emissions from heavy duty vehicles through vehicle simulation, Final report. Service contract CLIMA.C.2/SER/2012/0004 I 07/14/Rex EM-I 2012/08 699 from 25.06.2014, Consortium of TUV, TUV-Nord Mobilitat, Heinz Steven and TNO, 2014. p. 90

A. R. Mahayadin, I. Ibrahim, I. Zunaidi, A. B. Shahriman, M. K. Faizi, M. Sahari, M. S. M. Hashim, M. A. M. Saad, M. S. Sarip, Z. M. Razlan, M. F. H. Rani, Z. M. Isa, N. S. Kamarrudin, A. Harun, and Y. Nagaya. Development of Driving Cycle Construction Methodology in Malaysia's Urban Road System. In *2018 International Conference on Computational Approach in Smart Systems Design and Applications (ICASSDA)*, pages 1–5, Kuching, August 2018. IEEE. ISBN 978-1-5386-8369-9. doi: 10.1109/ICASSDA.2018.8477619. p. 90

Sai Kiran Mayakuntla and Ashish Verma. A novel methodology for construction of driving cycles for Indian cities. *Transportation Research Part D: Transport and Environment*, 65:725–735, December 2018. ISSN 13619209. doi: 10.1016/j.trd.2018.10.013. p. 90

Peter Nyberg, Erik Frisk, and Lars Nielsen. Generation of Equivalent Driving Cycles Using Markov Chains and Mean Tractive Force Components. *IFAC Proceedings Volumes*, 47(3):8787–8792, 2014. ISSN 14746670. doi: 10.3182/20140824-6-ZA-1003.02239. p. 92

Peter Nyberg, Erik Frisk, and Lars Nielsen. Using Real-World Driving Databases to Generate Driving Cycles With Equivalence Properties. *IEEE Transactions on Vehicular Technology*, 65(6):4095–4105, June 2016. ISSN 0018-9545, 1939-9359. doi: 10.1109/TVT.2015.2502069. p. 92

OpenStreetMaps. OSM. URL https://www.openstreetmap.org. p. 95

Duoguan Qiu, Yuan Li, and Dapeng Qiao. Recurrent Neural Network Based Driving Cycle Development for Light Duty Vehicles in Beijing. *Transportation Research Procedia*, 34:147–154, 2018. ISSN 23521465. doi: 10.1016/j.trpro.2018.11.026. p. 90

Volker Schwarzer and Reza Ghorbani. Drive Cycle Generation for Design Optimization of Electric Vehicles. *IEEE Transactions on Vehicular Technology*, 62(1):89–97, January 2013. ISSN 0018-9545, 1939-9359. doi: 10.1109/TVT.2012.2219889. p. 90

Peihong Shen, Zhiguo Zhao, Jingwei Li, and Xiaowen Zhan. Development of a typical driving cycle for an intra-city hybrid electric bus with a fixed route. *Transportation Research Part D: Transport and Environment*, 59:346–360, March 2018. ISSN 13619209. doi: 10.1016/j.trd.2018.01.032. p. 90

Shuming Shi, Nan Lin, Yan Zhang, Jingmin Cheng, Chaosheng Huang, Li Liu, and Bingwu Lu. Research on Markov property analysis of driving cycles and its application. *Transportation Research Part D: Transport and Environment*, 47:171–181, August 2016. ISSN 13619209. doi: 10.1016/j.trd.2016.05.013. p. 92

Shuming Shi, Nan Lin, Yan Zhang, Chaosheng Huang, Li Liu, Bingwu Lu, and Jingmin Cheng. Research on Markov Property Analysis of Driving Cycle. In *2013 IEEE Vehicle Power and Propulsion Conference (VPPC)*, pages 1–5, Beijing, October 2013. IEEE. ISBN 978-1-4799-0720-5. doi: 10.1109/VPPC.2013.6671737. p. 92

SUMOGit. AbstractNetworkGeneration, 2019. URL http://sumo.dlr.de/wiki/Networks/Abstract_Network_Generation. p. 95

Bingying Sun and Dapeng Qiao. Driving cycle construction methodology based on Markov process and uniform distribution. In *2016 35th Chinese Control Conference (CCC)*, pages 9300–9304, Chengdu, China, July 2016. IEEE. ISBN 978-988-15639-1-0. doi: 10.1109/ChiCC.2016.7554835. p. 92

Qidong Wang, Hong Huo, Kebin He, Zhiliang Yao, and Qiang Zhang. Characterization of vehicle driving patterns and development of driving cycles in Chinese cities. *Transportation Research Part D: Transport and Environment*, 13(5):289–297, July 2008. ISSN 13619209. doi: 10.1016/j.trd.2008.03.003. URL https://linkinghub.elsevier.com/retrieve/pii/S1361920908000333. p. 90

Zhang Xiao, Zhao Dui-Jia, and Shen Jun-Min. A Synthesis of Methodologies and Practices for Developing Driving Cycles. *Energy Procedia*, 16:1868–1873, 2012. ISSN 18766102. doi: 10.1016/j.egypro.2012.01.286. p. 90

Biao Zhang, Xia Gao, Xisen Xiong, Xiaodan Wang, and Hailiang Yang. Development of the Driving Cycle for Dalian City. In *2014 8th International Conference on Future Generation Communication and Networking*, pages 60–63, Hainan Island, China, December 2014. IEEE. ISBN 978-1-4799-7780-2 978-1-4799-7779-6. doi: 10.1109/FGCN.2014.22. p. 90

Jingyuan Zhao, Yinhan Gao, Jianhua Guo, and Liang Chu. The creation of a representative driving cycle based on Intelligent Transportation System (ITS) and a mathematically statistical algorithm: A case study of Changchun (China). *Sustainable Cities and Society*, 42:301–313, October 2018. ISSN 22106707. doi: 10.1016/j.scs.2018.05.031. p. 90

Chapter 7

Use case: ADAS evaluation on a Long-Haul Cycle

Contents

This chapter presents the application of the methods presented in this thesis. The previous chapter (Chapter 6), details the methodology to automatically generate realistic road networks through statistical information from usual cycles. It was highlighted that the created networks, from a statistical point of view, are consistent to the usual cycles studied.

This chapter investigates the relevance of simplified road network usage for FC estimation and assessment of ITS and ADAS. Driving cycles (DC) relevance has been studied in the literature (Achour and Olabi, 2016; Chindamo and Gadola, 2018; Hereijgers et al., 2017), however, as the creation of simplified networks for simulation has not been widely studied, to the best author's knowledge, their relevance has not been validated either. The conclusions about DC impact on FC estimation differ a lot depending on the DC used.

Chindamo and Gadola (2018) compare three DC: the New European Driving Cycle (NEDC), the World Harmonized Light Vehicles Test Procedures (WLTC) and the Common Artemis Driving Cycles (CADC) used by a Light Duty Vehicle (LDV). This study compares the pollutant emissions of the LDV on these three DC with real-world emission levels. It has been demonstrated that the synthetic NEDC cycles cannot to reproduce real-world driving conditions, but the WLTC and CADC cycles seem to offer a better estimate. The WLTC cycle is the closest to the real-world data but it still leads to the underestimation of the pollutant emissions.

Achour and Olabi (2016) propose to develop specific DC for each test case. The authors precise that the development of DC for the estimation of the impacts of road traffic energy consumption on the environment is more and more studied. However, a major problem with these DC is that they vary from one city to another due to the type of principle activities present. The authors propose a method based on recorded data on equipped vehicles and COPERT software to estimate vehicle emissions. The method was evaluated in two cities: Aleppo and Dublin. The results show that the created DC were close to real-world driving conditions and allow an accurate estimation of FC.

Hereijgers et al. (2017) propose a method based on Markov chains to create synthetized DC and compare them with the NEDC. The cycles are evaluated with three different vehicle types: conventional vehicles, full hybrid and mild-hybrid electric vehicles. The results show that using synthesized DC to build vehicle prototypes is possible. Using these DC instead of real-world DC or very simplistic DC like the NEDC, reduces considerably the simulations times and it results in more robust and less sub-optimal vehicle designs.

The two previous studies show that using generic DC to estimate FC can lead to important bias compared to real values. The differences between two cities do not allow the use of such DC. For the accurate estimation of vehicles energy consumption, defining a DC for each application seems better. The work presented in the previous chapter allows the generation of simplified simulation networks requiring only the GPS information on the route used by the vehicle. The evaluation of the generated networks according to the fuel consumption estimation and speed achieved by the studied vehicle is presented in this chapter. The possibility to test ITS and ADAS is also highlighted.

This chapter first presents the DC used for the method evaluation. Then, the results of simulations realized with the usual DC and the simplified networks are compared with measurements. Finally, an example of potential use for ITS or ADAS development of simplified networks is presented in section 7.2 (p.108).

7.1 The Long-Haul driving cycle

This section presents the DC used for the validation of the method to generate simplified networks for simulation.

7.1.1 Driving Cycle presentation

The DC used for the validation of the method is a long-haul cycle of about 101.5km long (Figure 7.1). This cycle begins in the south-east of Lyon and ends after the city of Chambéry (FRANCE).

This cycle contains four intersections: three traffic lights and one yield. The average number of lanes is equal to 2.4. This DC contains around 55 slopes and the same number of valleys, respectively about 1430m and 1200m long in average.

The speed limit of this cycle is equal to 118km/h in average. The observed speeds are equal to 106km/h for on-peak and off-peak conditions and to 109km/h under free-flow conditions, there are not so much traffic flow variations for long-haul usages.

Figure 7.1 – Long-haul driving cycle

7.1.2 Application: Comparison of usual DCs and simplified networks with measurements

To conclude on the accuracy of simplified networks for fuel consumption estimation, the simulation results are compared with measurements and simulation results obtained with the usual DC. The simulation architecture including Volvo vehicle model and SUMO software is detailed in Figure 7.2. Data are compared regarding the length of cycles, their duration, the average speed reached by the vehicle and the FC estimation.

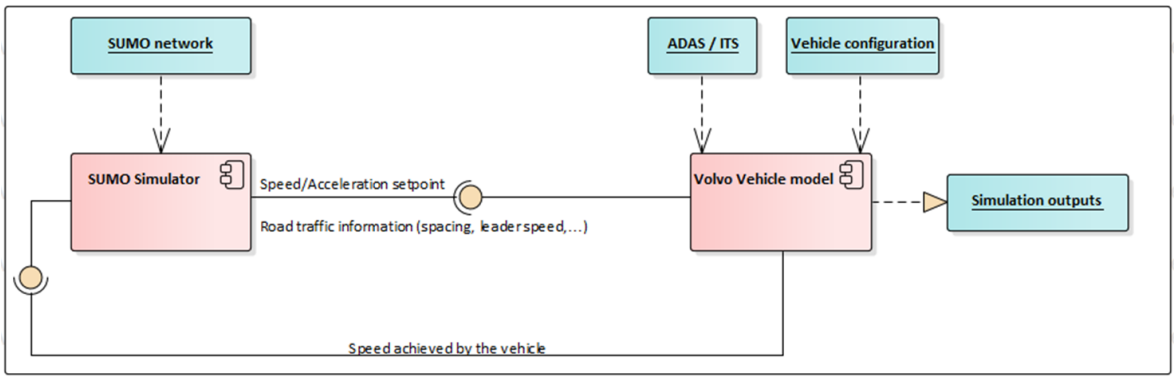

Figure 7.2 – Simulation architecture including Volvo vehicle model and SUMO software

7.1.2.1 Data presentation

Measurement

Several measurements, 15 in total, were realized along the route presented in Figure 7.1. The recorded cycles are in average 102.6km, last 1h21 in average with a mean vehicle speed equal to 76.3km/h.

Classical Driving Cycle

The corresponding DC of this route is defined to be 102.5km long, with an average set speed equal to 70.7km/h. The simulation is realized with the vehicle simulator of Volvo Group. The software has been configured to correspond to the vehicle used to record the data presented in previous paragraph.

Simplified Network

The simplified network has been generated for off-peak traffic conditions (106km/h in average for the vehicle flow). The route used by the studied vehicle is about 100.3km. The Volvo vehicle model is coupled in close loop with the SUMO traffic simulation software for simulations. The speed set points are sent to the vehicle model at each time step, the vehicle model computes the true speed that the vehicle can achieve according to its configuration, and finally write the achieved speed into the traffic simulator.

The simplified network was generated with a fixed seed value equal to 11 to ensure reproducibility. For the simulations, SUMO also allows to modify the value of the seed. This value is used for the initialization of the random number generator. It will influence the speed distribution and the behaviour of vehicles during the simulation. The simulations were run with 64 different seed values to observe a distribution of the potential behaviour of the studied vehicle.

7.1.2.2 Results comparison

The comparison of the three data is presented in the following paragraphs. Figures 7.3, 7.4, 7.5 and 7.6 respectively compare the duration of cycles, their length, the average speed achieved by the vehicle and its FC. On these figures, boxplots illustrate the distribution of values for measurements and SUMO-simulations, their mean value is represented thanks to the red circles, and the usual cycle simulation value is represented by the green dotted line.

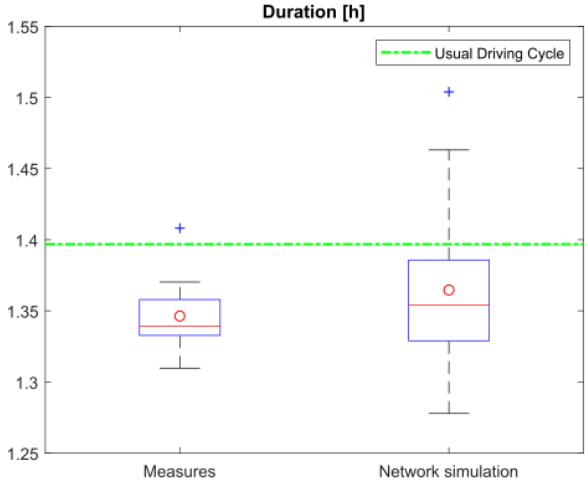

Figure 7.3 – Cycle duration comparison

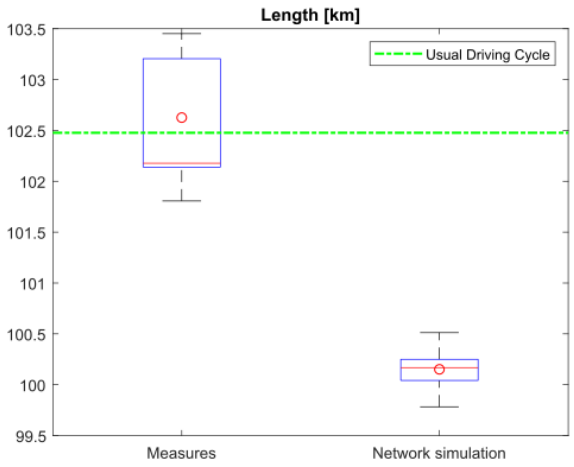

Figure 7.4 – Cycle length comparison

In Figure 7.3 we can see that the usual DC is a little slower (around 5min) than the measurements and the SUMO-simulations in average. However, we can see that the range of values obtained with SUMO-simulations is larger than the one measured. The usual DC duration is contained in the SUMO-simulations while it is not the case in the measurements.

There are also some differences between the lengths of the cycles. The generated network is 2km smaller in average than usual DC and measurements. Moreover, the generated network has also a smaller dispersion around the average length of the route.

The two previous observations are consistent with the average speed values. The measurements are longer and faster, which implies a higher average speed than for SUMO-simulations. The usual DC average speed is closer to the average speed observed in SUMO-simulations than to the one measured but it is still in the range of measured values. Correlated with the cycle duration, the average speed range in SUMO-simulations is larger than in measurements.

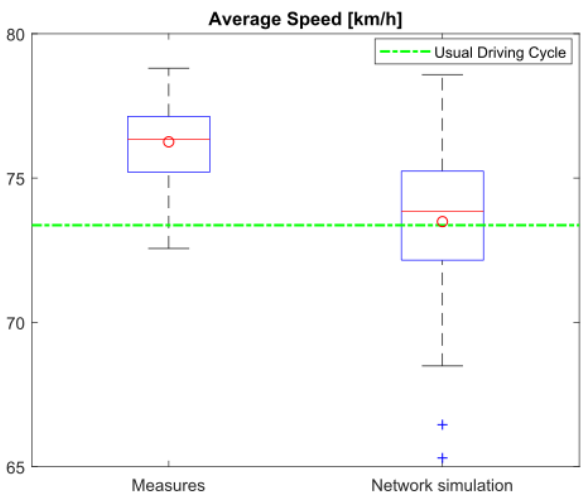

Figure 7.5 – Cycle average speed comparison

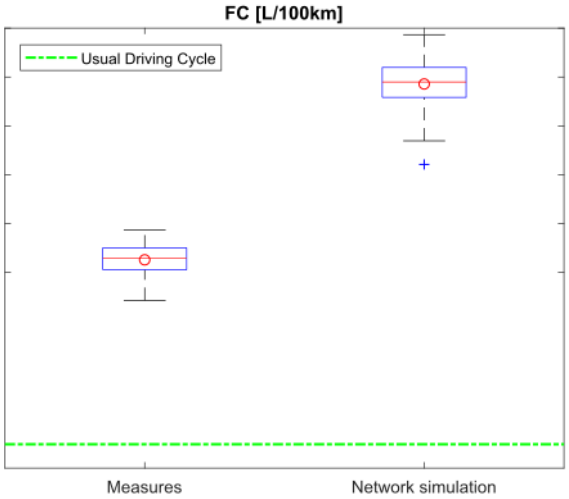

Figure 7.6 – Cycle average FC comparison

Major differences can be observed between the FC computed. The usual DC provides the smallest value for the FC estimation while the SUMO-simulations provide the biggest one. The values computed during the measures are halfway between the other data, however, the dispersion of values is similar for measurements and SUMO-simulations. In order to find the origin of these differences, the instantaneous speed and the cumulated FC are investigated more in depth.

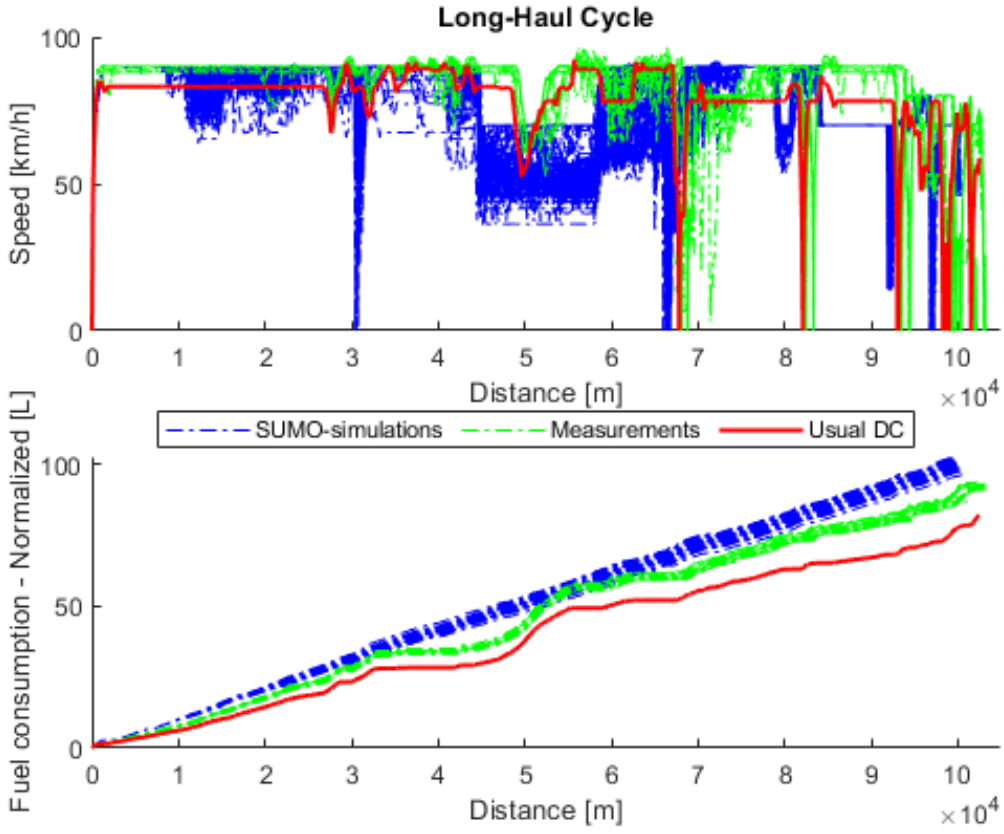

Figure 7.7 – Instantaneous speed and cumulated FC comparison

Figure 7.7 presents the speed profiles and the normalized cumulated FC obtained with SUMO-simulations, measurements and usual DC. The three types of speed profiles are similar with speed reductions and stops at equivalent locations.

First, we can observe that there are more oscillations (due to road traffic) in the SUMO-simulations and in the measurements than in the usual DC. Particularly, SUMO-simulations generate a lot of oscillations between 10 and 30km. Between 40 and 75km, high speed oscillations can also be observed for SUMO-simulations and measurements. Moreover, when the speed is almost constant (between 0 and 25km, between 70 and 75km and between 85 and 90km) we can observe that the vehicle is generally slower in the usual DC than in the SUMO-simulations or measurements. These differences in constant speed and oscillations have an important impact on the FC.

For example, in the first part of the route (until 30km) we can see that the cumulated FC increases more slowly for the usual DC than for the two other data where the vehicle speed is higher and with more oscillations.

We can also notice that the cumulated FC has similar shapes for the measurements and for usual DC. However, its shape for SUMO-simulations is more linear. This should be explained by the fact that the slope is not exactly the same when generating a simplified network as it is in the usual DC. We would only like to keep the average length of valleys and peaks, and the slope values are computed thanks to Markov Matrices that imply some randomness in the slope values even if they fulfil the observed values.

We can see that the usual DC and the simplified SUMO network have equivalent accuracy when estimating the FC, even if the usual DC underestimates the FC, because there is no interaction with other vehicles or the infrastructure, and the SUMO-simulations overestimates the FC, because of a different network regarding the slope, and more interactions with other vehicles. The usual DC underestimates the FC by -11.3%, while the SUMO-simulations overestimate it by 10.8%.

However, the SUMO-simulations have important advantages compared to the usual DC. First, the generated network used in this chapter is only one of the possible network that can be generated and it could not be the closest to the measurements. Moreover, SUMO-simulations give the possibility, by varying the seed value, to evaluate a lot of possible situations that a vehicle can encounter along the same route, which is not possible with the usual DC that only represents one functional point. SUMO-simulations, by modelling other vehicles and the infrastructure, also offer the possibility to design, test and optimize ITS and/or ADAS. The following section illustrate that point with the evaluation of an Adaptive Cruise Control (ACC) algorithm.

7.2 Adaptive Cruise Control (ACC) evaluation

7.2.1 ACC algorithm

ACC is an ADAS allowing the vehicle to adapt its speed when approaching a slower vehicle to prevent collision without necessary action from the driver. Vehicle control is based on sensor information, like radar or camera, which measures the distance to the vehicle ahead.

ACC is one of the first steps to reach a completely autonomous vehicle. According to the levels of driving automation defined by the SAE international (SAE, 2014), the ACC system corresponds to the level 1 of driving automation, named Driving Assistance. This level is defined by the *driving mode*-specific execution by a driver assistance system of either steering or acceleration/deceleration using information about the driving environment and with the expectation that the *human driver* performs all remaining aspects of the *dynamic driving task*.

Many ACC algorithms exist, the one used in this chapter is under development in the Volvo Group.

7.2.2 ACC evaluation

The ACC has been evaluated on the same network used in previous sections. Several simulations were run with different seed values to obtain an image of the possible range of benefit that can be reached with the ACC. In total, 128 simulations were realized, 64 without ACC and 64 with. The network contains vehicles that are slower than the studied ones to generate situations where the ACC can be activated.

Figures 7.8 and 7.9 present the comparison of average speed values and FC estimation with and without the use of the ACC.

The average speeds without or with ACC are really close to each other, respectively 72.0km/h and 71.9km/h. The distributions of the average speeds, in Figure 7.8, highlight that the averaged speed values are better shared when using the ACC than when it is deactivated.

The FC estimated are also close to each other, the FC estimated without ACC is 0.03$L/100km$ smaller than the one estimated when using ACC. The distributions of FC values, in Figure 7.9 highlight that there are more median values with ACC than without it. The use of ACC smooths the vehicle trajectories and so their FC.

The simulations prove the effect of the ACC on the vehicle trajectories by smoothing the speed profile and decreasing the FC variability along the same route.

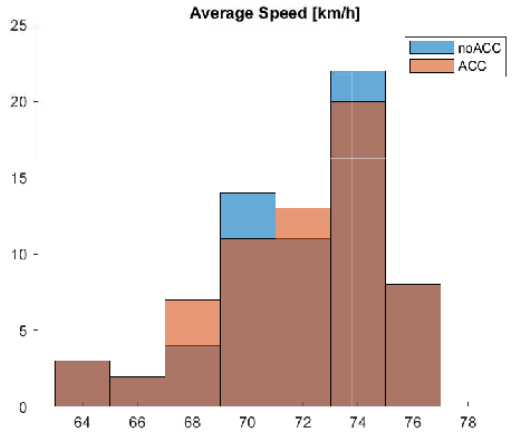

Figure 7.8 – Speed distribution on Long-Haul cycle, with and without ACC use

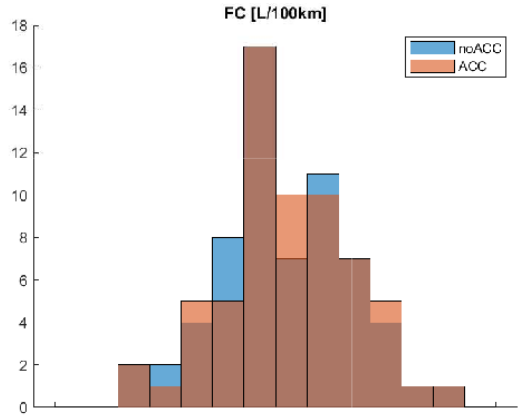

Figure 7.9 – FC distribution on Long-Haul cycle, with and without ACC use

7.3 Conclusion of the chapter

This chapter presented an application of the methods and works developed during the thesis. The advantages of using simplified networks for simulations instead of usual DC has been highlighted in the first section. Then, the use of the developed models for ITS or ADAS evaluation has been proven with the evaluation of the ACC impact on a Long-Haul road.

7.4 References

H. Achour and A.G. Olabi. Driving cycle developments and their impacts on energy consumption of transportation. *Journal of Cleaner Production*, 112:1778–1788, January 2016. ISSN 09596526. doi: 10.1016/j.jclepro.2015.08.007. p. 104

Daniel Chindamo and Marco Gadola. What is the Most Representative Standard Driving Cycle to Estimate Diesel Emissions of a Light Commercial Vehicle? *IFAC-PapersOnLine*, 51(5):73–78, 2018. ISSN 24058963. doi: 10.1016/j.ifacol.2018.06.213. p. 104

Kobus Hereijgers, Emilia Silvas, Theo Hofman, and Maarten Steinbuch. Effects of using Synthesized Driving Cycles on Vehicle Fuel Consumption. *IFAC-PapersOnLine*, 50(1):7505–7510, July 2017. ISSN 24058963. doi: 10.1016/j.ifacol.2017.08.1183. p. 104

SAE. Levels of Driving Automation are Defined in New SAE International Standard J3016, 2014. p. 108

Conclusion of Part II

The second part of this thesis focuses on the road infrastructure that an industrial vehicle can encounter and how to simulate it in order to be able to evaluate ITS and ADAS and their impact on industrial vehicles FC. This study deals with the research of indicators linked to the usual routes used by industrial vehicles. This part is divided into two chapters.

The first one (Chapter 6) presents the statistical study of a usual cycles database. Several statistical indicators are investigated and they can be divided into two categories:

(i) the static indicators: the number of lanes, the intersections and their types, the slope, the speed limit..., and,

(ii) the dynamic indicators: the average flow speed observed under different traffic conditions: free-flow, on-peak or off-peak conditions.

The usual cycles roads have been first sorted into five categories: urban, mid-urban, regional, ring road and highway, for which the statistical indicators have been computed. The categories and their indicators are presented in Tables 6.1 and 6.4.

Then, chapter 6 proposes a methodology to automatically generate SUMO-networks based on those statistics for simulation. The process allows the user to choose the type of cycle he wants to create, its length and the road traffic conditions. It is also possible to assign a value to the seed factor for the reproducibility of the results. The process can be used to generate general networks based on the predefined categories, or it can also be used to simplify a particular road.

The second chapter (Chapter 7) of this part deals with the application of the results and methods proposed during this thesis.

A simplified Long-Haul network, based on a usual Volvo DC, has been generated with the method proposed in Chapter 6. The route driven by the vehicle is about $102km$ long between two cities.

First, the generated network accuracy is verified by comparing the SUMO-simulations with measurements and a usual DC simulation. It is highlighted that the generated simplified network, can be considered as accurate as the usual DC but with the advantage of allowing the evaluation of ITS and ADAS, thanks to the co-simulation between a traffic simulation software and the Volvo FC estimation tool. Moreover, this method also allows to simulate many situations that the studied vehicle can encounter by changing the seed value, while the usual DC allows the simulation of only one particular case.

Then, the generated network is used to illustrate a possible application of such a model. The network is used to evaluate the impact of using ACC algorithm on a Long-Haul cycle. It is shown that the ACC smooths the vehicle speed which results in a more narrow distribution of the average speed.

Conclusion and Perspectives

The objective of this thesis was to propose methods and models to integrate a road traffic model into the Volvo FC estimation tool in order to design and to evaluate the impact of ITS or ADAS use on industrial vehicles. ITS and ADAS have two important characteristics:

(i) They are the first step towards vehicle automation, and,

(ii) They allow a vehicle trajectory optimization in the objective of FC reduction and safety increase.

These two characteristics make ITS and ADAS one of the most important challenges for vehicles manufacturers.

The development and evaluation of these systems are first realized in simulation. The microscopic traffic scale of simulation, representing each vehicle as a particular agent with a personal behaviour, is the most adapted scale to do it. This thesis focuses on the definition of simulation methods and models for ITS and ADAS evaluation.
This thesis is divided in two parts. The first one focuses on the definition and calibration of a car-following model adapted to HDV. The aim of this study is to integrate a realistic representation of the dynamic parameters that the vehicle can encounter in order to take into account the road traffic conditions in the estimation of FC and to offer the possibility of evaluating ITS and ADAS. The realistic notion was evaluated by the capacity of the model to generate trajectories which are relevant for both driving and consumption points of view.
The second part deals with the generation of simplified simulation road networks for SUMO software. The networks statistics (percentage of intersections, speed limits,...) must be consistent with the statistics of usual cycles computed. The second objective completes the previous one. It focuses also on the representativeness of traffic conditions modelling while integrating the network structure of the road by the research of statistical indicators linked to the routes.

Results

The first part is divided into four chapters. The first one presented the materials and the methodology used in this part (Chapter 2). Particularly, the scales of simulation and models retained to model trucks reactions to other vehicles (car-following model) are presented. Then, the calibration method used to adapt usual car-following models to trucks behaviour is described.

Chapter 3 presented the setup of a database of real cycles needed for the calibration of the car-following models. We would like to define a method to reconstruct the entire needed trajectories for calibration, from measurement containing only the speed of the studied vehicle and spacing to its leader. This chapter proposed several methods to reconstruct the trajectory of the Follower and its Leader. Moreover, these methods were compared and one of them has been defined as the most suitable for our study.
The selected method first consists in filtering the measured speed of the truck with a moving average to remove the noise due to the measure. Then, its position is computed thanks to the trapezoidal scheme, and the position of its leader is computed by adding the measured spacing and the length of the vehicle to the position of the truck. Then, the speeds are computed by derivating the positions with trapezoidal scheme, and they are filtered. The acceleration profiles are computed in the same manner. The cycles computed in this chapter are used in Chapter 4 to calibrate, assess and compare the car-following models ability to reproduce the truck behaviour. In Chapter 5, these cycles will be used to evaluate the car-following models on FC estimation.
Once the reconstruction method has been defined, the complete couples (Follower and Leader) of trajectories are computed and the cycles are classified into four categories: urban, mid-urban, regional and ring road cycles, having similar characteristics.

Then, Chapter 4 deals with the calibration of the four well-known car-following models: Gipps model, IIDM, Newell model and Wiedemann model, on real cycles presented in Chapter 3.
The study presented in this chapter proposed a robust method to calibrate each of the selected car-following models on trucks trajectories by comparing several GoF functions (section 4.2), several simulation time steps (section 4.3) and several solvers (section 4.4).
According to the results of the calibration, the Gipps' car-following model appears to be more relevant to reproduce the behaviour of an industrial vehicle. It is the model with the lowest error values even when optimal parameters are switched to mean values per cycle categories. Moreover, the importance of calibrating the car-following models not only based on spacing, speed or acceleration but based on the joint combination of all these variables has been demonstrated by studying the intersections of optimal parameters domains (section 4.2).
Contrary to the Wiedemann's model and the Newell's model, the Gipps' model and the IIDM are more robust and less sensitive to the use of averaged parameters instead of optimal one per cycles. The models proposed by Newell and Wiedemann are clearly not robust enough to be used as shown in section 4.5.2. The rest of the work of this part focuses on the two other models: the Gipps model and the IIDM.
This chapter also highlights some dependencies of the car-following model parameters to the simulation time step (section 4.3.3) and to the solver (section 4.4.3).

To complete this work, the energy consumption of the vehicle is estimated on all cycles simulated with the Gipps' model and the IIDM. The estimation of the FC was not included in the study presented in Chapter 4 due to high computation times for a complete study including traffic and FC.

Chapter 5 highlighted the influence of simulated trajectories on FC estimation and proposed a solution to reduce gaps between measured and simulated values. The two car-following models: the Gipps' car-following model and the IIDM, are compared on their ability to provide trajectories accurate enough to estimate properly the FC of the studied vehicle.
The first comparison is realized using the trajectories resulting on the models calibration on trajectory MoP (spacing, speed and acceleration). Although these models provide good results in terms of trajectory representativeness, the errors on the FC estimation are high. To solve this issue, it has been proposed to calibrate the models again including the FC estimation in the process. Two calibrations are done: one with the cumulated FC as the fourth MoP, and the other with the instantaneous FC as the fourth MoP. The computation time is increased, but the results are really better. The error on the FC estimation has been reduced for the two models.
However, the two models do not react similarly to these new parameters. For the Gipps' car-following model, the error on the trajectory indicators are only a little higher than previously, whereas for the IIDM these errors increase significantly. The Gipps' model is still better than the IIDM to represent the truck's trajectory.
For all categories, the calibration of the IIDM with the instantaneous FC as the fourth MoP is the least efficient. For the cumulated and instantaneous FC, the Gipps' model results are always better than the IIDM results.
According to the observations, a good compromise between the values of the errors on the trajectory, on the FC and the stability of the method seems to be the use of the Gipps' car-following model, calibrated on four MoP: the spacing, the speed, the acceleration and the cumulated FC.

The first part of this thesis proposed methods to obtain a well calibrated car-following model to reproduce trucks behaviour and its energy consumption. Moreover, car-following models were calibrated and compared, and one of them is selected to be used with Volvo simulation tools.

The second part of the thesis is divided into two chapters. The first one (Chapter 6) deals with the statistical representation of usual cycles and the automatic generation of simplified cycles for simulation. This chapter presents the methodology used to easily create representative SUMO simulation networks with traffic.
In this chapter, a highlight on HDV usual cycles was done. Their static and dynamic statistics (average speed, intersection density, number of lanes,...) are presented. Then, a methodology to generate simplified networks for SUMO simulations based on these statistics is proposed. By comparing the statistics of usual DC and the ones of the generated simplified networks, it is pointed out that the proposed methods allow an easy creation of relevant simulation networks.

The last chapter of the second part (Chapter 7) presents the results on a test case chosen to illustrate the complete developed simulation model.
The advantages of using simplified networks for simulations instead of usual DC has been highlighted. The literature review shows that using generic DC to estimate FC can lead to important bias compared to real values. The differences between two cities do not allow the use of such DC. For the accurate estimation of vehicles energy consumption, defining a DC for each application seems better. The work presented in Chapter 6 allows the generation of simplified simulation networks requiring only the GPS information on the route used by the vehicle.
Then, the potential use of the developed models for ITS or ADAS evaluation has been proven with the evaluation of the ACC impact on a Long-Haul road. The generated network was evaluated according to the FC estimation and speed achieved by the studied vehicle. The study compares measurements, and simulation realized with a classical DC and with the simplified SUMO network.

Limits and perspectives

The work presented in this thesis proposed several methods to improve the actual tool used in the Volvo group for the FC estimation when evaluating ITS and ADAS. However, some work can be added to improve the current results and other research axis could be investigated.

First, about the calibration of the car-following models the results can be improved by increasing the number of cycles used for the calibration. Moreover, it would be interesting to use another set of cycles for a proper validation of the calibration.
The calibration study has another limit imposed by the fact that HDV behaviour is strongly linked to the vehicle weight and configuration. Even if the calibration methods proposed for the four car-following models are relevant in all situations, the values proposed for the car-following model parameters are consistent with the behaviour of the studied truck, and these values could not be optimal for another vehicle. If there are sufficient available data, it would be interesting to compare the optimal car-following models parameters depending on the configuration of the truck (rigid or semi-trailer for example) and its weight to propose sets of car-following model parameters adapted to several vehicles.

The generation of simplified networks also points out several questions. First, the usual cycles statistics presented in Chapter 6 were computed in and around the city of Lyon, France. Even if the process to compute these statistics is usable on every zone covered by the HERE database, the statistics presented in this thesis could be different in another city or country. This implies to compute them every time a simplified network is needed on a new city.
Moreover, the use of statistical information (Markov Matrices) and randomness in the generation of the networks could lead in some cases to unrealistic networks. For example, it could appear that some roads can have a lot of lanes on a very short distance, or that the average speed conditions under the different road traffic conditions could not be fulfilled easily, which increases considerably the network creation time.
Another limit of this method, is that it is based on the data proposed by the HERE database, and this data could be incomplete (particularly for the average speed) on some roads which leads to unrealistic values when extracting them. To improve the accuracy of the computed statistics, it would be interesting to merge the information from different sources like Google Maps or Open Street Map for example.

Appendices

Appendix A

Calibration results of Gipps'model, IIDM, Newell's model and Wiedemann's model

A.1 Gipps' car-following model

Table A.1 – Errors in % (Theil's inequality coefficient), on the trajectory simulated with Gipps' car-following model

Urban									
N°	2	3	4	5	6	7	8	9	10
Position [%]	0.65	1.43	0.72	0.68	1.50	1.21	1.51	0.51	0.60
Spacing [%]	5.00	12.16	5.74	5.65	10.81	5.45	6.44	10.93	2.32
Speed [%]	2.11	10.43	4.42	4.65	4.70	3.22	7.30	3.10	0.97
Acceleration [%]	14.93	40.83	33.43	26.20	31.96	25.33	18.04	30.47	9.94
N°	13	14	15	16	17	18	33	34	
Position [%]	0.82	0.28	2.93	0.47	0.90	1.90	0.29	1.15	
Spacing [%]	2.66	2.36	7.13	4.71	2.75	3.10	3.93	6.62	
Speed [%]	2.21	1.86	7.16	1.96	4.12	6.04	2.05	2.13	
Acceleration [%]	14.35	24.25	42.79	13.19	25.25	24.23	21.20	26.46	

Mid-urban					
N°	1	11	12	19	35
Position [%]	0.40	0.70	0.94	1.22	1.16
Spacing [%]	3.18	7.55	9.10	15.22	10.35
Speed [%]	2.47	3.58	4.86	5.74	3.27
Acceleration [%]	20.88	30.78	24.45	26.28	21.49

Ring road					
N°	20	21	22	23	24
Position [%]	0.48	0.75	1.02	0.25	1.22
Spacing [%]	9.28	8.93	11.48	2.51	12.34
Speed [%]	3.03	3.82	6.40	1.56	4.57
Acceleration [%]	21.59	26.08	31.11	12.54	36.81

Regional								
N°	25	26	27	28	29	30	31	32
Position [%]	1.92	0.59	0.22	0.56	0.45	0.63	0.43	0.79
Spacing [%]	11.04	13.70	6.98	8.30	11.75	8.76	3.58	8.50
Speed [%]	2.79	2.65	2.32	2.63	2.01	3.66	1.31	2.86
Acceleration [%]	22.12	32.60	21.50	24.88	23.22	25.53	20.14	31.31

A.2 IIDM

Table A.2 – Errors in % (Theil's inequality coefficient), on the trajectory simulated with IIDM

Urban									
N°	2	3	4	5	6	7	8	9	10
Position [%]	1.73	1.49	4.30	1.08	0.55	4.72	0.76	1.43	5.86
Spacing [%]	11.69	13.15	26.23	9.18	4.22	18.19	3.20	24.52	18.58
Speed [%]	10.33	1.77	6.68	5.95	3.10	7.82	6.64	6.28	14.81
Acceleration [%]	48.40	42.18	31.74	32.63	26.29	47.68	29.41	47.15	50.35

N°	13	14	15	16	17	18	33	34
Position [%]	3.96	0.41	3.14	5.49	1.01	2.41	0.83	2.72
Spacing [%]	11.41	3.33	7.86	36.08	3.05	3.83	10.53	14.32
Speed [%]	7.83	3.44	8.33	10.11	3.48	5.02	3.91	4.24
Acceleration [%]	43.74	33.05	36.13	43.34	21.91	30.16	26.38	34.13

Mid-urban					
N°	1	11	12	19	35
Position [%]	2.02	1.30	1.88	2.67	0.46
Spacing [%]	13.25	14.36	18.15	28.70	4.46
Speed [%]	6.54	8.49	10.25	8.44	3.38
Acceleration [%]	29.13	62.29	43.38	53.30	24.24

Ring road					
N°	20	21	22	23	24
Position [%]	2.89	0.95	1.22	1.69	2.62
Spacing [%]	35.34	11.12	13.50	19.03	22.68
Speed [%]	12.66	7.63	6.76	9.85	4.92
Acceleration [%]	41.13	47.89	33.46	49.36	42.09

Regional								
N°	25	26	27	28	29	30	31	32
Position [%]	0.98	0.98	0.76	1.45	0.51	1.69	1.84	0.96
Spacing [%]	4.51	20.96	20.64	19.09	13.20	20.97	13.71	10.40
Speed [%]	3.14	4.04	3.50	4.68	3.35	5.12	3.79	4.36
Acceleration [%]	21.64	35.50	32.95	34.27	33.15	35.32	26.86	34.10

A.3 Newell's car-following model

Table A.3 – Errors in % (Theil's inequality coefficient), on the trajectory simulated with Newell's car-following model

Urban									
N°	2	3	4	5	6	7	8	9	10
Position [%]	0.93	1.31	1.27	0.65	0.41	0.74	1.05	0.50	1.72
Spacing [%]	6.78	11.47	10.01	5.50	3.23	3.59	4.38	10.88	6.43
Speed [%]	5.14	9.86	6.22	4.59	2.81	3.96	7.44	3.99	6.39
Acceleration [%]	26.16	38.55	40.04	30.33	37.22	31.47	26.91	38.57	31.72
N°	13	14	15	16	17	18	33	34	
Position [%]	0.89	0.61	2.62	0.83	0.57	1.40	0.16	1.48	
Spacing [%]	2.89	5.02	6.78	8.52	1.72	2.35	2.28	9.01	
Speed [%]	3.58	3.71	8.53	3.55	3.14	4.12	2.09	4.91	
Acceleration [%]	36.67	33.73	45.51	27.34	22.94	29.23	22.04	36.90	

Mid-urban					
N°	1	11	12	19	35
Position [%]	0.68	0.97	1.17	1.22	2.09
Spacing [%]	5.16	10.71	11.25	15.47	17.39
Speed [%]	3.78	5.61	6.24	6.54	5.88
Acceleration [%]	26.16	47.91	31.23	53.79	27.55

Ring road					
N°	20	21	22	23	24
Position [%]	0.30	0.72	0.57	0.23	0.84
Spacing [%]	5.43	8.82	6.74	2.27	9.37
Speed [%]	3.38	5.19	5.59	2.51	4.98
Acceleration [%]	24.83	35.73	38.52	19.62	42.25

Regional								
N°	25	26	27	28	29	30	31	32
Position [%]	0.53	0.47	0.17	0.62	0.44	0.96	0.64	0.46
Spacing [%]	3.37	12.06	5.56	9.63	11.35	13.20	5.50	5.21
Speed [%]	3.13	3.70	2.52	3.32	2.83	3.98	3.65	2.80
Acceleration [%]	41.09	38.73	27.17	43.98	26.86	27.73	35.29	38.42

A.4 Wiedemann's car-following model

Table A.4 – Errors in % (Theil's inequality coefficient), on the trajectory simulated with Wiedemann's car-following model

Urban									
N°	2	3	4	5	6	7	8	9	10
Position [%]	0.75	51.68	2.19	4.01	6.56	5.62	10.26	8.43	0.46
Spacing [%]	5.33	76.83	15.05	33.13	35.97	21.92	30.04	64.89	1.73
Speed [%]	6.49	70.84	7.68	17.67	26.77	17.95	27.92	18.29	4.40
Acceleration [%]	28.25	79.48	47.89	63.25	65.52	48.15	70.69	61.21	20.46

N°	13	14	15	16	17	18	33	34
Position [%]	1.99	1.21	81.53	0.56	12.27	9.98	8.46	11.51
Spacing [%]	6.15	10.49	54.60	6.03	51.40	18.41	70.20	44.84
Speed [%]	10.65	6.67	91.20	3.45	21.33	23.20	26.73	24.87
Acceleration [%]	74.45	34.70	89.40	20.45	36.86	46.59	66.90	53.80

Mid-urban					
N°	1	11	12	19	35
Position [%]	10.05	1.60	3.27	1.46	7.12
Spacing [%]	47.20	18.75	30.08	20.13	43.35
Speed [%]	31.62	8.23	13.28	6.28	24.15
Acceleration [%]	69.81	47.95	41.03	47.21	76.86

Ring road					
N°	20	21	22	23	24
Position [%]	2.96	1.16	68.47	1.14	9.78
Spacing [%]	43.49	15.26	84.17	10.32	56.35
Speed [%]	10.13	8.20	77.72	3.87	29.89
Acceleration [%]	40.65	38.93	75.19	26.96	68.01

Regional								
N°	25	26	27	28	29	30	31	32
Position [%]	0.73	3.22	2.24	3.50	3.27	3.12	3.48	4.82
Spacing [%]	4.85	57.88	59.19	43.90	67.76	49.12	33.34	35.65
Speed [%]	3.30	21.91	8.95	22.43	20.21	7.47	12.61	10.08
Acceleration [%]	41.10	78.95	59.13	82.02	78.45	47.56	54.52	52.61

Appendix B

Estimation of the fuel consumption using EstimFC with the measured trajectories

Table B.1 – Errors in %, on the fuel consumption computed in $L/100km$, and on the cumulated and instantaneous fuel consumption in L

Urban									
N°	2	3	4	5	6	7	8	9	10
FC cumulated Theil's inequality [%]	4.30	4.11	6.51	7.31	24.04	4.92	7.91	10.86	4.69
FC instantaneous Theil's inequality [%]	33.90	44.60	38.01	35.82	31.41	31.37	40.13	48.63	27.66
N°	13	14	15	16	17	18	33	34	
FC cumulated Theil's inequality [%]	2.68	10.61	9.44	7.74	4.70	3.67	2.93	6.00	
FC instantaneous Theil's inequality [%]	26.34	56.91	37.52	29.62	38.06	38.08	40.11	38.42	

Mid-urban					
N°	1	11	12	19	35
FC cumulated Theil's inequality [%]	4.30	4.25	3.13	2.71	9.22
FC instantaneous Theil's inequality [%]	33.90	16.86	36.89	23.41	23.60

Ring road					
N°	20	21	22	23	24
FC cumulated Theil's inequality [%]	5.08	2.53	6.32	4.01	3.48
FC instantaneous Theil's inequality [%]	29.42	22.05	45.34	17.40	27.45

Regional								
N°	25	26	27	28	29	30	31	32
FC cumulated Theil's inequelity [%]	14.25	0.91	0.80	1.49	6.52	3.31	2.42	4.88
FC instantaneous Theil's inequality [%]	20.72	20.98	12.90	23.31	35.32	33.21	29.95	21.99

Appendix C

Estimation of the fuel consumption using EstimFC with the trajectories generated thanks to the Gipps model and the IIDM calibrated without fuel consumption MoP (3D)

C.1 Gipps' model (3D)

Table C.1 – Errors in %, on the fuel consumption computed in $L/100km$, and on the cumulated and instantaneous fuel consumption in L - Simulated trajectories thanks to the Gipps' car-following model

Urban									
N°	2	3	4	5	6	7	8	9	10
FC cumulated Theil's inequality [%]	3.24	7.06	10.95	53.11	4.27	16.24	12.97	12.74	13.26
FC instantaneous Theil's inequality [%]	3.24	41.44	33.77	57.50	44.01	43.25	45.24	39.29	40.18
N°	13	14	15	16	17	18	33	34	
FC cumulated Theil's inequality [%]	30.59	8.77	6.51	11.53	2.78	8.77	2.74	9.11	
FC instantaneous Theil's inequality [%]	44.57	51.26	40.41	45.17	35.14	39.74	45.13	36.57	

Mid-urban					
N°	1	11	12	19	35
FC cumulated Theil's inequality [%]	3.96	11.13	14.90	13.15	6.52
FC instantaneous Theil's inequality [%]	39.01	39.71	38.58	37.70	36.93

Ring road					
N°	20	21	22	23	24
FC cumulated Theil's inequality [%]	11.45	3.77	13.16	4.74	6.21
FC instantaneous Theil's inequality [%]	44.66	28.32	44.72	26.39	43.71

Regional								
N°	25	26	27	28	29	30	31	32

FC cumulated								
Theil's inequality [%]	22.14	2.07	1.80	2.86	13.41	3.98	3.36	0.89
FC instantaneous								
Theil's inequality [%]	36.22	28.21	15.19	27.06	26.92	34.27	27.59	22.42

C.2 IIDM (3D)

Table C.2 – Errors in %, on the fuel consumption computed in $L/100km$, and on the cumulated and instantaneous fuel consumption in L - Simulated trajectories thanks to the IIDM

Urban									
N°	2	3	4	5	6	7	8	9	10
FC cumulated									
Theil's inequality [%]	30.43	8.61	15.60	57.04	3.54	14.37	18.30	17.20	54.46
FC instantaneous									
Theil's inequality [%]	56.11	39.67	44.69	65.33	38.90	47.81	44.24	48.09	69.64
N°	13	14	15	16	17	18	33	34	
FC cumulated									
Theil's inequality [%]	47.72	8.61	11.57	58.19	8.01	9.80	6.28	9.22	
FC instantaneous									
Theil's inequality [%]	73.07	54.89	49.86	70.66	39.53	42.18	39.69	42.89	

Mid-urban					
N°	1	11	12	19	35
FC cumulated					
Theil's inequality [%]	8.40	39.18	39.03	62.46	17.99
FC instantaneous					
Theil's inequality [%]	43.14	48.74	49.29	74.58	38.35

Ring road					
N°	20	21	22	23	24
FC cumulated					
Theil's inequality [%]	35.32	30.69	8.30	23.51	7.00
FC instantaneous					
Theil's inequality [%]	57.01	41.82	38.98	58.75	45.31

Regional								
N°	25	26	27	28	29	30	31	32
FC cumulated								
Theil's inequality [%]	29.47	2.97	5.22	10.68	49.14	12.71	10.08	5.13
FC instantaneous								
Theil's inequality [%]	43.96	28.77	24.52	33.16	51.28	39.93	35.54	21.91

Appendix D

Estimation of the fuel consumption using EstimFC with the trajectories generated thanks to the Gipps model and the IIDM calibrated with fuel consumption MoP (4D)

D.1 Gipps' model (4D)

D.1.1 Cumulated fuel consumption as MoP

Table D.1 – Calibration taking into account fuel consumption estimation
Errors in %, on the fuel consumption computed in $L/100km$, and on the cumulated and instantaneous fuel consumption in L - Simulated trajectories thanks to the Gipps' CF model

Urban									
N°	2	3	4	5	6	7	8	9	10
FC cumulated Theil's inequality [%]	3.85	6.21	6.99	37.89	3.91	3.24	5.38	5.86	6.64
FC instantaneous Theil's inequality [%]	40.85	42.22	39.45	50.59	42.46	42.11	44.12	32.23	32.06
N°	13	14	15	16	17	18	33	34	
FC cumulated Theil's inequality [%]	9.73	8.49	7.24	6.87	3.10	8.50	3.11	8.40	
FC instantaneous Theil's inequality [%]	39.29	51.42	40.82	44.12	42.48	40.48	45.12	36.13	

Mid-urban					
N°	1	11	12	19	35
FC cumulated Theil's inequality [%]	4.32	8.13	13.74	10.15	5.74
FC instantaneous Theil's inequality [%]	40.75	40.21	41.21	43.24	30.90

Ring road					
N°	20	21	22	23	24
FC cumulated Theil's inequality [%]	9.06	3.89	5.58	5.34	7.67
FC instantaneous Theil's inequality [%]	40.32	27.45	44.27	26.87	40.44

	Regional							
N°	25	26	27	28	29	30	31	32
FC cumulated Theil's inequality [%]	16.45	2.16	0.86	2.85	9.62	2.07	2.03	0.97
FC instantaneous Theil's inequality [%]	34.74	28.35	17.24	27.54	30.79	35.41	29.24	20.86

Evolution of FC estimation errors per cycle categories

Urban cycles

For urban cycles errors have been reduced from 12.6% to 8.0% on the cumulated FC. Moreover, the standard deviation is also significantly reduced, from 12.0%to 7.8%. The calibration also reduces a little the errors on instantaneous FC, from 43.0% to 41.6% in average, and the standard deviation is reduced by 1%.

We can also observe that for the cycles n°5 and 13, for which the error on the cumulated FC, respectively 53.1% and 30.6%, were really high, the errors have been noticeably reduced: respectively 37.9% and 9.7%. However, if we consider another particle of the optimal swarm, the one with the smallest error on FC, named *Best_FC*, the necessity of the MO calibration is pointed out. For the cycle n°5 and the particle *Best_FC*, the error on the cumulated FC is quite low (8.0%), whereas it was equal to 53.1% (for the *Compromise* particle) when the FC was not taken into account in the calibration. Despite this, the errors on the trajectory are really high: 59.9% for the position, 78.3% for the spacing, 66.6% for the speed and 71.8% for the acceleration. Here it is obvious that the set of parameters of the Gipps' car-following model is not good because even if the error on the FC is quite low, the errors on the trajectory of the vehicle are not acceptable. This result highlights the necessity of the MO calibration to find a good set of parameter that enables to model properly the trajectory of the vehicle and its energy consumption.

Mid-Urban cycles

For mid-urban cycles, the results are a little improved. The average error for the cumulated FC goes from 9.9% (with a standard deviation of 4.1%) to 8.4% (with a standard deviation of 3.3%). It could be explained by the fact that those cycles are longer and more stable than the urban ones, so the most important is the estimation of the desired speed. This is also valid for ring road an regional cycles.

The errors on position, spacing, speed, acceleration and instantaneous FC are not changed.

Ring road cycles

On ring road cycles, the error on the cumulated FC is slightly reduced. It goes from 7.9% (with a standard deviation of 3.8%) to 6.3% (with a standard deviation equal to 1.8%). However, the error on the FC (expressed in $L/100km$) has increased a little from 5.7% to 36.0%. The errors on the other indicators are quite the same.

Regional cycles

The average error is reduced from 6.3% to 4.6%. As for urban cycles, the standard deviation decreases also, from 7.0% to 5.2%. These results mean that errors are not only lower for the FC estimation, but the accuracy of the estimate is also improved.

The errors on the other indicators remain constant.

D.1.2 Instantaneous fuel consumption as MoP

Table D.2 – Calibration taking into account fuel consumption estimation
Errors in %, on the fuel consumption computed in $L/100km$, and on the cumulated and instantaneous fuel consumption in L - Simulated trajectories thanks to the Gipps' CF model

Urban									
N°	2	3	4	5	6	7	8	9	10
FC cumulated Theil's inequality [%]	2.54	8.71	9.02	36.82	3.59	14.35	9.14	3.53	12.31
FC instantaneous Theil's inequality [%]	32.41	36.78	33.51	49.74	35.95	34.35	37.62	24.93	18.66
N°	13	14	15	16	17	18	33	34	
FC cumulated Theil's inequality [%]	8.01	23.90	5.79	8.91	2.56	12.87	5.48	8.43	
FC instantaneous Theil's inequality [%]	32.38	46.13	35.52	29.34	30.27	33.89	34.89	34.43	

Mid-urban					
N°	1	11	12	19	35
FC cumulated Theil's inequality [%]	2.88	9.93	13.77	15.27	22.93
FC instantaneous Theil's inequality [%]	33.14	38.36	33.88	36.65	27.29

Ring road					
N°	20	21	22	23	24
FC cumulated Theil's inequality [%]	9.67	8.11	8.43	5.99	6.61
FC instantaneous Theil's inequality [%]	39.33	23.04	39.09	21.91	39.24

Regional								
N°	25	26	27	28	29	30	31	32
FC cumulated Theil's inequality [%]	36.78	1.97	1.53	3.07	8.87	4.22	3.60	1.00
FC instantaneous Theil's inequality [%]	38.76	24.55	15.12	25.57	21.92	31.40	28.69	13.75

Evolution of FC estimation errors per cycle categories

Urban cycles

The estimation of the instantaneous FC is improved, error was equal to 43.0% in average in the previous calibration, whereas it is equal to 34.17% here. The errors on cumulated FC were also reduced; from 12.6% to 10.4%. The average errors on position and speed stay constant. However, the errors on spacing and acceleration are increased, respectively from 5.8% to 8.3% and from 24.9% to 27.5%.

Mid-Urban cycles

For the mid-urban cycles, the errors on instantaneous FC go from 38.4% to 33.9%. However, the errors on cumulated FC go up, from 9.9% to 13.0%.

The errors on position, speed and spacing are a little smaller, however, the error on the acceleration increases from 24.8% to 28.6%.

Ring road cycles

As for the other categories of cycles the error on the estimated instantaneous FC has been reduced by the calibration in four dimensions. The error was equal to 37.6% previously, and now it is equal to 32.5%. The errors on the position, the speed, the acceleration and the cumulated FC remain acceptable whereas they shoot up for the spacing, from 8.9% to 11.6%.

Regional cycles

The errors on the instantaneous FC decreased from 27.2% to 25.0% by adding the FC estimation as an additional MoP. The error on the position, the speed are not really changed, respectively without and with the FC in the calibration process, from 0.7% to 0.8% and from 2.5% to 2.6%. The error on the cumulated FC increased slightly, from 6.3% to 7.6%.

However, the errors on the spacing and the acceleration remain close to the error of the previous calibration. For the spacing the error goes from 9.1% to 9.8, and for the acceleration it goes from 25.2% to 26.3%.

D.2 IIDM (4D)

D.2.1 Cumulated fuel consumption as MoP

Table D.3 – Calibration taking into account fuel consumption
Errors in %, on the fuel consumption computed in $L/100km$, and on the cumulated and instantaneous fuel consumption in L - Simulated trajectories thanks to the IIDM

Urban									
N°	2	3	4	5	6	7	8	9	10
FC cumulated Theil's inequality [%]	12.70	2.91	20.40	8.91	4.80	21.45	6.65	6.52	10.89
FC instantaneous Theil's inequality [%]	53.55	39.73	49.27	46.70	34.69	46.50	46.15	41.73	59.28
N°	13	14	15	16	17	18	33	34	
FC cumulated Theil's inequality [%]	18.89	7.81	9.81	26.20	3.46	5.41	3.10	6.60	
FC instantaneous Theil's inequality [%]	45.37	56.90	45.72	52.28	36.13	40.65	38.15	42.91	

Mid-urban					
N°	1	11	12	19	35
FC cumulated Theil's inequality [%]	2.14	11.89	16.95	12.98	13.20
FC instantaneous Theil's inequality [%]	37.38	49.71	49.99	34.99	36.26

Ring road					
N°	20	21	22	23	24
FC cumulated Theil's inequality [%]	17.39	10.62	6.83	16.57	9.52
FC instantaneous Theil's inequality [%]	54.62	46.24	39.58	57.41	41.92

Regional								
N°	25	26	27	28	29	30	31	32
FC cumulated Theil's inequality [%]	28.38	3.19	4.55	5.59	10.74	6.51	3.46	3.56
FC instantaneous Theil's inequality [%]	38.74	27.38	25.26	31.36	52.45	36.29	32.96	21.53

Evolution of FC estimation errors per cycle categories

Urban cycles

On the urban cycles, the errors on the cumulated and instantaneous FC are reduced, respectively from 22.3% to 10.4%, and from 51.0% to 45.6%.

The errors on the position are not changed, the error on the speed and on the spacing increased (respectively from 7.0% to 9.9%, and from 12.9% to 18.4%), and the error on the acceleration is really different, with an average error of 52.8% whereas it was equal to 36.8% previously.

Mid-Urban cycles

As for the urban cycles, the average errors on FC indicators have been drastically reduced: from 33.4% to 11.4% for the cumulated FC and from 50.8% to 41.7% for the instantaneous FC.

However, the errors on the trajectory indicators increase. The error on the position goes from 1.7% to 6.8% in average, the error on the spacing goes from 15.8% to 34.2%. The speed error goes from 7.4% to 14.2%, and the error on the acceleration profile goes from 42.5% to 67.1% in average.

Ring road cycles

For the ring road cycles, the average error on cumulated FC has been reduced from 21.0% to 12.2%. The average error on the instantaneous FC has not been improved (about 48%).

As for the mid-urban cycles, the errors on the trajectory of the vehicle have been deteriorated: from 1.9% to 6.9% for the position, from 20.3% to 44.2% for the spacing, from 8.4% to 16.1 for the speed and from 42.8% to 56.9% for the acceleration.

Regional cycles

The same observations can be done for the regional cycles as for the other categories: the errors on the FC indicators are reduced, but the errors on the trajectory indicators increase.

The error on the instantaneous FC are quite identical: 34.9% and 33.3% respectively for the calibration without and with cumulated FC as MoP. For the cumulated FC, the error decreases from 15.7% to 8.3%.

For the trajectory indicators, the average errors go up from 1.1% to 4.3% for the position, from 15.4% to 28.3% for the spacing, from 4.0% tp 7.4% for the speed and from 31.7% to 43.0% for the acceleration.

D.2.2 Instantaneous fuel consumption as MoP

Table D.4 – Calibration taking into account fuel consumption
Errors in %, on the fuel consumption computed in $L/100km$, and on the cumulated and instantaneous fuel consumption in L - Simulated trajectories thanks to the IIDM

Urban									
N°	2	3	4	5	6	7	8	9	10
FC cumulated Theil's inequality [%]	11.36	3.33	19.38	15.02	4.64	21.20	14.13	14.84	14.42
FC instantaneous Theil's inequality [%]	42.82	41.13	48.18	49.95	35.91	47.22	40.14	38.56	39.60
N°	13	14	15	16	17	18	33	34	
FC cumulated Theil's inequality [%]	22.44	7.95	10.60	25.16	19.51	9.37	4.28	19.89	
FC instantaneous Theil's inequality [%]	46.76	52.71	44.81	53.74	30.42	35.70	35.77	33.74	

Mid-urban					
N°	1	11	12	19	35
FC cumulated Theil's inequality [%]	5.26	16.34	20.36	12.84	12.01
FC instantaneous Theil's inequality [%]	38.43	51.95	40.31	36.41	31.34

Ring road					
N°	20	21	22	23	24
FC cumulated Theil's inequality [%]	15.88	8.80	7.35	19.86	11.77
FC instantaneous Theil's inequality [%]	51.31	45.46	37.10	45.84	37.49

Regional								
N°	25	26	27	28	29	30	31	32
FC cumulated Theil's inequality [%]	30.15	3.18	5.65	11.42	34.72	6.99	6.15	4.50
FC instantaneous Theil's inequality [%]	37.41	27.50	24.13	27.99	43.58	36.67	26.60	22.94

Evolution of FC estimation errors per cycle categories

Urban cycles

On the urban cycles, the errors on the FC indicators have been drastically reduced: from 22.3% to 14.0% for the cumulated FC and from 51.0% to 42.2% for the instantaneous FC. But the errors on the position, spacing, speed and acceleration have been increased, respectively from 2.5% to 4.6%, from 12.9% to 21.6%, from 7.0% to 10.2% and from 36.8% to 49.8%.

Mid-Urban cycles

For the mid-urban cycles, the instantaneous FC is reduced from 50.8% to 39.7%. The cumulated FC is also highly reduced, from 33.4% to 13.4%.

As for urban cycles, the errors on the trajectory indicators have been deteriorated: from 1.7% to 3.4% for the position, from 15.8% to 29.2% for the spacing, from 7.4% to 11.3% for the speed and from 42.5% to 62.7%.

Ring road cycles

As for the two previous categories, the errors on the FC MoP are reduced whereas the errors on the trajectory MoP are higher.

The average error on cumulated FC goes down from 21.0% to 12.7% and on instantaneous FC error goes down from 48.4% to 43.4%.

The error on the position goes up from 1.9% to 4.4%, the spacing error goes from 20.3% to 30.6%, the speed error increases from 8.4% to 10.8% and the error on the acceleration increases from 42.8% to 55.0%.

Regional cycles

The calibration on regional cycles provides the same results as the calibration on the other categories.

The average errors on the cumulated and instantaneous FC are reduced, respectively from 15.7% to 12.9% and from 34.9% to 30.9%.

For the trajectory indicators, the average error increases: from 1.1% to 1.3% for the position, from 15.4% to 18.7% for the spacing, from 4.0% to 5.6% for the speed and from 31.7% to 46.0% for the acceleration. We can nevertheless notice that the trajectory MoP are less deteriorated on regional cycles than on the cycles of the other categories.

Appendix E

Statistical description of Local and Regional Delivery usages

E.1 Local Delivery

Table E.1 – Statistics of Local Delivery usage

	Urban	**Mid-Urban**	**Regional**	**Ring Road**	**Highway**
Mean length $[km]$			42.1		
Mean length per category $[m]$	8297	755	1106	3733	0
Percentage of cycles type	74.8	4.3	0.4	20.5	0.0
Mean number of intersections	33.7	1.1	0.3	0.0	-
Percentage of intersection type					
Traffic lights	93.4	96.2	0.0	0.0	-
Yields	1.5	1.9	100.0	0.0	-
Stops	1.7	0.0	0.0	0.0	-
Roundabouts	3.4	1.9	0.0	0.0	-
Density of intersections	0.39	0.25	0.08	0.0	-
Mean spacing between intersections $[m]$	308	365	-	-	-
Mean number of peaks	30	2	2	5	-
Mean length of peaks $[m]$	139	222	376	310	-
Mean number of valleys	29	2	2	5	-
Mean length of valleys $[m]$	143	169	157	341	-
Mean number of lanes	1.6	1.9	1.2	2.7	-
Mean speed limit $[km/h]$	48.0	70.1	89.5	89.9	-
Mean speed under ON peak conditions $[km/h]$	28.7	46.2	69.7	71.9	-
Mean speed under OFF peak conditions $[km/h]$	32.0	54.7	76.3	79.5	-
Mean speed under FREE flow conditions $[km/h]$	34.8	59.9	83.4	83.9	-

E.2 Regional Delivery

Table E.2 – Statistics of Regional Delivery usage

	Urban	**Mid-Urban**	**Regional**	**Ring Road**	**Highway**
Mean length $[km]$			200.2		
Mean length per category $[m]$	2269	775	2706	5569	13900
Percentage of cycles type	29.5	11.0	16.9	16.9	25.8
Mean number of intersections	5.5	0.8	1.4	0.3	0.0
Percentage of intersection type					
Traffic lights	58.6	35.4	11.5	0.0	-
Yields	6.4	16.9	1.9	60.0	-
Stops	2.4	6.2	11.5	0.0	-
Roundabouts	32.6	41.5	75.0	40.0	-
Density of intersections	0.33	0.23	0.07	0.04	-
Mean spacing between intersections $[m]$	546	553	566	562	-
Mean number of peaks	8	2	5	4	9
Mean length of peaks $[m]$	169	212	305	728	907
Mean number of valleys	8	2	5	4	9
Mean length of valleys $[m]$	168	210	338	892	1074
Mean number of lanes	1.2	1.3	1.2	2.4	2.7
Mean speed limit $[km/h]$	53.4	71.6	86.0	90.5	120.1
Mean speed under ON peak conditions $[km/h]$	34.8	50.1	65.1	72.2	108.1
Mean speed under OFF peak conditions $[km/h]$	38.1	55.1	68.0	80.3	108.8
Mean speed under FREE flow conditions $[km/h]$	40.9	59.2	71.1	84.7	112.1

Appendix F

Extended Summary (French) / Résumé Étendu (Français)

Prise en compte des conditions de trafic dynamique dans l'évaluation des consommations énergétiques des véhicules industriels en intégrant les stratégies d'aide à la conduite

F.1 Introduction

Les problématiques de réduction de la pollution sont au coeur des enjeux des villes, mais également des constructeurs automobiles. Responsable de près de 38% des émissions de CO_2 en 2017, le secteur du transport est l'un des plus polluants en France (CITEPA, 2017).

Dans ce cadre, les normes européennes sont de plus en plus strictes envers les véhicules pour limiter les émissions de polluants. Afin de respecter ces nouvelles mesures, et grâce à l'évolution des technologies et l'augmentation des objets connectés, les constructeurs se tournent aujourd'hui vers les nouveaux systèmes d'aide à la conduite : *Intelligent Transportation Systems* (ITS) et *Advanced Driver Assistance Systems* (ADAS), dans le but de réduire les consommations de leurs véhicules tout en augmentant la sécurité des usagers.

Pour développer ces nouveaux systèmes, l'industrie automobile cherche à représenter au mieux le réel pour concevoir des outils et produits les plus adaptés aux enjeux et marchés actuels, en diminuant les délais de mise au point et les coûts de prototypage. Dans ce but, il est de plus en plus fait appel à la modélisation et à la simulation.

Dans cette optique, le groupe Volvo a développé de puissants outils pour la simulation de la dynamique de ses véhicules industriels. Ces outils permettent notamment l'optimisation de composants véhicules ou de stratégies de contrôle. De nombreuses activités de recherche portent sur des technologies innovantes, permettant de réduire la consommation des véhicules industriels et d'accroître la sécurité de leurs usages dans différents environnements. En particulier, le développement des systèmes d'aide à la conduite (ADAS) et systèmes de transports intelligents (ITS) est en plein essor.

Afin de pouvoir développer ces systèmes, un environnement de simulation permettant de prendre en compte les différents facteurs pouvant influencer la conduite d'un véhicule doit être mis en place. Les outils de simulation de la cinématique véhicule étant déjà développés, le travail se concentre sur la simulation de l'environnement du véhicule et des interactions entre le véhicule et son environnement direct, i.e. le véhicule qui le précède.

L'environnement du véhicule peut être représenté par deux catégories de paramètres : (i) les paramètres statiques et (ii) les paramètres dynamiques. Les paramètres statiques décrivent les informations liées à l'environnement qui ne changent pas au cours du temps : le nombre de voies, la pente, la limitation de vitesse par exemple, tandis que les paramètres dynamiques sont susceptibles d'évoluer au cours du trajet du véhicule : l'état des feux tricolores rencontrés, la vitesse et l'inter-distance du véhicule qui le précède, l'état du réseau (congestionné ou non), par exemple.

Les interactions entre le véhicule étudié (*Follower*) et le véhicule qui le précède (*Leader*) sont modélisées à l'aide de modèles mathématiques, nommés lois de poursuites (*car-following models*). De nombreux modèles

existent dans la littérature. La plupart d'entre eux utilisent comme paramètres la vitesse désirée et l'accélération du *Follower*, l'inter-distance et la différence de vitesse entre les deux véhicules, le temps de réaction du *Follower* par exemple.

Le travail réalisé dans cette thèse se divise en deux parties. La première, divisée en quatre chapitres, se concentre sur l'étude des lois de poursuites et le calage de leurs paramètres sur des données poids lourds. La seconde partie, divisée en deux chapitres, présente une étude de l'environnement usuel rencontré par un véhicule industriel lors de son usage. En particulier, des indicateurs statistiques permettant de décrire ces usages sont estimés, puis utilisés pour générer des scénarios de simulation réalistes.

F.2 Partie 1 : Adaptation des lois de poursuite au comportement d'un poids lourd

Le but de cette thèse est de permettre l'estimation des consommations énergétiques des véhicules industriels en intégrant les stratégies d'aide la conduite. Pour répondre à cette problématique, il est proposé de compléter l'outil d'estimation des consommations énergétiques utilisé au sein du groupe Volvo, en permettant, dans un premier temps, au véhicule simulé (*Follower*) de réagir à son environnement direct, c'est à dire, le véhicule qu'il suit (*Leader*).

Cette partie se concentre sur le développement de méthodes de calage pour adapter les paramètres des lois de poursuites usuelles au comportement d'un véhicule industriel. Quatre chapitres seront ainsi développés :

i. La définition des méthodes et données nécessaires au calage des paramètres (section F.2.1)

ii. La mise en place d'une base de données de trajectoires sur lesquelles caler les paramètres (section F.2.2)

iii. La comparaison de plusieurs méthodes de calage et plusieurs lois de poursuites (section F.2.3)

iv. L'impact de la méthode de calage sur l'estimation des consommations énergétiques à partir des trajectoires simulées (section F.2.4)

F.2.1 Données et méthodes

Cette section présente les méthodes et données utilisées dans la première partie de la thèse pour définir une loi de poursuite adaptée pour reproduire de manière précise le comportement d'un véhicule industriel.

F.2.1.1 Les modèles microscopiques de simulation trafic

La simulation du trafic routier peut-être réalisée suivant différentes échelles : les modèles macroscopiques et les modèles microscopiques sont les plus utilisés.

Les modèles macroscopiques sont principalement utilisés pour modéliser de grands réseaux. Ils sont choisis lorsque des informations détaillées pour chaque véhicule ne sont pas nécessaires mais seulement une évaluation des flux de véhicules dans le réseaux. A cette échelle, le trafic est représenté comme un fluide compressible décrit par trois paramètres : le volume de véhicules ($q(x,t)$), la vitesse du flot de véhicules ($u(x,t)$) et sa densité ($k(x,t)$).

Ces trois paramètres sont liés par des relations décrites par le diagramme fondamental. Plusieurs études ont étudié ce diagramme (Gerlough and Huber, 1975; Greenshields, 1935; Lighthill and Whitham, 1955; Richards, 1956). Les études expérimentales les plus récentes ont mis en évidence que ce diagramme pouvait être modélisé de manière triangulaire sur autoroute (Chiabaut et al., 2009; Coifman and Wang, 2005; Windover and Cassidy, 2001) et linéaire en zone urbaine lors des phases de congestion (Leclercq, 2005).

Les modèles microscopiques sont quant à eux centrés sur les véhicules. La simulation est réalisée grâce à des particules interagissant entre elles dans le but de conserver une position sécurisée dans le trafic. Il s'agit d'une échelle de simulation détaillée, où chaque véhicule est modélisé ainsi que l'infrastructure. Ces modèles permettent ainsi de tester divers systèmes d'aide à la conduite.

Les lois de poursuite, décrivant comment un véhicule suit le véhicule qui le précède, font partie des modèles microscopiques. Une étude approfondie leur est consacrée.

F.2.1.2 Le cas des lois de poursuites pour les poids lourds dans la littérature

La littérature sur les lois de poursuite pour les véhicules légers (VL) est très vaste. Cependant, jusqu'à aujourd'hui peu de recherches ont été effectuées concernant les poids lourds (PL) (Aghabayk et al., 2015; Nodine et al., 2017).

Les principales études traitant des lois de poursuite pour les PL se concentrent sur les différences de comportement de suivi selon le *Leader* (PL ou VL) (Aghabayk et al., 2012, 2016; Nodine et al., 2017; Sarvi, 2011). D'autres études mettent en évidence l'impact de l'hétérogénéité du trafic sur celui-ci (Chen et al., 2016; Liu et al., 2016; Yang et al., 2014).

Les précédentes études sur des lois de poursuites adaptées aux PL étaient basées sur des modèles complexes existant (Aghabayk et al., 2016) ou sur le développement de nouveaux modèles (Aghabayk, 2013; Aghabayk et al., 2013). Dans cette étude, nous cherchons à établir si un modèle courant et existant, avec des paramètres adaptés, pourrait reproduire les trajectoires d'un poids lourd de manière suffisamment précise pour estimer sa consommation énergétique.

Quatre lois de poursuites connues et fréquemment utilisées sont étudiées et comparées :

- le modèle de Gipps (Gipps, 1981),
- l'*Improved Intelligent Driver Model* (IIDM) (Treiber and Kesting, 2013a),
- le modèle de Newell (Newell, 2002), et,
- le modèle de Wiedemann (Wiedemann and Reiter, 1992; Wiedemann, 1974).

F.2.1.3 Méthodes permettant de reconstruire les trajectoires d'un véhicule

La définition des trajectoires pour le calage des lois de poursuite occupe une place importante dans les études d'optimisation de ces modèles. Les trajectoires peuvent venir de différentes sources : véhicules équipés, enregistrements vidéo ou données simulées (Thiemann et al., 2008; Toledo et al., 2007; Vieira da Rocha et al., 2015).

Plusieurs études ont mis en évidence les impacts que la reconstruction des trajectoires pouvait avoir sur les résultats des calages des paramètres des lois de poursuites (Ossen and Hoogendoorn, 2008; Punzo et al., 2005; Toledo et al., 2007). Ces études se concentrent principalement sur le lissage des données et sur l'ordre dans lequel appliquer lissage et dérivation/intégration.

Afin de proposer une méthode adaptée aux données disponibles, différents schémas d'intégration/dérivation (schémas d'Euler explicite et implicite, et schéma trapézoïdal), combinés à différentes méthodes de lissages (pas de lissage, moyenne glissante, interpolation) seront comparés. Au total 54 méthodes de reconstruction seront étudiées (section F.2.2).

F.2.1.4 Définir une méthode de calage adaptée au modèle

Le calage des lois de poursuite vise à trouver le jeu de paramètres qui permettra de minimiser les erreurs entre les trajectoires mesurées et les trajectoires simulées. Pour caler ces paramètres, plusieurs paramètres doivent être définis :

(i) La fonction de coût : la fonction avec laquelle l'écart entre mesures et simulations est évalué,

(ii) Les mesures de performances (*Measure of Performance*, MoP) : les indicateurs sur lesquels l'erreur est calculée,

(iii) Le pas de temps de simulation, et ,

(iv) Le solver : le schéma d'intégration/dérivation liant position, vitesse et accélération.

On s'intéressera dans un premier temps à quatre fonctions de coût fréquemment utilisées pour caler les paramètres de lois de poursuites : le *Root Mean Squared Error* (RMSE), le *Root Mean Squared Percentage Error* (RMSPE), le *Squared Error* (SE) et le coefficient d'inégalité de Theil (U). La comparaison de ces fonctions sera basée sur leur forme (plate ou escarpée) définissant les domaines optimaux. On s'intéressera particulièrement aux intersections de ces domaines optimaux. L'efficacité de plusieurs pas de temps de simulation : $0.01s$, $0.1s$, $0.5s$ et $1s$; ainsi que de plusieurs solvers : schémas explicite et implicite, schéma trapézoïdal, schéma

mixte (explicite combiné avec trapézoïdal), et le schéma de Runge-Kutta d'ordre 4 sont également comparés sur la base des valeurs des erreurs observées après calage des paramètres des lois de poursuite.

L'algorithme d'optimisation utilisé est un algorithme d'optimisation par essaim particulaire, proposé par Kennedy and Eberhart (1995). Il s'agit d'un algorithme d'optimisation globale, comme l'algorithme génétique.

Cet algorithme est basé sur l'utilisation d'un essaim de particules (dont la position correspond à vecteur représentant les paramètres à caler), se déplaçant dans l'espace des solutions possibles. A chaque itération, chaque particule se déplace dans une direction combinant la position de la meilleure particule (celle qui génère la plus faible erreur) et la meilleure position rencontrée jusqu'alors par la particule elle-même, et ce jusqu'à ce que l'erreur acceptée soit atteinte ou que le nombre maximal d'itérations soit atteint.

Cet algorithme est décliné ici sous sa formulation multi-objectif, basé sur la définition de la dominance de Pareto (Coello Coello and Lechuga, 2002) et sur la méthode de guidage aléatoire globale (*RANDOM global guides*) proposée par Alvarez-Benitez et al. (2005).

F.2.2 Reconstruction des trajectoires nécessaires au calage des lois de poursuites

Cette section présente une comparaison des différentes méthodes de reconstruction de trajectoires présentées précédemment.

F.2.2.1 Présentation des données

Les données utilisées pour créer une base de données de trajectoires, nécessaires au calage des paramètres des lois de poursuite, ont été extraites d'un enregistrement d'environ 80km en région lyonnaise.

Cet enregistrement fournit les données GPS (latitude, longitude et altitude), la vitesse du véhicule ainsi que la distance entre celui-ci et son *Leader*. A partir de ces informations, il est nécessaire de reconstruire la trajectoire complète (position, vitesse et accélération) des deux véhicules, *Follower* et *Leader*, pour pouvoir procéder au calage des paramètres de lois de poursuite.

L'enregistrement a permis d'extraire 35 cycles, mesurant entre 166m et 2.6km.

F.2.2.2 Comparaison des méthodes de reconstruction

Pour comparer les différentes méthodes de reconstruction, chacune d'entre elles est utilisée pour calculer les trajectoires complètes des deux véhicules, sur chacun des cycles identifiés.

Pour sélectionner la méthode la plus adaptée, les positions, vitesses, accélérations, et jerks (dérivée de l'accélération) seront comparés.

Pour estimer la précision des positions reconstruites, les distances parcourues sont comparées. Ces distances sont quasiment identiques pour toutes les méthodes, avec un écart maximal de l'ordre de 60cm. La comparaison des positions ne sera pas discriminante dans le choix de la méthode de reconstruction.

Les vitesses reconstruites sont ensuite comparées avec les vitesses mesurées en utilisant le RMSE. On observe que certaines méthodes donnent des erreurs qui sont toujours supérieures au $75^{\text{ème}}$ quantile des erreurs. Ces méthodes sont celles utilisant l'interpolation comme méthode de lissage. Elles seront donc écartées par la suite comme étant celles générant les erreurs les plus élevées.

La comparaison des accélérations se fait par la recherche des valeurs extrêmes, les méthodes générant des valeurs supérieures en valeur absolue à $3m/s^2$ sont écartées pour des raisons de réalisme. Les $10^{\text{ème}}$ et $90^{\text{ème}}$ quantiles sont calculés et comparés pour chaque cycle. On observe que, de la même manière que pour la vitesse, certaines méthodes se distinguent en générant des valeur d'accélération plus élevées que les autres méthodes. Ces méthodes correspondent aux méthodes calculant l'accélération sans lissage, elles seront écartées.

L'étude des valeurs du jerk a permis de mettre en évidence que les trajectoires reconstruites respectaient la physique d'un véhicule, avec moins de 2% d'excès de la valeur maximale acceptée du jerk contre 10% dans la littérature (Punzo et al., 2011). Les méthodes générant les valeurs de jerk les plus élevées sont également écartées.

A ce stade, 14 méthodes sont finalement envisageables parmi les 54 testées. En se basant sur les conseils donnés dans la littérature (Punzo et al., 2011), seule une méthode parmi les 14, correspond au schéma proposé.

Cette méthode consiste à lisser la vitesse mesurée, puis intégrer cette mesure avec le schéma trapézoïdal, pour obtenir la position du *Follower*. L'interdistance est ajoutée à cette position pour obtenir la position du *Leader*. Puis, chacun de ces vecteurs position est dérivé avec le schéma trapézoïdal pour obtenir les vitesses, qui sont ensuite lissées avec une moyenne glissante, la même opération est répétée pour obtenir les accélérations des deux véhicules.

F.2.2.3 Classification des cycles

Les réactions d'un véhicules sont dépendantes de son environnement : le mouvement d'un véhicule peut être différent suivant s'il est en zone urbaine ou non par exemple.

Pour l'étape de calage des paramètres, les 35 cycles sont classés parmi quatre catégories : urbain, inter-urbain, régional et périphérique. Les cycles sont classés suivant leur vitesse moyenne, la vitesse maximale atteinte et leur localisation géographique.

La catégorie "urbain" contient 17 cycles, la catégorie "régional" contient 8 cycles, et les catégories "inter-urbain" et "périphérique" contiennent chacune 5 cycles.

F.2.3 Calage des lois de poursuite à partir de trajectoires poids lourd

La section précédente a présenté le choix d'une méthode de reconstruction de trajectoire, permettant à partir d'un enregistrement de la vitesse d'un véhicule et de la distance au véhicule qui le précède, de calculer l'ensemble de la trajectoire (position, vitesse et accélération) des deux véhicules, *Leader* et *Follower*.

Cette section va présenter l'étude de différentes méthodes pour le calage des paramètres de lois de poursuite. Cette section va proposer pour chacune des lois de poursuites étudiées, présentées à la section F.2.1, une méthode de calage adaptée. Les fonctions de coûts, le pas de temps de simulation ainsi que le solver sont à déterminer.

F.2.3.1 Étude de la forme des fonctions de coût et choix de MoP

Dans un premier temps, nous nous intéressons aux fonctions de coût, et en particulier à leur forme. Si la fonction de coût est plate, cela signifie que le domaine optimal est étendu, et qu'un grand nombre de combinaisons de valeurs de paramètres peuvent donner des résultats quasi-optimaux, le calage perd ainsi en précision.

Pour étudier la forme de ces fonctions, un maillage de chacune d'elle est réalisé. La forme des fonctions est déterminée en étudiant l'évolution de la taille des domaines optimaux avec l'erreur acceptée. Les domaines optimaux sont définis comme suit : le point donnant l'erreur minimale est recherché, ensuite cinq domaines optimaux sont définis. Le premier contient les points dont l'erreur est comprise entre l'erreur minimale et l'erreur minimale plus 10%. Le second domaine contient les points dont l'erreur se situe entre l'erreur minimale et celle-ci additionnée de 20% et ainsi de suite jusqu'au cinquième domaine.

Ce procédé a permis de mettre en évidence le fait que les domaines optimaux pour la position ou l'interdistance sont très pointus contrairement aux domaines optimaux pour la vitesse et l'accélération, et ce pour les quatre fonctions de coût.

Cependant, le but final de cette recherche est l'estimation des consommations énergétiques. Or, il est nécessaire d'avoir une estimation précise de la vitesse et de l'accélération pour celle-ci. Le calage des lois de poursuite uniquement basé sur les positions ou interdistances n'est donc pas pertinent dans ce cas d'étude. Nous nous intéressons donc ensuite à l'intersection des domaines optimaux afin de garantir une trajectoire simulée la plus précise possible sur ses trois composantes : position, vitesse et accélération.

Afin de garantir l'existence de l'intersections des domaines optimaux, le choix d'utiliser comme fonction de coût le coefficient d'inégalité de Theil est fait. Les lois de poursuites seront calées en utilisant une optimisation par essaim particulaire multi-objectif.

F.2.3.2 Influence du pas de temps sur le résultat du calage

L'influence du pas de temps de simulation dans le calage des paramètres des lois de poursuites n'est que très peu étudié dans la littérature. Afin de déterminer quel est le pas de temps idéal pour chaque modèle, leurs paramètres seront calés sur quatre cycles appartenant à des catégories différentes, pour chacun des pas de temps étudiés.

Ces calages ont mis en évidence que l'estimation des positions et des vitesses ne sont pas très sensibles aux variations de pas de temps, contrairement aux accélérations et interdistances.

Pour chaque modèle, le pas de temps de simulation permettant d'obtenir les erreurs les plus faibles est sélectionné.

F.2.3.3 Influence du solver sur le résultat du calage

De la même manière que pour le choix du pas de temps de simulation, les lois de poursuites sont calées pour chacun des solvers envisagés, et les résultats sont comparés.

En accord avec la littérature, l'usage du solver de Runge-Kutta d'ordre 4 ne permet pas d'avoir de meilleurs résultats qu'avec un solver plus simple (Treiber and Kesting, 2013b).

Contrairement au pas de temps, le même solver est sélectionné pour les quatre lois de poursuite : le solver mixte (schéma trapézoïdal pour lier positon et vitesse, et schéma explicite pour lier vitesse et accélération). Le tableau ci-dessous résume les méthodes choisies pour caler chacune des lois de poursuites étudiées.

TABLE F.1 – Méthode otpimale de calage des lois de poursuite

	Fonction de coût	Mesures de performance	Pas de temps	Solver
Gipps	Coefficient d'inégalité de Theil	Interdistance Vitesse Accélération	$0.1s$	Mixte
IIDM	Coefficient d'inégalité de Theil	Interdistance Vitesse Accélération	$0.01s$	Mixte
Newell	Coefficient d'inégalité de Theil	Interdistance Vitesse Accélération	$0.5s$	Mixte
Wiedemann	Coefficient d'inégalité de Theil	Interdistance Vitesse Accélération	$0.5s$	Mixte

F.2.3.4 Résultat du calage des paramètres des lois de poursuite

Après avoir défini une méthode de calage pour les lois de poursuites, leurs paramètres sont calés et les modèles sont comparés.

On met en évidence que les modèle de Gipps et de Newell donnent de très bons résultats dans l'estimation de la position et de l'interdistance avec des erreurs respectives autour de 0.9% et 7.4%, et une erreur de 3.7% pour le modèle de Gipps et de 4.6% pour le modèle de Newell pour la vitesse. Les erreurs provenant du calage des paramètres de l'IIDM sont environ deux fois plus élevées. Le modèle de Wiedemann est celui qui donne les moins bons résultats avec des erreurs allant de 20% pour l'interdistance à 55% pour l'accélération.

F.2.3.5 Étude de la robustesse des modèles

Étant donné le faible nombre de cycles disponibles pour le calage des modèles, une validation n'est pas réalisable. Cependant, on s'intéresse à la robustesse du calage de ces modèles. En effet, ces modèles devant être intégrés dans un outil de simulation, il serait intéressant de pouvoir utiliser un paramétrage moyen par type de cycle plutôt que des paramètres optimaux pour chaque cycle.

La robustesse des modèles est vérifiée en simulant chacune des 35 trajectoires avec les paramètres optimaux moyens de sa catégorie à la place de ses paramètres optimaux propres.

Ces simulations permettent de conclure que les modèles de Newell et de Wiedemann ne sont pas du tout robustes à l'utilisation de paramètres moyens, avec des erreurs dépassant les 80% pour le modèle de Newell et 60% pour le modèle de Wiedemann.

Le modèle de Gipps et l'IIDM sont quant à eux très robustes, les erreurs sur les trajectoires simulées n'étant que très peu augmentées par rapport aux simulations avec les paramètres optimaux.

F.2.3.6 Conclusion

En conclusion, les différentes études dont les résultats sont présentés dans cette section ont permis de définir des méthodes de calage adaptées à chacune des lois de poursuites étudiées.

Les paramètres de ces lois de poursuite ont été calés et les résultats ainsi que la robustesse de modèles ont été évalués. Au vu des résultats de robustesse et de précision des modèles, seules la loi de Gipps et l'IIDM seront conservées pour la suite de l'étude concernant l'estimation des consommations énergétiques.

F.2.4 Estimation des consommations énergétiques à partir des trajectoires simulées

La précédente section a présenté le calage des paramètres des lois de poursuite de Gipps et de l'IIDM. Les trajectoires simulées peuvent à présent être utilisées pour estimer la consommation énergétique des véhicules industriels. Une comparaison entre les mesures et les simulations est réalisée.

F.2.4.1 Estimation des consommations énergétiques à partir des trajectoires simulées

L'estimation des consommations énergétiques est réalisée à l'aide de l'outil de simulation utilisé au sein du groupe Volvo. Cet outil utilise comme entrée le profil de vitesse du véhicule et la pente de la route.

Malgré les bons résultats du calage des modèles concernant les trajectoires du véhicule industriel, les erreurs sur l'estimation de la consommation énergétique sont très élevées. En moyenne, elles s'élèvent à 10% pour le modèle de Gipps et 22% pour l'IIDM.

Ce résultats est cohérent avec l'étude présentée dans Vieira da Rocha et al. (2015) sur les VL. Le calage d'une loi de poursuite peut-être très précis d'un point de vue des trajectoires, mais générer des grandes erreurs au regards des estimation des polluants. Or, dans la majorité des études, les modèles de simulation de trafic sont calés uniquement sur des objectifs liés aux trajectoires des véhicules, même si par la suite ils sont utilisés pour estimer des émissions.

F.2.4.2 L'estimation de la consommation énergétique, la 4ème Mesure de Performance

Afin de diminuer l'erreur observée sur l'estimation de la consommation énergétique à partir de trajectoires simulées, il est proposé d'ajouter l'estimation de la consommation énergétique dans le processus de calage en tant que quatrième Mesure de Performance.

Le modèle de Gipps et l'IIDM sont de nouveaux calés sur les 35 trajectoires. L'ajout de l'estimation de la consommation énergétique dans le processus de calage, multiplie le temps de calcul par trois ou quatre selon la longueur des cycles, mais cela reste acceptable.

Afin de confirmer l'intérêt d'un calage suivant quatre objectifs, les consommations énergétiques sont recalculées avec les nouvelles trajectoires.

On observe alors une amélioration significative des estimations de consommation. Les erreurs sont à présent de 7% et 10% respectivement pour le modèle de Gipps et l'IIDM.

La précision de la représentation des trajectoires pour l'IIDM est légèrement dégradée mais reste acceptable. On constate cependant que pour le modèle de Gipps les erreurs sur les trajectoires sont quasiment identiques dans les deux calages.

Dû à la platitude de la fonction de coût, l'ajout d'un objectif dans le processus de calage a permis d'améliorer les estimations des consommations énergétiques sans dégrader la précision des trajectoires. D'après les résultats de simulation, le modèle de Gipps est le plus adapté pour la modélisation du comportement d'un PL.

F.3 Partie 2 : Génération automatique de cycles de simulation à partir d'informations statistiques sur les trajets usuels des véhicules industriels

Dans le but de tester des systèmes d'aide à la conduite, il est nécessaire de pouvoir utiliser des scénarios de simulation réalistes. Pour permettre ces tests, il a été choisi d'utiliser le logiciel de simulation de trafic microscopique SUMO (Krajzewicz et al., 2012) couplé au modèle de cinématique véhicule.

Pour définir des scénarios de simulation, nous nous sommes intéressés à l'environnement rencontré par un PL lors de parcours usuels. En particulier, des indicateurs statistiques représentatifs de ces parcours ont été définis, et une méthodologie pour générer ces scénarios est proposée.

F.3.1 Utilisation des statistiques des trajets usuels pour générer des réseaux routiers

Cette section présente la base de données de trajets usuels utilisée pour la génération de scénarios de simulation. Ces trajets sont, dans un premier temps, étudiés afin de définir des indicateurs statistiques représentatifs, puis ces indicateurs sont utilisés pour créer les scénarios des simulations.

Dans la majorité des études, les cycles de simulation sont des cycles statiques, définis par un profil de vitesse. Ici, on s'intéresse à des réseaux complets, modélisés grâce à l'outil de simulation microscopique SUMO, dans le but de pouvoir tester des systèmes d'aide à la conduite.

F.3.1.1 Les cycles usuels

Afin de pouvoir définir des scénarios de simulation réalistes, nous nous appuyons sur une base de données de parcours usuels de PL dans la région lyonnaise. En complément, la base de données cartographiques HERE (HereMaps) est utilisée pour obtenir les informations nécessaires à la mise en place des scénarios (intersections, vitesses légales, vitesses moyennes,...).

La base de données de trajets contient 25 trajets (3 livraisons régionales et 22 livraisons locales). Comme dans la section F.2.2, ces trajets sont d'abord divisés en fonction de plusieurs type d'environnement : urbain, inter-urbain, régional, périphérique et autoroutier. Ces environnements sont définis par leur vitesse légale, les vitesses maximales et moyennes observées ainsi que le nombre de voies moyen.

Plusieurs informations sont nécessaires afin de définir un scénario de simulation (type d'infrastructure, état du trafic routier...). Ces informations sont extraites de la base de données HERE pour chaque sous-trajet puis moyennées par catégorie d'environnement.

On considère deux catégories d'indicateurs. Les indicateurs statiques et les indicateurs dynamiques. Les indicateurs statiques décrivent la géométrie du réseau routier et ses caractéristiques : nombre de voies, types et positions des intersections, pente, vitesse légale,... Les indicateurs dynamiques sont liés à l'état du trafic routier sur le réseaux, il est alors proposé trois états possibles définis par une vitesse moyenne par route : état congestionné, état fluide et état libre.

L'enchaînement des différents évènements/composants est estimé via des matrices de Markov.

F.3.1.2 Génération des scénarios de simulation

Une fois les indicateurs décrit précédemment calculés, les scénarios de simulation peuvent être générés. Un outil permettant de générer automatiquement un scénario a été développé. Cet outil est basé sur le langage de programmation Python.

L'utilisateur choisit le type d'environnement qu'il souhaite créer, la longueur du parcours (ou valeur par défaut dépendante de l'environnement) et les conditions de trafic. La génération du réseau dure de quelques secondes à quelques minutes. Le trafic présent dans le scénario est ensuite généré par le biais d'une optimisation par essaim particulaire. Cette étape peut durer jusqu'à une journée.

La méthode de génération des scénarios de simulation a été validée pour les différents environnements. Une centaine de scénarios ont été générés aléatoirement, puis les moyennes de leurs caractéristiques ont été comparées aux indicateurs calculés à partir des bases de données.

Les proportions d'intersections sont respectées dans tous les environnements. Les vitesses des scénarios sont parfois un peu plus faibles que les vitesses mesurées mais restent dans un intervalle cohérent.

F.3.2 Application : Evaluation d'un système d'ACC sur un trajet long-routier

Cette section présente les résultats de l'utilisation de la chaîne complète de simulation pour l'évaluation d'un algorithme d'*Adaptive Cruise Control* (ACC).

F.3.2.1 Application à la génération d'un scénario long-routier

L'ACC a un impact sur la distance à laquelle un véhicule suit le véhicule qui le précède dans le but d'éviter tout risque de collision. Ce système lisse ainsi les trajectoires des véhicules en anticipant les freinages.

F.3.2.2 Application à l'évaluation d'un algorithme d'ACC

Le système d'ACC est évalué sur un trajet long-routier, entre Lyon et Chambéry. Ce trajet est dans un premier temps généré sous forme de scénario de simulation pour le logiciel SUMO.

Plusieurs données sont disponibles pour la comparaison : le cycle statique défini par un profil de vitesse (une simulation unique), les mesures (une vingtaine d'enregistrements), et le scénario simplifié (possibilité d'un grand nombre de simulations, ici 100 avec et sans l'activation de l'ACC).

Des différences sont observables entre les trois sources de données. Le cycle statique est très lissé comparé aux deux autres, ce qui influe également sur la quantité de fuel utilisé. En comparant les profils de consommation cumulée on peut observer que les simulations résultant du scénario simplifié sont plus linéaires que les deux autres : les pentes, générées aléatoirement, peuvent différer de la réalité. Les vitesses moyennes sont quand à elles quasiment identiques entre les mesures et les scénarios simplifiés.

L'utilisation de paramètres moyens et d'aléatoire dans la génération des scénarios simplifiés, peut induire des écarts avec la réalité, même si statistiquement les cycles sont similaires. Cependant, l'usage de scénarios simplifiés permet d'évaluer de nouveaux systèmes d'aide à la conduite impossibles à tester à l'aide des cycles statiques traditionnels.

La comparaison des simulations, avec et sans activation de l'ACC, met en évidence le fait que cet algorithme lisse les trajectoires en décalant légèrement vers des valeurs un peu plus faibles la distribution des vitesses moyennes. Les consommations de carburant ne sont pas impactées par l'utilisation de cet ADAS.

F.4 Conclusion et perspectives

Les travaux réalisés durant cette thèse ont permis de proposer des modèles adaptés aux poids lourds et des méthodes permettant de mettre en place rapidement des scénarios de simulation réalistes pour l'évaluation des nouveaux systèmes d'aide à la conduite.

L'étude sur les lois de poursuite pourrait être complétée par l'utilisation d'autres données permettant d'effectuer une véritable validation des modèles. De plus, le calage a ici été réalisé pour un type de poids lourd, avec un poids défini, il serait intéressant de vérifier les résultats sur d'autres véhicules.

La génération des réseaux simplifiés apporte également plusieurs interrogations. Les trajets usuels ont été enregistrés autour de la même agglomération, on peut s'interroger sur la pertinence de ces valeurs pour une autre ville ou un autre pays. De plus, l'utilisation d'aléatoire nous éloigne parfois des moyennes, et pourrait rendre les scénarios générés non réalistes.

Les informations générées pourraient également être améliorées en combinant plusieurs sources d'informations géographiques en supplément de HERE, telles que Google Maps ou OpenStreetMaps.

F.5 Références

Kayvan Aghabayk. *Modelling heavy vehicle car-following in congested traffic conditions*. PhD thesis, Institute of Transport Studies, SDepartment of Civil Engineering, Monash University, 2013. p. XXI

Kayvan Aghabayk, Majid Sarvi, and William Young. Understanding the Dynamics of Heavy Vehicle Interactions in Car-Following. *Journal of Transportation Engineering*, 138(12):1468–1475, December 2012. ISSN 0733-947X, 1943-5436. doi: 10.1061/(ASCE)TE.1943-5436.0000463. p. XXI

Kayvan Aghabayk, Majid Sarvi, Nafiseh Forouzideh, and William Young. New Car-Following Model Considering Impacts of Multiple Lead Vehicle Types. *Transportation Research Record: Journal of the Transportation Research Board*, 2390:131–137, December 2013. ISSN 0361-1981. doi: 10.3141/2390-14. p. XXI

Kayvan Aghabayk, Majid Sarvi, and William Young. A State-of-the-Art Review of Car-Following Models with Particular Considerations of Heavy Vehicles. *Transport Reviews*, 35(1):82–105, January 2015. ISSN 0144-1647, 1464-5327. doi: 10.1080/01441647.2014.997323. p. XXI

Kayvan Aghabayk, Majid Sarvi, and William Young. Including heavy vehicles in a car-following model: modelling, calibrating and validating. *Journal of Advanced Transportation*, 50(7):1432–1446, November 2016. ISSN 01976729. doi: 10.1002/atr.1409. [3]. p. XXI

Julio E. Alvarez-Benitez, Richard M. Everson, and Jonathan E. Fieldsend. A MOPSO Algorithm Based Exclusively on Pareto Dominance Concepts. In David Hutchison, Takeo Kanade, Josef Kittler, Jon M. Kleinberg, Friedemann Mattern, John C. Mitchell, Moni Naor, Oscar Nierstrasz, C. Pandu Rangan, Bernhard Steffen, Madhu Sudan, Demetri Terzopoulos, Dough Tygar, Moshe Y. Vardi, Gerhard Weikum, Carlos A. Coello Coello, Arturo Hernández Aguirre, and Eckart Zitzler, editors, *Evolutionary Multi-Criterion Optimization*, volume 3410, pages 459–473. Springer Berlin Heidelberg, Berlin, Heidelberg, 2005. ISBN 978-3-540-24983-2 978-3-540-31880-4. doi: 10.1007/978-3-540-31880-4_32. URL http://link.springer.com/10.1007/978-3-540-31880-4_32. p. XXII

Danjue Chen, Soyoung Ahn, Soohyuk Bang, and David Noyce. Car-Following and Lane-Changing Behavior Involving Heavy Vehicles. *Transportation Research Record: Journal of the Transportation Research Board*, 2561:89–97, January 2016. ISSN 0361-1981. doi: 10.3141/2561-11. [9]. p. XXI

N. Chiabaut, C. Buisson, and L. Leclercq. Fundamental Diagram Estimation Through Passing Rate Measurements in Congestion. *IEEE Transactions on Intelligent Transportation Systems*, 10(2):355–359, June 2009. ISSN 1524-9050, 1558-0016. doi: 10.1109/TITS.2009.2018963. p. XX

CITEPA. Inventaire SECTEN, 2017. URL https://www.citepa.org/fr/activites/inventaires-des-emissions/secten. p. XIX

C.A. Coello Coello and M.S. Lechuga. MOPSO: a proposal for multiple objective particle swarm optimization. volume 2, pages 1051–1056. IEEE, 2002. ISBN 978-0-7803-7282-5. doi: 10.1109/CEC.2002.1004388. p. XXII

Benjamin A. Coifman and Yun Wang. Average Velocity of Waves Propagating through Congested Freeway Traffic. 2005. ISBN 978-0-08-044680-6. p. XX

Daniel L. Gerlough and Matthew J. Huber. *Traffic Flow Theory - A monograph*. Transportation Research Board Special Report 165. H.P. Orland, Washington, D.C., 1975. p. XX

P.G. Gipps. A behavioural car-following model for computer simulation. *Transportation Research Part B: Methodological*, 15(2):105–111, April 1981. ISSN 01912615. doi: 10.1016/0191-2615(81)90037-0. p. XXI

B. d Greenshields. A study of traffic capacity. *Proceedings of the 14th Annual Meeting of the Highway Research Board*, 1935:448–477, 1935. ISSN 0096-1027. p. XX

HereMaps. HERE. URL https://www.here.com. p. XXVI

J. Kennedy and R. Eberhart. Particle swarm optimization. volume 4, pages 1942–1948. IEEE, 1995. ISBN 978-0-7803-2768-9. doi: 10.1109/ICNN.1995.488968. p. XXII

Daniel Krajzewicz, Jacob Erdmann, Michael Behrisch, and Laura Bieker. Recent development and applications of SUMO–Simulation of Urban MObility. *International Journal On Advances in Systems and Measurments*, 5(3&4):128–138, December 2012. p. XXV

Ludovic Leclercq. Calibration of Flow-Density Relationships on Urban Streets. *Transportation Research Record: Journal of the Transportation Research Board*, 1934:226–234, January 2005. ISSN 0361-1981. doi: 10.3141/1934-24. p. XX

M. J. Lighthill and G. B. Whitham. On Kinematic Waves. II. A Theory of Traffic Flow on Long Crowded Roads. *Proceedings of the Royal Society A: Mathematical, Physical and Engineering Sciences*, 229(1178): 317–345, May 1955. ISSN 1364-5021, 1471-2946. doi: 10.1098/rspa.1955.0089. p. XX

Lan Liu, Liling Zhu, and Da Yang. Modeling and simulation of the car-truck heterogeneous traffic flow based on a nonlinear car-following model. *Applied Mathematics and Computation*, 273:706–717, January 2016. ISSN 00963003. doi: 10.1016/j.amc.2015.10.032. [8]. p. XXI

G.F. Newell. A simplified car-following theory: a lower order model. In *Transportation Research Part B: Methodological*, volume 36, pages 195–205, 2002. doi: 10.1016/S0191-2615(00)00044-8. p. XXI

Emily Nodine, Andy Lam, Mikio Yanagisawa, and Wassim Najm. Naturalistic Study of Truck Following Behavior. *Transportation Research Record: Journal of the Transportation Research Board*, 2615:35–42, January 2017. ISSN 0361-1981. doi: 10.3141/2615-05. [2]. p. XXI

Saskia Ossen and Serge P. Hoogendoorn. Validity of Trajectory-Based Calibration Approach of Car-Following Models in Presence of Measurement Errors. *Transportation Research Record: Journal of the Transportation Research Board*, 2088(1):117–125, January 2008. ISSN 0361-1981, 2169-4052. doi: 10.3141/2088-13. p. XXI

Vincenzo Punzo, Domenico Formisano, and Vincenzo Torrieri. Nonstationary Kalman Filter for Estimation of Accurate and Consistent Car-Following Data. *Transportation Research Record: Journal of the Transportation Research Board*, 1934:1–12, January 2005. ISSN 0361-1981. doi: 10.3141/1934-01. p. XXI

Vincenzo Punzo, Maria Teresa Borzacchiello, and Biagio Ciuffo. On the assessment of vehicle trajectory data accuracy and application to the Next Generation SIMulation (NGSIM) program data. *Transportation Research Part C: Emerging Technologies*, 19(6):1243–1262, December 2011. ISSN 0968-090X. doi: 10.1016/j.trc.2010.12.007. p. XXII

Paul I. Richards. Shock Waves on the Highway. *Operations Research*, 4(1):42–51, February 1956. ISSN 0030-364X, 1526-5463. doi: 10.1287/opre.4.1.42. p. XX

Majid Sarvi. Heavy commercial vehicles-following behavior and interactions with different vehicle classes: Following behavior analysis in heavy vehicles. *Journal of Advanced Transportation*, pages n/a–n/a, October 2011. ISSN 01976729. doi: 10.1002/atr.182. URL http://doi.wiley.com/10.1002/atr.182. p. XXI

Christian Thiemann, Martin Treiber, and Arne Kesting. Estimating Acceleration and Lane-Changing Dynamics from Next Generation Simulation Trajectory Data. In *Transportation Research Record: Journal of the Transportation Research Board*, volume 2088, pages 90–101, Washington D.C., 2008. doi: 10.3141/2088-10. p. XXI

Tomer Toledo, Haris N. Koutsopoulos, and Kazi I. Ahmed. Estimation of Vehicle Trajectories with Locally Weighted Regression. In *Transportation Research Record: Journal of the Transportation Research Board*, volume 1999, pages 161–169, Washington D.C., 2007. doi: 10.3141/1999-17. p. XXI

Martin Treiber and Arne Kesting. Car-Following Models based on Driving Strategies. In *Traffic Flow Dynamics: Data, Models and Simulation*, pages 187–198. Springer, 2013a. ISBN 978-3-642-32459-8. p. XXI

Martin Treiber and Arne Kesting. Elementary Car-Following models. In *Traffic Flow Dynamics*. Springer Berlin Heidelberg, Berlin, Heidelberg, 2013b. ISBN 978-3-642-32459-8 978-3-642-32460-4. doi: 10.1007/978-3-642-32460-4. p. XXIV

Thamara Vieira da Rocha, Ludovic Leclercq, Marcello Montanino, Céline Parzani, Vincenzo Punzo, Biagio Ciuffo, and Daniel Villegas. Does traffic-related calibration of car-following models provide accurate estimations of vehicle emissions? *Transportation Research Part D: Transport and Environment*, 34:267–280, January 2015. ISSN 13619209. doi: 10.1016/j.trd.2014.11.006. p. XXI, XXV

R. Wiedemann and U. Reiter. Microscopic traffic simulation: the simulation system MISSION, background and actual state. Proj. ICARUS Final report, Brussels, 1992. p. XXI

Rainer Wiedemann. Simulation des Strassenverkehrsflusses. Technical report, Instituts für Verkehrswesen des Universität Karlsruhe, 1974. p. XXI

John R. Windover and Michael J. Cassidy. Some observed details of freeway traffic evolution. *Transportation Research Part A: Policy and Practice*, 35(10):881–894, 2001. p. XX

Da Yang, Peter (Jing) Jin, Yun Pu, and Bin Ran. Stability analysis of the mixed traffic flow of cars and trucks using heterogeneous optimal velocity car-following model. *Physica A: Statistical Mechanics and its Applications*, 395:371–383, February 2014. ISSN 03784371. doi: 10.1016/j.physa.2013.10.017. [7]. p. XXI